EFFECTS OF Kv1.3 INHIBITION

IN TYPE 2 DIABETES-INDUCED

CARDIAC ELECTRICAL

REMODELING

JULIAN ZAYAS ARRABAL

PhD Thesis

2021

AGRADECIMIENTOS

tú, y estando con gente tan maja en los chupinazos o en las fiestas de Bernedo. A Marina, Albertus y Laura y todos los demás por formar esa cuadrilla de expatriados que ha sido imprescindible para mi felicidad en Gasteiz. Por muchos más momentos compartidos. A Dani, Itxaso, Naiara y Unai por todas las conversaciones, cervezas y momentos compartidos. Gracias por guiarme en Vitoria. Y, como no, a la gente del euskaltegi de AEK de Judimendi. Eskerrik asko denei. Zuen eskuz euskara ikasi dut, baina horretaz gain, merezi duen jendea ezagutu dut. Antoine, Sergio eta Iñaki, betiko laurak izango gara betirako. Espero dut harremana mantentzea, onena opa dizuet.

Eskerrik asko Oreretako jendeari, beso zabalik hartzeagatik. Maialanen kuadrilari, mutil eta neskei, bereziki Kattalini, azken boladan gasteiztarra bihurtu denari. Eskerrik asko ere Maialenen familiari beste bat banintz bezala tratatu nautelako. Jon, Oihane, Iraia, Iren, Miguel, Itziar, Juantxo eta Miren, eskerrik asko bihotzez.

A tot el grup vasco-català de la UAB i de la Vila. Més de 10 anys de compartir moments que no canviaria per res. Lidia, Rivas, Anita, Jokin, Franc, Carles, Jon y todos los demás, gracias. Porque sin nuestras quedadas todo hubiese sido mucho más difícil. Eskerrik asko denagatik!

A la meua colla de Tortosa, als de sempre, a la gent en la que m'he criat i he crescut i en los que he viscut i viuré moments inoblidables, gràcies de tot cor. Sense vatros no seria qui sóc. Especialment als més incondicionals, Roger, Oscar, Angi, Peu, Criska, Jacketa, Miki, Gaya, Kinto i Sara. Gràcies per estar en qualsevol moment, per a tot, sempre. Tampoc voldria deixar-me a la gent del barri millor barri de Tortosa. Ariño, Oriol, Fran, Fàtima, Ramon i tots els altres, gràcies. No podria estar més orgullos de ser d'on sóc i de tenir els amics que tinc.

A Vicente, porque me ha tratado como uno más de la familia. Sin todo su apoyo, ese año en Orduña y toda la ayuda que me ha dado, esta tesis no hubiera sido posible y mi vida sería diferente. Gracias de corazón, nunca podré devolverte tanto.

A toda la gente que ha pasado por mi vida dejando huella en estos 30 años. Fuese donde fuese, Graz, Dublin, Ankara, Roma, Barcelona o Euskal Herria por haber convertido cada sitio en mi segunda casa. Gracias por esos momentos compartidos y por todo lo que me habéis enseñado. Gracias, grazie, gràcies, thank you o Eskerrik asko.

A mi familia, a los que están y a los que ya no están. Por haberme querido tanto y por haberme enseñado tanto. Aunque me gustaría poder seguir disfrutando del cariño de los tíos y los abuelos que ya no están, me siento un afortunado de todo el cariño que recibo y he recibido. A mis primos Raquel, Roberto y David y a mis tíos José y Maria del Carmen. Muchas gracias por todo, os quiero.

A mis padres, porque sin su apoyo nada sería posible. Por ser un ejemplo y por haberme dado todo. Por quererme tanto. No podría estar más orgulloso de los valores y la educación que me han dado con todo su cariño y esfuerzo. Soy lo que soy gracias a vosotros. Os quiero mucho.

Azkenik, eskerrik asko Maialeni guztiagatik. Baldintzarik gabeko sostenguagatik, eutsi eta erortzen ez uzteagatik, hainbeste maitasun erakusteagatik eta hain maitatua sentiarazteagatik. Denbora honetan guztian erakutsi didazun guztiagatik eta eredu izateagatik. Pandemia batean tesi bat idaztea ez da erraza, eskerrik asko jasateagatik. Bide hau zoriontasunez egiten jarraitzea eta helburuak elkarrekin betetzen jarraitzea espero dut. Eskerrik asko bihotz-bihotzez. Asko maite zaitut.

FINANCIACIÓN

INDEX

INDEX OF FIGURES

INDEX OF TABLES

ACRONYMS AND ABBREVIATIONS

ADA: American Diabetes Association

Akt: Protein kinase B

AMP: Adenosine monophosphate

AP: Action potential

APD: Action potential duration

ATP: Adenosine triphosphate

AUC: Area under the curve

AV node: Atrioventricular node

BCA: Bicinchoninic acid

BMI: Body mass index

CAMKII: Ca^{2+}/calmodulin-dependent protein kinase II

CC: Current clamped

CCD Technology: Charge-coupled divice technology

Cf: Stray capacitance

Cm: Membrane capacitance

CNS: central nervous system

Cpip: Pipette capacitance

CRAC: Calcium release activated channel.

CTRL: Control

CVD: Cardiovascular disease

dH$_2$O: Distilled water

DMEM: Dulbecco's Modified Eagle Medium

DPP-4: Dipeptidyl peptidase-4

ECG: Electrocardiogram

Em: Transmembrane potential

ER: Endoplasmic reticulim

ERG-hERG: (Human) Ether-a-go-go–Related Gene Potassium Channels

EtOH: Ethanol

EWAT: Epididymal white adipose tissue

FDA: Food and drug administration

FFA: Free fatty acids

GLP-1: Glucagon-like peptide-1

GLUT2: Glucose transporter 2

GLUT4: Glucose transporter 4

HbA1c: Glycated hemoglobin

HDL: High-density lipoprotein

HFD: High-fat diet

HOMA index: Homeostatic model assessment

Ic: Capacitance current

ICa-L: L-type calcium current

IFNγ: Interferon gamma

IK: Potassium current

IK1: Inward rectifier potassium current

IKKβ: Inhibitor of nuclear factor kappa-B kinase subunit beta

IKr: Rapidly delayed-rectifier potassium current

IKs: Slowly delayed-rectifier potassium current

IKur: Ultra-rapid delayed-rectifier potassium current

IL-1β: Interleukin 1 beta

IL-6: Interleukin 6

Im: Current through a membrane

IP: Intraperitoneal

Ip: Pipette current

IPIGTT: Intraperitoneal insulin-glucose tolerance test

IR: Insulin resistance

IRS: Insulin receptor substrate

Ito: Transient outward potassium current

JNK: C-Jun N-terminal kinases

KCNE: Gene that codifies potassium voltage-gated channel subfamily E members

Kir: Inwardly rectifying potassium channels

Kvβ2: Voltage-gated potassium channel subunit beta-2

LDL: Low-density lipoprotein

MAPK: Mitogen-activated protein kinase

mTor: Mechanistic target of rapamycin

NCX: Sodium-calcium exchange

NF-κB: Nuclear factor kappa-light-chain-enhancer of activated B cells

PAP-1: 5-(4-Phenoxybutoxy)psoralen

PBS: Phosphate buffered saline

PDK1: Mithochondrial pyruvate dehydrogenase lipoamide kinase isozyme 1

PI3K: Phosphoinositide 3-kinases

PKA: Protein kinase A

PKC: Protein kinase C

QTc: QT interval corrected to heart rate

QTd: QT interval dispersion

QTdc: QT interval dispersion corrected to heart rate

ROS: Reactive oxygen species

RT: Room temperature

RyR: Ryanodine receptor

SA node: Sinoatrial node

SA-PE: Streptavidin-phycoerythrin

SDS: Sodium dodecyl sulfate

SEM: Standard error of the mean

Ser: Serine

SERCA2: Sarco/endoplasmic reticulum Ca^{2+}-ATPase 2

SGLT2: Sodium-glucose linked transporter 2

SR: Sarcoplasmic reticulum

STZ: Streptozotozin

T1D: Type 1 diabetes

T2D: Type 2 diabetes

TAG: Triacylglyceride

TBS: Tris buffered saline

TCR: T-cell receptor

TG: Triglyceride

Thr: Threonine

TLR: Toll-like receptor

TNFα: Tumor necrosis factor

Tyr: Tyrosine

VC: Voltage clamped

Vcom: Command voltage

VLDL: Very low-density lipoprotein

Vp: Applied voltage to the pipette

Vrf: Pulses that change the membrane potential membrane potential

VRf: Voltage output of the amplifier

WAT: White adipose tissue

WHO: World health organization

RESUMEN TESIS

RESUMEN TESIS

INTRODUCCIÓN

La diabetes afecta a 422 millones de adultos en el mundo (OMS 2016), por lo que el coste sociosanitario asociado a esta enfermedad es enorme. Es una patología caracterizada por hiperglucemia debida a que el páncreas no produce suficiente insulina (diabetes tipo 1, DT1) o a que el organismo no puede utilizarla eficientemente (diabetes tipo 2, DT2). Más del 90% de los pacientes diagnosticados como diabéticos tienen diabetes tipo 2 pero, con el tiempo, en muchos de ellos el páncreas se agota y acaban necesitando insulina exógena igual que los diabéticos tipo 1. Por lo tanto, la principal diferencia entre ambos tipos es la resistencia periférica a la insulina característica de la diabetes tipo 2. Además, la diabetes es una enfermedad compleja que a menudo está relacionada con múltiples factores como una alteración de los lípidos circulantes (triglicéridos y colesterol), una mayor adiposidad o una activación inusual del sistema inmune que genera el llamado estado inflamatorio de bajo grado.

1. REMODELADO ELECTRICO CARDIACO

Una las complicaciones a largo plazo habituales de la diabetes es la cardiopatía diabética (Rubler et al., 1972), la cual provoca tanto alteraciones mecánicas como eléctricas que son independientes entre sí. De hecho, las alteraciones eléctricas suelen preceder a las alteraciones mecánicas (Casis & Echevarria, 2004; Gallego & Casis, 2014). El electrocardiograma de los pacientes diabéticos presenta un aumento de la duración del intervalo QT corregido a la frecuencia cardiaca (QTc), fenómeno que se acentúa a medida que progresa la enfermedad. El alargamiento del QTc es el reflejo de alteraciones en el comportamiento eléctrico cardiaco, concretamente indica que la repolarización ventricular sucede más lentamente de lo normal. Este alargamiento de la duración de la repolarización se asocia a un mayor riesgo de arritmias ventriculares y muerte súbita y es un predictor independiente de mortalidad cardiovascular en pacientes con DT2 (Joel et al., 1987; Veglio et al, 2002, Cox et al., 2014; Lu et al., 2017). Un estudio publicado en 2018 que analiza 35 millones de hospitalizaciones en los últimos 25 años observa un aumento de las hospitalizaciones por arritmias cardiacas en pacientes jóvenes con diabetes (Rios-Burrows et al., 2018). Es decir, la diabetes remodela el comportamiento eléctrico del corazón y lo hace más vulnerable y propenso a sufrir arritmias letales.

A lo largo de los últimos 25 años nuestro grupo y otros se ha descrito que la DT1 alarga la duración de la repolarización cardiaca porque reduce la expresión de dos tipos de canales de

potasio, y por consiguiente la amplitud de las corrientes iónicas que conducen. Se trata de las corrientes de potasio transitoria de salida, Ito, y rectificadora tardía lenta, IKs (Gallego & Casis, 2014, Magyar et al, 1992; Shimoni et al, 1994; Casis et al, 2000; Lengyel et al, 2007; Gallego et al, 2008; Torres et al, 2013). Por lo que respecta a la DT2, los datos son escasos. Solamente un estudio en pacientes, publicado recientemente, describe una reducción de la expresión de hERG (el canal responsable de la corriente rectificadora tardía rápida o IKr) y un aumento de la expresión de gen NCX (responsable del intercambiador Na/Ca) por mecanismos moleculares que no se conocen aún (Ashrafi et al., 2017).

2. MODELOS ANIMALES DE DIABETES

Hay que señalar que el estudio del remodelado eléctrico cardiaco en la DT2 ha presentado tradicionalmente un problema importante: la dificultad de encontrar un modelo animal adecuado. Los modelos basados en alteraciones genéticas (ratones ob/ob; db/dd; Zucker), en dietas ricas en fructosa, o en lesiones en el páncreas provocan obesidad, síndrome metabólico, hipertensión, diabetes tipo 1, pero algunos fallan en generar hiperglucemia, otros en la resistencia a insulina característica de los pacientes con diabetes tipo 2 y otros son tan caros que su precio dificulta mucho su uso. Ha sido muy recientemente cuando han empezado a surgir modelos que, combinando una dieta rica en grasa con un daño pancreático leve, están consiguiendo provocar resistencia a insulina e hiperglucemia.

3. TRATAMIENTO DE LA DIABETES TIPO 2

Desde los años 70 se sabe que los pacientes con DT2 tienen el doble de riesgo de morir de enfermedades cardiovasculares (Kannel et al., 1974) que las personas no diabéticas. Llama la atención que más de 40 años después los fármacos disponibles han conseguido controlar bien la glucemia y sin embargo la principal causa de muerte entre los enfermos con DT2 sigue siendo cardiovascular (Preis et al 2009; Xu et al 2017). Desde hace muchos años, la metformina es el fármaco de primera elección para la diabetes. Sin embargo, su efecto en reducir la mortalidad por causas cardiovasculares está en entredicho (Zhuang et al., 2018; American Diabetes Association, 2017). Además, aunque las alternativas terapéuticas son variadas (sulfonilureas, glitazonas, los inhibidores del DPP-1, etc) solamente los inhibidores del SGLT2 han demostrado sin dudas una reducción de la mortalidad en pacientes con riesgo cardiovascular (Zhuang et al., 2018).

4. PAPEL DEL SISTEMA INMUNE EN LA FISIOPATOLOGÍA DE LA DIABETES

Por otra parte, la diabetes genera un estado inflamatorio con elevación de los niveles de IL-1β, IL-6, NF-κB, TNFα y Toll Like Receptors (TLRs) (Devaraj et al., 2008; Tu et al., 2010; El-Atat et al., 2004; Lu et al., 2013). Actualmente es evidente que la inflamación tiene un papel clave en la fisiopatología de la diabetes (Danesh et al, 2004; Scheruebel et al., 2014). Así, la ADA matiza que: "la diabetes tipo 2 está asociada con defectos de la secreción de insulina relacionados con la inflamación y el estrés metabólico" (ADA, 2017b). A esto hay que añadir que la producción de citoquinas por el miocardio tiene un efecto quimiotáctico que provoca una inflltración del corazón por macrófagos, linfocitos T y neutrófilos (Xia et al., 2009; Weisheit et al., 2014). La acumulación de células inmunes en el corazón a su vez aumenta la secreción de más citoquinas que amplifican la respuesta inflamatoria (Weisheit et al., 2014; Wang et al., 2014). En este aspecto, parece ser que las citoquinas responsables del remodelado eléctrico cardiaco producido por la DT1 son generadas principalmente por los macrófagos residentes en el propio corazón, que actúan de manera paracrina sobre los miocitos cardíacos (Monnerat et al., 2016).

a. EL CANAL DE POTASIO KV 1.3 EN EL SISTEMA INMUNE

Una diferencia funcional entre las células inflamatorias en reposo y en estado activo, de la que podemos aprovecharnos farmacológicamente, es que su activación se acompaña de un aumento de la expresión de los canales de potasio Kv1.3 (Pérez-Verdaguer et al., 2016). Los animales knockout para el canal Kv1.3 muestran resistencia a desarrollar obesidad y diabetes (Xu et al 2002). Asimismo, el bloqueo farmacológico de estos canales aumenta la sensibilidad a la insulina tanto en animales sanos como en animales con resistencia a insulina (Xu et al., 2004; Upadhyay et al., 2013; resultados preliminares propios). Todo esto demuestra que la reducción del estado inflamatorio a través del bloqueo del canal Kv1.3 tiene efecto antidiabético.

Además, el canal Kv1.3 no se expresa en los principales tejidos diana de la insulina en humanos (tejido adiposo y músculo) y, como es esperable, sus bloqueantes no tienen efecto sobre la captación de glucosa en estos tejidos *in vitro* (Straub et al., 2011). Esto apoya la hipótesis de que el efecto hipoglucemiante y normalizador de la resistencia a insulina no es directo, sino que es secundario a una reducción del grado de activación del sistema inflamatorio.

OBJETIVOS

➢ Crear y validar un modelo metabólico de diabetes tipo 2 en ratas que además reproduzca las alteraciones en el ECG observadas en los pacientes diabéticos.

> ➢ Analizar si desarrolla inflamación de grado bajo y estudiar el papel de dicha inflamación en el remodelado eléctrico cardiaco.

> ➢ Intervenir sobre el sistema inmune para modular el estado inflamatorio de la diabetes tipo 2 con el fin de comprobar si la inmunomodulación corrige las alteraciones metabólicas y el remodelado eléctrico cardiaco.

RESULTADOS Y DISCUSIÓN

1. LAS RATAS DIABETICAS REPRODUCEN LA FISIOPATOLOGÍA DE LA ENFERMEDAD

A diferencia de la diabetes tipo I, la diabetes tipo II es una enfermedad con un gran componente metabólico, en la que factores ambientales como la dieta o el estilo de vida tienen un papel muy importante en el desarrollo de la enfermedad. Por lo tanto, un modelo genético no se ajusta a la realidad de la patología. Es necesario establecer un modelo que reproduzca las alteraciones metabólicas que son inducidas por factores ambientales. Para ello y, basándonos en modelos previamente publicados (Ionut et al., 2010; Podell et al., 2017), en esta tesis se ha establecido un modelo metabólico de diabetes tipo II en el que los animales recibieron dieta rica en grasa (45% kcal provenientes de grasas) durante 6 semanas para inducirles la resistencia a la insulina. Después de 2 semanas de dieta, los animales recibieron una inyección intraperitoneal de una dosis baja de streptozotocina (35 mg/kg) que les provocó un ligero daño en las células β-pancreáticas y, por lo tanto, les indujo hiperglucemia (Figura 1).
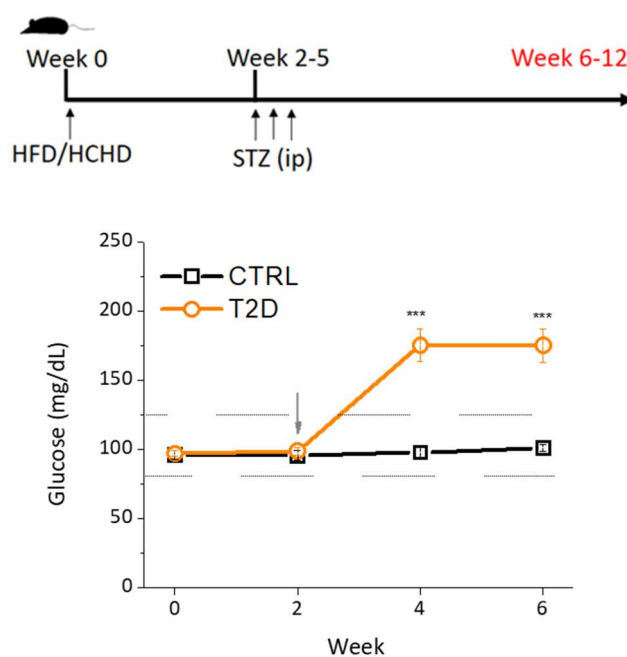
Figura 1. A) Modelo experimental de DT2. B) Glucosa plasmática a lo largo del periodo experimental.

La caracterización muestra que las ratas sometidas al modelo metabólico de inducción de diabetes tipo II reproducen las dos principales características de la patología: la hiperglucemia y la resistencia a la insulina. Después de 6 semanas, los animales que solo recibieron la dieta rica en grasa mostraron resistencia a la insulina, pero no hiperglucemia. Por otra parte, los animales que recibieron sólo la inyección de streptozotocina no desarrollaron resistencia a la insulina, pero si ligera hiperglucemia. Por el contrario, sólo los animales que recibieron dieta rica en grasa durante 6 semanas sumado a una inyección de una baja dosis de streptozotocina desarrollaron a la vez hiperglucemia y resistencia a la insulina. El modelo también presenta otras alteraciones que están relacionadas con el desarrollo de la patología como: hypertrigliceridemia o una mayor adiposidad, aunque no sobrepeso. Además, en los sueros de las ratas diabéticas también se han detectado unos niveles superiores de citoquinas proinflamatorias después de 4 semanas de diabetes. En el plasma de los animales diabéticos se detectaron mayores niveles de TNFα, IL-1β, IFNy y IL-6, entre otros. Este aumento de citoquinas proinflamatorias circulantes ha sido descrito repetidas veces en la literatura (Dandona et al., 2004; Shoelson et al., 2006) como uno de los principales causantes de la resistencia a la insulina que se observa en la diabetes tipo II (Figura 2).
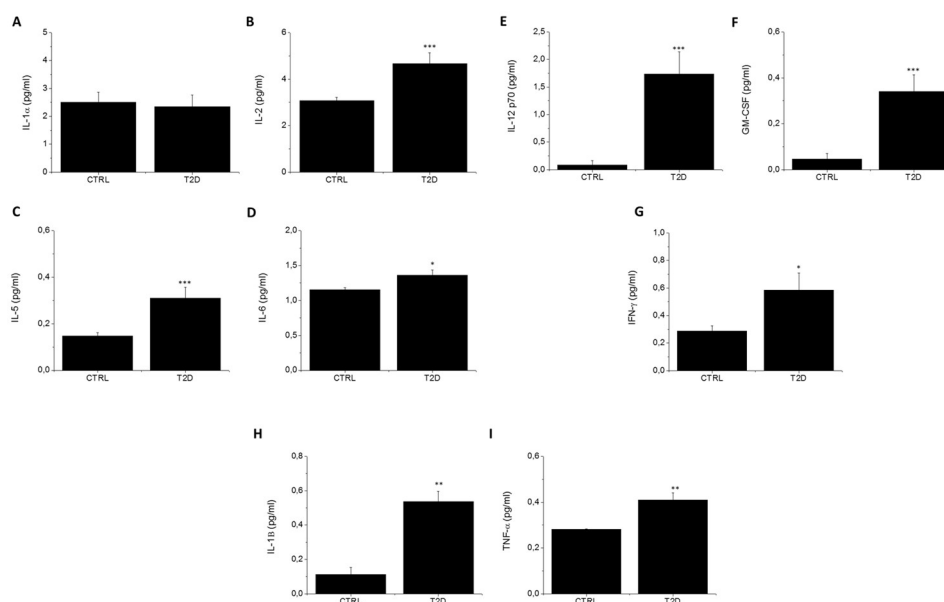
Figura 2. El modelo de diabetes tipo 2 GENERA un estado proinflamatorio de bajo grado. A-I) Los niveles plasmáticos de citocinas proinflamatorias son más altos en animales con diabetes tipo 2 que en controles de la misma edad. Esto revela un perfil inflamatorio alterado en la diabetes tipo 2. Todas las citocinas proinflamatorias circulantes analizadas muestran un aumento significativo en animales con diabetes tipo 2. Solo IL-1β no mostró ningún cambio significativo.

2.   LAS ANIMALES DIABETICOS PRESENTAN UN REMODELADO ELECTRICO CARDIACO

Pese a que se ha observado en pacientes con diabetes tipo II (Lu et al., 2017) poco se sabe de las causas de este remodelado eléctrico. Para su investigación, sería muy interesante un modelo animal en el que el corazón de las ratas con diabetes tipo II replicase el mismo remodelado eléctrico observado en los pacientes. En este sentido, los resultados electrocardiográficos de las ratas diabéticas sometidas al modelo metabólico muestran un alargamiento de la repolarización cardiaca ya que tienen los intervalos QT, QTc y Tpeak-Tend significativamente más largos que los animales diabéticos (Figura 3). Además, el potencial de acción de los animales diabéticos también se ha visto alargado respecto al de los controles. Esto deja claro que la fisiopatología de la diabetes tipo II afecta a la repolarización cardiaca.
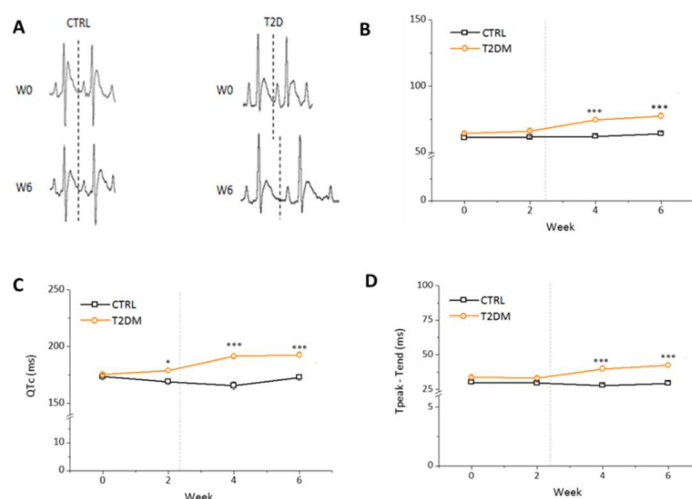
Figura 3. A) registros electrocardiográficos en una rata control y en una rata antes y 6 semanas después de la inducción de la diabetes. **B-D)** Remodelado eléctrico cardiaco inducido por la DT2 y que se observa en el ECG de las ratas diabéticas.

Por lo tanto, este modelo animal de inducción de diabetes tipo II en ratas, además de reproducir la fisiopatología de la enfermedad es el adecuado para para investigar las alteraciones de la repolarización cardiaca que se observan en la diabetes tipo II. En la actualidad, no existía ningún modelo en ratas para el estudio del remodelado eléctrico cardiaco de la DTII.

3. LA PROLONGACIÓN DE LA REPOLARIZACIÓN CARDIACA DE LAS RATAS DIABETICAS ES DEBIDA A UNA REDUCCIÓN DE LA CORRIENTE DE POTASSIO Ito A CAUSA DE UNA MENOR EXPRESIÓN DE SU CANAL

Pese a que su papel en la repolarización del potencial de acción de los cardiomiocitos humanos es menor, Ito es la principal corriente repolarizadora en las ratas. Además, en animales se ha visto reducida en animales con diabetes tipo I. Esto convierte a esta corriente iónica en la principal candidata en verse afectada por la diabetes tipo II. Como se esperaba, los cardiomiocitos provenientes de ratas diabéticas muestran una reducción sustancial de la corriente Ito. Kv4.3 es una de las dos subunidades que forman los canales que conducen la Ito. Los experimentos de western blot mostraron que los niveles de Kv4.3 eran menores en corazones de ratas con diabetes tipo II que en animales control. Por lo tanto, la reducción de la Ito es debida a una reducción de la expresión de las proteínas que forman el canal (Figura 4).
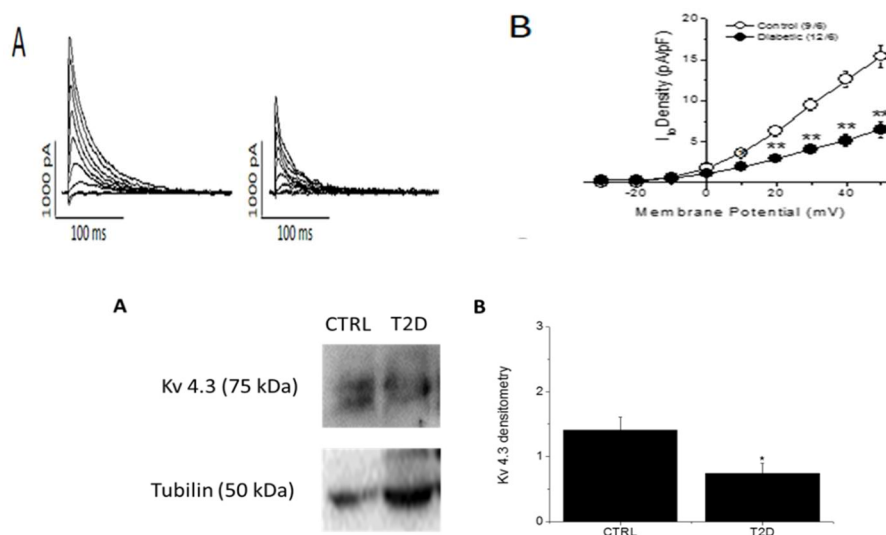
Figura 4. Panel superior: A) La DT2 reduce la amplitude de la Ito a todos los voltajes estudiados **Panel inferior: B)** La DT2 reduce la expresión del canal Kv4.3.

4. EL REMODELADO ELECTRICO CARDIACO CAUSA UNA MAYOR SUSEPTIBILIDAD A ARRITMIAS EN LAS RATAS DIABÉTICAS

Las alteraciones en la repolarización cardiaca llevan a los pacientes diabéticos a tener un mayor riesgo de sufrir arritmias letales. Por lo tanto, se sometió a los animales diabéticos a un protocolo de inducción de arritmias para comprobar que todas las alteraciones en la repolarización cardiaca vistas previamente en ellos causaban un mayor riesgo de sufrir arritmias

ventriculares severas. Los resultados mostraron que los animales diabéticos sufrieron un 50% más de taquicardias ventriculares que los animales control después del protocolo (Figura 5).
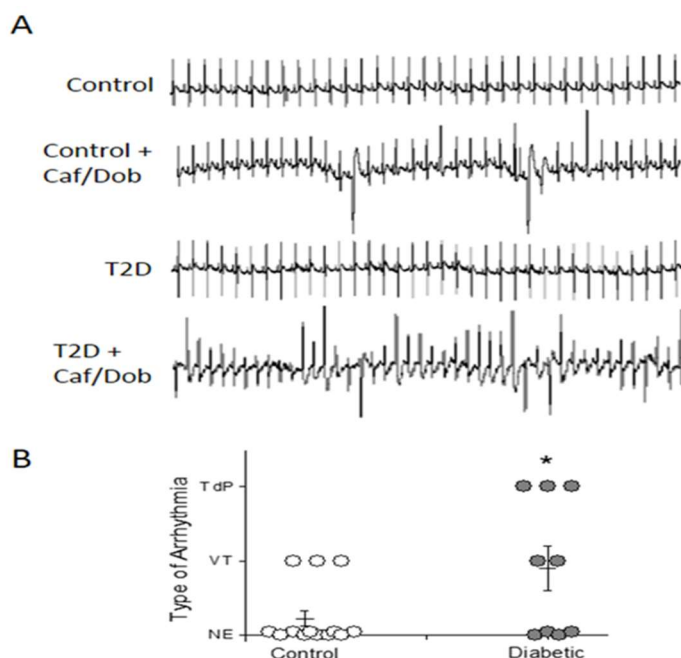
Figura 5. Susceptibilidad a las arritmias en el corazón diabético. A) Ejemplos de registros electrocardiográficos no arrítmicos y arrítmicos en animales de control y diabéticos antes y después del reto con cafeína / dobutamina (Caf / Dob). Sólo aparecen latidos ventriculares prematuros y salvas en el animal control, mientras que el animal diabético muestra episodios de torsade de pointes (TdP). **B)** Incidencia y severidad de taquicardias ventriculares y TdP en animales control y diabéticos. Cada arritmia se puntuó como No Eventos (NE) = 0; Taquicardia ventricular (VT) = 1; y Torsión de Puntas (TdP) = 2. La incidencia y gravedad de las arritmias ventriculares después de la estimulación cardíaca aumentan en animales diabéticos.

5. EL AUMENTO EN LAS CITOQUINAS CIRCULANTES PROVOCA EL REMODELADO ELECTRICO CARDIACO

En otras patologías como la enfermedad de Chagas (Santos-Cruz et al., 2017), se ha descrito que niveles altos de TNFα causan problemas en la repolarización cardiaca y arritmias (Monnerat et al., 2016). Además, se ha visto que las citoquinas y el sistema inmune también juegan un papel clave en el desarrollo del remodelado eléctrico cardiaco de la DTI. Por lo tanto, decidimos comprobar el papel de esas citoquinas como causantes de las alteraciones en la repolarización observadas en los corazones diabéticos.

Para ello, se incubaron cardiomiocitos sanos con sueros extraídos de ratas diabéticas y se observó que, después de 24h, los cardiomiocitos incubados con sueros diabéticos presentaban un alargamiento del potencial de acción que no se producía en los cardiomiocitos incubados con sueros control. Estos resultados indican que los componentes del suero diabético, con mayor presencia de citoquinas proinflamatorias, produjeron un alargamiento del potencial de acción. Además, al añadir al suero de animales diabéticos bloqueantes de los receptores de TNFα y de IL1β desparece el efecto sobre el potencial de acción (Figura 6).
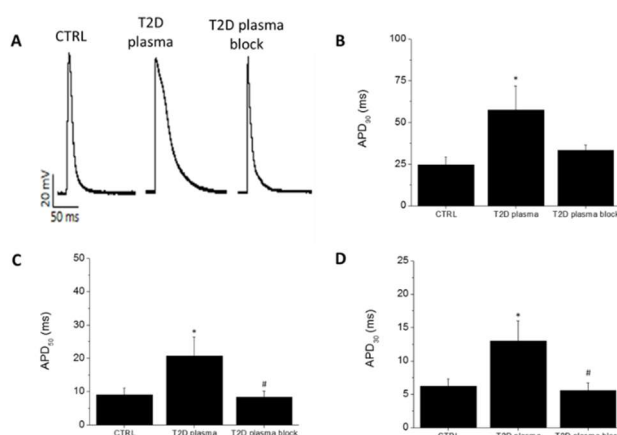
Figura 6. Papel de los mediadores circulantes en el remodelado eléctrico cardíaco. A) Potenciales de acción típicos registrados en miocitos aislados del ventrículo derecho de animales sanos incubados 24 horas en DMEM suplementado con plasma de animales sanos (Ctrl); en DMEM suplementado con plasma de animales diabéticos (T2D plasma); o DMEM suplementado con plasma extraído de animales diabéticos tipo 2 con bloqueadores del receptor de TNFα e IL-1β (T2D plasma blocked). **B-D)** El plasma diabético prolonga la duración del potencial de acción de los cardiomiocitos sanos en diferentes momentos de la repolarización. Los antagonistas de TNFα e IL-1β evitan la prolongación.

6. LA INMONOMODULACIÓN MEDIANTE LA INHIBICIÓN DEL CANAL DE POTASIO Kv1.3 MEJORA LA FISIPOATLOGÍA, EL REMODELADO ELECTRICO CARDIACO Y LA SUSCEPTIBILIDAD A ARRITMIAS PRESENTE EN LA DIABETES TIPO II

Como se ha mencionado, la inhibición del canal de potasio Kv1.3 modula al sistema inmune y tiene efectos antidabéticos. En ratones diabéticos, la inhibición del Kv1.3 controló la glucemia, redujo la resistencia a la insulina, el peso corporal y la adiposidad. Como además nuestros resultados muestran que la DTII tiene un estado inflamatorio que es uno de los causantes y perpetuanes de la enfermedad y de su remodelado eléctrico cardiaco, que causa un mayor riesgo de muerte súbita, podemos suponer que un fármaco que inhibiese el canal Kv1.3 y

produjese un efecto inmunomodulador en las ratas diabéticas podría mejorar tanto la fisiopatología de la diabetes como el remodelado eléctrico cardíaco.

Para testar esta hipótesis, tratamos a los animales diabéticos durante 4 semanas con PAP-1, un inhibidor selectivo del Kv1.3 y observamos que no desarrollaron la fisiopatología de la diabetes. Los animales tratados con PAP-1 tenían unos niveles de glucosa normales y similares a los de los animales control y a los animales diabéticos tratados con metformina. Además, mostraron beneficios que no se vieron en los animales tratados con metformina, como una mejora en la sensibilidad a la insulina (reduciendo así la resistencia a la insulina) una ligera reducción en peso y en la adiposidad, la cual se ha visto clave para el desarrollo de la diabetes.

En cuanto al remodelado eléctrico cardiaco, el PAP-1 y no la metformina redujo el alargamiento del intervalo QT y, sobre todo, la susceptibilidad a arritmias (Figura 7). Los animales diabéticos tratados con PAP-1 tienen una susceptibilidad a arritmias similar a la del control.
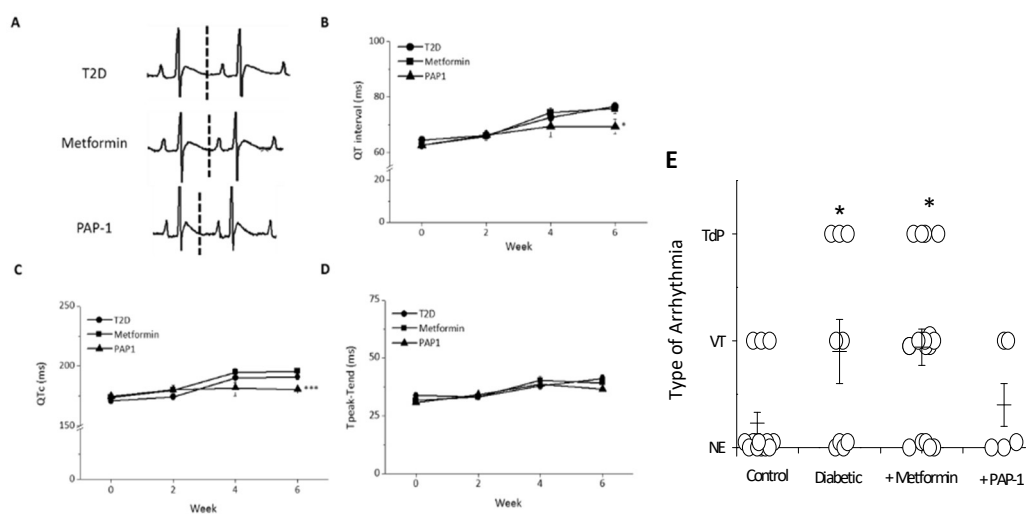
Figura 7. La inhibición del canal Kv1.3 con PAP-1 previene el remodelado eléctrico cardíaco diabético. A) Registros electrocardiográficos en animales diabéticos tipo 2, animales tratados con metformina y tratados con PAP-1. La línea de puntos muestra el final de la onda T. **B)** Repolarización cardíaca expresada como intervalo QT del ECG. **C)** Repolarización cardíaca expresada como intervalo QT corregido por frecuencia cardíaca. **D)** Dispersión transmural de la repolarización expresada como Tpeak-Tend. **E)** La inhibición de kv1.3 por pap-1 reduce la susceptibilidad a la arritmia en ratas diabéticas tipo 2.

Nuestros resultados están de acuerdo con los trabajos que proponen al canal Kv1.3 como posible diana terapéutica para el tratamiento de la diabetes. Asimismo, refuerzan la idea de que el estado inflamatorio es el responsable de las alteraciones eléctricas del corazón diabético.

7. LA INMONOMODULACIÓN INDUCIDA POR LA INHIBICIÓN DEL CANAL DE POTASIO Kv1.3 REDUCE LOS NIVELES CIRCULANTES DE CITOQUINAS PROINFLAMATORIAS

Finalmente, para confirmar que el efecto protector frente a arritmias que proporciona la inhibición del canal Kv1.3 es debido a una mejora del estado inflamatorio, medimos los niveles de citoquinas en animales diabéticos tratados con PAP-1. Como esperábamos, los niveles del TNFα y la IL-1β eran más bajos en estos animales que en los animales control y que en los diabéticos tratados con metformina. Por lo tanto, podemos suponer que la cardioprotección y la mejora del estado metabólico observadas en los animales diabéticos son debidas al efecto inmunomodulador de la inhibición del Kv1.3 mediante PAP-1 (Figura 8).
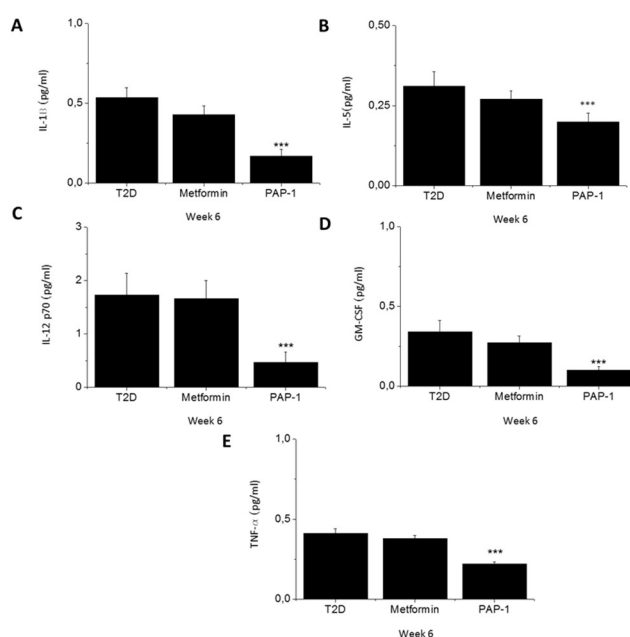
Figura 8. La inhibición farmacológica de Kv1.3, y no la metformina, reduce los niveles de citocinas proinflamatorias en animales con diabetes tipo 2. A-E) Niveles plasmáticos de citocinas proinflamatorias que encontramos más altos en animales con diabetes tipo 2 y se reducen por la acción del tratamiento con PAP-1. Los niveles del resto de citoquinas estudiadas no fueron modificados ni por la metformina ni por el PAP-1.

CONCLUSIONES

1. En ratas, una dieta rica en grasa mantenida durante dos semanas, seguida de una inyección intraperitoneal de una dosis baja de estreptozotocina, provoca una elevación de la glucemia y resistencia a la insulina, características de la diabetes tipo 2. El modelo provoca también una elevación de la grasa abdominal y dislipemia.

2. El modelo metabólico de diabetes tipo 2 reproduce las alteraciones en el electrocardiograma basal, como bradicardia y alargamiento del intervalo QT, y aumenta la susceptibilidad a las arritmias cardiacas.

3. Los animales con diabetes tipo 2 de origen metabólico sufren una inflamación de bajo grado, caracterizada por un aumento de los niveles de citoquinas plasmáticas.

4. La elevación de los niveles circulantes de citoquinas, especialmente IL-1β y TNFα, son responsables del remodelado eléctrico cardiaco.

5. La inhibición del sistema inflamatorio, mediante el bloqueo farmacológico del canal Kv1.3, mejora la fisiopatología de la diabetes tipo 2 y revierte el remodelado eléctrico cardiaco, reduciendo la propensión a las arritmias cardiacas.

ABSTRACT

Background: Diabetic patients have prolonged cardiac repolarization and a higher risk of arrhythmia. Besides, diabetes activates the innate immune system, resulting in higher levels of plasmatic proinflammatory cytokines such as TNFα and IL-1β, which are described to prolong ventricular repolarization. **Methods:** Most of the current knowledge on diabetic cardiac electrical remodeling derives from type 1 diabetic animals. Here, we characterize a metabolic model of type 2 diabetes with prolonged cardiac repolarization. Sprague-Dawley rats were fed on high fat diet (45% Kcal from fat) for 6 weeks, and a low dose of streptozotozin was intraperitoneally injected at week 2. Body weight and fasting blood glucose were measured and electrocardiograms to conscious animals were recorded weekly. Plasmatic lipid profile, insulin, cytokines, and arrhythmia susceptibility were determined at the end of the experimental period. The transient outward K^+ current and action potentials were recorded in isolated ventricular myocytes by patch-clamp. Animals were also treated with PAP-1, an inhibitor of Kv1.3 channel that has an immunomodulatory role. **Results:** Type 2 diabetic animals showed insulin resistance, hyperglycemia and higher levels of plasma cholesterol, triglycerides, TNFα and IL-1β than controls. They also developed bradycardia and prolonged QTc-interval duration that resulted in increased susceptibility to severe ventricular tachycardia under cardiac challenge. Action potential duration (APD) was prolonged in control cardiomyocytes incubated 24h with plasma isolated from diabetic rats. However, adding TNFα and IL-1β receptor blockers to the serum of diabetic animals prevented the increased APD. Inhibition of Kv1.3 reduced the circulating cytokines including TNFα and IL-1β. It had an antidiabetic effect improving insulin resistance and controlling the glucose while reduced the prolongation of QTc and the susceptibility to arrhythmia in the diabetic rats. **Conclusions:** The elevation of the circulating levels of TNFα and IL-1β are responsible for impaired ventricular repolarization and higher susceptibility to cardiac arrhythmia in our metabolic model of type 2 diabetes. Thus, immunomodulation by inhibition of Kv1.3 has antidiabetic effects while improving the electrical alterations of the diabetic heart. These results make the immune system a potential target for the treatment of diabetes and its associated alterations.

INTRODUCTION

INTRODUCTION

1. DIABETES MELLITUS

Diabetes mellitus is a group of metabolic disorders, whose first clinical symptom is high blood glucose levels, and that leads over time to serious clinical complications in the heart, blood vessels, eyes, kidneys, and nerves. The disease associates with a great socio-sanitary cost that is increasing year after year. In the last decades, the prevalence of diabetes mellitus among adults has been steadily rising and has become a major public health problem worldwide. The number of people with diabetes rose from 108 million in 1980 to 422 million in 2014, and this tendency is not expected to change in the next years. Current global estimates indicate that diabetes prevalence is set to escalate to 625 million by the year 2040. Rising prevalence caused a 5% increase in premature mortality from diabetes between 2000 and 2016. Nowadays, around 1.6 million deaths are directly attributed to diabetes worldwide each year, and another 2.2 million deaths were attributable to high blood glucose in 2012 (WHO 2020, figure 1).

Moreover, treatment of diabetes generates a great associated expenditure for healthcare systems worldwide. The estimated global direct health expenditure on diabetes in 2019 was USD 760 billion and is expected to grow to USD 825 billion by 2030 and USD 845 billion by 2045.

Characteristic hyperglycemia of diabetes occurs either when the pancreas does not produce enough insulin or when the body cannot effectively use the insulin it produces. This feature is used to establish the main two types of diabetes. Type 1 diabetes (T1D), the less common form, is caused by insufficient or no insulin production. Type 2 diabetes (T2D) accounts for more than 90% of the cases and starts with insulin resistance that later progresses towards various degrees of β-cell dysfunction, and many patients need exogenous insulin.
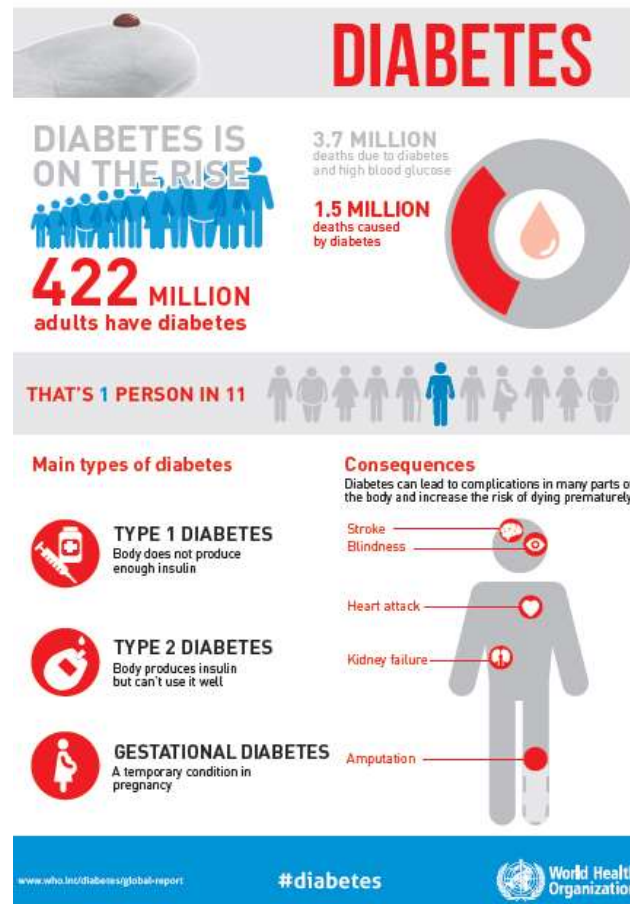
Figure 1. Diabetes impact on the public health. Adapted from World Health Organization (WHO) report (2018).

2. TYPE 2 DIABETES MELLITUS

Type 2 diabetes is characterised by high blood glucose levels associated to a relative insulin deficiency caused by pancreatic β-cell dysfunction and insulin resistance (IR) in target organs.

2.1. EPIDEMIOLOGY OF THE DISEASE

As cited before, 415 million people live with diabetes worldwide, and an estimated 193 million people have undiagnosed diabetes. Type 2 diabetes accounts for more than 90% of patients with diabetes and leads to microvascular and macrovascular complications that cause profound psychological and physical distress to both patients

and healthcare professionals and put an enormous burden on healthcare systems. Despite increasing knowledge regarding risk factors for type 2 diabetes and evidence for successful prevention programmes, the incidence and prevalence of the disease continues to rise globally.
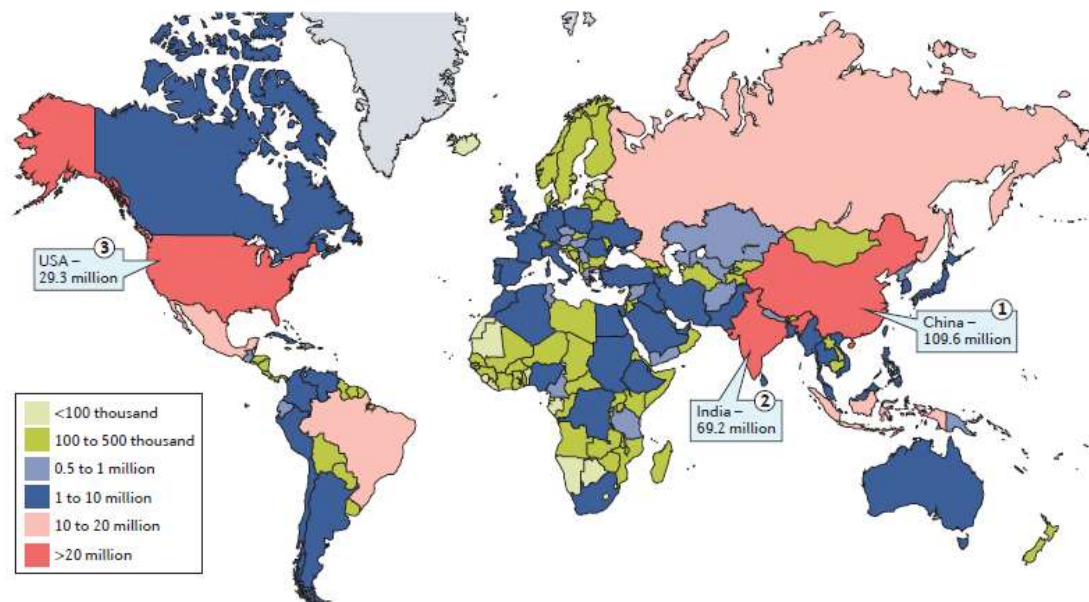
Figure 2. Type 2 diabetes prevalence worldwide. Adapted from WHO report (2016).

Between 1980 and 2014, the global rise in obesity, sedentary lifestyles, and an ageing population have quadrupled the incidence and prevalence of type 2 diabetes. However, intensive lifestyle modification, pharmacotherapy, or both can reverse or delay development of type 2 diabetes. Even then, type 2 diabetes is the sixth leading cause of disability in 2015, and places considerable socioeconomic pressures on the individual and overwhelming costs to global health economies, estimated at USD 825 billion (figure 2). Patients with T2D have a 15% increased risk of all-cause mortality. Furthermore, cardiovascular disease (CVD) is the greatest cause of mortality associated according to geographical region, with more than 80% of patients living in low-to-middle-income countries, but the overall trend is an increase in diabetes prevalence in every country since 1980 [1] (figure 2).

2.2. TYPE 2 DIABETES RISK FACTORS

Several factors significantly increase the risk of type 2 diabetes. Many of these factors are associated to a sedentary lifestyle and unhealthy diet but can also be related with genetic factors or smoking habits among others (figure 3).

Figure 3. Type 2 diabetes risk factors. Adapted from WHO report (2018).

A. GENETIC FACTORS

T2D risk factors include a complex combination of genetic, metabolic, and environmental factors that interact with one another contributing to its prevalence. Although individual predisposition to T2D due to non-modifiable risk factors (ethnicity and family history/genetic predisposition) has a strong genetic basis, evidence from epidemiological studies suggests that many cases of T2D can be prevented by improving the main modifiable risk factors (obesity, low physical activity and an unhealthy diet).

Globally, the incidence and prevalence of T2D are found to vary widely depending on ethnicity and geographical region. However, no clear reasons have been found, and contributing factors such as modern lifestyle factors socioeconomic and direct genetic propensity or gene environmental interactions have been postulated [2].

Although is not completely clear, genetic predisposition plays a part in the risk of developing T2D. Over the past decade, several T2D genome-wide association studies have shown the complex polygenic nature of T2D in which most of these loci increase T2D risk through primary effects on insulin secretion, and a minority act through reducing insulin action. Since these studies demonstrated that T2D is highly polygenic, and additional association studies are needed to identify most loci. The diversity of phenotypes and missing heritability of type 2 diabetes patients is due to the impact of a given genetic variant can be modulated by the environmental factors (and vice versa) as evidenced by both observational studies and clinical trials [3].

B. SEDENTARY LIFESTYLE AND UNHEALTHY DIET

A sedentary lifestyle is another risk factor for T2D. For instance, walking 2-3 h a week or at least 40 min a week showed a 34% and 56% reduction, respectively, of developing T2D in participants. There are primary benefits of physical activity on the delay of T2D onset. First, the contraction of skeletal muscle cells induces an increase in blood flow into the muscle, enhancing glucose uptake from plasma as well as moderate-intensity exercise has been shown to improve glucose uptake by 40% [4]. Moreover, physical activity reduces the notorious intra-abdominal fat, which is a known risk factor that promotes IR [4]. Therefore, physical activity improves glucose uptake and insulin sensitivity, but it can also improve or even reverse inflammation and oxidative stress, which are T2D predisposing factors [5].

Many prospective studies have found relations between fat intake and subsequent risk of developing T2D. Therefore, unhealthy diet, in terms of food intake and composition, is an important risk factor of T2D. For instance, elevated fatty acid levels during fasting are associated with decreased glucose uptake by skeletal muscle. Then, a

high intake of some food such as red meat, sweets and fried foods, also contributes to the increased risk of insulin resistance and T2D [6].

C. OBESITY AND OVERWEIGHT

Lifestyle including sedentariness and unhealthy diet are one of the main causes that lead to obesity, defined as an overweight caused by a body fat accumulation. People is considered obese when the body-mass index (BMI) is over 30 kg/m^2. However, obesity by itself is the strongest risk factor for T2D, independently of diet and lifestyle. There is an inverse linear relationship between BMI and the age at diagnosis of T2D. Obesity is also associated with metabolic abnormalities resulting in insulin resistance, the main pathophysiology associated to T2D. The exact mechanisms by which obesity induces T2D and IR remain to be elucidated. However, numerous factors have shown a significant role in the development of this pathological process such as the elevated circulating free fatty acids (FFA). Most studies highlight the important role of FFAs on peripheral glucose homeostasis and insulin sensitivity. During fasting, lipids need to be often mobilized to provide energy. For this purpose, the triglycerides (TG) stores are hydrolyzed and relieved from adipocyte and are carried by plasma albumin to provide energy for tissues during fasting. The hydrolyzed and circulating TG are called free fatty acids (FFA), which are critical oxidative substrates [7, 8].

D. SMOKING HABITS

A meta-analysis found a dose-response relationship between the number of cigarettes smoked and risk of T2D, and current smokers had a 45% higher risk of T2D than non-smokers. Smokers are more likely to have central fat accumulation than non-smokers, and smoking is known to induce insulin resistance and compensatory insulin-secretion responses, which could explain the increased risk of T2D in people who smoke [9].

3. TYPE 2 DIABETES PATHOPHYSIOLOGY

The pathophysiology of the Type 2 diabetes starts with insulin resistance. Previously mentioned factors such as diet or sedentary lifestyle may lead to insulin resistance. To maintain normal glucose levels and avoid that the impaired functionality of insulin causes hyperglycemia, the pancreas secretes more insulin causing hyperinsulinemia that sustained in time produces a beta cell failure, which creates an impaired insulin secretion and subsequent hyperglycemia and T2D (figure 4). Besides, insulin resistance importantly contributes to the development of other conditions such as dyslipidemia, hypertension and atherosclerosis.
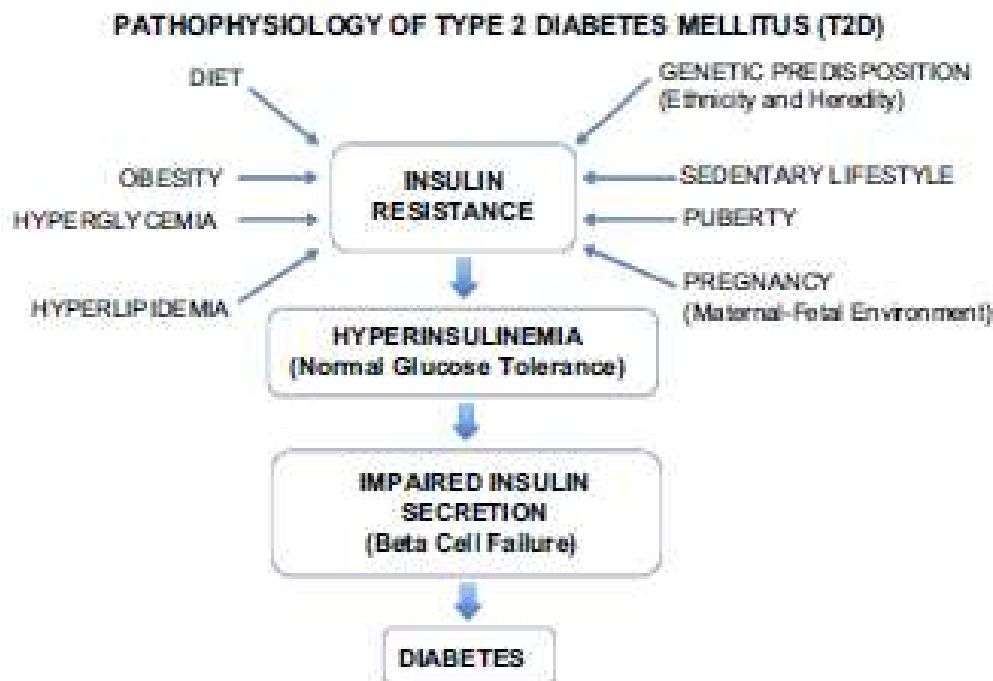
Figure 4. **T2D pathophysiology development since insulin resistance to B-cell failure leads to hyperglycemia and diabetes.** Adapted from Significance of Organ Crosstalk in Insulin Resistance and Type 2 Diabetes. Harvard Medical School. Bhatt, S. (2010).

Regarding the pathophysiology of the disease, a malfunctioning of the feedback loop that causes insulin secretion results in hyperglycemia. This feedback loop relies on crosstalk between the β-cell and the insulin sensitive tissues (figure 5A). Insulin secretion involves a sequence of events in β-cells that lead to fusion of secretory granules with the plasma membrane. Insulin is secreted primarily in response to glucose, while other

nutrients such as free fatty acids and amino acids can augment glucose-induced insulin secretion. In a physiological situation, insulin released in response to β-cell stimulation mediates the uptake of circulating glucose by insulin-sensitive tissues (figure 5A). When insulin resistance is present, the β-cell increases its insulin output to maintain normal glucose tolerance (figure 5B). However, when the β-cell is incapable of this task, the result is an elevation in plasma glucose (figure 5C). Thus, the reduction degree in the ability of β-cell function to produce insulin determines the degree of elevation in plasma glucose. In early stages of type 2 diabetes, insulin resistance is well established, but glucose level remains normal because of a compensatory increase in insulin secretion [10, 11].
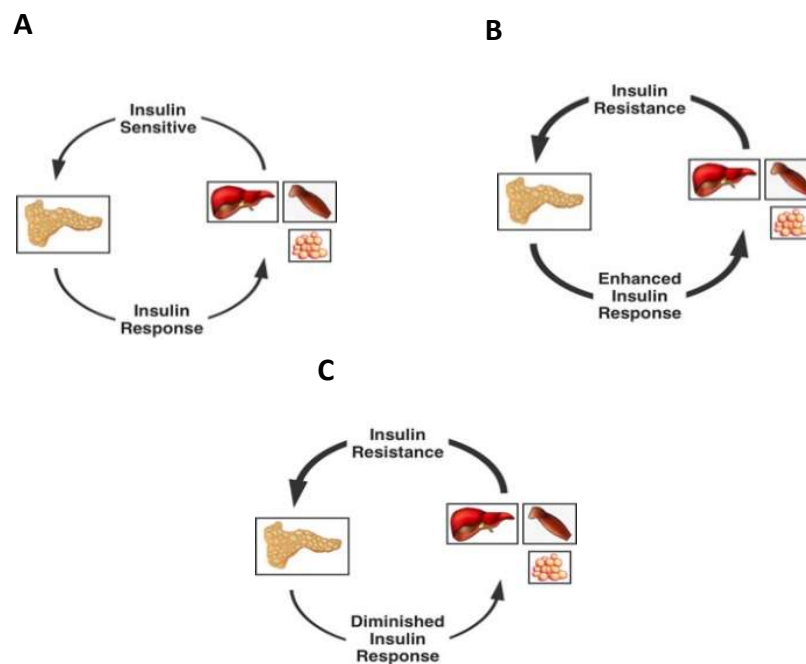
Figure 5. Steps of the pathophysiology of type 2 diabetes. A) Correct balance between insulin sensitivity and insulin response. **B)** Insulin resistance leads to β-cell to enhance insulin secretion to keep normal levels of blood glucose. **C)** Sustained insulin resistance causes β-cell damage that leads to decrease of insulin secretion and subsequent hypeglycemia. Adapted from Inflammation and metabolic disorders. *Nature Review*. Hotamisligil GS. (2006).

3.1. INSULIN RESISTANCE

Insulin, a 51-amino acid peptide, is the key hormone responsible for maintaining glucose homeostasis. Insulin resistance is typically defined as decreased sensitivity

and/or responsiveness to metabolic actions of insulin that promote glucose disposal. IR refers to a decrease in the metabolic response of insulin-responsive cells to insulin or, at a systemic level, an impaired/lower response to circulating insulin by blood glucose levels. Unfortunately, the little understanding of insulin resistance has restricted T2D treatment. However, it is known that some altered conditions sustained in time can induce and maintain insulin resistance and subsequent T2D [12] (figure 6).
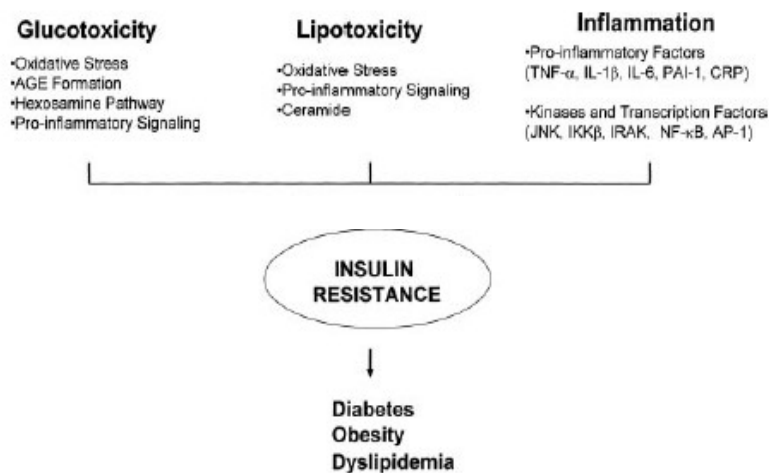
Figure 6. **Pathological factors involved in the feedback development of insulin resistance and T2D**. Adapted from Reciprocal Relationships between Insulin Resistance and Endothelial Dysfunction. *Circulation*. Kim, J. (2006).

A. CANONICAL INSULIN SIGNALING PATHWAY

Glucose homeostasis is maintained by coordinating the production of glucose in the liver through the pathways of glycogenolysis and gluconeogenesis in times of fasting with the disposal of glucose into skeletal muscle through glycogen synthesis and glucose metabolism and to a much lesser extent adipose tissue during feeding.

The hormone insulin, secreted by the beta cells of the pancreas in times of nutrient uptake, inhibits hepatic glucose output while enhancing glucose uptake into muscle and adipose tissue. Glucose is released through the glucose transporter GLUT2 in liver, while the insulin-sensitive GLUT4 mediates glucose uptake in muscle and fat [13]. Akt protein kinase is required for insulin regulation of the pathways that control systemic glucose

homeostasis, including glucose transport in adipocytes and muscle, inhibition of hepatic gluconeogenesis as well as cell autonomous activation of hepatic lipogenesis [14, 15].

Biological actions of insulin are initiated by the binding of insulin to its cell surface receptor, a ligand-activated tyrosine kinase. This binding activates its intrinsic tyrosine kinase activity that phosphorylates Insulin Receptor Substrate (IRS) proteins on tyrosine residues. This serve as anchoring sites (the p85 regulatory subunits of p85/p110) for PI-3 kinase at the cell membrane. There, it generates the formation of a phospholipid that facilitates recruitment and interaction between the protein kinases PDK1 and Akt. Finally, this interaction leads to phosphorylation (on threonine 308) and activation of the Akt. As summary, figure 7 represents the canonical signaling cascade of insulin [12].
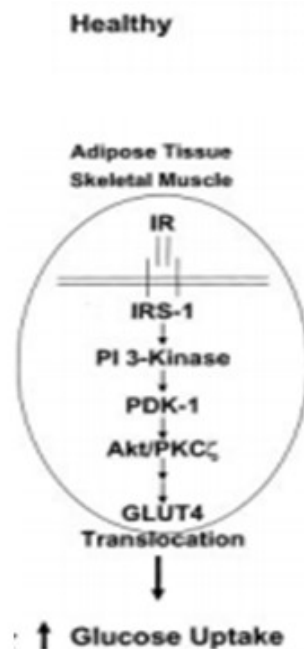
Figure 7. **Canonical peripheral insulin signaling in healthy tissues**. Adapted from Reciprocal Relationships between Insulin Resistance and Endothelial Dysfunction. *Circulation*. Kim, J. (2006).

B. PERIPHERAL INSULIN RESISTANCE

Three broad categories of insulin resistance or insulin-deficient conditions are mainly described in literature: diminished insulin secretion by β-cells as happens in developed stages of type 2 diabetes; insulin antagonists in the plasma, due either to counter-regulatory hormones or non-hormonal bodies that impair insulin receptors or signaling

like cortisol or growth hormone that are elevated in some syndromes such as cushing's disease or acromegaly; and impaired insulin response in extra-pancreatic insulin-sensitive organs like skeletal muscle, adipose tissue and liver. A defective action of insulin in these tissues often precedes the development of systemic IR, thus progressively leading to T2D. Peripheral insulin resistance is often caused by the desensitization of the insulin receptor that is produced by the hyperphosphorylation in the cell-signaling cascade.
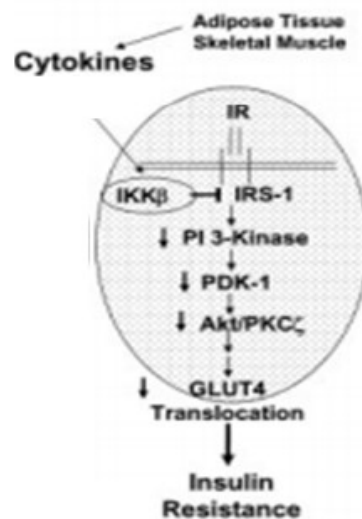
Figure 8. **Molecular mechanism that disrupts Insulin Receptor altering the insulin signaling and causing insulin resistance.** Adapted from Reciprocal Relationships between Insulin Resistance and Endothelial Dysfunction. *Circulation*. Kim, J. (2006).

Most common insulin resistance alterations include a decrease in the number of insulin receptors and of their catalytic activity; an increased Ser/Thr phosphorylation state in insulin receptor and IRS; an increase in Tyr phosphatase activity, which participate in receptor and IRS dephosphorylation; a decrease in PI3K and Akt kinases activity and defects in GLUT-4 expression and function. These alterations reduce glucose uptake in muscular and adipose tissues and promote alterations at the metabolic level. An essential factor contributing to insulin resistance is Ser/Thr hyperphosphorylation of IRS proteins. IRS hyperphosphorylation decreases its phosphorylation in Tyr and reduces its interaction with PI3K, thus altering Akt kinase phosphorylation and activation. Additionally, IRS phosphorylation on Ser/Thr residues has been reported to accelerate its degradation. Different agents, such as pro-inflammatory cytokines, free fatty acids

(FFA), and hyperinsulinemia, increase the activity of kinases, such as several IKKβ, PKC isoforms, JNK stress kinase, mTOR, 70-kDa S6 ribosomal protein kinase, PKA and MAPK, which phosphorylate IRS [12, 16, 17] (figure 8).

I. SKELETAL MUSCLE INSULIN RESISTANCE

Skeletal muscle insulin resistance is the most important extra-pancreatic factor in the development of T2D. Under physiological conditions, insulin stimulates muscle glycogen synthesis by enhancing glucose uptake from plasma. Upon insulin binding to insulin receptor in muscle cells, GLUT4 translocates from intracellular compartments to the plasma membrane. This process allows glucose uptake and reduces circulating glucose levels.

Genetics may be a reason for the skeletal muscle insulin resistance. Mutations that affect phosphorylation sites, expression of insulin receptor or GLUT4, as well as defects in either upstream or downstream signaling pathway would reduce glucose intake into the muscle resulting in a hyperglycaemic state. However, environmental factors usually play an important role in glucose uptake by muscle. For instance, elevated circulating free fatty acids_due to an inappropriate diet_increase immune cell infiltration and secretion of proinflammatory molecules in intermyocellular and perimuscular adipose tissue, and leads to skeletal muscle inflammation, which cause impaired myocyte metabolism, and contributes to IR via paracrine effects [12, 18, 19] (figure 10).

II. ADIPOSE TISSUE INSULIN RESISTANCE

Adipose tissue is a metabolically dynamic tissue capable of synthesizing a wide range of biologically active compounds that regulate metabolic homeostasis at a systemic level. In fact, adipose tissue participates in a broad range of biological processes involving, among others, immunity, appetite regulation, body weight homeostasis and glucose and lipid metabolism.

Insulin acts on adipose tissue in two different ways: stimulating glucose uptake and triglyceride synthesis; and suppressing triglyceride hydrolysis and inducing the uptake of FFA and glycerol from circulation. In the fed state, GLUT4 allows uptake of glucose

from the bloodstream into adipocytes, where forms triacylglycerol (TGA) that is stored in lipid droplets. To the contrary, during metabolic stress, lipid stores, the TGA droplets of the adipocyte, are depleted, resulting in the liberation of FFA that are used as an energy source in other tissues. Accumulation of visceral fat has been proposed as a risk factor for T2D. High-fat diet and obesity lead to adipose tissue dysfunction and inflammation due to the endoplasmic reticulum stress effect of FFA in the adipocytes [20, 21].

The endoplasmic reticulum (ER) is a large membrane-enclosed cellular organelle, found in all eukaryotes, that is the site of folding of membrane and secreted proteins, synthesis of lipids and sterols, and storage of free calcium. Physiologic stresses, such as increased secretory load, or pathological stresses, such as the presence of mutated proteins that cannot properly fold in the ER, can lead to an imbalance between the demand for protein folding and the capacity of the ER for protein folding, thereby causing ER stress, a state that can regulate processes like cell survival and cell death. Chronic exposure to high FFAs concentrations causes ER stress, which may contribute to a cell dysfunction and ultimately cell apoptosis. Growing evidence suggests that ER stress signaling has been associated with T2D and many other human diseases [22].

Furthermore, this metabolic stress is followed by the release of cytokines by the adipocyte such as TNFα, IL-1β or IL-6 among others capable of causing local paracrine effects (i.e. on macrophages), and more distal endocrine effects such as muscle and liver insulin resistance. Adipose tissue-resident immune cells like macrophages contribute to increased circulating levels of TNFα and IL-1β and IL-6 (figure 9). The increase in circulating proinflammatory molecules facilitates the emergence of a chronic state of low-grade systemic inflammation, also known as metabolic inflammation. This chronic inflammatory state is considered a key part in the pathogenesis of insulin resistance and T2D [23-25].

This low-grade inflammatory status leads to an adipose tissue-insulin resistance. It can cause impaired suppression of lipolysis, impaired glucose uptake, and enhanced FFA release into plasma even in the presence of high insulin levels. Among the signalling elements affected by low-grade inflammation and subsequent adipose-insulin resistance, Akt activation impairs GLUT4 translocation to the membrane and promotes

the activation of lipolytic enzymes that aggravate hyperglycemia. Moreover, all this alterations in the adipose tissue, besides to be related with insulin resistance, are also associated with glucose intolerance and elevated circulating FFA in other tissues such as muscle or liver (figure 10). In the case of the liver, FFA accumulation results in impaired insulin signaling that promotes hepatic gluconeogenesis and impairs the glucose-stimulated insulin response, inducing T2D development [12, 26].
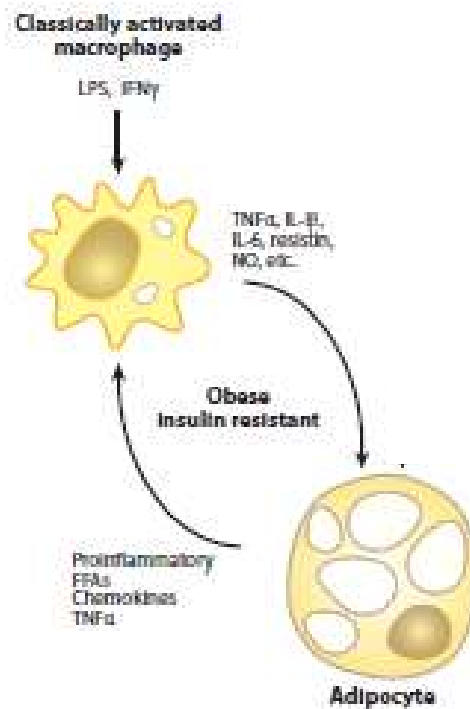
Figure 9. **Adipose tissue and inflammation lead to insulin resistance.** Adapted from Macrophages, Inflammation, and Insulin Resistance. *Annu. Rev. Physiol.* Olefsky, JM (2010).

III. LIVER INSULIN RESISTANCE

In the liver, insulin does not only regulate glucose production/utilization but also affects lipid metabolism. In physiological states, the combined action of glucagon and insulin allows the precise regulation of hepatic glucose output. While glucagon induces hepatic glucose production, insulin acts as a potent inhibitor of glucose production when its concentration in the blood is elevated. The effect of insulin on hepatic glucose production is due to both direct and indirect mechanisms. However, the relative importance of each one remains unclear. In addition, insulin promotes glucose storage as glycogen and inhibits glucose synthesis and hepatic glucose output [27].

Furthermore, in the liver, insulin resistance impairs glycogen synthesis, fails to suppress glucose production, enhances lipogenesis, and increases the synthesis of proinflammatory proteins. Liver insulin resistance is strongly correlated with the proinflammatory status induced by adipocytes (figure 10). The abnormal production of cytokines, combined with conditions such as oxidative stress, lead to an inflammatory state responsible for altered insulin response by the liver. Similar to the case in other insulin-sensitive tissues, in liver insulin resistance, physiologic levels of circulating insulin are also insufficient to elicit the appropriate insulin response in hepatic cells [28].
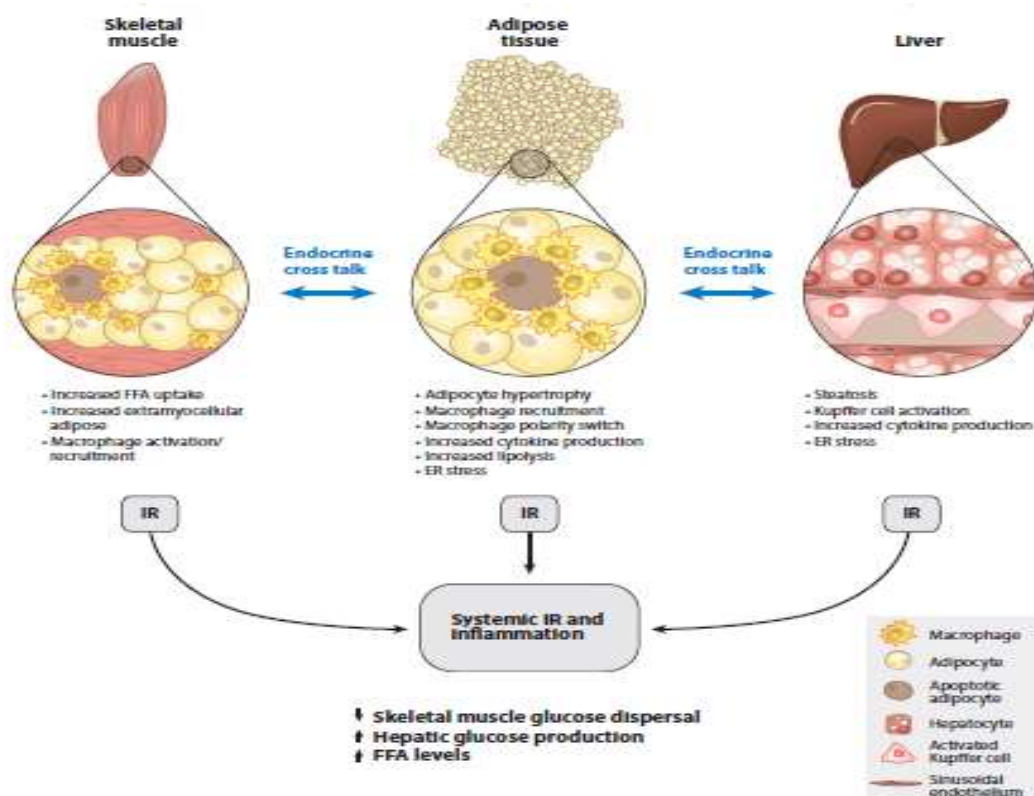
Figure 10. **Pathophysiology of peripheral insulin resistance and inflammation.** Adapted from Macrophages, Inflammation, and Insulin Resistance. *Annu. Rev. Physiol.* Olefsky, JM (2010).

On the other hand, increased plasma FFA concentrations cause hepatic insulin resistance, impair insulin signalling, and stimulate hepatic glucose production by driving both hepatic gluconeogenesis and glycogenolysis. Furthermore, adaptation of FFA-induced hepatic insulin resistance involves an increase in insulin secretion but also a reduction of hepatic insulin clearance that results in peripheral hyperinsulinemia. Liver insulin resistance is one of the causes of T2D hyperglycemia. Fasting hyperglycemia in T2D is closely correlated to the rate of endogenous glucose production, of which more

than 90% corresponds to glucose production by the liver. The increase in endogenous glucose production in T2D is believed to be primarily due to excessive rates of hepatic gluconeogenesis, whereas glycogenolysis autoregulation is better preserved [7, 29].

3.2. β-CELL DYSFUNCTION

β-cells are responsible for insulin production. Insulin release is primarily triggered by a response to high glucose concentrations. It is known that some other factors can also induce insulin release such as amino acids, fatty acids, and hormones. Under previously described circumstances like dyslipidemia, hyperglycemia, FFA excess, insulin resistance or low-grade inflammation, β-cells are subject to toxic pressures including inflammation, inflammatory stress, ER stress, metabolic/oxidative stress, amyloid stress, with the potential of ultimately leading to a loss of islet integrity [30].

Lipotoxicity, glucotoxicity and glucolipotoxicity occurring in T2D, induce metabolic and oxidative stress that leads to β-cell damage. An excess of FFAs and hyperglycemia lead to β-cell dysfunction by inducing ER stress through the activation of the apoptotic unfolded protein response (UPR) pathways. This ER stress generates proapoptotic signals and induce interleukin IL-1 release that recruits macrophages and enhances local islet inflammation [31]. Multiple studies have shown that fatty acids can induce β-cell death by apoptosis and that this effect is potentiated by glucose. Therefore, it is conceivable that the combination of elevated FFA and chronic hyperglycemia synergize to create a milieu conducive to B-cell dysfunction and failure [31].

Moreover, insulin secretion must be finely regulated to accurately meet metabolic demand. For that reason, proper islet integrity must be conserved to allow β-cells to respond to metabolic needs. Under T2D pathophysiological condition, the ER stress and local islet inflammation can ultimately lead to disruption of islet integrity/organization, impairing optimal cell-to-cell communication within pancreatic islets, contributing to poor regulation of insulin and glucagon release, and ultimately exacerbating the hyperglycemia. Thus, defects in the synthesis of any insulin precursors, or insulin itself, as well as disruption of the secretion mechanism, can lead to insulin secretory dysfunction, the primary driver of β-cell failure, and a foundation of T2D [32].

Finally, we can summarize the process as following: the pancreatic islets respond to insulin resistance by enhancing their cell mass and insulin secretory activity. However, when the functional expansion of islet β-cells fails to compensate, insulin deficiency and ultimately T2D develop.

3.3. HYPERGLYCEMIA

In T2D patients, hyperglycemia is a symptom that appears after insulin resistance due to overload of β-cells, caused by the compensation effort for maintaining euglycemia under insulin resistance, which leads to dysfunction of pancreas β-cells. Although β-cells have an incredible ability to compensate and increase insulin production, the combination of obesity, chronic hyperglycemia, and worsening insulin resistance ultimately lead to b-cell apoptosis. Hyperglycemia is particularly toxic for the beta cells. Glucotoxicity induced by prolonged hyperglycemia causes b-cell dysfunction and loss of β-cell mass. The proposed mechanism is that chronically high blood glucose might increase glucose metabolism through oxidative phosphorylation and increase production of ROS (reactive oxygen species). This could overload the mitochondria, ultimately causing β-cell apoptosis [33-36].

3.4. DYSLIPIDEMIA

Dyslipidemia, characterized by high circulating free fatty acids is one of the major abnormalities in the lipid profile of patients with type 2 diabetes. The hallmark of diabetic dyslipidemia is a characteristic profile consisting of elevated triglycerides and low-density lipoprotein (LDL), and reduced high-density lipoprotein (HDL) levels. Although the pathophysiology of dyslipidemia in T2D is not completely characterized, concomitant—hyperglycemia, insulin resistance, abnormalities in adipocytes and cytokines, are involved. Under physiological conditions, lipoprotein production, metabolism, and clearance are efficient processes. However, insulin resistance associated to T2D is among the most important metabolic derangements in these process and they give rise to impaired metabolism and clearance of lipoproteins [37, 38].

Peripheral insulin resistance leads to diabetic dyslipidemia, whose dominant feature is the increased production rate of VLDL by the liver. Moreover, FFAs derived from adipose tissue are also a major source of liver TGs and very low-density lipoproteins. As mentioned above, T2D is characterized by increased production of FFAs by adipose tissue. Therefore, an increase in TG lipolysis in adipose tissue and FFA influx serves as another source of lipid to the liver, and ultimately causes the dysfunction of insulin handling by the liver and hyperglycemia. Additionally, hepatic insulin resistance also contributes to impaired clearance of TG by the liver. On the other hand, it has been observed that the deleterious effects of lipids are observed predominantly in the presence of high glucose, and toxic actions of FFA on tissues become apparent in the context of hyperglycemia [39-41].

3.5. INFLAMMATION

Inflammation plays a critical role in the development of type 2 diabetes. It is now commonly accepted that diabetes is associated with low-grade inflammation that is characterized by abnormal cytokine production, increased acute-phase reactants, and activation of a network of inflammatory signaling pathways. Experimental, epidemiological and clinical evidence produced during the last years causally links inflammation, or the molecules and networks integral to inflammatory responses, to the development of metabolic diseases like diabetes and/or the complications that emerge from these pathologies, particularly in the context of obesity and type 2 diabetes [42].

Many lines of evidence have shown that chronic activation of intracellular proinflammatory pathways within insulin target cells can lead to insulin resistance. Several cytokines, such as IL-6, IL-1β, and TNFα, can be released by both adipocytes and macrophages. Consistent with this, elevated levels of the proinflammatory cytokines TNFα and IL-6 have been shown in individuals with insulin resistance and diabetes [43]. Furthermore, TNFα levels are elevated in adipose tissue and blood from obese rodents, and neutralization of TNFα improves insulin sensitivity in these animals. An important initiator of the inflammatory response to the development of T2D is adipose tissue. It is now well understood that adipose tissue is not simply a storage depot for excess calories

but that it also actively secretes hormones and cytokines that function in an endocrine or a paracrine fashion. The adipose tissue consists of a variety of cell types, including adipocytes, immune cells (macrophages and lymphocytes), preadipocytes, and endothelial cells. Adipose tissue and macrophages are a major source of proinflammatory cytokines, which can function in a paracrine and potentially an endocrine fashion to cause decreased insulin sensitivity [44, 45].

In type 2 diabetes, high fat diet induces the increasing of circulating FFA that activates the Toll-like receptors (TLR) in adypocytes. TLR are important factors in the pathophysiology of chronic low-grade inflammation. TLRs are able to sense pathological levels of lipids. In these sense, TLR4 is involved in macrophage activation and cytokine production in response to saturated fatty acids [46]. Activation of these tissue macrophages leads to the release of a variety of cytokine, which in turn recruit additional macrophages, setting up a feed-forward process that further increases adipose tissue macrophages content and propagates the chronic inflammatory state. Adipose tissue macrophages appear to have either an anti-inflammatory phenotype (M2, producing anti-inflammatory cytokines such as IL-10) or a proinflammatory phenotype (M1, producing inflammatory cytokines such as IL-1, IL-6 and TNFα) [47].

Therefore, the low-grade inflammation observed in T2D is linked with altered levels of several circulating factors, including TNFα, IL-1β, IL-6 and other inflammation markers. Adipocytes share some properties with macrophages: both can activate complement and produce inflammatory cytokines and many other factors. Adipocytes also store lipids and regulate metabolic homoeostasis whereas macrophages can also accumulate lipids to become foam cells [48, 49]. TNFα, IL-6, IL-1β, and possibly other cytokines and macrophage-secreted factors exert paracrine effects to activate inflammatory pathways in insulin target cells. These cytokines are thought to play a major role in the pathophysiology of insulin resistance in insulin target tissues. Through phosphorylation of the insulin receptor substrate-1 (IRS-1) protein on serine residues. All kinase phosphorylation pathways interact with insulin signaling via serine/threonine inhibitory phosphorylation of IRS [50].

Low-grades inflammation is associated with the stimulation of various serine/threonine kinases and the activation of the transcription factors NF-κB, which

lead to insulin resistance. Activation of serine/threonine kinases c-Jun NH2-terminal kinase (JNK), PKCs, and IκB kinase complex β (IKKβ) leads to serine phosphorylation of IRS-1, which impairs its ability to bind and activate PI 3-kinase. This leads to diminished activation of downstream kinases Akt and PKC-ζ, which results in decreased GLUT4 translocation and glucose transport (figure 11). In addition, activation of NF-κB and AP-1 regulates transcription of proinflammatory genes, including interleukin IL-6, IL-1β, and TNFα. On the other hand, direct effects of inflammation on β-cells arise from activation of the intra-islet immune response. In this sense, the strongest support is for the key role of IL-1β due to increased glucose levels and fatty acids increase IL-1β production in islets [51-54].
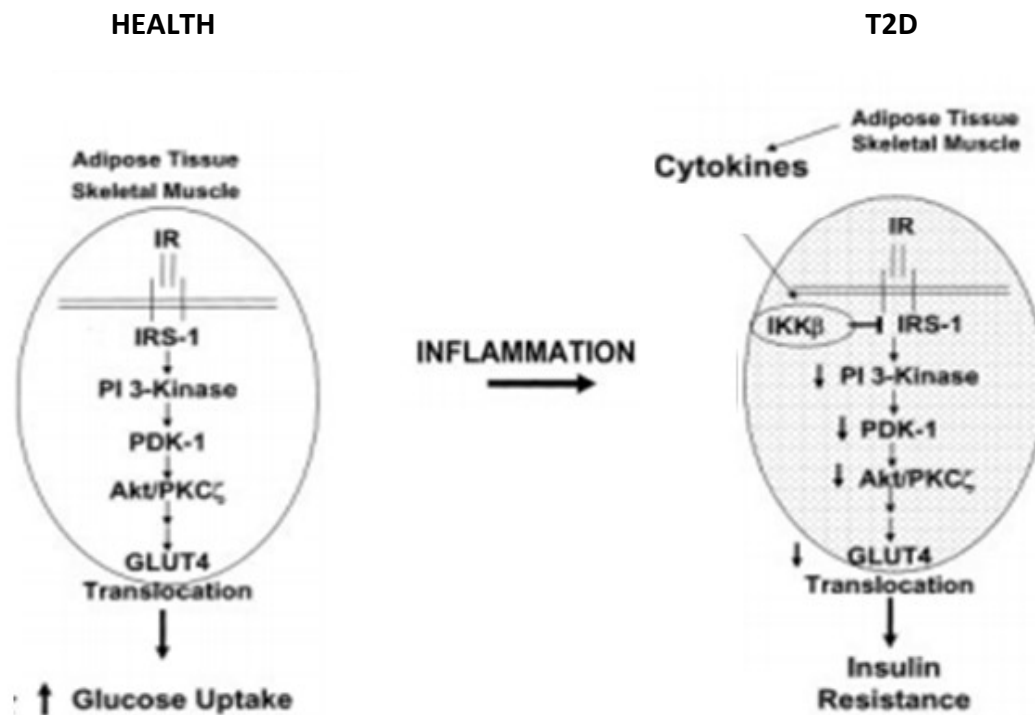
Figure 11. **Effects of the inflammation in the insulin signaling.** Adapted from Reciprocal Relationships between Insulin Resistance and Endothelial Dysfunction. *Circulation*. Kim, J (2006).

4. TYPE 2 DIABETES ANIMAL MODELS

Unfortunately, virtual or human in vitro systems are not suitable, for the moment, for studying the structural, electrical and metabolic remodelling that takes place in the diabetic heart, and therefore animal models are required. As usual, rodents have been

the most common choice, but other mammals have been used like guinea-pigs, rabbits, dogs and pigs. Currently there are many different animal models for type 1 and type 2 diabetes. It is important that they reproduce the pathophysiology of the disease, especially in type 2 diabetes where is often more difficult. These have been extensively reviewed and include spontaneous, transgenic as well as surgically, chemically and diet-induced [55-57] (figure 12).

Most of our knowledge regarding cardiac electrical remodelling, including ECG, ionic currents and action potentials in diabetes derives from type 1 diabetic animals [58-62]. Type 2 diabetes has a different origin and pathophysiology. In humans, it starts with insulin resistance, but for some time the pancreas compensates with increased insulin secretion and the glycemic control is maintained. Eventually, there is a loss of functional beta cells resulting in hyperglycemia and the patient is diagnosed as diabetic. Up to the last decade, the type 2 diabetes animal models were mainly genetic. Since the last decade, several non-genetic animal model that had better reproduce the pathophysiology of the disease have been developed.
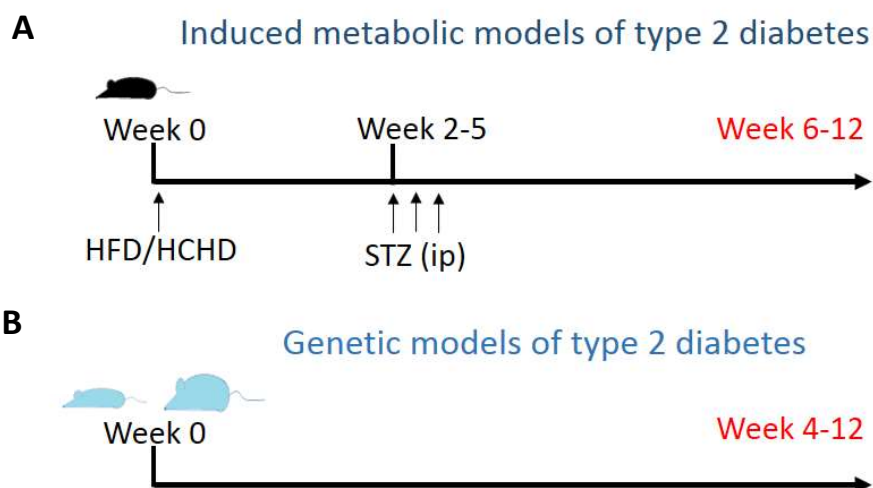
Figure 12. **T2D animal models. A)** Metabolic models for type 2 diabetes include diet-induced insulin resistance followed by mild to medium pancreatic toxicity. Animals are fed with high fat and/or high carbohydrate diet (HFD and HCHD respectively) for some weeks to generate insulin resistance and then receive one or more intraperitoneal injections of low dose streptozotocin to reduce beta cell mass. **B)** Genetic hyperinsulinemic and/or hyperglycemic animals, lean and obese, spontaneously develop diabetes over time.

Among the non-genetic animal models of type 2 diabetes, metabolic models are becoming popular and replicate that sequence of events. They combine high fat and/or high-carbohydrate diet with a low-dose of STZ intraperitoneal [63, 64]. Feeding on high caloric food progressively leads to glucose intolerance and insulin resistance, whereas STZ provides the loss of functional beta cell mass required to establish diabetes. There are different versions depending on the percentage and composition of the fat in the diet, the source of carbohydrates (sucrose, fructose), the dose of STZ, the animal species or the duration of the diet. All variations yield animal models that differ in severity, ranging from mild insulin resistance to overt diabetes with associated complications [63] Thus, each model can be carefully characterized and be suitable for studying particular aspects of the disease. For instance, a metabolic model that develops myocardial hypertrophy and fibrosis [65] will be good for studying diabetic cardiomyopathy [65].

5. ELECTROPHYSIOLOGY OF THE HEART

Electrocardiogram (ECG) is a graph of voltage versus time of the electrical activity of the heart using electrodes placed on the skin. These electrodes detect the small electrical changes that are a consequence of cardiac muscle depolarization followed by repolarization during each cardiac cycle (heartbeat). Just like skeletal muscles, heart muscles are electrically stimulated to contract. This stimulation also called activation or excitation triggers the generation of an action potential. The electrical activity of a single cell can be registered as the action potential. Therefore, the individual action potentials of the individual cardiomyocytes are averaged and the result that is the average of billions of microscopic electrical signals (action potentials) from cardiomyocytes is shown on the ECG (figure 13)4.

During each heartbeat, heart has an orderly progression of depolarization that results in an electrical force that has a direction and magnitude, an electrical vector. The depolarization starts with pacemaker cells in the sinoatrial node, spreads throughout the atrium, and passes through the atrioventricular node down into the bundle of His and the Purkinje fibers, spreading down and to the left throughout the ventricles. This orderly pattern of depolarization gives rise to the characteristic ECG tracing. There are

three main components to an ECG: The P wave, which represents the depolarization of the atria; the QRS complex, which represents the depolarization of the ventricles; and the T wave, which represents the repolarization of the ventricles (figure 14).
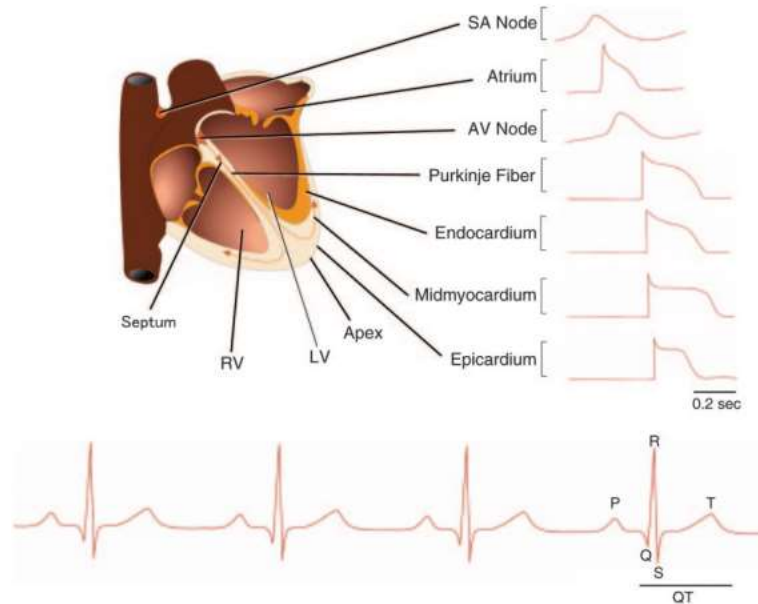
Figure 13. **Heart regions, action potentials (above), and resulting ECG trace (below).** Adapted from Molecular Physiology of Cardiac Repolarization. *Physiol Rev*. Nerbonne, JM (2005).

The analysis of the waves and intervals of the ECG provides information about the electrophysiological behavior of the heart (figure 14).

P wave: The P wave represents depolarization of the atria. Atrial depolarization spreads from the SA node towards the AV node, and from the right atrium to the left atrium.

PR interval: The PR interval is measured from the beginning of the P wave to the beginning of the QRS complex. This interval reflects the time the electrical impulse takes to travel from the sinus node through the AV node. A short PR interval suggests that the electrical impulse is bypassing the AV node. Otherwise, a long PR interval diagnoses atrioventricular block.

QRS complex: The QRS complex represents the rapid depolarization of the right and left ventricles. The ventricles have a large muscle mass compared to the atria, so the QRS complex usually has a much larger amplitude than the P wave. A wide QRS complex

suggests disruption of the heart's conduction system, or ventricular rhythms such as ventricular tachycardia.

T wave: The T wave represents the repolarization of the ventricles.

QT interval and Corrected QT interval (QTc): The QT interval is measured from the beginning of the QRS complex to the end of the T wave. It is related to the time taken from when the cardiac ventricles start to contract to when they finish relaxing. Acceptable ranges vary with heart rate; therefore it must be corrected to the heart rate. Different formulas can be used; the most commons are Frederica's and Bazzet's formulas. A prolonged QTc interval is a risk factor for ventricular tachyarrhythmias and sudden death.
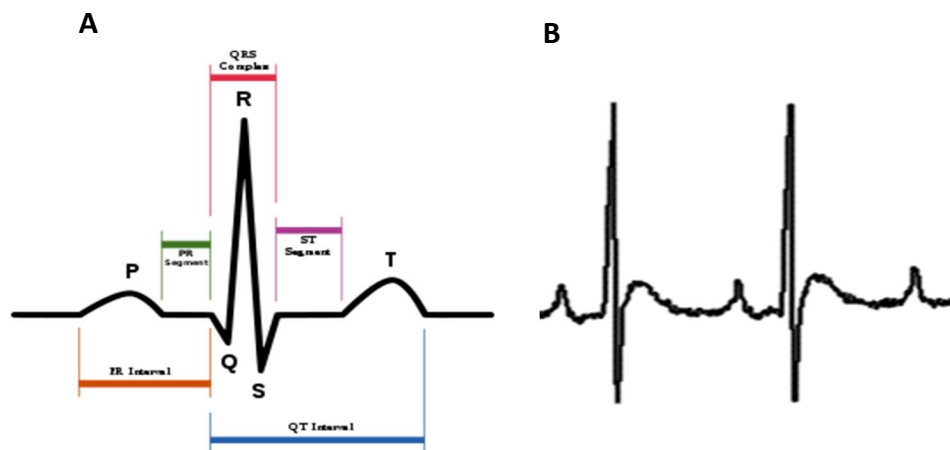
Figure 14 ECG beat intervals and waves. A) Representation of ECG intervals and waves. **B)** Recorded ECG beats.

The normal sequence and synchronous contraction of the atria and ventricles require the rapid activation of groups of cardiac cells. An activation mechanism must enable rapid changes in heart rate and respond to the changes in autonomic tone. The propagating cardiac action potential fulfils these roles. Figure 15 illustrates the 5 phases of the normal action potential:

Phase 4, or the resting potential, is stable at ≈−90 mV in normal working myocardial cells.

Phase 0 is the phase of rapid depolarization. The membrane potential shifts into positive voltage range. This phase is central to rapid propagation of the cardiac impulse.

Phase 1 is a phase of rapid repolarization. This phase sets the potential for the next phase of the action potential.

Phase 2, a plateau phase, is the longest phase. It is unique among excitable cells and marks the phase of calcium entry into the cell.

Phase 3 is the phase of rapid repolarization that restores the membrane potential to its resting value [66].
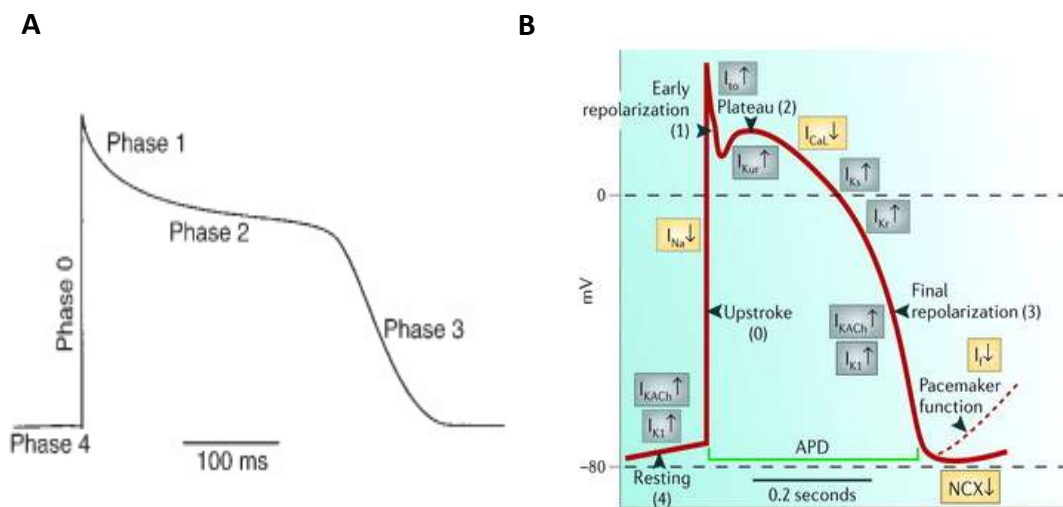
Figure 15. **Cardiac action potential A)** Phases of cardiac action potential. **B)** Phases of cardiac action potential and implicated ion currents. Adapted from Cardiac Ion Channels. *Circulation.* Grant, AO (2009).

Ion channels are pore-forming membrane proteins that allow ions to pass through the channel pore. Voltage-gated ion channels are a class of transmembrane proteins that form ion channels that are activated by changes in the electrical membrane potential near the channel. The membrane potential alters the conformation of the channel proteins, regulating their opening and closing. Myocardial action potentials reflect the coordinated functioning of inward (Na^+ and Ca^{2+}) and outward (K^+ and Cl^-) current carrying channels that open and close in a voltage- and time-dependent manner (figure 15B).

Voltage-gated K^+ (Kv) channels are the primary determinants of action potential repolarization in the mammalian myocardium, and compared with cardiac Nav and Cav channels, there is considerable electrophysiological and functional cardiac Kv channel diversity with distinct gating properties that determine the heights and durations of

myocardial action potentials [67]. Two broad classes of repolarizing cardiac Kv currents have been distinguished: transient outward K⁺ currents (Ito) and delayed, outwardly rectifying K⁺ currents (Ik). The transient currents (Ito) activate and inactivate rapidly on membrane depolarizations to potentials positive to approximately 30 mV and underlie the early phase (phase 1) of repolarization in ventricular and atrial cells (fig.14B). Cardiac delayed rectifiers (Ik) activate at similar membrane potentials and with variable kinetics, and these currents determine the latter phase (phase 3) of repolarization back to the diastolic potential (fig. 15B) [68].

6. DIABETIC CARDIOMYOPATHY

The vascular complications of type 2 diabetes mellitus have traditionally been divided into macrovascular complications (cardiovascular disease) and microvascular complications (complications affecting the kidney, the retina, and the nervous system). Complications of T2D are very common, with half of patients with T2D presenting with microvascular complications and 27% with macrovascular complications. The relative risk of microvascular and macrovascular disorders among patients with T2D was estimated to be at least 10-20 times higher and 2-4 times higher, respectively, than in people without diabetes. There is a large increase in the number of prevalent cases of T2D, and undiagnosed T2D. Advances in the treatment of T2D lead to people longer life expectancy. Higher prevalence together with advances in treatment of the disease has resulted in a costly increase in the incidence of diabetic complications. For instance, 53% of the lifetime medical costs of T2D have been attributed to treating the major complications of T2D such as nephropathy, neuropathy, retinopathy, stroke and coronary heart diseases [69, 70].

Among T2D-associated complications, cardiovascular disease is particularly important because is the major cause of mortality and morbidity in diabetic patients. Framingham study reported that patients with type 2 diabetes were twice likely to die from cardiovascular diseases than healthy people [71]. Currently, with the advances in diabetes management, many diabetic patients achieve good glycemic control, but in spite of that, cardiovascular complications remain the leading cause of death [72, 73].

Beyond the cardiovascular disease, diabetes increases the risk of heart failure in the absence of heart failure risk factors such as cardiac ischaemia, hypertension or other. This condition is known as diabetic cardiomyopathy, and consists in changes in the myocardial structure induced by T2D, which leads to cardiac dysfunction [74, 75].

Diabetic cardiomyopathy is currently defined as a ventricular dysfunction in the absence of coronary artery disease or hypertension. The Cardiovascular Health study [76] and the Strong Heart study [77] confirmed the association between diabetes and increased left ventricular mass and wall thickness with compromised diastolic and systolic function.

Unlike other diabetes-associated complications like cardiac autonomic neuropathy and coronary artery disease that are caused by damage in nerves and blood vessels of the heart, diabetic cardiomyopathy is a primary alteration of the myocardial tissue. Different mechanisms have been proposed to promote the development of diabetic cardiomyopathy. As previously mentioned, these mechanisms include: cardiac insulin resistance; metabolic remodeling with abnormal free fatty acids metabolism and lipotoxicity; mitochondrial dysfunction with increased ROS production; accumulation of advanced glycation end products and collagen; abnormalities in calcium handling; pro-inflammatory responses; activation of the renin-angiotensin-aldosterone system; and autonomic neuropathy with increased sympathetic activity [78-81].

Metabolic disturbance triggered by nutrients, such as hyperglycaemia, and increased free fatty acid levels, induces chronic low-grade inflammation in metabolically important organs, like the liver and adipose tissue. Peripheral metabolic disturbance also induces subcellular low-grade inflammation in the heart [82]. The early stage of diabetic cardiomyopathy is not accompanied by substantial changes in myocardial structure and cardiac function. However, in turn, the systemic metabolic disorders induce subcellular component abnormalities, such as oxidative stress, mitochondrial dysfunction, ER stress, and impaired calcium handling, leading to impaired myocardial relaxation. In the advanced stage, increased subcellular component abnormalities, inflammatory cell infiltration, neurohumoral activation, and their vicious cycle, induce cardiomyocyte injury and death, and subsequent cardiac fibrosis, resulting in impairment of both diastolic and systolic functions [83, 84].

6.1. DIABETIC CARDIAC ELECTRICAL REMODELLING

The processes that take place in the diabetic myocardium can modify the expression and electrophysiological properties of different ionic channels [85], even in the absence of structural changes, leading to an electrical remodelling. The main characteristic of diabetic cardiac electrical remodelling is the prolonged ventricular repolarization, reflected as a prolonged duration of the QT interval in the electrocardiogram. At the cellular level, diabetes lengthens the cardiac action potential duration, and alters the expression of ion channels proteins. All these alterations increase the risk of developing ventricular arrhythmias and sudden death [86, 87]. Moreover, arrhythmogenesis in diabetes can be amplified by other factors like autonomic dysregulation [88-90], inflammation [91], and by the presence of comorbidities like hypertension [87].

A. ELECTROCARDIOGRAPHIC DISORDERS IN DIABETES

A variety of inherited and acquired cardiac diseases are associated with changes in the expression and/or the biophysical properties of myocardial ion channels, changes that can lead to alterations in the waveforms and/or the propagation of action potentials in different regions of the heart, predisposing individuals to potentially life-threatening arrhythmias and sudden cardiac death. Detailed understanding of disease-linked alterations in cardiac ion channel expression and/or properties is needed to facilitate accurate diagnosis of risk and the development of optimal treatment strategies. Thus, characterizing the functional expression and properties of myocardial ion channels is important to understand these electrical cardiac alterations.

I. ATRIAL FIBRILLATION

Diabetes is an independent risk factor for atrial fibrillation (AF) and diabetic patients have one-third greater risk of incidence of AF compared with unaffected individuals [92]. Although the underlying pathophysiological mechanisms are not completely understood, diabetic-induced atrial remodeling share some mechanisms with diabetic cardiomyopathy. Atrial autonomic dysregulation, oxidative stress, fluctuations of

glucose levels and structural and electrical remodelling contribute to the development of arrhythmia [93]. Regarding the electrical remodelling, diabetic Zucker obese rats with higher susceptibility to AF showed prolonged atrial action potential duration. This effect was caused by a reduction of the repolarizing currents Ikur and Ito, as well as the corresponding channel forming proteins [94].

II. PROLONGED QT INTERVAL DURATION

Although some diabetic patients have slow ventricular depolarization that is visible in the electrocardiogram as an increase in QRS duration [95], the most-studied electrical alteration of the diabetic myocardium is the prolonged ventricular repolarization. Diabetes lengthens the duration of both the QT interval and the QT corrected to the heart rate (QTc) of the ECG. It is widely described that QT and QTc prolongations are associated with higher risk of developing ventricular arrhythmias and sudden cardiac death. At the beginning, prolonged QTc was first reported in individuals with diabetic neuropathy [96-98]. Later, it was also observed in newly diagnosed type 2 diabetic patients with no apparent complications [99]. It is difficult to estimate the prevalence of longer QTc among diabetics. The different characteristics of the patient population in each study and the formula used to adjust the QT for heart rate (Bazett, Fridericia, Hodges, others) lead to heterogeneous results, where prevalence ranges from 3% to 44% [100-103]. Moreover, recruited participants usually exhibited diabetes with several years of duration, and therefore received antidiabetic medication [104].

On the other hand, the QT dispersion or QTd reflects the difference between the longer and the shorter QT interval duration in the 12 leads electrocardiogram. An increase in the QTd is typically associated to an increased predisposition to ventricular arrhythmias. Diabetic patients show increased QTd and heart-rate corrected QT dispersion (QTdc) compared to non-diabetic subjects in the absence of other cardiovascular pathologies. Furthermore, the presence of concomitant cardiovascular abnormalities such as left ventricular hypertrophy or hypertension increased the QT dispersion in diabetes mellitus [105].

C. IONIC CHANNELS AND CURRENTS IN THE DIABETIC MYOCARDIUM

The basic electrical activity of the cardiac cells is based in the action potential that consists of a rapid depolarization phase followed by a repolarization phase with a plateau. It is described a lengthening of the cardiac action potential duration (APD) in a rat model of type 1 diabetes [58]. This effect is consistently confirmed in both rodent and non-rodent models [61, 106], and correlates with the prolonged QTc duration in diabetic patients. Besides, in type 1 ventricular myocytes, APD prolongation was not homogeneous throughout the heart, and the effect was more pronounced in the endocardium than in the epicardium [60].

However, although steps forward in the research of this field has been done in the last years, there is not as much evidence about the ion channels alterations in type 2 diabetes as in type 1. Alterations in the expression and behaviour of several ionic channels that conduct depolarizing (sodium and calcium) and repolarizing (potassium) currents cause the prolonged APD in diabetes. (summarized in Figure 16).

AP Phase	Current	Protein	Type of Diabetes
0	↓I_{Na} ↑I_{Na-L}	↓Nav1.5	T1D
1	↓I_{to} ↓I_{Kur}	↓Kv4.3, Kv4.2 ↓Kv1.5	T1D & T2D T1D & T2D
2	↓I_{CaL}	↓Cav1.2	T1D & T2D
3	↓I_{Ks} ↓I_{Kr}	=Kv7.1, ↓minK ↓hERG	T1D T1D & T2D
4	= I_{K1} ? I_{K1} ? I_{NCX}	=Kir2.1 ↓Kir2.1 ↑NCX	T1D T2D T2D
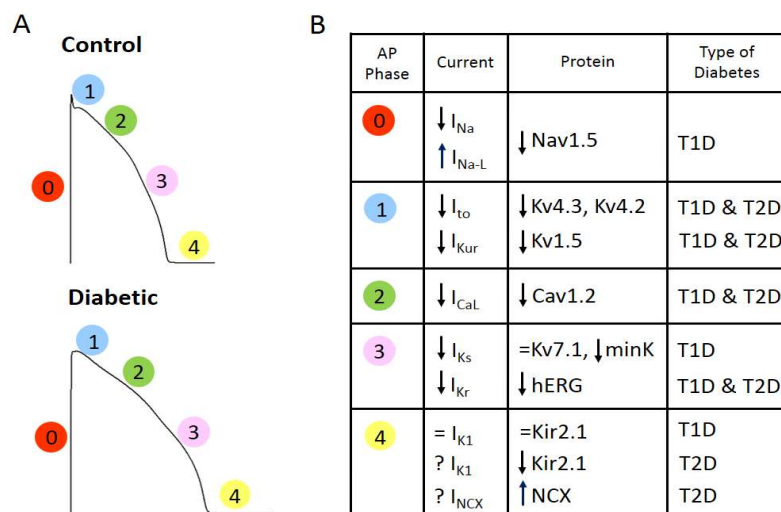
Figure 16. Diabetes affects the depolarizing and repolarizing currents responsible for the cardiac action potential. A) Action potential depictions of a control and a diabetic heart (numbers indicate the phase of the AP) showing that diabetes changes action potential shape and prolongs duration. **B)** Summary of the alterations in the cardiac ionic currents and the respective channel-forming proteins obtained in animal models of type 1 (TD1) and type 2 diabetes (T2D).

I. CALCIUM CURRENT AND CALCIUM HANDLING

The L-type calcium current (ICa-L) is a depolarizing current active during the repolarization and responsible for the plateau phase or phase 2. Regarding the ICa-L, experiments with diabetes animal models have yielded confusing results. Some groups found no effects upon the current amplitude and the biophysical behaviour of the calcium channel in type 1 diabetic models [61, 62, 107, 108]. On the contrary, other groups described a reduction in the current amplitude and a slowing in the current inactivation kinetics. Finally, some groups reported a reduction of ICa-L but no effect on the channel behaviour. In this sense, the reduction in the cardiac ICa-L current density correlates with a decreased expression of its channel-forming protein Cav1.2 in Akita mice, a genetic model of type 1 diabetes with defective insulin production. This effect has been also described in type 2 diabetic model like the db/db obese mice and Zucker obese rats [86, 109, 110]. In addition, electrophysiological recordings of single-channel activity showed that the biophysical properties of the calcium channel were similar in control and diabetic animals [110].

It is not clear the reason for these discrepant results. They might be related with methodological aspects in the current recordings such as the patch-clamp configuration and the charge carrier used in the experiment (Ca^{2+} or Ba^{2+}). There could also be intrinsic differences in the diabetic models, for instance induced vs genetic. The experimental conditions for the current recording are also crucial since the amplitude of the L-type calcium current is very sensitive to the intracellular calcium content.

Aside from calcium currents, diabetes also showed alterations in the intracellular calcium handling. Changes several proteins involved in the intracellular calcium handling, which leads to an increase in cytosolic $[Ca^{2+}]$. This leads to the prolongation of the duration of both the contraction and the relaxation phases of the cardiac cycle in diabetes [111-113]. In the diabetic heart Ca^{2+} release from the sarcoplasmic reticulum during systole is depressed, mainly because of a reduction in Ca^{2+}-releasing proteins at the SR membrane. In this sense, mRNA and protein levels of ryanodine receptors (RYRs) are reduced in diabetes, and became fully restored after insulin supplementation in type 1 diabetes animals [114, 115].

However, more characteristic of the diabetic myocardium is the diastolic calcium overload, which is increased about three-fold compared to healthy persons [116]. It has been reported that type 2 diabetes increases the opening probability of RYRs and leads to diastolic Ca^{2+} leak to the cytoplasm [117]. In addition, calcium reuptake to the SR is also compromised because diabetic cardiomyopathy reduces the expression of sarcoplasmic reticulum Ca^{2+}-ATPase (SERCA2) as well as its apparent affinity for Ca2+ [114, 115, 118, 119]. As a result, diabetic cardiomyocytes have higher diastolic calcium levels caused by a markedly impaired calcium uptake [120-123]. Thus, diabetic cardiomyocytes have less calcium available for the contraction during systole together with an excess of diastolic calcium that impairs relaxation during diastole.

II. THE REPOLARIZING POTASSIUM CURRENTS

Repolarization of the action potential is the most common and described alteration of the diabetic electrocardiogram, and it is closely related with a prolongation of the QT interval ECG. Several potassium currents determine the action potential repolarization in the human heart. The transient outward or Ito and the ultrarapid delayed rectifier or IKur are responsible for the initial repolarization or phase 1; the slow delayed rectifier, IKs, and specially the rapid delayed rectifier, IKr, repolarize the phase 3; finally, the inward rectifier or IK1 contributes to the final repolarization or phase 4 [124]. Patch-clamp experiments in type 1 diabetic cardiomyocytes show that all are modified except IK1 [58, 60].

Ito has been extensively studied in rodents because is the dominant repolarizing current in the ventricle. Ito is highly affected by type 1 diabetes regarding current density, biophysical properties, and regulation. The reduction in the amplitude of Ito [58-60, 125] was caused by a reduction in the expression of the channel-forming proteins Kv4.3 and Kv4.2 and the accessory subunit KChIP2 [61, 106, 126]. In addition, diabetes accelerated Ito current inactivation [58, 60] due to a reduction in the Kv4.3 channel phosphorylation by CaMKII [127]. This contributed to the reduction of the total current and the lengthening of the action potential duration. Like Ito, diabetes inhibited the IKur because of a decrease in the expression of the pore forming protein Kv1.5 [60, 106].

The delayed rectifiers, virtually absent in rodents, have been analyzed mostly in type 1 diabetic rabbits and dogs. The amplitude of the slow delayed rectifier IKs was reduced and this was caused by a reduction in the expression of the accessory subunit mink, whereas the pore-forming subunit Kv7.1 was not or little affected [61, 62, 128]. Regarding the rapid delayed rectifier, most of the studies reported no effect of diabetes on IKr amplitude and properties [61, 62, 128]. However, experiments made in rabbits with longer diabetes duration showed significant reduction of IKr amplitude and the expression of the pore-forming protein ERG [128, 129].

A combination of factors can lead to the reduced electrical activity and expression of cardiac potassium channels. In type 1 diabetic animals, insulin treatment restored some but not all the altered currents. The impaired metabolic status of the diabetic cells might also affect the protein synthesis. Thus, in vitro activation of the AMP-dependent protein kinase reduced several K^+ repolarizing currents in a similar fashion than diabetes [106]. On the other hand, diabetes induced a sterile inflammation that increased the IL-1β release from cardiac macrophages and lead to the reduction of the Ito [130]. Thus, the possible role of proinflammatory status in the cardiac electrical remodelling cannot be discarded in type 2 diabetes.

The literature regarding cardiac electrical remodelling in type 2 diabetes, however, is very limited, and the experiments are often performed in type 2 diabetes genetic models. Even then, a few studies reported a prolongation of APD and a reduction of the amplitude of the ventricular Ito current in the genetic model WBN/Kob rats [107, 131], in db/db mice [132] or the Otsuka-Long-Evans-Tokushima Fatty rats [133]. Similarly, Ito, IKur and ICa-L currents, as well as their channel-forming proteins were reduced in the atria of Zucker diabetic fatty rats [94].

A recent study in elderly type 2 diabetic patients showed a reduction of the mRNAs encoding for hERG and Kir channels, responsible for IKr and IK1, and an increase of the Na^+/Ca^{2+} exchanger (NCX) expression. Channel protein levels and current recordings were not assessed, and the study was performed in few, aged and poly-medicated patients [134]. This is the first work that compares for the expression of cardiac channels between diabetic and non-diabetic humans [135].

7. TREATMENT OF DIABETES

Metformin has become the oral hypoglycemic of choice for the treatment of T2D [136]. However, there are several meta-analysis studies that question whether metformin has beneficial effects on mortality [137-140] A recent meta-analysis published in 2018 and including more than 166,000 patients with T2D shows that metformin is not superior to placebo in terms of the incidence of serious cardiovascular events or in terms of all-cause mortality [141].

Furthermore, T2D is a progressive disease. As time passes, patients require increasing doses of antidiabetic, and even combined treatment of several drugs [142]. The American Diabetes Association (ADA) establishes that, if the goal of glycosylated hemoglobin (A1C) is not reached in three months with metformin, the combination with: Sulfonylureas, DPP-4 (DiPeptidyl Peptidase 4) inhibitors, GLP-1 receptor, Thiazolidinediones (Glitazones), GLP-1 receptor agonists (Glucagon Like Peptide-1), SGLT2 inhibitors (Na / Glucose type 2 co-transporter) and Insulin.

7.1. TREATMENT OF DIABETES IN PATIENTS WITH CARDIOVASCULAR RISK

Diabetic patients have two-fold risk of developing cardiovascular disease (CVD) and atherosclerotic cardiovascular disease is still the leading cause of morbidity and mortality in this group (ADA 2017). Results from the Framingham Heart Study original and offspring cohorts showed that, although the incidence of cardiovascular disease has declined in both adults with and without diabetes over the last few decades, diabetic patients still have 2-fold greater risk of CVD compared with the non-diabetic population [143, 144].

For years, the principal target of the drugs is to reduce the hyperglycemia to healthy levels avoiding hypoglycemia in type 2 diabetes patients. According to this target, metformin is the first choice to start glycemic control due to the positive results obtained in overweight patients [145]. However, type 2 diabetes is a progressive disease, and patients need increasing doses of antidiabetic drugs and even the

combined treatment of several drugs [145]. The American Diabetes Association establishes that, if in three months metformin does not reach the goal of glycosylated hemoglobin (HbA1c), a second drug among the following options should be added: sulfonylureas; thiazolidinediones; DPP-4 inhibitors; SGLT2 inhibitors; GLP-1 receptor agonists; ultimately insulin. In addition, there are meta-analysis studies that raise into question whether metformin has beneficial effects on mortality in patients with T2D [137, 139, 140], but although the therapeutic alternatives are varied, not all have the same cardiovascular safety (Table 1).

As the concerns about cardiovascular risk in diabetic patients has guided the policy of the regulatory agencies to establish the safety of new drugs necessary for their approval and, in the clinical settings, it may also determine the treatment of choice. In 2008, FDA issued the guidance for the pharmacological industry regarding evaluating cardiovascular risk during the development of new antidiabetic therapies for type 2 diabetes. This information has been incorporated into the standards of medical care

Despite metformin does not reduce cardiovascular mortality [137, 140], it continues to be the drug of choice in this group of patients, often in combination with other drugs, taking into account a number of important limitations (ADA, 2020). However, metformin combined treatment with either sulphonylurea or thiazolidinediones has shown significant higher mortality and development of heart failure [146-148]. Regarding the DPP-4 inhibitors, although the studies are contradictory, the FDA do not recommend this treatment either. Some of these studies reported increased heart failure [149] while others non-significant association [150, 151]. These results indicate that sulfonylureas, thiazolidinediones and DPP-4 inhibitors should be avoided, or used with great caution in diabetic patients with cardiovascular disease or risk.

On the other hand, the effect of a GLP-1 receptor agonist, showed a reduction of the set of myocardial infarction, angina or cardiovascular death in diabetic patients with high risk or established cardiovascular disease [152, 153]

Moreover, the Na^+/Glucose cotransporter 2 (SGLT2) inhibitors showed a reduction in the mortality of patients with T2D and established cardiovascular disease [154]. In addition, SGLT2 inhibitors has been described to reduce the risk of developing potentially lethal arrhythmias [155] independently of its glucose-lowering effect [156].

Therefore, in patients with cardiovascular risk, the recommended drugs are reduced to metformin, GLP-1 agonists and SGLT2 inhibitors [157].

Finally, although metformin is still considered the first choice treatment, the American Diabetes Association (ADA) recommends to consider a sodium–glucose cotransporter 2 inhibitor or glucagon-like peptide 1 receptor agonist with demonstrated cardiovascular disease benefit for type 2 diabetic patients with established atherosclerotic cardiovascular disease or indicators of high risk, established kidney disease, or heart failure (ADA 2020). Nevertheless, most prevalence studies do not differentiate subjects on monotherapy from those on combined therapy, but the fact is that antidiabetic medication does not seem to be efficient to restore normal QTc values [158-160].

ADA´s recommendation for treatment of type 2 diabetes	Recommended when CV risk	CVOTs conducted	Associated with CV benefit
Metformin	Metformin	-	-
(*) Sulfonylureas	-	-	-
(*) Thiazolidinediones	-	-	-
(*) DPP-4 inhibitors	-	+	-
(*) SGLT2 inhibitors	SGLT2 inhibitors	+	*Empagliflozin, Canagliflozin*
(*) GLP-1 receptor agonists	GLP-1R agonists	+	*Liraglutide*

(*) Options to be added to metformin if necessary

Table 1. **Recommended treatments for type 2 diabetes**. Only SGLT2 inhibitors and GLP-1R agonists have been associated with cardiac benefit.

8. THE VOLTAGE-DEPENDENT CHANNEL Kv1.3.

Kv is the largest superfamily of channels containing 12 subfamilies (Kv1 – Kv12) and comprising more than 40 genes. Kv channels are tetramers of pore-forming subunits, each one with six transmembrane helices (S1–S6) connected by intra- and extracellular loops. The NH_2- and COOH-terminal domains are intracellular regions of variable length (figure 17). The Kv1 subfamily (Shaker) includes eight voltage-gated potassium channels belonging to the delayed rectifier class (Kv1.1 – Kv1.8). The third member, Kv1.3, is encoded by the intronless KCNA3 gene on chromosome 1p13.3 in humans and accounts

for a 575 amino acid long protein. The transmembrane helices of each Kv subunit contain two functionally and structurally independent domains: The K^+ selective pore (formed by S5 and S6 helices and their linker) and the voltage sensor domain (the S1–S4 transmembrane helices). Kv1.3 associates with Kvβ2 and KCNE auxiliary subunits [161].
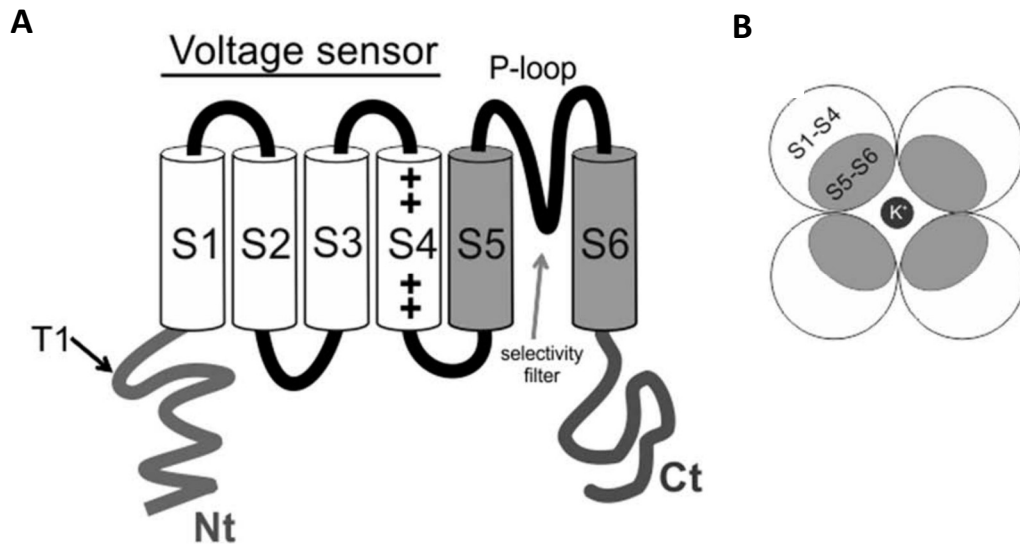
Figure 17. **Main structural features of the voltage-gated potassium channel Kv1.3. A)** Schematic representation of the membrane topology. **B)** Top view of a functional tetramer. Each monomer is represented by a circle. Adapted from the voltage-gated potassium channel Kv1.3 is a promising multitherapeutic target against human pathologies. *Taylor and Francis. Expert opinion*. Perez-Verdaguer, M (2015).

In the case of Kv1.3, It efficiently targets the cell surface activating upon membrane depolarization > -35 mV (with a single channel conductance of 13 pS). In addition to the cell surface, Kv1.3 also targets to the inner mitochondrial membrane, Golgi apparatus and nuclear membrane, exhibiting different biophysical properties [162-164]. Its activation and inactivation are voltage-dependent. Activation threshold occurs at potentials between -60 and -50 mV. The voltage-dependence of inactivation is also very steep, with a midpoint around -45 mV for heterologous channels. These biophysical properties determine a small range of voltages at which there is a finite probability that Kv1.3 channels are open and not inactivated. In T cells, this region overlaps with resting potential, allowing its effective control by Kv1.3 currents [165, 166]. Kv1.3 activation time course is fast (a few milliseconds) whereas the inactivation is time constant and cumulative and, therefore inactivation time is much larger (~200 ms). Then, Kv1.3

channels require a considerable time to reopen again [167, 168]. Many of these biophysical and kinetic properties are relevant for the modulation of firing patterns in excitable cells. However, their possible role shaping membrane potential in non-excitable cells remains to be elucidated.

The expression of the kv 1.3 was originally identified in T-lymphocytes. Thus, it is not surprising that most of our knowledge regarding the kinetic and pharmacological properties ties of Kv1.3 channels, their molecular associations, their contribution to cellular homeostasis, and their role in the pathways leading to activation and proliferation has been characterized in T-lymphocytes. However, Kv1.3 is mostly expressed in neurons, mainly in the hypothalamus and the olfactory bulb [162, 169]. It is also expressed in kidney, osteoclasts, testis, insulin-sensitive tissues such as adipose tissue, liver and skeletal muscle [170] and immune cells including T [171, 172] and B lymphocytes [173], and macrophages [174].

The channel has been implicated in the regulation of a wide range of physiological functions and its role is still controversial. Kv1.3 contributes to the resting membrane potential, apoptosis, cell volume regulation and leukocyte activation and proliferation. It participates in the activation and proliferation of T lymphocytes by regulating membrane potential and Ca^{2+} signalling pathways. In this sense, Kv1.3 hyperpolarizes the membrane potential, promoting a Ca^{2+} influx through the calcium release activated channel (CRAC), and triggering TCR downstream signalling. Kv1.3 channels and the intermediate conductance Ca^{2+}-activated K channels (KCa3.1 channels) are the main K^+ conductance in T cells. Their activation, either by membrane depolarization (Kv1.3) or by increases in intracellular Ca^{2+} (KCa3.1), leads to membrane hyperpolarization, increasing the driving force for Ca^{2+}. These two channels determine T cell resting membrane potential, thus regulating the magnitude of the Ca^{2+} signal required for gene transcription and cell proliferation. This process is involved in the regulation of inflammatory cytokine production by the T lymphocytes [175]. Although less extensively studied, B lymphocytes show also dramatic changes in K^+ channel phenotype during differentiation and activation, paralleling T-cell changes [173]. Kv1.3 channel expression has been also reported to increase upon activation and differentiation in response to inflammatory injury in macrophages, and its blockade inhibits migration and

proliferation [174]. Kv1.3 also participates in cholesterol metabolism and flux regulation in macrophages by reducing the cholesterol contents [176]. According to these effects, it is clear that Kv1.3 affect the specific immune responsiveness by the regulation of synthesis and secretion of inflammatory cytokines like TNFα and IL-6 and the participation in proliferation and differentiation of the immune cells. Thus, Kv1.3 is recognized as one of the main actors in the immune system response. Such an important role has its downsides, as dysregulation or malfunction produces severe and often chronic inflammatory diseases.

On the other hand, other studies suggest that Kv1.3 may participate in the pathways that regulate energy homeostasis and body weight due to it is expression in neurons may affect in the central nervous system (CNS) [177]. However, the exact mechanism by which Kv1.3 regulates energy homeostasis and body weight is not yet understood. Additionally, Kv1.3 seems to play a role in central insulin sensitivity at the olfactory bulb sensing the body metabolic state [178] due to some results suggest that the functional linkage between Kv1.3 and insulin receptor in the CNS is implicated in insulin signalling [179]. As it is expressed in insulin-sensitive tissues [174, 180-182], Kv1.3 has also been found to participate in the peripheral insulin response. Another study showed that Kv1.3 gene deletion and channel inhibition enhanced peripheral insulin sensitivity by increasing the amount of glucose transporter 4 (GLUT4) at the plasma membrane and the uptake of glucose in insulin sensitive cells via intracellular Ca^{2+} signalling. The hyperpolarization of the membrane causes a decrease in the secretion of TNFα and IL-6 that leads to improve the signal cascade of insulin receptor [182] (figure 18). Therefore, Kv1.3 may play a critical role in insulin action by controlling peripheral insulin sensitivity, although this channel is not associated with insulin secretion in pancreatic β-cells. Due to this, Kv1.3 has been suggested as a putative target for obesity and T2D [183].

8.1. Kv1.3 INHIBITION AND INSULIN RESISTANCE

Several physiological effects are attributed to Kv1.3 and, particularly, to its inhibition. Among them, we can find the participation in energy homeostasis and body weight control [177]; in the peripheral insulin sensitivity; and in the inflammatory system

participating in the proliferation and differentiation of immune cells including the regulation of the synthesis and secretion of cytokines, which plays a central role in chronic inflammation diseases [184]. According to this, inhibition of Kv1.3 can be considered as a putative pharmacological target for the treatment of metabolic diseases like obesity or type 2 diabetes mellitus (T2D) and autoimmune diseases with chronic inflammation diseases such as psoriasis [185].
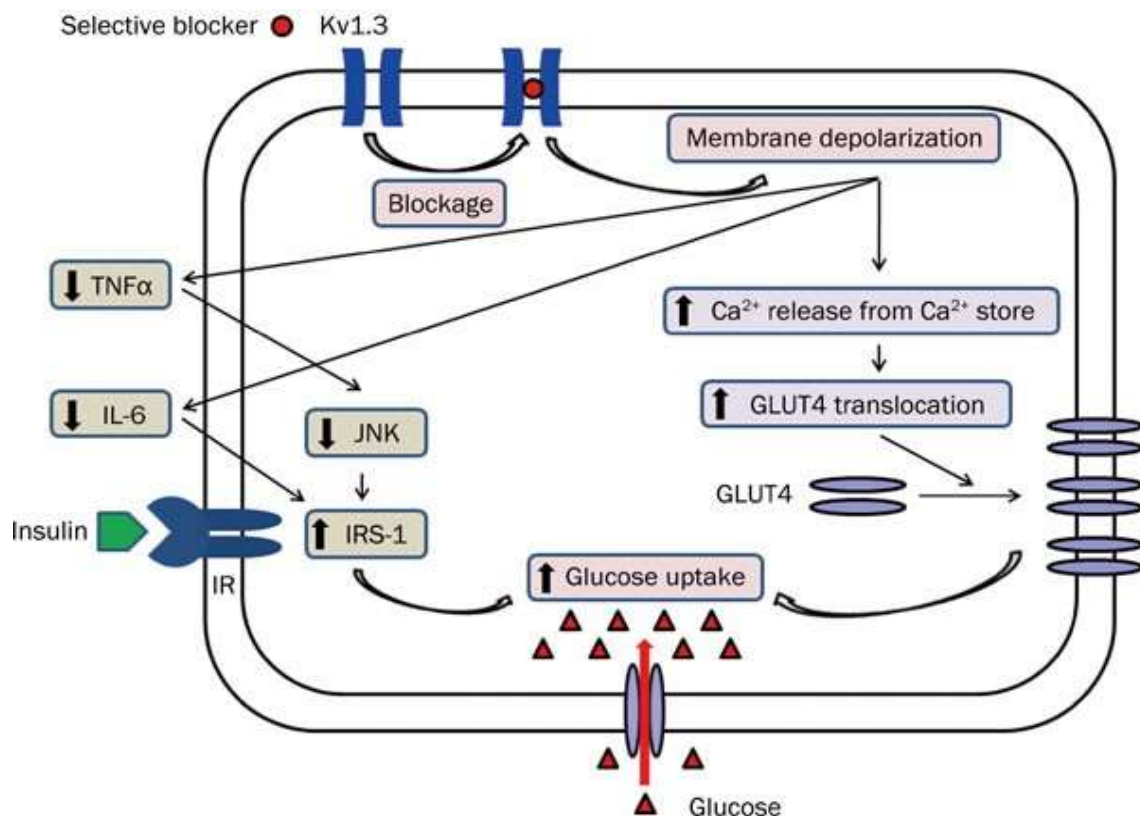
Figure 18. Effects of the inhibition of Kv1.3 on insulin sensitivity and glucose homeostasis in insulin sensitive cells like adipocytes. Adapted from Kv1.3: a potential pharmacological target for diabetes. *Acta Pharmacologica Sinica*. Choi, BH (2010).

Inhibition of Kv1.3 channel increases peripheral insulin sensitivity in skeletal muscle and adipose tissue through GLUT4 membrane translocation in a Ca^{2+}-dependent process [182] as previously explained (figure 18). However, the role of Kv1.3 in adipose tissue is controversial [186, 187]. In previous publications, the use of Kv1.3 blockers in the treatment of obesity and insulin resistance induces brown, more than white, adipocyte activity, leading to enhanced metabolism, increased body temperature and impaired adipogenesis, which mimics the $Kv1.3^{-/-}$ lean phenotype [183]. Furthermore, central insulin sensitivity improvement as well as body weight and energy homeostasis

regulation associates with effect in the olfactory bulb. In fact, a study with Kv1.3[-/-] mice displayed a lean phenotype and diet-induced obesity protection associated with a higher basal metabolic rate. Mice remained euglycemic and exhibited low blood insulin levels [181]. This phenomenon could be a consequence of increases in physical activity and basal metabolic rate, which depends on the olfactory bulb. Another study reported that Kv1.3 gene deletion reduced adiposity and total body weight in the melanocortin-4 receptor-null mice, a genetic model of obesity, by increasing both locomotor activity and mass specific metabolism [188]. This may be also related to the CNS effect.

Moreover, Kv1.3 promotes cytokine secretion and migration through Ca^{2+} signalling regulation in macrophages. Although the open debate, and the disparity of data, Kv1.3 plays an important role in the immunomodulation of the immune cells. Inhibition of Kv1.3 has been reported that inhibits the differentiation and proliferation of different T-Cells, B-cells and macrophages [173-175]. Kv1.3 blockade also decreases the secretion of proinflammatory cytokines, which cause chronic inflammation, by T-cells and macrophages [189].

These findings envisage Kv1.3 as a target in the pharmacological treatment of insulin resistance related pathologies like obesity and T2D that have links with inflammation, new pandemic diseases in industrialized countries, calling for new pharmacological strategies.

8.2. PAP-1, A PHARMACOLOGICAL INHIBITOR OF Kv1.3 CHANNEL

The previously explained effects of Kv1.3 ablation and pharmacological inhibition on insulin sensitivity suggest that this channel could be an attractive target for the treatment of type 2 diabetes. Several specific inhibitors of Kv1.3 have been identified, allowing for detailed investigations of channel function to be performed. As previously explained, K^+ channels are the most diverse family of ion channels and contribute to many important physiological functions in various tissues. Thus, a K^+ channel blocker, as an ideal and safe therapeutic drug, should act selectively and potently on the specific target K^+ channels without affecting other ion channels. In this sense, the best selective

inhibitor that showed the best effect in peripheral insulin resistance improvement as well as in glycemic control is PAP-1 [183].

PAP-1, 5-(4-Phenoxybutoxy) psoralen), was developed as a selective small molecule inhibitor of Kv1.3. PAP-1 potently inhibits Kv1.3 with an EC50 of 2 nM and exhibits good selectivity over other Kv channels (23-fold over Kv1.5, 33-fold over other Kv1 family members). PAP-1 binds to the C-type inactivated state of Kv1.3, thus functioning as a use-dependent blocker of the channel. PAP-1 further exhibits an excellent selectivity for Kv1.3 over other ion channels, transporters, receptors, and P450-dependent enzymes; and it is not found to be phototoxic, cytotoxic, or mutagenic [190].

Taken together with its relatively high lipophilicity, this pharmacological profile might make PAP-1 an ideal drug for the clinical treatment of disease related with chronic inflammation or insulin resistance.

HYPOTHESIS AND OBJECTIVES

HYPOTHESIS

The data on cardiac arrhythmic morbidity and mortality in diabetic patients lead us to hypothesize that the differences in the response to the different antidiabetic treatments available may be due to differences in their antiarrhythmic potential. Based on clinical evidence, experimental work, and our preliminary results with the drug PAP-1, we hypothesized that a reduction in cytokine release, through modulation of the inflammatory system, will both improve insulin resistance as well as cardiac electrical remodeling. The results obtained from both genetic and pharmacological blockade of the Kv1.3 channel place it as a very promising new therapeutic target. In this regard, PAP-1 (Kv1.3 channel blocker) is a drug currently in clinical study for other inflammatory diseases, which would facilitate its use in diabetes.

In summary, our hypothesis is that blocking Kv1.3 channels is an effective hypoglycemic treatment that improves cardiac electrical remodeling and could decrease the susceptibility to arrhythmias in patients with T2D.

OBJECTIVES

➢ To establish and validate a metabolic model for type 2 diabetes.

➢ To study whether the established metabolic model of type 2 diabetes reproduces the type 2 diabetes electrocardiogram alterations.

➢ To describe whether the type 2 diabetes model also has a low-grade inflammation status.

➢ To establish the role of low-grade inflammation in the cardiac electrical remodelling.

➢ Targeting the immune system to modulate the inflammatory status of type 2 diabetes to observe whether this immunomodulation improves the pathophysiology of diabetes in both metabolic disturbances and cardiac electrical remodeling.

MATERIAL AND METHODS

MATERIAL AND METHODS

1. MAIN MATERIALS:

- ❖ **PAP-1:** Oxchem

- ❖ **Cremophor:** Sigma-Aldrich

- ❖ **Metformin:** Sigma-Aldrich

- ❖ **Streptozotocin:** Sigma-Aldrich

- ❖ **Glucose:** Sigma-Aldrich

- ❖ **Insulin:** Sigma-Aldrich

- ❖ **Insulin ELISA kit** Cloud-Clone Corp.

- ❖ **Cholesterol and Triglycerides reactive kits:** Spinreact

- ❖ **Cytokine multiplex detection kits:** Bio-Plex Pro TM, Bio-Rad

- ❖ **High fat diet:** D12451, Research Diet Inc

- ❖ **ECG recordings:** Biopac MP35 and cable SSL2 (Biopac Systems Inc.).

- ❖ **Patch clamp recordings:** Axopatch 200B amplifier (Molecular Devices) connected to the digitizer Digidata 1140 (axon Instruments Inc) and Leica inverted microscope.

2. ANIMAL HANDLING AND ETHICS

The investigation fulfils the European (86/609/EEC) and the Spanish (RD 53/2013) rules for the care of animals used for experimental and other research purposes, and has been approved by the Ethics Committee for Animal Care of the University of the Basque Country with reference CEBA/273M/2012.

Male Sprague-Dawley rats (8 weeks aged and 180-220g weight) were housed in a room of a certified animal-housing facility with temperature (22±1ºC) and humidity (50%) controlled under a 12:12 light: dark alternant cycle. Water and diet were provided ad libitum.

3. METABOLIC-INDUCED TYPE 2 DIABETES ANIMAL MODEL
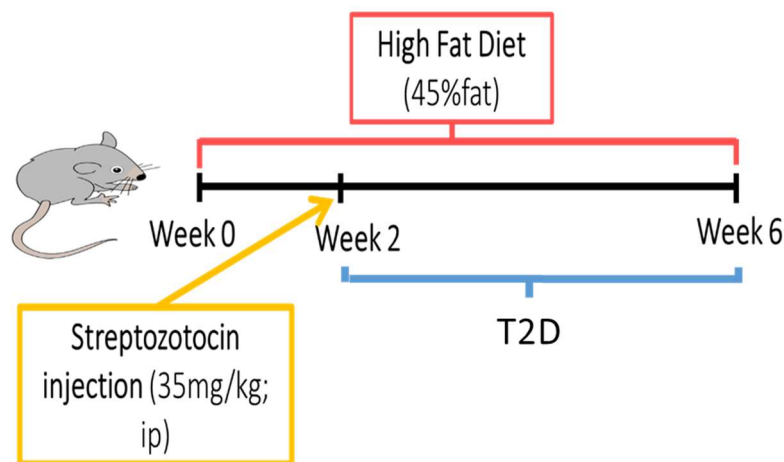
Figure 19. Type 2 diabetes rat model

According to previous literature [63-65, 191], the materialization of the disease pattern was achieved by combining the feeding of a high-fat diet (HFD) with a low dose injection of streptozotocin (STZ). In figure 19, we schematize the type 2 diabetes animal model.

Diabetic rats were fed during 6 weeks with a HFD (Research Diets Inc.) that induces insulin resistance. It is known that increased fat intake is associated with metabolic diseases such as type 2 diabetes. Fat is the main source of energy of HFD. Therefore, nutrients contribution to the energy of the used HFD was 45% fat, 20% protein and 35% carbohydrate, as a percentage of total kcal. Specific nutrients composition of the diet is provided below. Besides, control animals were fed with chow diet that has a completely different nutrients contribution to the energy. In fact, carbohydrates mainly provide chow diet energy. In this case, the diet composition was 65% carbohydrate, 20% protein and 15% fat, as a percentage of total kcal.

After 6 weeks, the feeding with a high-fat diet induces insulin resistance but does not induce hyperglycaemia. Because of that, hyperglycaemia was achieved by a low dose STZ injection. Thus, at week 2 of the experimental period, rats received an intraperitoneal injection (IP) of STZ. Rats were maintained under overnight fasting

before the injection. According to previously cited literature, the chosen STZ dose was 35 mg/kg. STZ was dissolved in 0.1 mol/L citrate buffer, pH 4.5. IP injection was done in anesthetized animals with a sterile single-use syringe of 25G (B|Braun).

❖ **High fat diet (D12451, Research Diet Inc.) composition:** 200g Casein, 80 Mesh; 3g L-Cystine; 72.8g Corn Starch; 100g Maltodextrin 10; 172.8g Sucrose; 50g Cellulose BW200; 25g Soybean Oil; 177.5g Lard; 10g Mineral Mix S10026; 13g DiCalcium Phosphate; 5.5g Calcium Carbonate; 16.5g Potassium Citrate, 1 H2O; 10g Vitamin Mix V10001; 2g Choline Bitartrate; 0.05g FD&C Red Dye #40. Total: 858.15g

In any case, an intraperitoneal injection of low dose streptozotocin such as 35 mg/kg is expected to cause damage in the β-cell mass enough to induce a relative lack of insulin and lead to hyperglycemia but not for destroying all beta cells, which would cause type 1 diabetes. Because of that, glucose and insulin levels were controlled to ensure that animals have type 2 diabetes. Thus, after 72 hours of the STZ injection, fasting plasmatic glucose levels were measured, and only animals with a glucose range between 130 mg/dl and 250 mg/dl were selected for carrying out with experiments. The rest of the animals, including animals that did not show any plasma insulin level, were discarded. Non-discarded animals followed with the HFD feeding for 4 weeks more after the STZ injection. The efficiency of the method was about 75%.

Additionally, the model had to be validated, confirming that the effects observed in the model were due to the pathology, and not because of the isolated effect of the HFD or STZ. According to this, two more animal groups were created for the validation of the model. So, the same experimental protocols than for diabetic and control animals were applied to these groups. In the table 2, we summarize the groups for the validation of the type 2 diabetes animal model. The HFD group was only fed with the high fat diet for 6 weeks. In other words, in the HFD group animals were fed with high fat diet and had no STZ injection at any point of the experimental period. The STZ group was only fed with standard chow diet (as control animals) for 6 weeks. However, animals received a STZ injection (as in the diabetes model). Thus, at week 2 of the experimental period,

animals received a 35 mg/kg IP injection of STZ. Then, animals were controlled until the end of the 6 weeks experimental period.

Week 0   Week 2   Week 6

72 h
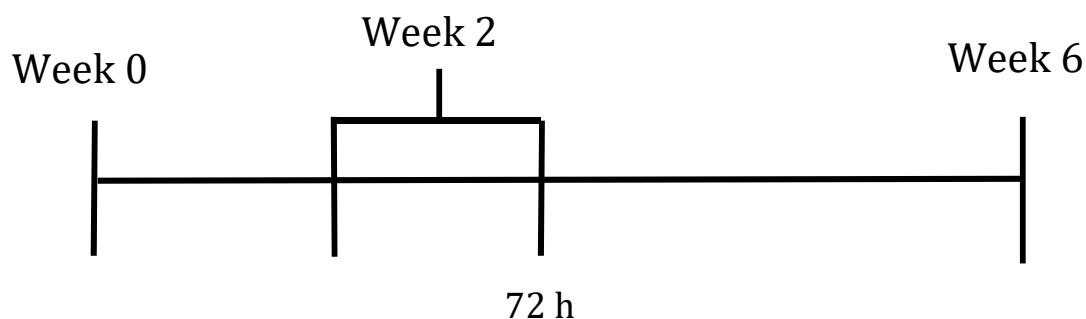
CNTRL	Chow	Vehicle	-		IPIGGT, TG and Cholesterol, Insulin, cardiomyocytes isolation, electrophysiology recordings, WB and calcium sparks.
HFD	HFD	Vehicle	-	Weekly glucose levels and ECG	
STZ	Chow	i.p; 35 mg/kg; STZ injection	High glucose confirmation		
T2D	HFD	i.p; 35 mg/kg; STZ injection	High glucose confirmation		

Table 2. Type 2 diabetes rat model follow-up. The chronological line of our experimental period is above the table of the experimental groups. The diet administrated, the injection as well as the experiments done correlates in the chronological bar to the time-point when was done in our experimental period.

4. TREATMENTS FOR T2D

4.1. PAP-1, A NOVEL THERAPEUTIC TARGET

We use a Kv1.3 channel blocker, PAP-1, in our animal model of T2D. PAP-1 was manufactured by Oxchem and was chemically formulated as previously described [192]. PAP-1 is a poorly water-soluble pharmacological agent. Therefore, it had to be dissolved

in 25% Cremophor (Sigma-Aldrich) solution, a mixture of 25% Cremophor and 75% phosphate-buffered saline (PBS). Cremophor is a mixture of polyoxyethylated triglycerides, by reacting castor oil with ethylene oxide in a molar ratio of 1:35, which acts as a nonionic surfactant and serves as a formulation vehicle for poorly-water soluble pharmacological agents. Cremophor 25% solution was prepared in advance and the stock solution was kept at 4ºC for several weeks. Furthermore, to facilitate the solution of PAP-1 in the Cremophor 25% solution, medium heat was applied while shaking the solution.

For in vivo treatment and, after type 2 diabetes was confirmed as previously described, the animals treated with PAP-1 received a daily intraperitoneal injection for 4 weeks. The dose was adjusted to control the glucose levels. Thus, the doses varied from 5 mg/kg to 10 mg/kg. Doses were selected according to previous bioavailability and effectiveness studies made in rats that received intraperitoneal injections of PAP-1 [193]. However, for in vitro treatments, PAP-1 was administered to the cultured medium of isolated cardiomyocytes in a concentration of 1 mM. Cells were incubated or 24h with PAP-1 before the electrophysiological recordings.

A novel therapeutic approximation to any pathology has to demonstrate that it is more beneficial than the current treatments for the pathology. Thus, we had to compare PAP-1 treatment with metformin, the first-choice drug for T2D. In rats, we emulated the clinical administration of the drug. Therefore, metformin was administered orally, and the dose was adjusted for an intensive glucose control as in clinic. Metformin was dissolved in water and was administered daily in drinking water, and metformin dose was adjusted to the weight of the rats and the metabolic rate.

On the other hand, according to literature, the metabolic rate of the rats is 6.4 times faster than humans. As type 2 diabetes patients usually receive a dose between 1500 mg/day and a 2550 mg/day (maximum dose), and we considered a 70 kg patient as a standard patient, then, a 70 kg patient with a maximum dose of metformin (2550 mg/kg) receives a dose of 36 mg/kg*day. Thus, applying the metabolic rate of the rat (6.4), the maximum dose of metformin in rats would be 233 mg/kg*day, according to our established parameters. Considering all these, we ranged our doses for an intensive

control glucose between 50 and 200 mg/kg*day depending on the weekly glucose levels of the animals. In the table 3, we summarize the treatments of the model.

Week 0   Week 2   Week 6

72h

CNTRL	Chow	Vehicle	-	-		
T2D	HFD	i.p; 35 mg/kg; STZ injection	Hyperglycemia confirmation	-	Weekly glucose levels and ECG	IPIGTT, TG and Cholesterol, Insulin, myocytes isolation, electro-physiology recordings, WB and calcium sparks.
T2D+ MET	HFD	i.p; 35 mg/kg; STZ injection	Hyperglycemia confirmation	Intensive glucose control with metformin (50-200 mg/kg)		
T2D+ PAP-1	HFD	i.p; 35 mg/kg; STZ injection	Hyperglycemia confirmation	Intensive glucose control with PAP-1 (5-10 mg/kg)		

Table 3. Type 2 diabetes treatment follow-up. The chronological line of our experimental period is above the table of the experimental groups. The diet administrated, the treatment used and the injection as well as the experiments done correlates in the chronological bar to the time-point when was done in our experimental period.

5. BIOMETRIC MEASUREMENTS

5.1. IN VIVO BIOMETRIC MEASUREMENTS

Possible biometric obesity markers such as body weight, abdominal perimeter, and body length were measured weekly during the entire procedure. These non-invasive measures were done in vivo to the rats while the glucose measurements.

The body weight was measured to conscious rats that were weighted in a commercial lab-scale (NVT, Ohaus). Abdominal perimeter and body length were measured to isoflurane-anesthetized rats. Thus, rats were quiescent, and the measurements were more reliable. The abdominal perimeter was measured with a measuring tape around the abdomen of the rat, always measuring the same area. Additionally, body length was measured from the nose to the tail base with a measuring tape.

With all these parameters, the body mass index (BMI) was calculated. BMI is a value derived from the mass (weight) and height of an animal. The body length of the rat was used as a body height. The BMI is defined as the body mass divided by the square of the body height and is universally expressed in units of kg/m^2. Thus, the following formula was used for calculation: BMI = Weight (kg) / Body length^2 (m^2).

5.2. POST-MORTEM BIOMETRIC MEASUREMENTS

Some biometric measurements cannot be performed in vivo because they are too invasive and can induce unnecessary suffering and even death. Thus, it is not ethical to sacrifice animals only for this purpose. Thus, when at the end of the experimental time rats were sacrificed for other purposes such as patch-clamp, these invasive biometric measurements were also obtained from the same rats. The relevant biometric measurements collected were tibia length, periepididymal fat and heart weight.

A. HEART WEIGHT

The heart was removed by cutting the aorta, was mechanically stripped of fat and appendages, and was weighted with a Laboratory balance. Furthermore, the rat was weighted with a balance before anesthesia.

B. TIBIA LENGTH

Tibia length provided a more accurate indication than body weight of the relative heart weight of the rat. For measuring the tibia length, one leg was severed above the knee joint, and the muscle and skin of the tibia were removed by mechanical stripping. Then, the length of the tibia from the condyles to the tip of the medial malleolus was measured with micrometre Vernier callipers.

C. PERIEPIDIDYMAL FAT

We collected periepididymal fat as a representative part of visceral fat. First, the peritoneum was cut from the diaphragm to the rectum mid coronally to expose abdominal organs. Then, the testes were located and the attached white adipose tissue was identified. Once it is located, epididymal fat depots were carefully dissected from both the testes, epididymides, and vasa deferentia. When it is completely cleaned, it was weighed with a previously tared balance. Finally, fat pads were transferred to 2 ml tubes and were kept at -80ºC for conservation.

6. FOOD AND WATER INTAKE

Rats were individualized in cages, in other words, one rat was placed in one cage. As previously explained, food and water was provided ad libidum (figure 20). However, measurements of the food and water intake were done as explained. The food was weighted weekly with a calibrated balance. 400g of pellet diet were placed on each cage. Then, 7 days later at the same time point, the remaining diet was collected and was weighted again with the same calibrated balance. We checked that the rat did not hid

any food into the cage. The weight difference between the provided diet amount and the resting diet amount was considered the weekly food intake. When we split this into 7 days, we can estimate the daily food intake.

Similar procedure was used for the water intake measurement. A bottle filled with 1L of water was placed on each cage. Then, 7 days later at the same time point, the remaining water into the bottle was collected and was measured with a graduated cylinder. The difference in the liquid volume between the provided water and the remaining water was considered the weekly water intake. When we split this into 7 days, we can estimate the daily water intake. Data was collected in excel for analysis and plot.

Figure 20. Individualized animal drinking water in a cage with HFD.

7. SERUM COLLECTION FOR ANALYSIS

Serum is used in numerous diagnostic tests because it allows measuring the concentration of many molecules. Because of this, we collected quite amount of blood and we extracted the serum from it at the end of our experimental period. To obtain serum, a blood sample is allowed to clot. The sample is then centrifuged to remove the clot and blood cells, and the resulting liquid supernatant is considered the serum.

For this procedure, rats were fasted overnight. At the beginning, rats were immobilized in a trap and the tail of the rat was immersed in a bath at 37ºC for 1 minute for inducing vasodilation. Additionally, the trap containing the rat was laid on an electrical blanket avoiding the loss of body temperature (figure 21).

Then, a fast and not very deep cut above the vein was done with a scalpel. Blood was collected into a 1.5 ml eppendorf using heparinized capillaries. If collected blood was not enough either a smooth massage in the tail for helping the blood to come out or another cut in the tail could be done for collecting more blood. Immediately after of the blood collection, Eppendorf was kept on ice while other procedures are done.

When all the blood collections were finished, eppendorfs were kept at room temperature for 30' to let the clot to form. Then, they were centrifuged between 2000 and 3000 G for 15 minutes. Just after the centrifugation, the supernatants of the Eppendorf were collected in another 1.5 ml eppendorf, were labelled, and were quickly stored at -80ºC for long-term conservation.

A   **B**
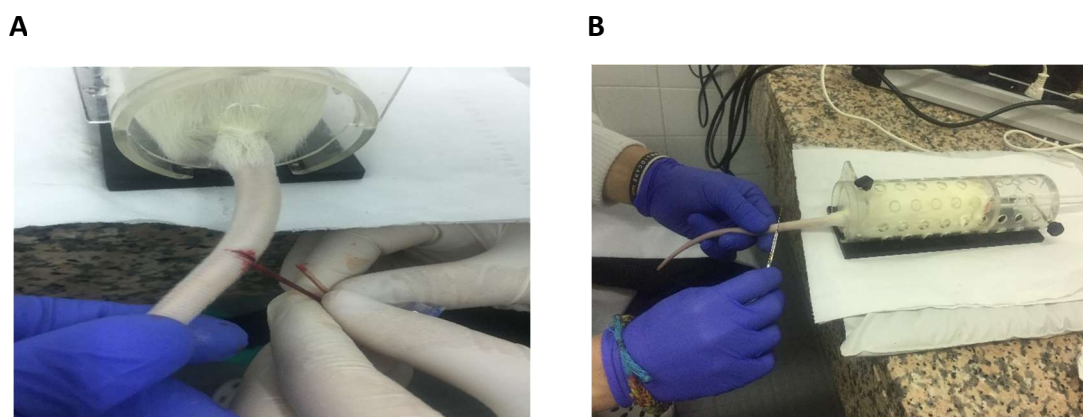
Figure 21. Blood collection. **A)** Blood collection from a tail vain cut using a heparinized capillary. **B)** Rat placed in a trap while doing a cut with a scalpel

8. BLOOD GLUCOSE LEVELS

Blood glucose levels were measured weekly during the entire procedure. These measurements were made after an overnight (16 h) fasting. In the late afternoon, rats were changed to a clean cage that contained new sawdust to ensure that no food rests remained in the cage. Sixteen hours later, blood glucose levels were measured from the tail vein of the rats. For this procedure, rats were anesthetized by isoflurane inhalation. Anesthesia is applied by using a full anesthesia equipment (MSS International, LTD). Animals were placed in a closed box insufflate with vaporized isoflurane in oxygen

(figure 22). When the animal is under unconscious state, it is moved to a platform where can be manipulated while it is still receiving anesthesia through the upper respiratory tract. The concentration of isoflurane can be adjusted by the researcher. Unconsciousness state was induced with 3-4% isoflurane and maintenance was done with a lighter concentration (between 1-2%). Blood was collected from a small drop of the tail vein of the rat. By using a 23G needle (B| Braun) a small prick was done in the tail vein and a drop of blood was collected with the glucometer (figure 22). Glycaemia was measured with blood drop glucose strips (Glucomen, Menarini) in a commercial glucometer (Glucomen aero 2k, Menarini diagnostics).

A   **B**
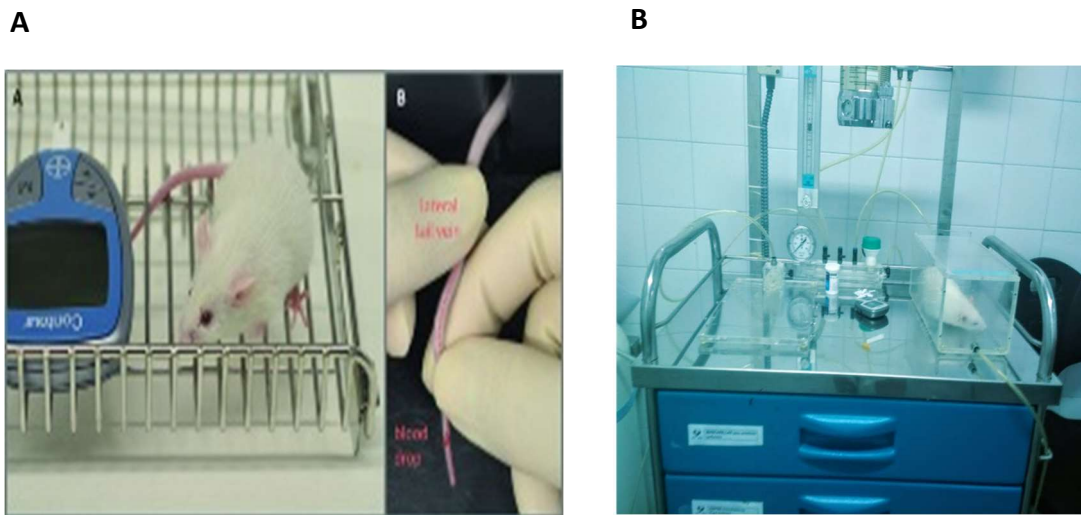
Figure 22. Glucose measurements. A) Blood drop collection for glucose measurement. **B)** Anesthesia set-up

9. INSULIN RESISTANCE

There are multiple ways to measure insulin resistance such as fasting insulin levels or glucose/insulin tolerance tests. Presence of insulin in hyperglycemic animals indicates insulin resistance as well as does difference between control and diabetic in glucose/insulin tolerance test. Then, to make our results more consistent, we performed both kind of experiments.

9.1. INTRAPERITONEAL INSULIN GLUCOSE TOLERANCE TEST

Insulin resistance can be analyzed by the glucose tolerance test, as it is reported in previous literature. However, insulin sensitivity can be analyzed by the insulin tolerance test. Insulin resistance and insulin sensitivity are two sides of the same coin. If you have insulin resistance, you have low insulin sensitivity. Conversely, if you are sensitive to insulin, you have low insulin resistance. In preliminary studies made in our lab, separated tolerance tests caused both severe hyper and hypoglycemia in rats. Thus, we decided to do a combined test consisting of an intraperitoneal glucose injection followed by an intraperitoneal insulin injection. This combined test called intraperitoneal insulin-glucose tolerance test (IPIGTT) is based on a previously described protocol [194].

Solutions were freshly prepared just before the protocol. Glucose (Sigma-Aldrich) was dissolved in distilled water and was prepared for a dose administration of 1 g Glucose/kg rat. On the other hand, insulin (Sigma-Aldrich) was dissolved in 1.5 Molar Tris-HCl buffer (pH 7) and was prepared for a dose of 1 Units of Insulin/kg rat. Volumes and concentrations of solutions were adjusted according to the number of animals and the weight of the animals. For our commercial insulin, 1 mg of insulin corresponds to 25 units.

Figure 23. IPIGTT set-up and material ready to use

Animals were undergone to an overnight fasting (16h) and they were anesthetized by isoflurane inhalation, as previously described. Once the rat is anesthetized and before the injections, the blood glucose level of the rat was measured from the tail vein. This

was considered the first time point (O minutes). Then, the unconscious rat received an intraperitoneal glucose injection following by an intraperitoneal insulin injection. Injections were done using a 1 ml syringe with 23G needle (B| Braun) (figure 23). After injections, blood glucose measurements were performed as explained before and they were repeated at 15, 30, and 60 minutes time points. Finally, results were collected and plot using OriginPro Lab software. Insulin resistance was measured by the area under the curve (AUC) that was calculated by the OriginPro Lab software from the resulting graph of the glucose levels at different time points.

9.2. SERUM INSULIN LEVELS

Serum from overnight fasted rats was obtained as described below and serum levels of insulin were measured with a commercial ELISA kit (Cloud-Clone Corp). The Elisa kit was kept at 2-8ºC until use. Reagents were tempered at room temperature just before use. Elisa has different steps. First, standards, reagents, and solutions were prepared. Standard was reconstituted in 500 μl of standard diluent. After shake it gently and wait 10 minutes at RT, we made 1:3 dilution series by diluting 300 μl of reconstituted standard in 600 μl of standard diluent and 300 μl from this dilution in 600 μl of standard diluent). We did this procedure 4 times. Reagent A was reconstituted in 150 μl of diluent reagent and, after gently shake and wait 10 minutes at room temperature, it was diluted to a working concentration (1:100) in Assay diluent A. Reagent B was also diluted to working concentration (1:100) in Assay diluent B. Wash solution was diluted from 30X concentration to a 1X (20 μl of 30X in 580 μl distilled water).

Once the solutions are ready, we started the assay. For this, we first added 50 μl of standard, blank, or samples to each well. Afterward, we added 100 μl of prepared reagent A to each well and incubate the plate at 37 ºC for 1 hour. After washing 3 times, we added 100 μl of prepared reagent B to each well and incubate the plate at 37 ºC for 30 minutes. Then, we washed 5 times all the wells and we added 90 μl of substrate solution. Again, we incubated the plate for 10-20 minutes at 37 ºC. Finally, we added the stop solution and we read the plate at 450 nm in a spectrophotometer.

The HOMA index was calculated according to previous literature and the formula used was: HOMAi = [fasting glucose (mg/dL) x Fasting insulin (mUI/L)] / 22.5.

10. ANALYSIS OF DYSLIPIDEMIA

Since dyslipidemia is often associated with type 2 diabetes, we tested whether our model reproduces the lipid alterations observed in patients with diabetes mellitus. Thus, serum levels of cholesterol and triglycerides obtained from rats at the end of the experimental period were determined by enzymatic colorimetric using a commercial kit (SPINREACT).

In enzymatic colorimetric analysis, widely used in medical laboratories, the color reaction is preceded by a reaction catalysed by an enzyme. As the enzyme is specific to a particular substrate, accurate results are obtained. Enzymatic analysis are always carried out in a buffer solution at a specified temperature (usually 37°C) to provide the optimum conditions for the enzymes to act. In our case, enzymatic colorimetric procedures consist of the following reactions:

❖ **Cholesterol:**

$$\text{Cholesterol esters} + H_2O \xrightarrow{\text{CHE}} \text{Cholesterol} + \text{fatty acids}$$

$$\text{Cholesterol} + O_2 \xrightarrow{\text{CHOD}} \text{4-Cholestenona} + H_2O_2$$

$$2\,H_2O_2 + \text{Phenol} + \text{4-Aminophenazone} \xrightarrow{\text{POD}} \text{Quinonimine} + 4H_2O$$
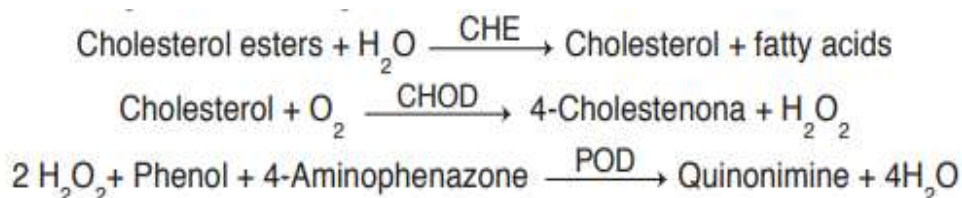
*CHE: Cholesterol esterase; CHOD: Cholesterol oxidase; POD: Peroxidase

❖ **Triglycerides:**

$$\text{Triglycerides} + H_2O \xrightarrow{\text{LPL}} \text{Glycerol} + \text{free fatty acids}$$

$$\text{Glycerol} + \text{ATP} \xrightarrow{\text{Glycerolkinase}} \text{G3P} + \text{ADP}$$

$$\text{G3P} + O_2 \xrightarrow{\text{GPO}} \text{DAP} + H_2O_2$$

$$H_2O_2 + \text{4-AP} + \text{p-Chlorophenol} \xrightarrow{\text{POD}} \text{Quinone} + H_2O$$
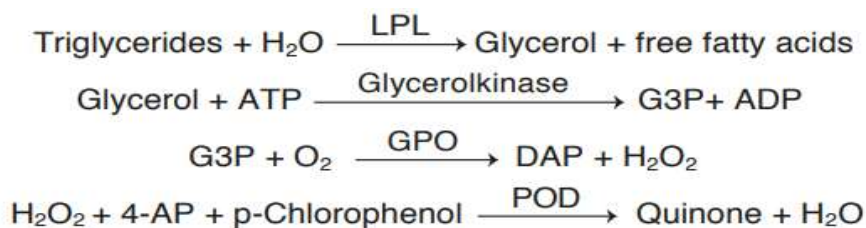
*LPL: Lipoproteinlipase; G3P: glycerol-3-phosphate; GPO: glycerol phosphate dehydrogenase; POD: Peroxidase

Due to these enzymatic reactions, the serum levels of triglycerides and cholesterol are measured because the intensity of the color formed is proportional to the cholesterol and triglycerides concentration in the sample.

Before using them, kits were kept at 2-8ºC. The kit use is quite simple. First, working reaction (WR) was prepared by the reconstitution of the 1 part of enzymes in 1 part of buffer; both part of the kit. Afterward, 1 ml of blank, standard, or sample was added to the tubes. Following, 1 ml of previously prepared WR was applied to each tube. Then, samples were incubated at 37 ºC for 10 minutes until the colorimetric reaction is finished. Finally, samples were read at 505 nm in a spectrophotometer.

Formula below was used for the determination of sample concentration:

$$\frac{(A)\ Sample - (A)\ Blank}{(A)\ Standard - (A)\ Blank} \times 200\ (Standardconc.) = mg/dL$$

11. CYTOKINE DETECTION

A Bio-Plex ProTM (Bio-Rad), specifically the rat Th1/Th2 12-Plex immunoassay, was used for the detection of cytokines. The kit enables researchers to quantify multiple cytokines in a single well of a 96-well plate in 3–4 hours. Bio-Plex Pro Assays are essentially immunoassays formatted on magnetic beads. The assay principle is similar to that of a sandwich ELISA. Capture antibodies directed against the desired biomarker are covalently coupled to the beads. Coupled beads react with the sample containing the biomarker of interest. After a series of washes to remove unbound protein, a biotinylated detection antibody is added to create a sandwich complex. The final detection complex is formed with the addition of streptavidin-phycoerythrin (SA-PE) conjugate. Phycoerythrin serves as a fluorescent indicator or reporter. The Bio-Plex Multiplex System is built upon the xMAP technology. This is based in the fluorescently dyed microspheres (also called beads), each with a distinct color code or spectral address to permit discrimination of individual tests within a multiplex suspension. This allows simultaneous detection of types of molecules (up to 50) in a single well of the 96-well microplate on the Luminex MAGPIX System where the entire sample load volume is injected into a chamber and magnetized into a monolayer. The beads and reporter

fluorophores are excited by LEDs, imaged and detected by CCD technology. Then, a high-speed digital signal processor that efficiently manages the fluorescence data. Data from the reactions are acquired using a Bio-Plex System or similar Luminex based reader. When a multiplex assay suspension is drawn into the Bio-Plex 200 Reader, a red (635 nm) laser illuminates the fluorescent dyes within each bead to provide bead classification and thus assay identification. At the same time, a green (532 nm) laser excites PE to generate a reporter signal, which is detected by a photomultiplier tube (PMT). A high-speed digital processor manages data output, and Bio-Plex Manager Software presents data as median fluorescence intensity (MFI) as well as concentration (pg/ml). The concentration of analyte bound to each bead is proportional to the MFI of the reporter signal.

Both serum and cell culture supernatant were used in this protocol. Only 15 µl of serum or 50 µl of cell culture supernatant were needed for the immunoassays. Serum was achieved from rat blood that was collected at the end of the experimental period, as previously explained.

Kit contents were stored at 4°C and never frozen. Coupled magnetic beads and streptavidin-PE were stored in the dark. All components are guaranteed for a minimum of six months from the date of purchase when stored as specified. Vortexing, shaking, and incubation times have to be done carefully and with special attention. Calibrated pipettes were used for the delivery of accurate volumes during transfer, dilution, and addition steps.

Before running the assay, the total number of wells in the experiment were determined using the Plate Layout Template. It has to be considered that duplicates of standards and blank as well as for the working samples are recommended to be done. Furthermore, the Bio-Plex system has to be calibrated with Bio-Plex Manager Software before setting up the assay. The calibration kit should be run daily or before each use of the instrument to standardize the fluorescent signal.

First, the Bio-Plex® System was started up for warming it up (30 min). Assay buffer, wash buffer, and sample diluent were accommodated to room temperature (RT) and other items such as samples were kept on ice until needed. Working samples were frozen at -80ºC, therefore they were begun to thaw while keeping on ice. Furthermore,

the wash buffer has to be prepared. The working solution has to be at 1X concentration. However, the stock solution is 10X, thus, it has to be diluted in 9x (1 part of stock 10X wash buffer in 9 parts of dH$_2$0). Before the preparation, the 10X stock was mixed by inversion and was ensured that all salts are in solution.

Secondly, samples were prepared for use. For rat serum cytokines, the manufacturer recommends a dilution of 1:4 in the provided Bio-Plex sample diluent. For cell culture supernatant, a recommended dilution was not provided for the manufacturer. Thus, samples were diluted in dilution bufferin a 1:4 ratio.

Thirdly, a single vial of standards was reconstituted in 500 μl of a diluent similar to the final sample type or matrix. It was vortexed for 5 sec and was incubated on ice for 30 min. Prepare dilution series and blank as shown in figure 24. Vortex for 5 seconds between liquid transfers.
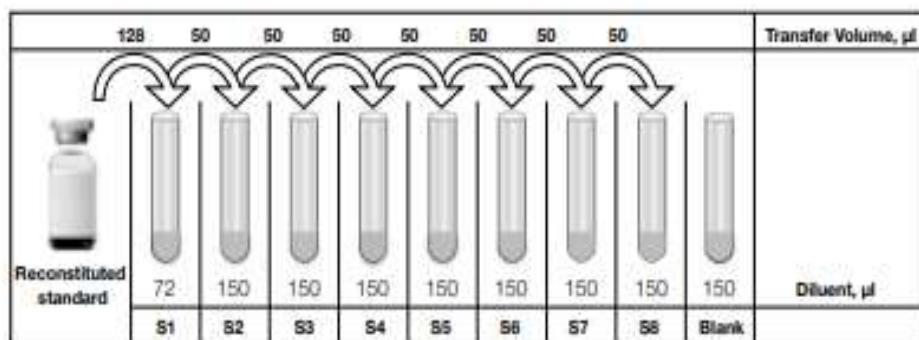
Note: Change tips between each dilution.

Figure 24. Serial dilution of Standard in cytokine detection by Bio-Plex Adapted from Bio-Rad protocol.

Fourthly, 10X coupled beads were vortexed for 30 seconds and were diluted to 1X in Assay Buffer (1 part of coupled beads in 9 parts of assay buffer).

Once all the solutions were ready, the assay procedure started. First, the diluted (1X) beads were vortexed for 10-20 seconds and then, 50 μl was added to each well of the assay plate. Following, the plate was washed 2 times with 100 μl wash Buffer

Afterward, samples, standards, and blanks were vortexed and 50 μl of each were added to the corresponding wells. Next, the plate was covered with sealing tape and was incubated on a shaker at 850 rpm at RT for 1 hour.

After 10 minutes in the incubation, the detection antibodies were diluted to 1X in the provided detection antibody diluent. The stock solution was 10X (1 part of the stock solution and 9 parts of the detection antibody diluent). Before the dilution, detection antibodies were vortexed for 5 seconds and were quick-spun to collect liquid. Once the incubation time was finished, the plate was washed 3 times by adding 100 µl of wash buffer to each well. Next, antibodies were softly vortexed and 25 µl were added to each well. Then, the plate was covered with sealing tape and was incubated on a shaker at 850 rpm at RT for 30 minutes.

Again, the same procedure as with the detection antibodies was performed for the 100X SA-PE. With 10 minutes left in the incubation, the 100X SA-PE was diluted to 1X in the provided assay buffer. The stock solution was 100X (1 part of the stock solution and 90 parts of the detection antibody diluent). Before the dilution, 100X SA-PE were vortexed for 5 seconds and were quick-spun to collect liquid. Next, SA-PE were gently vortexed, and 50µl were added to each well. Then, the plate was covered with sealing tape and was incubated on a shaker at 850 rpm at RT for 10 minutes.

Once the incubation times were finished, the plate was washed 3 times with 100 µl of wash buffer to each well. Next, the beads were resuspended by adding 125 µl of assay buffer to each well. Following, the plate was covered with sealing tape and was incubated on a shaker at 850 rpm at RT for 30 seconds. Finally, the solution was removed and the plate was read using a MAGPIXTM system. Results were exported to excel for handling.

12. CELL ISOLATION AND CULTURE

12.1. CARDIOMYOCYTES ISOLATION

For the study of cardiomyocytes electrophysiology, we had to isolate them (figure 25). Cardiac myocytes were isolated in a Langendorff apparatus. The Langendorff is an *ex vivo* technique used for longer than 90 years in physiological animal research. In the Langendorff preparation, the heart is removed from the animal's body, severing the blood vessels and it is then perfused in a reverse fashion (retrograde perfusion) via the

aorta. This preparation also allows the organ to be digested into individual cells by adding collagenase to the perfuse.
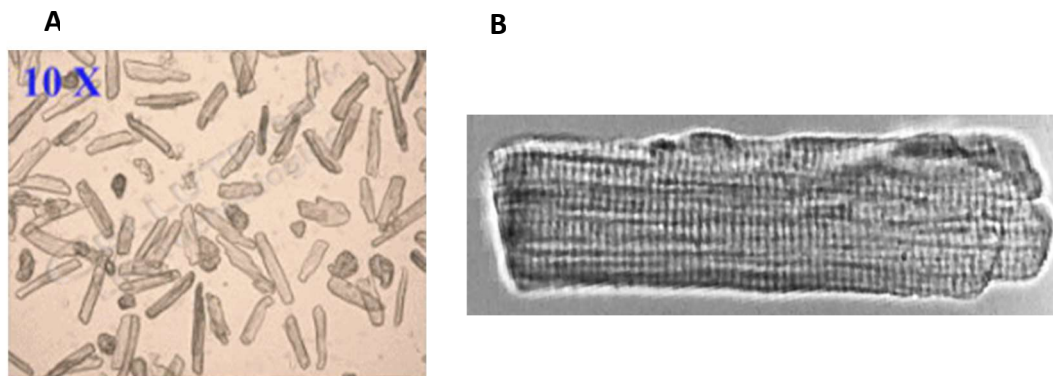
Figure 25. Isolated cardiomyocytes. **A)** Isolated cardiomyocytes in KB medium observed in an optic microscope at 10X. **B)** Isolated cardiomycyte at 40X

The procedure was performed at the end of the experimental period (end of week 6). Thus, animals used were adult male Sprague-Dawley rats between 300-420g. The isolation was performed according to the previously described by our group in the literature [195]. All the solutions used in this experiment, unless otherwise specified, were freshly prepared, oxygenated with 100% oxygen (Air Liquide), and kept at 37ºC. Solutions must be prepared freshly and cannot be stocked longer than 24 hours at 4ºC and have to be set at room temperature before using. The composition and concentrations of the solutions are listed below. The procedure was done under deep anesthesia of the animal. Anesthesia was induced by an intraperitoneal injection of a combination of Ketamine and Xylazine. It is known that this combination shows a synergistic effect resulting in anesthesia with extended analgesia and immobility. Doses used for the drugs were 80 mg/Kg in the case of Ketamine (Anesketin, Dechra) and 10 mg/kg in the case of Xylazine (xilagesic, Laboratorios Calier). Injections of both drugs were always done intraperitoneal.

After the unconsciousness state was induced, rats were surgically cut from the sternum towards the ribs, opening the rib cage, and allowing free access to the heart, which was removed from the body by cutting the aorta. Following, the heart was moved to a beaker containing a fresh Tyrode solution at 4ºC to carefully and mechanically remove the blood by softly pushing to the bottom of the beaker, facilitating the blood

to come out. This was rapidly made for around 15 seconds and repeated twice in another beaker with a new Tyrode solution at 4ºC. Then, using tweezers number 7 (FST, Dumont), the aorta of the heart was immediately inserted into a Langendorff apparatus by using a medical needle (23G) as a cannula and, straight away, it was tied to the needle with a silk suture size 4-0 (figure 26).
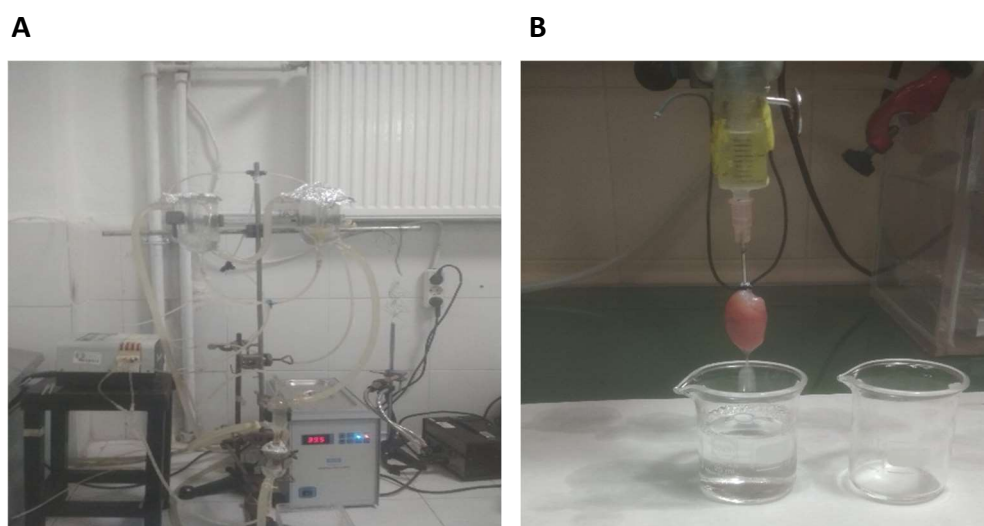
Figure 26. Langhedorff apparatus. A) Langhendorff apparatus used for the isolation**. B)** Rat heart hung in the Langhendorff apparatus for the isolation.

Next, a retrograde perfusion through the aorta was made by gravity, and all the solutions used for perfuse the heart and mentioned below were administrated by this method. Despite of gravity, the flux was tried to keep constant at around 8 ml/min. Different solutions were used for the perfusion of the heart.

First, the heart was perfused with a Tyrode solution, containing 1.8 millimolar of calcium, during a short time (5 minutes maximum). This solution with calcium provokes the heart contraction and helps to remove all the remaining blood in the heart. Thus, we perfused with this solution until we observed that the colour of the solution coming out from heart was clear and not red which means that main blood of the heart was removed.

Secondly, and always with no interruption of the flux, the heart was perfused with a free calcium Tyrode solution for 10 minutes. Calcium may interfere in the effectiveness of the enzymes and make the cardiomyocytes prone to die. Perfusion with free calcium Tyrode will improve the effectiveness of the enzymes as well as reduce the

cardiomyocytes mortality. Furthermore, the free calcium situation induces a stop of the heart contraction that should be observed in the first two minutes after the perfusion with free calcium Tyrode. Thus, the stop of the heart beating after the perfusion with free calcium Tyrode can be used as a checkpoint of the correct perfusion of the heart.

Thirdly, the enzymatic digestion of the heart was done to isolate the cardiomyocytes from the cell matrix. For this purpose, and always without interrupting the flux, the heart was perfused for 15 minutes with an enzyme solution, containing 1 mg/ml (approximately 260-320 UI/ml) of type II collagenase (Worthington Biochem Corp) and 0.03 mg/ml of protease XIV (Sigma-Aldrich) dissolved in free calcium Tyrode solution. In our case, we prepared 30 ml of the enzymatic solution for one isolation and reused them by refilling the perfusion system with the used solution to optimize the enzyme consumption. Importantly, collagenase activity varies significantly between lots which requires the new acquired batches to be tested for isolation at a range of concentrations.

During the enzymatic digestion, the heart should become softer and, as the enzymes digest the cellular matrix, although the flux is constant, the resistance is lower and the pass through the heart should be faster as time passes. At the end of the digestion, isolated cardiomyocytes can be observed from a drop of the perfusion. Little alterations in the time of the enzymatic digestion could be done according to the empirical observations made during the perfusion or in previous isolations.

Finally, the heart was perfused with 60-80 ml of KB medium for cleaning the heart, stopping the enzymatic digestion, and improving the survival of the cardiomyocytes. When the perfusion was finished, the heart was taken down from the Langedorff apparatus, it was dissected, disposing of the atrium, and the ventricles were moved to a glass Petri dish that contained a small amount of KB medium. There, each ventricle was isolated by cutting it with scissors and using the help of tweezers number 7. The isolated ventricle was placed in a plastic beaker that contained 10 ml of KB medium and making small cuts to the ventricle, but without dispersing the ventricle. Then, using the tweezers, the ventricle with the small cuts was strongly shaken against the borders of the plastic beaker (from side to side) for a few times to disperse the digested cardiomyocytes. The color of the solution should change to a yellow shade because of

the presence of the digested cardiomyocytes. Moreover, the color of the heart should turn into a paler shade due to the absence of cardiomyocytes. To check the success of the isolation, we took a drop from the beaker, dropped it on a coverslip, and observed at 10 X magnification in an optic microscope. In this way, we can observe the survival of the cells and the morphology and the contractibility. Depending on the following procedures, cells were treated in different ways since this point.

- ❖ **Calcium free Tyrode (in mM):** NaCl 130; KCl 5.4; $NaHCO_3$ 24; $MgCl_2$ 1.05; NaH_2PO_4 0.42; Dextrose 12; Taurine 20. The pH was adjusted to 7.4 with NaOH.
- ❖ **Tyrode with calcium (in mM):** Same composition than Tyrode free calcium but suplemeted with 1.8 mM of $CaCl_2$.
- ❖ **Enzymatic solution (in mM):** 1 mg/ml of type II collagenase (Worthignton Biochem. Corp.) and 0.03 mg/ml of Protease XIV (Sigma-Aldrich) dissolved in calcium free Tyrode solution with the same composition than explained above**.**
- ❖ **KB medium (in mM):** Taurine 10; Glutamic acid 70; Creatine 5; Succinic acid 5; Dextrose 10; KH_2PO_4 10; KCl 20; HEPES-K 10; EGTA-K 0.2. The pH was adjusted to 7.4 with KOH.

12.2. CARDIOMYOCYTES CELL CULTURE

For the culture to be successful several important features of the initial conditions must be considered. The initial quality of the isolation must be as high as possible, yielding a high percentage of rod-shaped myocytes. Moreover, the cells must be Ca^{2+} tolerant to avoid sarcoplasmic reticulum calcium overload and terminal contracture. Thus, cardiac myocytes must be subjected to a calcium adaptation protocol to make them tolerant to calcium and improve cell survival.

Calcium is critical for the suitability of the cardiomyocytes in physiological conditions. Furthermore, the medium used contains calcium. Thus, several washes with calcium gradient solutions had to be done to adapt the cells to calcium and reduce the cell mortality. The calcium gradient went from free calcium to the medium final concentration of calcium, 1.8 mM. The adaptation to calcium consisted of four steps.

Calcium increasing concentration was prepared by the addition of $CaCl_2$ to filtered Tyrode solution. Four different calcium concentrations were used: 0.1 mM; 0.5 mM; 1 mM and 1.8 mM. Solutions were prepared freshly on the day of the experiment and were kept at 37ºc for use. Only when the plates are coated, the medium is prepared and the calcium gradient is ready, the cell culture can start.

After the isolation, freshly isolated myocytes to be plated are brought into the laminar flow cabin. Cardiomyocytes floating in KB were moved to a 15 ml falcon that was kept at 37ºC. Once the cells settled down in a pellet, the supernatant was removed, and 10 ml of Tyrode 0.1 mM calcium were added again to the falcon while softly resuspending. Once the cell pellet is formed again, the same procedure was repeated for the next Tyrode solutions: 0.5 mM and 1 mM and 1.8 mM calcium. After resuspending the cells with 2 ml of Tyrode 1.8 mM calcium, the cells were seed through the plate with a pipette. 1 ml of cell suspension was used for each 60 mm diameter culture dish and 300 ml for each coverslip of the 12-well plate. Following, seeded cells were kept in an incubator at 37ºC and 5% CO_2 for 30 minutes. Cells that are not alive or are in a poor condition will die during the calcium adaptation or will not attach to the laminin. Thus, after 30 minutes, the liquid was carefully collected from the plate, and cells were softly washed with tempered Tyrode 1.8 mM for 3 times by using a pipette. Afterward, the preheated medium at 37ºC was kindly added to the plate until covering the bottom. For the 60 mm dish, 2 ml of medium were added to each dish. For the 12-well plate, 500 μl of medium were added to each well. Once the medium was added, the plates were placed in the incubator at 37ºC and 5% CO_2 and were kept for 24 hours. Before the incubation, it is recommendable to look at the plate on the microscope and check the cell shape and survival. With this method for the primary culture of cardiomyocytes, we reach to a 95% of purity and up to 70% of survival. Furthermore, survivor cardiomyocytes are tolerant of calcium and, thus, suitable for molecular and electrophysiological studies.

According to literature [196], rapid attachment to the plate results in better retention of *in vivo* myocyte morphology and functionality and ease of use in experiments. This method consists of a rapid cell attachment using a serum-free medium and coating of the culture substrate with a material to aid adherence. Thus, we decided to use this

method for our cardiomyocytes cell culture. In this method, an adhesion factor has to be added to induce the cardiomyocytes cell attachment to the culture plate. Substrate agents used to coat the coverslips or dishes must be selected with care to avoid unwanted changes in cell function. There are a wide variety of attachment proteins in the extracellular matrix and different types can be used depending on the cell type that wants to grow. Commonly used culture substrate coatings include laminin, fibronectin, poly-d-lysine, or synthetic peptides. Laminin, a component of the extracellular matrix, is the most used attachment factor in the bibliography. The use of laminin as a culture substrate produces strong myocyte adherence by binding of β1-integrin surface receptors. However, it must be noticed that attachment factors such as laminin can affect several cell functions. For example, atrial myocytes plated on laminin exhibited significantly reduced NO-dependent rebound in ICa-L following acetylcholine withdrawal and enhanced β2 along with reduced β1 signaling as published by other authors [197]. Despite this, we did not observe any effect on the studied cell functions in our experiments. Therefore, before the cardiomyocytes culture, plates have to be coated with laminin.

Cell plates were coated with laminin (Sigma-Aldrich) in a concentration of 50 μg/ml. For this, laminin was first dissolved in distilled water in a 1/20 proportion (for example, 100 μl laminin in 1900 μl distilled water). Then, the bottom of the plate was completely coated with the laminin solution. Laminin has to polymerize, and this procedure can take at least 1 hour at room temperature. After waiting for 1 hour, the remaining liquid fraction in the plate (non-polymerized laminin solution) can be collected again and kept at 4ºC for a fresh reuse for a maximum of 3 times. If glass coverslips were used, they were wiped with 70% EtOH and let air dry before coating. Unused dishes may be stored by aspirating the coating solution, drying in the hood cabin, and storing at 4 °C. However, coated dishes should rest in the incubator at least one hour before plating myocytes.

We have used different plates or dishes for cell cultures. For 2-dimensional culture a wide variety of glass coverslips and plastic culture dishes are commercially available. Glass coverslips that fit into small culture dishes are useful for culturing myocytes that are later transferred to a microscope perfusion chamber for electrophysiology or fluorescence experiments. The cells remain adherent to the glass, which can easily be

moved about using forceps. However, cells can be also cultured in plastic dishes, which are sterile, inexpensive, and commercially available in a range of sizes and number of wells per dish. In our experiments, most of the records for non-treated cells were done in a cell culture dish of 60 mm diameter and 15 mm high with a culture area of 21.5 cm2 (Thermo-Fisher Scientific). However, recordings with treatment were done in a 12 well plate (Thermo-Fisher Scientific) with a coverslip that fit into the small culture dish of the plate.

The main considerations for the choice of culture medium are buffering, ionic composition, and nutritional supplements. The basic choice for the culture of adult cardiac myocytes is sodium bicarbonate buffered Medium, which maintains a pH of 7.3 to 7.4 in the standard incubator atmosphere of 5% CO2. Sometimes, basic media may be mixed with Dulbecco's Modified Eagle Medium (DMEM).

It is critically important to maintain aseptic conditions during all steps of culturing. Therefore experiments were done in a culture room with a laminar flow cabin equipped with a vacuum, a water bath, and an incubator that can keep cultures at 37°C and an atmosphere of 95% O_2 −5% CO_2. Moreover, all steps should be performed in the laminar flow cabin, wearing lab gloves (latex or nitrile). Besides, all items brought into the cabin should be sprayed with 70% ethanol (EtOH) before each entry. Fresh, sterile media is warmed to 37°C in the water bath before plating the cells.

Before the cardiac myocytes culture, cell culture medium has to be prepared. The medium used was a modification of the M199 medium (GIBCO). The medium prepared was a medium mixed between a DMEM medium (Lonza) and an M199 medium (GIBCO) in a proportion of 4:1 (vol/vol). This mixed medium was supplemented with 1% of penicillin- streptomycin (Penicilin Streptomycin, GIBCO) and L-glutamine (Sigma-Aldrich). Nevertheless, the medium was not supplemented with any kind of fetal serum. Finally, the medium was filtered for higher sterilization using a 0.2 μm filter bottle-top filter (Corning) and stored at 4°C for weeks. The composition of the two commercial mediums used is reported below:

❖ **M-199 composition (mM):** $CaCl_2$, 1.8; NaCl, 116; Na acetate, 0.6; NaHPO4, 1; KCl, 5.3; $MgSO_4$, 0.8 plus all amino acids except glutamine, and vitamins.

❖ **DMEM composition (mM):** $NaHCO_3$, 44; Salt sodium pyruvate, 1; $CaCl_2$, 1.8; Dextrose, 5.5; $Fe(NO_3)_3$, 2,48; $MgSO_4$, 0.8; KCl, 5.3; NaCl, 110; HCl, 0.4; Glycine 0.4; Phenol red 0.4; plus all amino acids except glutamine, and vitamins.

13. CARDIAC ELECTROPHYSIOLOGICAL RECORDINGS

13.1. IN VIVO ELECTROCARDIOGRAM RECORDINGS

Electrocardiogram recording is non-invasive. Thus, to reproduce the clinical settings as much as we can, *in vivo* electrocardiogram recordings were carried out in conscious animals.

At least two days before the recordings, subcutaneous electrodes were implanted in the animals. The electrodes consisted of commercial circular-ring piercings (Crazy Factory) of surgical stainless steel, 8 mm diameter and 0.8 mm width of the bar. It is recommended to do the implants as in advance as possible before the records.

ECG tracing was obtained from the lead-II (figure 27), a limb lead of human ECG. Thus, subcutaneous piercings were placed in the right front leg and the left rear leg of the rats. A third electrode was implanted in the right rear leg of the rats as a ground electrode. Electrodes were implanted to anesthetized rats at the beginning of the experimental period. The procedure for the implantation was similar to a human piercing implantation by using a piercing catheter of 16G (Crazy Factory). Piercings were periodically replaced to avoid electrical noise and get a more stable output signal.
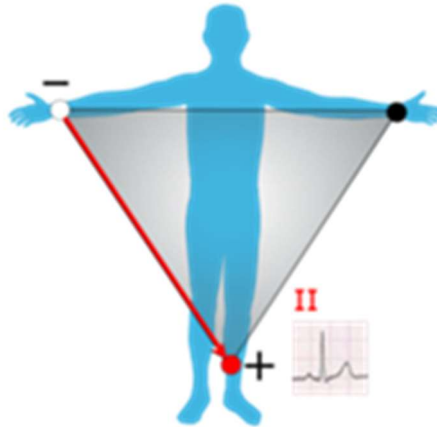
Figure 27. ECG lead-II electrodes representation. Adapted from Wikipedia.

To implant the electrodes, rats were anesthetized by isoflurane inhalation. Once the rat was anesthetized, a small portion of the skin was shaved with an electric razor and cleaned with ethanol 70%. The piercings were placed in the shaved regions and under the skin (subcutaneously) by using a stainless steel needle while the skin was stretched up with the fingers in a tweezer manner. The piercings were closed with pliers to make them completely circular and avoid them to fall. After the piercing placement, the antiseptic povidone-ionone was administrated topically in the region where the piercings were placed to avoid future infections. Furthermore, after the piercings implantation, animals had to be placed in individual cages due to the possibility that other animals pulled the piercings out.

For recording the ECG, conscious animals were transferred into another room that was dedicated to this procedure. Rats were let for 10 minutes for adaptation to the new room. Then, the subcutaneous electrodes of the rat were connected through copper cables of 0.5mm diameter to the electrode lead set (SS2LB) of the Biopac MP35 recording hardware (Biopac Systems Inc.). It was controlled by the BSL Pro software 8.0 (Biopac Systems Inc) in a windows 7 laptop (figure 28). The signal was filtered at 100 Hz and digitized at 1 kHz with this software. This connection must be as minimally invasive as possible for not disturbing the rats. After the electrodes were connected, the cage where the rat is, can be covered to provide darkness that helps to calm down the rat. It is also recommended to wait for a few minutes before starting the records for letting the rat to calm down.

A

B
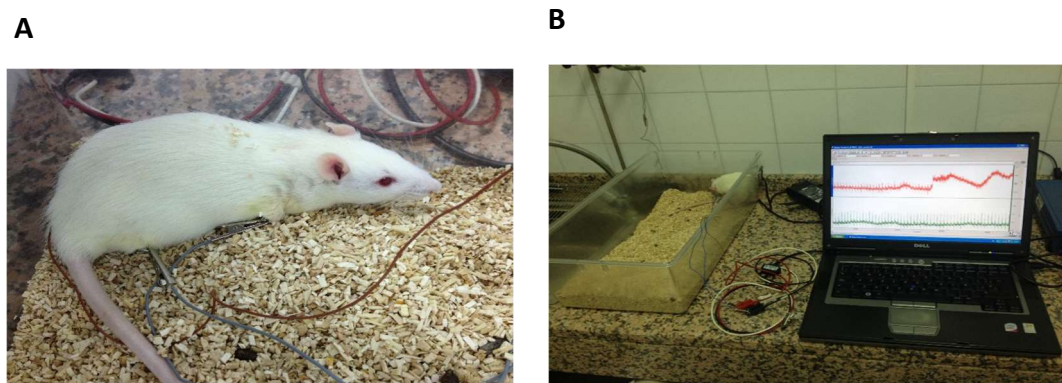
Figure 28. In vivo electrocardiogram recording. A) Rat with piercings and electrodes while recording ECG. **B)** Set-up for ECG recording.

Afterward, 15 minutes of the ECG were recorded with the BSL Pro software trying to get the best record possible with the best baseline. Electrocardiographic parameters were calculated by chosen 10 fractions of 10 beats each from the whole records and were analyzed with the Lab Chart 7.0 software (AD Instruments). Thus, parameters were showed as the average of 100 beats. Chosen beats were the best fractions of the records with the best baseline (around 0 mV) and with minimal electrical noise. All the records were analyzed by double-blind to avoid possible researcher bias. The Following electrocardiographic parameters were extracted from each record: PR interval, RR interval, P wave, QRS interval, QT interval, corrected QT interval (QTc), and T peak to T end interval duration. The QT interval was measured from the beginning of the QRS complex to the end of the T wave. Corrected QT interval was calculated using the Fridericia's formula: QTc = QT / $\sqrt[3]{RR}$.

13.2. ARRHYTHMIA SUSCEPTIBILITY TEST

Classification criteria used for arrhythmias are not universally agreed upon. For the classification of the arrhythmia, we based on the Lambeth convention that is the most accepted attempt to standardize the study of arrhythmias. This convention described, quantified and classified the most usual and lethal arrhythmogenic events such as ventricular tachycardia (VT) and ventricular fibrillation (VF).

An arrhythmia induction protocol that standardize the conditions of the cardiac challenge while monitoring is needed to test the prone to arrhythmia of the animals as

well as the type and severity of the developed arrhythmia. In our project, we used a caffeine-dobutamine cardiac challenge for testing the susceptibility to arrhythmia of our model and our treatments, as previously described [198].

The procedure was performed in rats at the end of the experimental period (end of week 6). To induce the unconscious state, animals were anesthetized by isoflurane inhalation. Although the majority of the animals survived, animals were not used for any other proposal after the challenge due to the severity of this protocol. Before the protocol, we must be sure that all the rats have the piercings and the ECG signal is adequate. If needed, we would replace the piercings either for improving the signal or because they had fallen down. ECG recordings were done as explained before. We used the same materials, hardware and software but the animal was anesthetized for this procedure.

A

B
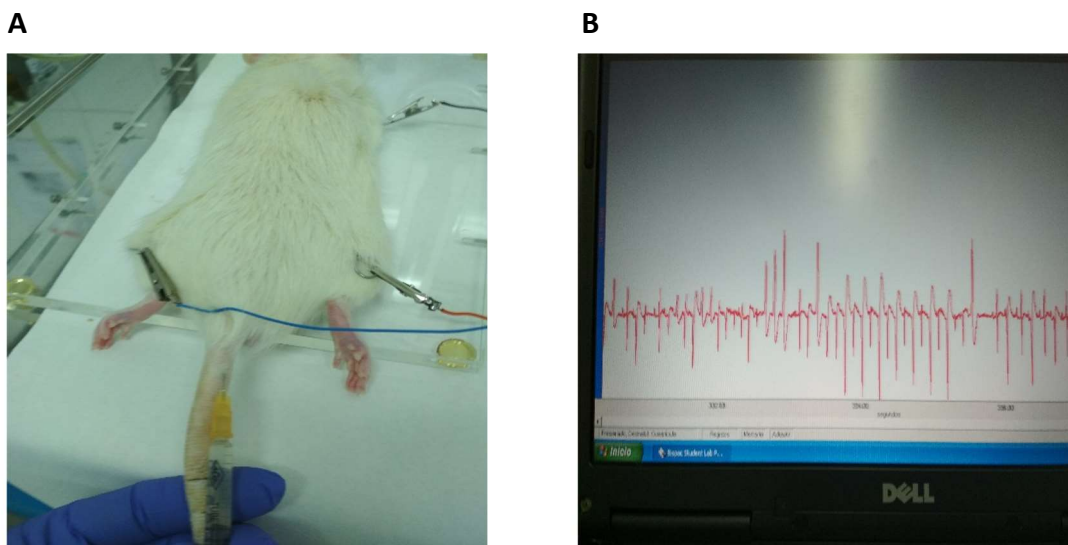
Figure 29. Arrhythmia induction protocol. A) Intravenous injection of dobutamine in isoflurane anestethized rat. **B)** ECG recording of arrhythmias after injections.

First, the animal was anesthetized with isoflurane. When the animal is anesthetized, rat electrodes were connected, and a control baseline electrocardiogram was recorded for 5 minutes. Then, the animals received an intravenous injection of dobutamine in the tail vein (Sigma-Aldrich) in a dose of 50 µg/kg followed by an intraperitoneal injection of caffeine (Sigma-Aldrich) in a dose of 120 mg/kg. After the injections, ECG was recorded for 10 minutes more (figure 29). The type of arrhythmia was identified according to the

Lambeth Convention guidelines. The incidence of ventricular arrhythmias was also quantified by severity criteria in accordance with the Lambeth Convention.

13.3. PATCH-CLAMP RECORDING

Characterizing the functional expression and properties of myocardial ion channels is important to understand mechanisms responsible for the electrical cardiac alterations. This requires voltage-clamp, an experimental approach designed to provide precise temporal and spatial control of the cellular membrane potential (voltage) to allow current flow through membrane ion channels to be measured directly. These measurements are made using the patch-clamp technique.

Patch-clamp recording technique combines a low-noise, high-resistance feedback amplifier with a low-resistance patch pipette and requires a high-resistance seal (called gigaseal) between the recording pipette and the cell membrane that combine to minimize noise and permit the measurements of currents, including currents through single ion channels, across the membranes of the excitable cells.

A. VOLTAGE-CLAMP

We performed experiments using voltage-clamp technique in whole-cell configuration. The whole-cell recording configuration is achieved by rupturing the cell membrane by applying negative suction across the membrane patch while in the cell-attached configuration, establishing a low-resistance pathway between the cell cytoplasm and the solution inside the pipette. The whole-cell configuration allows control of the composition of both the intracellular and extracellular compartments, permitting the measurement of whole-cell membrane potential changes (in the current-clamp mode) as well as whole-cell macroscopic currents (in the voltage-clamp mode) under a variety of conditions.

For performing the patch-clamp technique, we need an electrophysiological recording set-up that includes specific equipment such as a vibration isolation table,

upright or inverted microscope, micromanipulator, recording amplifier, AC/DC converter, Faraday cage and microelectrode puller.

It is also possible to control the composition of the intracellular pipette solution. In combination with well-designed voltage-clamp protocols, the ability to control the compositions of the extracellular bath and the intracellular pipette solution facilitates the isolation of individual current components.
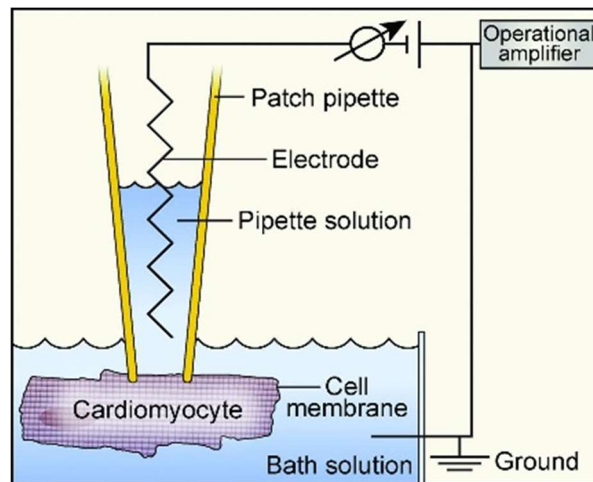
Figure 30. Components of the recording circuit. Adapted from manual of research techniques in Cardiovascular Medicine. Wiley Blackwell. Ardehali H (2014).

The key components of the circuit are illustrated in figures 30 and 31. The recording pipette, illustrated in contact with an isolated myocyte, is connected to the negative input of a high-gain, high-input resistance operational amplifier. The applied voltage to the pipette (Vp) follows the command voltage (Vcom) of the amplifier and the pipette current (Ip), which is proportional to the voltage output (VRf) of the amplifier, flows through the feedback resistor (Rf). The circuit will contain a frequency correction current circuit (FR) that allows reduction (or elimination) of the stray capacitance (Cf) and VRf. The analog signals from the head-stage are passed through an analog-to-digital (AD/DA) converter; the signal is digitized and sent to a computer for storage and offline analysis. In summary, the software generates the pulses that change the membrane potential (Vrf). The digitizer converts the signal from digital to analog and, through an amplifier, amplifies it to the electrode and this to the cell. The current generated in the cell passes through the electrode to the amplifier, where it is filtered at 1 KHz and it is converted from analog to digital and, finally, stored in the computer.

In voltage-clamp configuration, the membrane potential of the cells (Vm) is clamped and the ionic currents through the membrane are recorded due to the potential changes. The electrode is connected to a current / voltage converter by a chlorinated silver wire. The current through the membrane (Im) can be determined from the following expression:

$$Im = \frac{Vrf \cdot Vcom}{Rf}$$
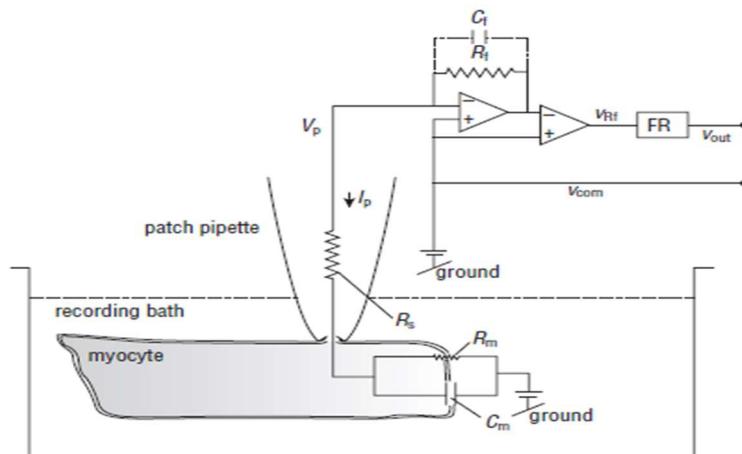
Figure 31. Voltage-clamp circuit representation. Adapted from manual of research techniques in Cardiovascular Medicine. Wiley Blackwell. Ardehali H (2014).

I. PIPETTES

One of the most critical components needed for successful patch-clamp recordings is the recording pipette. The geometry of the shank and the size of the tip of the pipette are readily controlled by the specific glass selected and temperature and timing of the heating and pulling of the glass.

The micropipettes were obtained from borosilicate glass capillaries (Sutter Instrument) with an external diameter of 1.1 mm. Borosilicate glass is selected because it has a low softening temperature and low electrical noise and, besides, seals readily to biological membranes. Pipettes are pulled immediately before use.

A

B
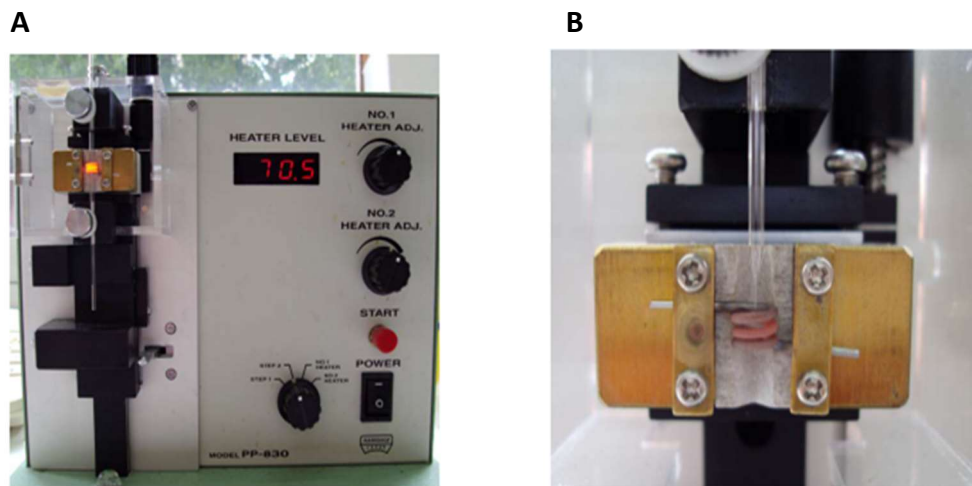
Figure 32. Pipette puller. A) PC-10 Narishige pipette puller. **B)** Resistance of the puller heating a borosilicate glas for the micropipette preparation.

The micropipettes were made using a horizontal dual-stage micropipette puller (PC-10, Narishige) that uses gravity as traction. Puller has a resistance that heats up when an electric current passes through and this heat causes the glass to melt. Procedure is done in two stages. In the first stage, intense heat is applied to the capillary, and in the second stage, heat application is lower. The puller can also control temperature applied to the capillaries and it is modified depending on the wanted characteristics of our pipette. While heating is applied, a stretch of the glass capillary occurs due to gravity-induced traction in both stages while heat is applied. Furthermore, the puller has weights that can increase or decrease the traction applied and that can be modified depending on our needs. Then, the micropipettes were filled with an internal solution (see compositions below) using a fine tip, trying not to form bubbles. For our records, pipettes had an access resistance between 1 and 3 MΩ when the pipette is immersed in the bath containing an external solution.

II. IONIC CURRENT RECORDING

All ionic currents were recorded by the patch-clamp technique adapted to our laboratory [60, 199]. All the experiments were performed at room temperature (20-22ºC). All the patch-clamp recordings were done using the whole-cell configuration with an Axopatch 200B patch-clamp amplifier (Molecular Devices) connected to the digitizer Digidata 1140 (axon Instruments Inc) that converts the signal from analog to digital. On the other hand, the microscope connected to the set-up is an inverted microscope (Leica). All the set-up was connected to a computer (windows) that also controlled the experiment with Clampex 10.2 software (Axon Instruments). All patch-clamp setup was placed on a vibration isolation table inside a Faraday cage, except the digitizer, the amplifier, and the computer that were placed outside the cage (figure 33).

A   **B**
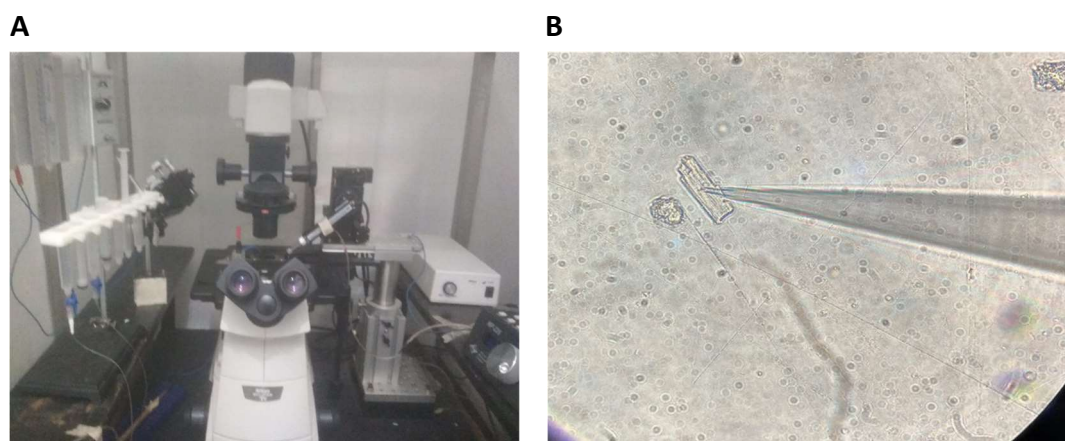
Figure 33. Patch-clamp recording set-up. A) Set-up used for patch-clamp recording. **B)** Cardiomyocyte while is recorded with the patch-clamp set-up.

Cardiomyocytes were isolated as previously explained. We used freshly cardiomyocytes as well as cultured cardiomyocytes at 37ºC for 24 hours.

For recording fresh cardiomyocytes, we kept them at 4ºC in a plastic beaker with 10 mL of KB medium. Before starting the records, we had to wait at least 2 hours to let the cells to stabilize. Then, cells were carefully taken with a plastic Pasteur pipette and were transferred to the recording chamber that is a low depth plate connected with the solutions and the suction pump. After waiting for 10 minutes until the cells were settled down to the bottom of the chamber, cardiomyocytes were perfused with a specific external solution for Ito current recording. This perfusion was done to replace the KB medium, where the cells were kept, for the external solution for the patch-clamp

recording. Perfusion must be extremely balanced between the solution flow and the suction because whether it would be unbalanced it could remove the cardiomyocytes from the plate. When the external solution starts to perfuse the cardiomyocytes, wait for a few minutes until we are sure the entire KB medium was removed, and the cells were only immersed into an external solution.

For the registration of the cultured cardiomyocytes, if cells were cultured in coverslip glasses in 12-well plates, the coverslip with the attached cells was placed in a culture plate for recording. However, if cells were cultured in a culture plate, we directly use this plate for the recording. In both cases, the culture medium was removed, and the cells were carefully washed with the external solution. Then, cells were covered with external solutions.

For registration, two different types of solutions are used: the external solution, which is in contact with the external surface of the plasma membrane, and the internal solution, with which the micropipettes are filled, and which is in contact with the internal surface of the membrane and, in the whole-cell configuration, it is dialyzed inside the cell.

During registration, the external solution was kept at room temperature. The external solution must be fresh, so it is prepared the same day while the internal solution was stored at -20ºC in tubes containing 1.5 ml of the solution. Before registration, internal solution was thawed and temper to room temperature. See the composition of the solutions used below:

- ❖ **Internal solution for I_{to} (mM):** L-Asp 80; KH_2PO_4 10; $MgSO_4$ 1; ATP-Na 3; EGTA-K 10; KCl 50; HEPES-K 5. Solution was adjusted to pH 7.2 with KOH
- ❖ **External solution for I_{to} (mM):** NaCl 86; KCl 4; $CaCl_2$ 0.5; $MgCl_2$ 1; $CoCl_2$ 2; HEPES-Na 10; TEA-Cl 50; glucose 11. Solution was adjusted to pH 7.4 with NaOH

i. GIGASEAL

The pipette was filled with an internal solution using a syringe with a fine, flexible and long needle, ensuring there are no air bubbles in it. Once the bath and pipette solutions

have been selected and pipettes have been fabricated and filled, the next step is the formation of a high resistance seal between the pipette tip and the cell membrane (figure 34).
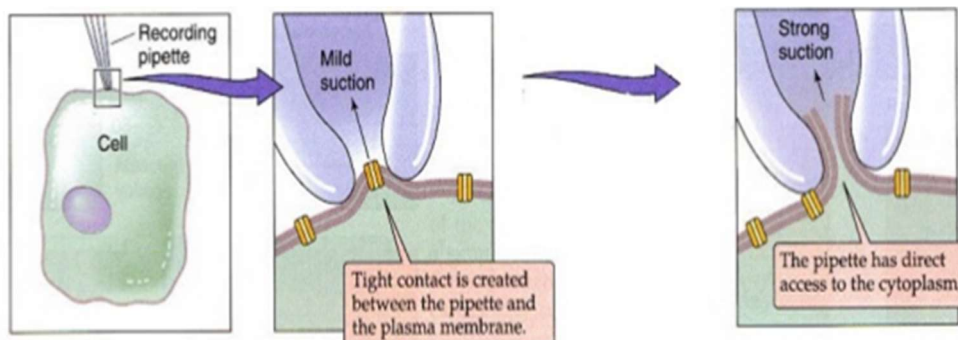
Figure 34. Steps for the gigaseal formation. Adapted from manual of research techniques in Cardiovascular Medicine. *Wiley Blackwell*. Ardehali H (2014).

First, a proper cell has to be located. The cells that presented a healthier appearance, shape, and refringence, were selected to carry out the records. The establishment of a high resistance seal (Gigaseal, GΩ) is of great importance since it allows completely electrically isolating the micro patch in the membrane and reducing noise to control the potential and obtain a cleaner register. To facilitate the formation of gigaseals, the cell surface membrane should be devoid of debris or damage and both the bath and the recording pipette solutions should be filtered (at 0.2 µm) to avoid clogging of the tip. Then, the pipette tip was dipped in the bath solution. For this, place it in the holder, and bring it under visual control near a candidate cell in the bath or chamber. Light positive pressure on the pipette suction port helps keep debris away from the tip. Pipette offset was adjusted for zero current. Small rectangular test pulses (10 mV) were applied to verify pipette resistance. These pulses were applied continuously, but only while not recording data. With the application of a potential across the tip, the pipette resistance can be monitored continuously. Thus, when contact is made with the cell, an increase in resistance occurs, which is reflected in the oscilloscope as a change in the amplitude of the signal Vp. According to this, pipette resistance can be calculated. While the electrode is out of the bath, the output signal has one transition at the start and one at the end of the pulse due to the capacitive components of the system. When the micro-pipette is introduced into the bath, the circuit between the recording electrode and the reference

electrode is electrically closed, generating a current. From Vp and the other known parameters, the resistance of the electrode can be determined using the expression:

$$R = \frac{Vrf \cdot Rs}{Vp - Vrf}$$

Moreover, when the pipette lumen becomes partly obscured, a reduced pipette current response to the test pulses is detected visually.

Later, contact with the cardiomyocytes must be done. This approach has to be done gently because the cardiomyocytes are sensitive cells, and the contact has to be soft (figure 33). Otherwise, the cell could die whether the approaching is too abrupt. Contact between the pipette tip and the cell membrane is signaled by an abrupt increase (two to tenfold) in pipette resistance. At this point, we applied a gentle suction that facilitates the formation of a seal between the pipette and the cell membrane by the introduction of a small piece of the cell membrane into the electrode micropipette tip (figure 34). This is signaled by a marked increase in pipette resistance (figure 35). Suction is performed by pulling a 1 mL syringe that is connected to the micropipette and the required strength of suction will depend on pipette tip size, cell stiffness, and pressure losses. The suction has to be enough to make the seal but not too much to break the membrane as it could kill the cell. Then, the seal should begin to form (substantial loss of pipette current response). The best seals reduce pipette current response to just a few pA. Sealing may require a few seconds to several minutes

As we were performing a ruptured patch, we had to do additional suction to break down the membrane patch inside the pipette. Thus, a slight suction was applied to the micropipette, causing the rupture of the membrane surface delimited by the tip (figure 34). Some cells respond best to steady gentle suction while others respond to strong impulsive suction. On successful rupture, the transient response to the test pulses will increase dramatically as Cm becomes part of the pipette circuit (figure 35). That causes an increase in the capacitive transients of the Vs signal. This increase is due to the capacity of the cell membrane. This Vs signal must be registered and saved in the computer.
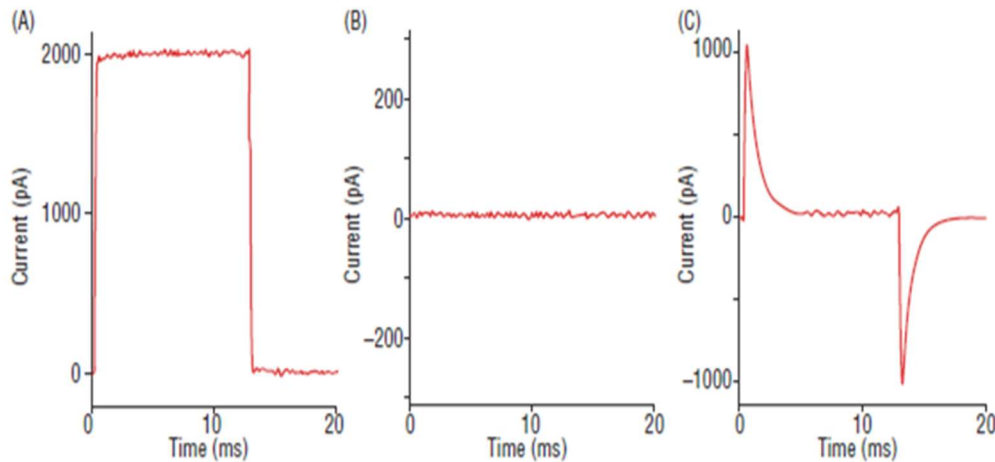
Figure 35. Ilustration of a gigaseal formation in the clampex software. **A)** Current recorded with the pipette in the bath before to seal formation **B)** High-resistance gigaseal formation. **C)** Seal has been broken and the acquisition of the whole-cell configuration has been reached.

ii. TRANSIENT OUTWARD POTASSIUM CURRENT, Ito, RECORDING

When the gigaseal was already achieved, we can obtain the whole-cell patch recordings. The whole-cell configuration was achieved by the application of a brief pulse of suction and was signaled by the appearance of large current transients in response to the (10 mV) test pulse, reflecting the whole-cell capacitive current (figure 35). Once the whole-cell configuration was achieved, the cell membrane potential was clamped to the desired voltage, typically at or near the cell resting membrane potential that is in the range of −60 to −80 mV. Furthermore, in the whole-cell configuration, the access resistance and the cell input resistance and capacitance can be calculated from records. Integration of the capacitive transient, evoked in response to a low-amplitude voltage step, provides the capacitive current (IC), from which the whole-cell membrane capacitance (Cm), can be calculated according to the formula IC= Cm (dV/dT). Series resistance was compensated by 80% to minimize voltage errors.

As mentioned before, the whole-cell voltage-clamp technique is very useful in experiments that detail myocyte membrane currents. For this purpose, there are specific strategies used to isolate and characterize individual current components. To begin, experimental (recording) conditions are established to eliminate all of the

currents other than the current of interest. For example, the intracellular pipette and extracellular bath solutions are optimized to facilitate the isolation of the current of interest, sometimes involving the inclusion of selective pharmacological blockers of the different types of ion channels. Besides, specific voltage-clamp protocols, involving step depolarizations or hyperpolarizations of fixed durations are designed and are used to facilitate the isolation of the specific current component of interest.

According to this, we used different strategies for the recording of transient outward potassium current. The external solution for registration contained cobalt, which blocks calcium channels, and tetraethylammonium (TEA), which inhibits most of the potassium channels but not those responsible for I_{to} (in the concentration used). In addition, the recording protocol was used to inhibit the sodium current because the resting cell potential used (-60 mV) was higher than that which allows the sodium channels to open. The recording protocol for I_{to} consisted of voltage pulses (500 ms long) to a test potential ranging from -30 to +50 mV, starting from a holding potential of -60 mV, were applied at a frequency of 0.1 Hz to ensure the full channel recovery from inactivation. An example of Ito current recording can be seen in figure 36.
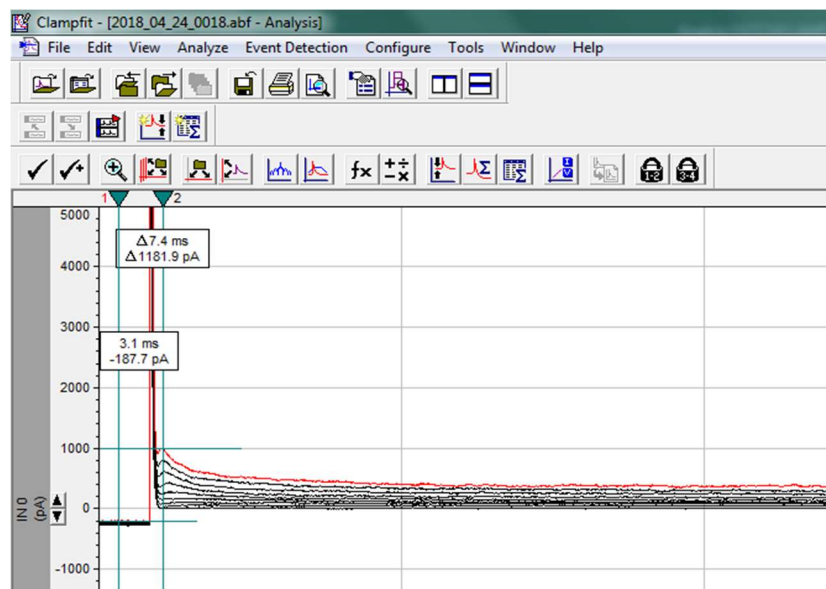
Figure 36. Recorded Ito current in our lab while analysis with clampfit 10.1

B. CURRENT-CLAMP

I. ACTION POTENTIAL

In cardiac cells, the Action potential (AP) is the time-dependent transmembrane potential (Em) associated with excitation and contraction. The cardiac AP is shaped by time-dependent changes in ion fluxes through numerous ion channels and transporters (figure 15). Thus, changes in ionic currents must be reflexed in the shape of AP. Moreover, intervals between APs as well as AP waveform properties may relate to clinical features such as heart rate and QT interval variability. If our model and our treatment have any electrophysiological effect on this, we will observe the effect on the AP duration and shape.

Action potentials were recorded from isolated cardiomyocytes and were cultured at physiological conditions for 24h, as explained before. Our recordings of APs were done from isolated myocytes, using a glass pipette, which provides direct contact between an electrode and intracellular space, along with an extracellular reference electrode.

Recordings were done in both a dish of 60 mm diameter (Thermo-Fisher scientific) cultured cells and a coverslip of 12 well plate (Thermo-Fisher Scientific) where cardiomyocytes were cultured. Mainly, recordings in serum treated myocytes were performed in cover glasses from a 12-well plate because the volume of the serum used was smaller for the concentration needed.

After 24h of incubation, the medium was gently removed with a pipette in the flow cabin and the dish was washed twice with an external solution. Medium was replaced for an external solution that covered the cells. However, whether we used a cover glass, then, the cover had to be carefully moved from the 12-well plate to a 60 mm diameter dish with thin tip tweezers. Finally, they were washed twice and were covered with an external solution as done with the dish-cultured cells.

As usually in the patch-clamp technique, criteria for choosing the recorded cardiomyocytes for recording was their shape and their refringence.

Action potentials were recorded following the instructions of Belma Turan's lab in Ankara (Turkey) and explained in the literature [200].

Patch pipettes were prepared with a pipette puller (PC-10, Nirishige) using borosilicate capillaries (Sutter instruments) filled with solutions mimicking intracellular composition (typical resistances 1–4 MΩ).

Gigaseal was achieved using the same method for voltage-clamp recordings and that is explained above. As the recording amplifier allows it, we started in Voltage Clamp mode, to establish whole-cell recording quality, and then switched to Current Clamp mode. Most commercially available amplifiers, including our Axopatch 200B patch-clamp amplifier (Molecular Devices), can also be used in the current-clamp mode to control the membrane current and allow the measurement of membrane voltage.

When a Voltage Clamped (VC) amplifier is switched to Current Clamped (CC), the normal user-chosen VC commands are replaced by an internal command derived from the pipette current. By feedback, this command continually drives Em toward the value which results in pipette current of zero or another specified value, accomplishing CC. Pipette capacitance (Cpip) strongly affects AP recording. In our case, the setup used for the action potential records was the same that we used for the ionic currents. It is convenient to synchronize computer recording with AP stimuli where relevant. Popular data acquisition program/interface packages can generate stimuli synchronous with recording via the same computer.

Once the gigaseal was achieved, the record was switched from voltage to current clamp. It is essential first to set clamp current to 0, to protect cells from damage by unintended current or voltage forcing. Typical Current-Clamp amplifiers have an I=0 mode. At this time, the resting Em should appear and we observed this in the computer. If the previous Voltage-Clamp period was prolonged, some seconds may be required for ion re-equilibration and Em stabilization.

Next, current commands were enabled to current-clamp and the stimuli for AP triggering was applied. When needed to induce APs, depolarizing current is passed through the pipette via the CC amplifier, or by external field stimulation. Pipette-delivered commands need to be large enough to trigger AP reliably, even if excitability

changes, but not so large as to introduce noise and/or unintended Em shifts in sensitive cells. For ventricular myocytes, we injected a small pulse of inward current to mimic the activating current, which in the intact heart would spread passively via gap junctions from neighboring cells, which are actively producing APs. Field stimuli in the range of ~50 V/cm may be required, due to the volume and low resistivity of bath solution. Some stimulus energy will be capacitively coupled into the recording system, causing artifacts in the AP record. Using the shortest duration effective stimuli will make these easier to remove. In our case, we applied an starting stimuli that consisted of an input of 15 mV. Unfortunately, sometimes, these stimuli were not enough for triggering the action potential, and start stimuli could be slightly increased toward a reliable suprathreshold response. The stimuli duration was always 4 ms. Finally, adjust Cpip neutralization and bridge balance and begin the experiment. Action potentials in left ventricular cardiomyocytes were determined under electrical stimulation at 0.5 Hz frequency.
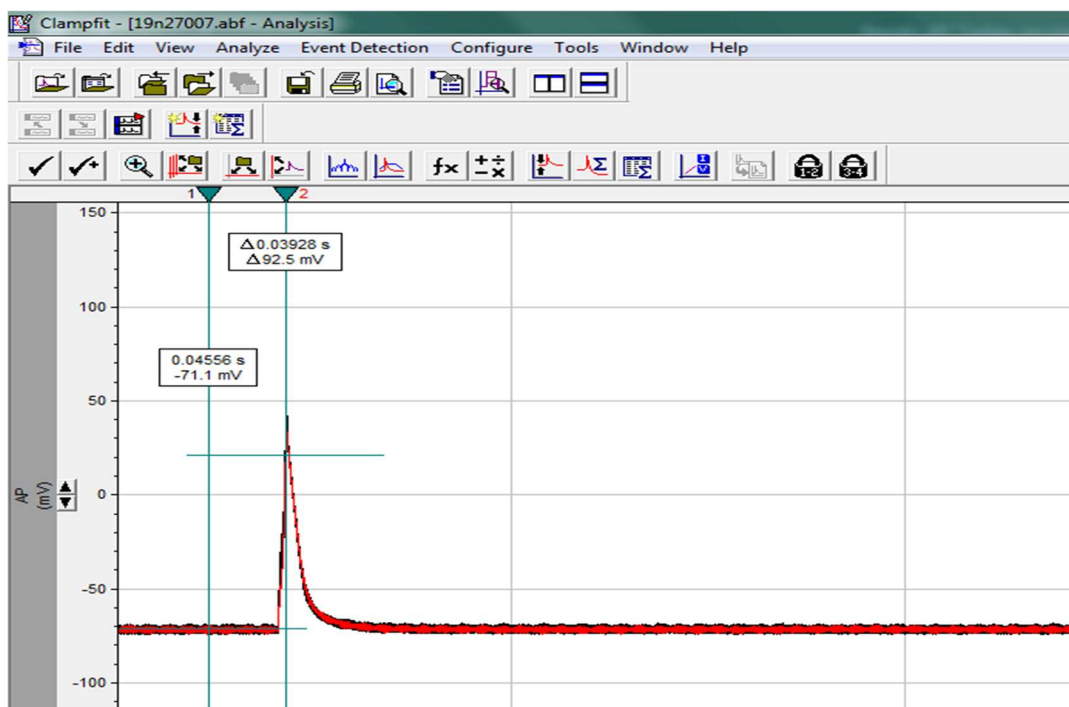
Figure 37. Recorded action potential in our lab while analysis with clampfit 10.1.

The parameters of action potential including resting membrane potential, the amplitude of action potential, and depolarization phase and repolarization phases at 30, 50, and 90 % of full AP duration were determined using Clampfit 10.2 software. However, for the AP analysis, consider that AP duration runs up or down during an

experiment. This is frequent in ruptured patch due to diffusion of signaling molecules from cell to pipette. APs must be recorded with sufficient time and amplitude resolution for analysis (figure 37).

❖ **External solution (in mM):** NaCl 136; KCl 5.4; $CaCl_2$ 1.8; $MgCl_2$ 1; HEPES-Na 10; Glucose 11. The pH was adjusted to 7.4 with NaOH.

❖ **Internal solution (in mM):** L-Asp 80; KH_2PO_4 10; $MgSO_4$ 1; ATP-Na 3; EGTA-K 10; KCl 50; HEPES-K 5. The pH was adjusted to pH 7.2 with KOH.

14. CALCIUM SPARKS

A calcium spark is the microscopic release of calcium (Ca^{2+}) from a store known as the sarcoplasmic reticulum (SR). A confocal microscope is essential for the calcium sparks detection. However, the detection by the microscope is only possible by using a calcium dye. Then, the calcium release is detected because calcium is highlighted using a substance known as fluo-3, which glow when interacts with Ca^{2+}.Finally, observed luminescence using the confocal has to be captured and interpreted. Thus, specific transductor signals and software have to be used to obtain the results.

Ca^{2+} sparks were measured from Fluo-3 loaded freshly isolated cardiomyocytes. Before the calcium measurements, isolated control cardiac myocytes, as explained before, were incubated with control and type 2 diabetes serums for 24h at physiological conditions. Isolation and cell culture were done as previously explained in this thesis.

Myocytes were loaded with the membrane-permeant fluorophore fluo-3 (Molecular Probes Inc.). Loading conditions consisted of a 1 h dark incubation at 37ºC in a HEPES-buffered solution containing 2 mM of fluo-3. The cells were then washed with HEPES. Following, cardiomyocytes were placed at room temperature into the recording chamber using a Pasteur pipette. Recording setup was placed in a dark room where the light was only used when required. The recording chamber was set onto the stage of an inverted confocal microscope equipped with a laser scanning (Leica, SP5). In the experiments, 40 X (numerical aperture of 1.2) water immersion objectives were used for

imaging cardiomyocytes that were located over the cover glass base of the recording chamber. After focusing the cells, a good-shaped cardiomyocyte was searched with the microscope to perform the protocol. When it was detected and well-focused, a 488-nm laser line from an argon laser (25 mW) was used to excite the Ca^{2+}-sensitive dye, Fluo-3. The emitted fluorescence was collected at 505 nm. Changes in intracellular calcium were recorded in line-scan mode (spatial [x] vs. temporal [t], 1.9 ms/line). To prevent photo-bleaching and cell damage, the laser line was kept at 4-6% of maximal intensity and the confocal pinhole set to 1–1.5 airy units to achieve the best resolution and emission intensity.
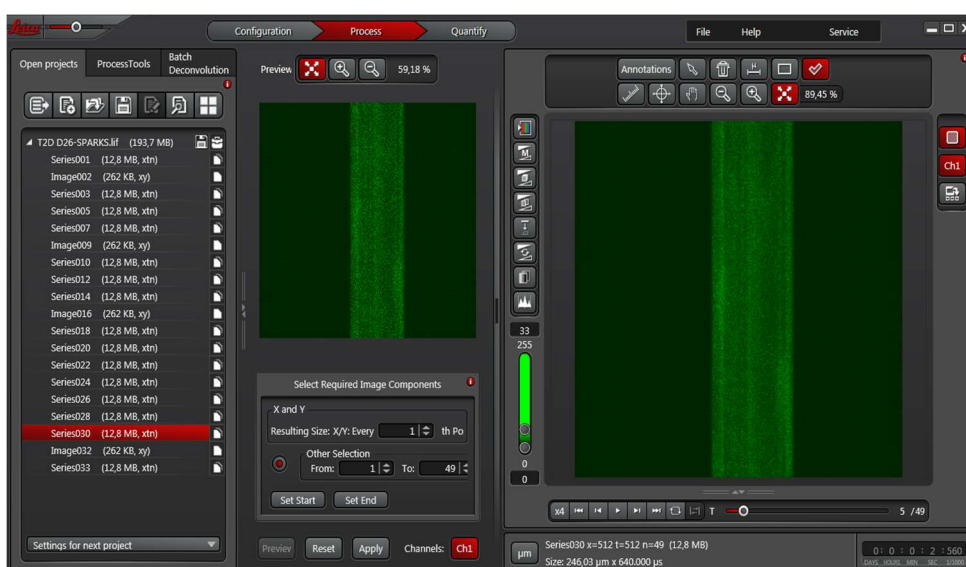
Figure 38. Recorded cardiomycyte calcium spark during analysis with LAS X software

Image analysis was performed using LAS X Image Examiner (figure 38). The parameters of fluorescence changes such as peak amplitude, Time to Peak (TP), spatial width (full width at half-maximum intensity, FWHM), and full duration half maximum (FDHM) were calculated automatically by using Image J program. LAS X images had to be converted to an 8-bit type for the analysis with Image J. The F0 value for fluorescence intensity of image was calculated by averaging pixels other than potential spark areas. Then, F/F0 image was created by using this F value (DF/F0, where DF=F2F0; F was identified as local maximum elevation of fluorescence intensity over basal level, F0). Despite calcium sparks were automatically calculated and detected, sometimes manually corrections were done to improve the detection. Time to peak, peak amplitude of fluorescence intensity, and decrease time to half-maximum were measured. Since

background and cell autofluorescence were usually about 10 times less than that measured from fluo-3 loaded myocytes, they were considered negligible and no correction was made in the calculation of $[Ca^{2+}]$.

❖ **HEPES-buffered solution** (in mM): NaCl 120, KC1 5.4, NaPO, 1.2, MgCl, 1.7, CaCl, 1.8, glucose 10, HEPES 10. Solution was adjusted to pH 7.4 with NaOH

15. PROTEIN DETECTION

15.1. CELL LYSIS AND PROTEIN EXTRACTION

Firstly, we have to get the complex mixture of proteins extracted from cells for their analysis with western blot technique. The cells used for wester blotting were isolated rat cardiomyocytes. The isolation of the cardiomyocytes was done as previously explained. After the isolation, left ventricular myocytes suspended in KB medium were collected in 1.5 ml eppendorfs. After waiting for 10 minutes until the cells were settle on the bottom of the Eppendorf, the KB medium was carefully removed using a pipette. The eppendorfs containing the cells (only cells, with no liquid) can be kept at -80ºC until they are used.

During the lysis procedure, we have to work on ice in order to avoid the degradation of the proteins. After thawing the cells on ice, 100-200 µl of homogenizing buffer (RIPA buffer), depending on our samples, was added to the eppendorfs. Samples with a homogenizing buffer were left for 30 minutes on ice. The hyposmotic buffer provoked an osmotic imbalance caused by the excess water moving into the cell that leads to cell burst. After 30 minutes of chemical lysis by the buffer, cells were mechanically lysed with an electrical pestle by giving 10 pulses of 10 seconds with 3 seconds of rest between each pulse.

❖ **RIPA buffer composition:** 140 mM NaCl; 25 mM Tris-HCl; 1 mM EDTA; 0.5 mM EGTA; 1 mM PMSF; 1mM NaF; 1% Triton X-100; 0.1% SDS; 0.1% Protease inhibitors cocktail Bring to volume with ultrapure water. Adjust the pH to 7.4 with HCl.

The objective of the lysis is to extract the protein form the cells, thus, whether the lysis have worked, we would expected to obtain the cellular protein dissolved in buffer. This protein mixture dissolved in buffer was used for the western blot but prior the protein concentration in the samples was quantified. As long as the protein is not used, lysed samples can be stored at -20ºC for a short time (maximum of one week). Longer storages were done at -80ºC.

For protein quantification, we used the bicinchoninic acid assay (BCA). It is a biochemical assay for determining the total concentration of protein in a solution (range: 0.5 μg/mL to 1.5 mg/mL). The total protein concentration is exhibited by a color change of the sample solution from green to purple in proportion to protein concentration, which can then be measured using colorimetric techniques.

The bicinchoninic acid Cu^{2+} complex is influenced in protein samples by the presence of cysteine/cystine, tyrosine, and tryptophan side chains. The BCA assay primarily relies on two reactions.

First, the peptide bonds in protein reduce Cu^{2+} ions from the copper (II) sulfate to Cu^+ (a temperature dependent reaction). The amount of Cu^{2+} reduced is proportional to the amount of protein present in the solution.

Next, molecules of bicinchoninic acid chelate with Cu^+ ion, forming a purple-colored complex that strongly absorbs light at a wavelength of 562 nm. Therefore, absorbance at this wavelength is directly proportional to the amount of protein present in the solution. Moreover, the amount of protein present in a solution can be quantified by comparing with protein solutions of known concentration.

We used known concentrations of bovine serum albumin (in mg/ml: 0, 0.2, 0.4, 0.6, 0.8, 1, 1.5 and 2) for the standard curve preparation. This allowed us to determine the concentration of unknown concentration samples by comparing their absorbance to a set of standard sample absorbance of known concentration. The standard curve results

in a plot where the x-axis corresponds to the concentration and the y-axis to the absorbance where we could obtain the graph equation (y=ax+b) from. Equation has several elements where Y was the observed absorbance of the unknown concentration samples, A and B were constants provided from the equation and X was the concentration variable. Therefore, isolating the X variable will give us the concentration of our sample.

A dilution of the samples is highly recommended because, usually, the concentration of the samples is too high and can be out of range of the standard curve concentrations. However, to make a dilution and the dilution factor applied always depend on the samples concentration, which is unknown. Therefore, it is up to the researcher and his experimental knowledge. The dilutions were done by diluting the sample in dH_2O. Be aware of applying the dilution factor to the final concentration when it is calculated.

For the protein quantification, we had to induce the colorimetric reaction. We used a kit reagent (Bio-Rad) that consisted of bicinchoninic acid and $CuSO_4$ and that had to be mixed in a 50: 1 ratio. 2 ml of the formed reagent were added to each sample. They were incubated for 30 minutes at 37ºC. Finally, the absorbance was read with a spectrophotometer (WPA 1101 Biotech Photometer) at 562 nm and the sample concentration was calculated as explained before.

15.2. WESTERN BLOT

Western blotting is an important technique used in cell and molecular biology. By using western blot, researchers are able to identify specific proteins from a complex mixture of proteins extracted from cells. The technique uses three elements to accomplish this task: (1) separation by size, (2) transfer to a solid support, and (3) marking target protein using a proper primary and secondary antibody to visualize.

The separation by size consists in the migration of proteins through a denaturing acrylamide gel in which an electric field is generated. Acrylamide forms a porous matrix through which proteins migrate based on their size. The smaller the protein is, the easier they pass though and the further they migrate. The acrylamide concentration of the gel can change. Higher concentration of acrylamide leads to a tighter pores where the

weightier proteins will have troubles to pass though. Otherwise, lower concentrations of acrylamide leads to wider pores where the weightier proteins will pass through easier. Therefore, acrylamide concentration changes depending on the size of the proteins that you want to migrate. For this project, we used 10% acrylamide gels.

A Laemmli buffer is added to the sample before running the electrophoresis in a 1:4 concentration. The proteins structure blocks their migration through the gel so, to allow the movement of proteins, they are previously denatured both by heating at 100ºC for 10 minutes and by adding SDS, a detergent that denatures proteins, and that is part of the Laemmli buffer.

Once the proteins are denatured, the electric field moves them from negative to positive pole and they separate according to their size. However, whether the electric field has to move the denatured proteins from pole to pole according to their size, the protein charge should be the same for all proteins to have any influence in the migrations. Laemli buffer also gives the homogeneity of charges. The SDS binds to the non-polar areas of the polypeptide in a same ratio for all proteins (one SDS molecule for every two amino acid residues, corresponding to about 1.4 g SDS / g protein) and provides to all proteins a similar net negative charge and therefore a similar charge-to-mass ratio.

❖ **Laemli buffer composition:** Tris 60 mM, 3% SDS 10%; 10 % Glicerol; 0.003% Bromophenol blue; 1% β-mercaptoetanol. Adjust the pH to 6.8 with HCl.

For this project, we used 1.5 mm thickness gels that allow loading abundant amounts of samples and therefore of protein (between 40 µg and 120 µg in our case). Then, the glasses used for the gels assembly were chosen according to the gel thickness. Gels has two phases with different concentration of acrylamide. One used to concentrate the samples (with 5% acrylamide) and another for the separation of the proteins (with 10% acrylamide). To assembly the gel, separation gel is added before the concentration gel that only can be added when the separation gel is polymerized. Following the addition of the separation gel, a comb have to be embedded into the gel in order to create the

wells where the sample will be charge. It has to be done before the polymerization of the gel.

❖ **Separation gel composition:** 44% dH$_2$O; 27% Tris HCl 1.5 M pH 8.8; 28% Acrylamide/Bisacrylamide at 30%; 1% SDS at 10%; 1% APS at 100 mg/ml; 0.1% TEMED.

❖ **Concentration gel composition:** 56% dH$_2$O; 25% Tris HCl 1.5 M pH 8.8; 16% Acrylamide/Bisacrylamide at 30%; 1% SDS at 10%; 0.5% APS at 100 mg/ml; 0.25% TEMED.

Gels were immersed in an electrophoresis/transference tank (mini-protean, Bio-Rad) that contains electrophoresis buffer. Then, 40 µl of samples were added to each well using a calibrated 100 µl pipette. Samples have to be gently vortexed before their use. The electrophoresis was run until the front was gone (2h approximately) at 100-120 mV with a power supply (PowerPac 300, BioRad). Time of electrophoresis can change depending on the protein we look for. Electrophoresis of proteins with higher molecular weight can last up to 4 hours.

❖ **Electrophoresis buffer:** Tris 50 mM; Glicine 384 mM; 0.1% SDS at 10%. Adjust pH to 8.5 with HCl.

Transfer to a solid support consisted in transfer of the proteins from the acrylamide gel onto a nitrocellulose membrane. For this, we used the electroblotting method that uses capillarity and an electric current to pull the negatively charged proteins from the gel towards the positively charged anode into the nitrocellulose membrane. Nitrocellulose membranes are chosen for their non-specific protein binding properties (i.e. binds all proteins equally well). Protein binding is based upon hydrophobic interactions, as well as charged interactions between the membrane and protein.

Before using it, the membrane was cut in the needed size and was activated by immersing it in dH$_2$0 for 5 minutes. The following process had to be done in wet conditions with a transfer buffer. Membrane, gel, 6 Watman papers and 2 sponges were immersed in a tray that contained a transfer buffer. Then, the assembly of the transfer buffer was done by introducing the element between the sandwiches in the following order: transparent face of the sandwich, sponge, 3 Watman papers, activated membrane, gel, 3 Watman papers, sponge and black face of the sandwich. Wet sponges and Watman papers are used to induce the capillarity.

When the sandwich is prepared, it is introduced in the support with electrodes and, then, in the cuvette that is connected to the power supply. The transfer was run at 300 mA for 90 minutes generating an electric field that led proteins to migrate from the gel to the membrane. Due to the high voltage applied to the transfer, this process reaches a high temperature, therefore, this part of the western blot is done at 4ºC. In case of not having a cold room, it can be done by placing an ice cube in the cuvette and placing the cuvette in a container with ice and keeping the buffer in agitation.

Once the transfer was finished, a Ponceau stain was done in order to check that the procedure performance was good. The stain is a sodium salt of a diazo dye of a light red color that stains for a rapid reversible detection of protein bands on nitrocellulose membranes of western blotting. A Ponceau stain is useful because it does not appear to have a deleterious effect on the sequencing of blotted polypeptides as well as it is also easily reversed with water washes, facilitating subsequent immunological detection.

We simply dipped the membrane in Ponceau red for 5 minutes. After this time, it is washed with distilled water until the bands corresponding to the proteins that have migrated can be observed. If there is a signal and, therefore, the transfer has occurred correctly, the experiment can be continued with the certainty that the protein has migrated. It is recommendable to take a picture of the Ponceau staining. Before continuing, the membrane must be completely unstained with the aid of a transfer buffer.

❖ **Ponceau stain:** 0.1% Ponceau S; 5% acetic acid. Brought to the volume with ultrapure water.

Before marking target protein using proper antibodies a prior step has to be done, the blocking. Since the membrane has been chosen for its ability to bind protein and as both antibodies and the target are proteins, steps must be taken to prevent the interactions between the membrane and the antibody used for detection of the target protein. Blocking of non-specific binding is achieved by placing the membrane in a dilute solution of protein from non-fat dry milk (both are inexpensive) in Tris-buffered saline (TBS). The protein of the milk attaches to the membrane in all places where the sample proteins have not attached. Thus, when the antibody is added, it cannot bind to the membrane, and therefore the only available binding site is the specific target protein. This reduces background in the final product of the western blot, leading to clearer results, and eliminates false positives.

For our project, the membrane was dipped in a blocking solution that is composed of 5% non-fat milk diluted TBS during (5g in 100 ml) for 1 hour. During this time, the membrane was gently agitated with a mixer.

❖ **Blocking Solution:** 5% non-fat milk; brought to the volume with TBS
❖ **TBS:** 50 mM Tris; NaCl 150 mM. Adjust pH to 7.5 with HCl.

Next, marking the target protein with antibodies was done in a two steps process: first, the primary antibody incubation and second, the secondary antibody incubation.

The primary antibodies are generated when a host species or immune cell culture is exposed to the protein of interest (or a part thereof). Normally, this triggers an immune response therefore the generated antibodies are harvested and used as sensitive and specific detection tools that bind the protein directly.

The primary antibody was incubated at 4 ºC overnight diluted in blocking solution and under gentle agitation. The dilution will depend on both how effective the antibody

is and the amount of protein of interest in the sample. Usually, manufacturers provide a recommended dilution but it is always up to the research and his experimental knowledge.

- ❖ **Primary antibody:** 1**.** Mouse anti-α tubulin 1:1000 (Santa-Cruz Biotechonoly); 2. Rabbit anti-Kv4.3 1:250 (Alomone labs).

Between both incubations, the membrane was washed 3 times for 10 minutes with a washing solution (TBST), TBS that contains a detergent (0.5% Tween-20) and under gentle agitation.

- ❖ **TBST:** 50 mM Trisl; NaCl 150 mM; 0.5% Tween-20.

Secondary antibodies come from animal sources (or animal sourced hybridoma cultures). They recognize and bind to the species-specific portion of the primary antibody. Furthermore, to allow detection of the target protein, the secondary antibody is commonly linked to a reporter enzyme such as horseradish peroxidase. This means that secondary antibodies will bind to one primary antibody and enhance the signal, allowing the detection of proteins.

The primary antibody was incubated at room temperature for 2h diluted in blocking solution and under gentle agitation. The dilution will depend on the same criteria than the primary one. Usually, the secondary antibody dilution factor is higher.

- ❖ **Secondary antibody:** 1**.** Donkey anti-mouse 1:2500 (Sigma-Aldrich); 2. Donkey anti-rabbit 1:2500 (Santa Cruz Biotechnology).

After the secondary antibody incubation, the membrane was washed again 3 times for 10 minutes, as explained before. Washing the membrane helps to remove excess antibodies and avoid nonspecific noise in development.

After all this procedure, the western blot is ready for chemiluminescent detection of the probes that are labeled and bound to the protein of interest. The antibody provides the specificity to locate the protein of interest, and the HRP enzyme, in the presence of a substrate, produces a detectable signal. The chemiluminescent substrate is cleaved by HRP, resulting in the production of luminescence. Therefore, the production of luminescence is proportional to the amount of HRP-conjugated secondary antibody, and therefore, indirectly measures the presence of the target protein. Then, membrane exposure to the light from the reaction creates an image of the antibodies bound to the blot. The light is then detected by CCD cameras which capture a digital image of the western blot.

Size approximations are taken by comparing the stained bands to that of the marker or ladder loaded during electrophoresis. The process is commonly repeated for a structural protein, such as actin or tubulin that should not change between samples. The amount of target protein is normalized to the structural protein to control between groups.

In our case, 2 ml of substrate (Super Signal West Pico, Pierce) were added to the membranes and they were incubated for 5 minutes, protecting from light. After this time, membranes were drained and were carefully placed in the development equipment. Before developing, the molecular weights of the membrane were marked with a permanent marker for a later ladder recognition when developed. Finally, they were exposed for a variable time, depending on the antibody signal, in the Kodak Gel logic 2200 digital imaging equipment.

The image is analyzed by densitometry, which evaluates the relative amount of protein staining and quantifies the results in terms of optical density. We used the Image J program to measure the intensity of the bands. This analysis is considered semi quantitative. Image J gives an intensity related number to each selected band. Background intensity has to be calculated and then subtracted from the band's intensity.

The intensity number of each band was divided by the corresponding tubulin. Once this is done, the data is expressed numerically and can be compared, plotted and analyzed.

16. STATISTICAL ANALYSIS

Data are presented as means ± standard error of the mean (SEM). As variables were normal and showed homoscedasticity, analysis was carried out by parametric tests of means using the Student test when comparing two independent groups Data were compared with Student's t-test or analysis of variance followed by Bonferroni's t-test. When working with more than two study groups, the analysis of variance (ANOVA) was used, followed by the Tukey test or the Student-Newman-Keuls test. The differences obtained have been considered significant when the p-value is less than 0.05 (*), less than 0.01 (**), or less than 0.005 (***)

RESULTS AND DISCUSSION

RESULTS AND DISCUSSION

PART 1. CHARACTERIZATION OF A METABOLIC-INDUCED MODEL OF TYPE 2 DIABETIC RAT

One of the purposes of our project was the characterization of a metabolic-induced model of type 2 diabetic rat that reproduces the metabolic and cardiac electrical disturbances observed in type 2 diabetic patients. Different combinations of high-caloric diets (fructose rich, fat rich) and low STZ doses have been used to induce type 2 diabetes in mammals [63-65, 191]. As previously explained in section 3 of material and methods, we used a diet with 45% Kcal from lipids to cause progressive insulin resistance. After two weeks, we injected a 35 mg/kg of STZ intraperitoneal to induce mild impairment of insulin secretion by the destruction of some beta cells. 48 hours after STZ administration diabetes was confirmed by elevated fasting glucose and animals continued consuming high fat diet throughout the whole experimental period. We weekly measured metabolic and electrocardiographic parameters. Thus, in this work we characterized an animal model with the main metabolic and electrocardiographic characteristics of type 2 diabetic patients in a reasonable period of 6 weeks.

Our protocol for inducing diabetes combines two variables: feeding on high-fat diet for 6 weeks and a single streptozotocin injection at week 2. According to previous publications, we assumed that HFD induces insulin resistance and the STZ injection induces hyperglycemia. Hence, we established two more control groups for the type 2 diabetes rat model to confirm that the effects observed in the model were due to the pathology, and not to isolated effects of the HFD or the STZ. The same experimental protocols were applied to the four groups: control; HFD; STZ; and diabetic.

1. METABOLIC ALTERATIONS OF TYPE 2 DIABETIC RATS

1.1. TYPE 2 DIABETIC RATS ARE HYPERGLYCAEMIC

The World Health Organization (WHO) diabetic diagnosis criteria established the definition of diabetes (both type 1 and type 2) in either a single raised glucose reading with symptoms or two raised values measured in different occasions, of fasting plasma glucose ≥ 126 mg/dl. Thus, a person who has a consistent glycemic range between 100–126 mg/dl is considered slightly hyperglycemic. If glycaemia rises above 126 mg/dl is is considered to have diabetes according to American Diabetes Association guidelines. We monitored fasting blood glucose levels weekly to ensure that animals have hyperglycemia like 2 diabetes patients. 72 hours after STZ injection, plasmatic glucose levels were measured in overnight fasting rats. Only animals with a glucose range between 130 mg/dl and 250 mg/dl were selected. As can be observed in figure 39, after STZ injection fasting glucose levels rapidly rose from 95 mg/dL to approximately 170 mg/dL in the diabetic group (p<0.01) and remained elevated and significantly higher than those of the control group. Therefore, Type 2 diabetic rats had sustained hyperglycemia, as happens in Type 2 diabetic patients [201].
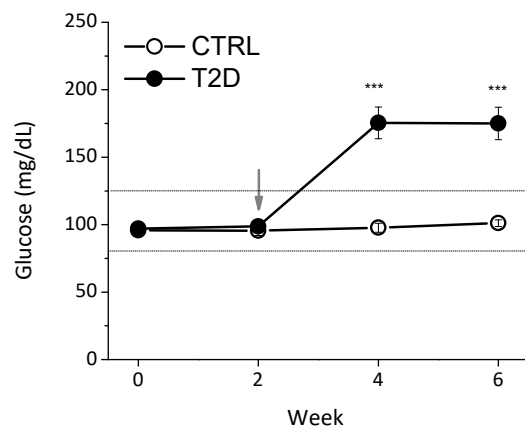
Figure 39. Type 2 diabetic rats show elevated plasma glucose. Weekly fasting plasma glucose throughout the experimental period. The dotted lines indicate the physiological interval for plasma glucose. The arrow indicates the injection of STZ or vehicle. CTRL n=23; T2D n=18; ***p<0,005

1.2. TYPE 2 DIABETIC ANIMALS HAVE INSULIN RESISTANCE

In states of insulin resistance, insulin receptors desensitize, preventing insulin from lowering blood glucose levels. Therefore, insulin resistance increases hyperglycemia because normal insulin levels are not sufficient to regulate glucose homeostasis.

As Type 2 diabetes characterizes by hyperglycemia and insulin resistance, a valid type 2 diabetic animal model should have both. To confirm that in our type 2 diabetic animals hyperglycemia is caused by insulin resistance we made tolerance tests for insulin and glucose. Insulin resistance can be determined by a glucose tolerance test, whereas insulin sensitivity can be analyzed by the insulin tolerance test. Insulin resistance and insulin sensitivity are two sides of the same coin. Someone who has insulin resistance will have low insulin sensitivity, and someone sensitive to insulin, will have low insulin resistance.

In previous experiments in our lab, we observed that some animals became severely hypoglycemic during the insulin tolerance test. To avoid hypoglycemia, that *per se* is arrhythmogenic, we switched to a combined insulin and glucose tolerance test. This test, called intraperitoneal insulin-glucose tolerance test (IPIGTT), is based on a previous protocol [194] and is valid for testing insulin resistance.
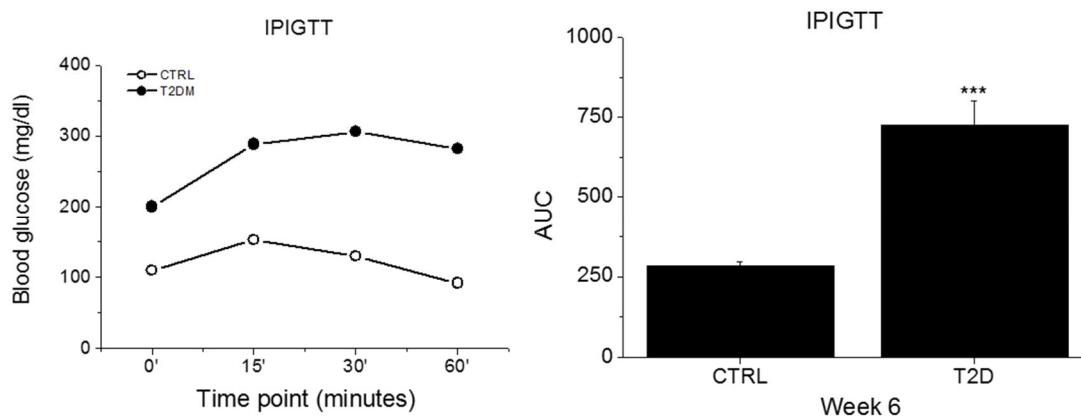
Figure 40. Type 2 diabetic rats show insulin resistance. **A)** IPIGTT performed at the end of the experimental period (week 6). **B)** The corresponding Area Under the Curve (AUC). CTRL n=15; T2D n=18; ***p<0,005.

Therefore, to confirm that the high fasting glucose levels observed in diabetic animals was due to insulin resistance, we performed an intraperitoneal glucose/insulin tolerance test at the end of the experimental period (week 6). After the injection of the bolus of glucose and the insulin, plasma glucose levels in diabetic rats were significantly higher than in control at all the time points tested (figure 40 A, B). In control animals, insulin normalizes blood glucose in 30 minutes. However, diabetic animals could not restore glycemia even after 60 minutes, indicating significant insulin resistance. Thus, IPIGTT confirms that our model displays the insulin resistance characteristic of type 2 diabetes patients.
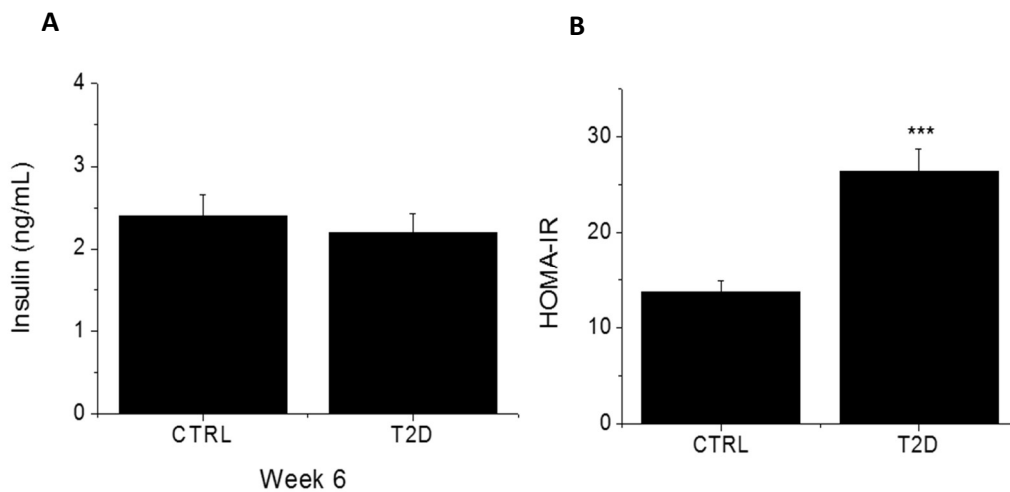
Figure 41. Type 2 diabetic rats show elevated insulin resistance. **A)** Plasma Insulin levels after 4 weeks of diabetes. CTRL n=16; T2D n=10. **B)** HOMA-IR index after 4 weeks of diabetes. CTRL n=10; T2D n=8; ***p<0,005.

Unlike type 1 diabetes, type 2 diabetes does not associate with a complete lack of insulin at early stages. We determined serum insulin levels at the end of the experimental period. Four weeks after diabetes induction insulin levels were not significantly different between control and diabetic animals (figure 41 A). Thus, as expected 35 mg/kg STZ slightly damaged the pancreas and destroyed some but not all β-cells, since insulin secretion was not abolished. Since fasting plasma insulin was similar in diabetics than in control animals, the high blood glucose was due to insulin resistance and the inability of the pancreas to compensate by increasing as is described in type 2 diabetes patients [202].

Complementary, the HOMA index (Homeostatic Model Assessment) was calculated. HOMA-IR is a simple method that assesses insulin resistance using fasting glucose and insulin parameters and, it is used for quantifying insulin resistance. As in patients [202], HOMA-IR is significantly higher in type 2 diabetic animals, indicating insulin resistance (figure 41 B).

This group of experiments shows that the combination of HFD and STZ injection in rats is an effective method to induce insulin resistance and hyperglycemia. Thus, our animal model reproduces the two main characteristic of type 2 diabetes.

1.3. TYPE 2 DIABETIC ANIMALS SHOW ALTERED LIPID PROFILE

Dyslipidemia is the abnormal amount of lipids (e.g., triglycerides or cholesterol) in the blood. Hyperlipidemia is a common feature of diabetes and one of the risk factors for cardiovascular disease. The most common hyperlipidemia in type 2 diabetes involves high levels of serum triglycerides and cholesterol particles. In contrast to type 1 diabetes, in type 2 diabetes achieving glycemic control does not usually correct hyperlipidemia. Therefore, defects in insulin action, and not hyperglycemia per se, associate with abnormal lipid profile in type 2 diabetes [203].
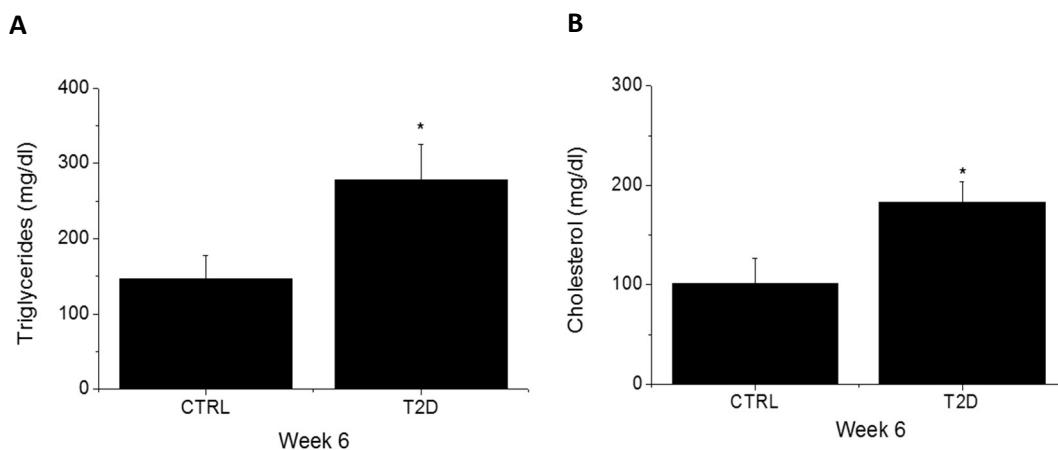
Figure 42. Hyperlipidemias of the type 2 diabetic model. Plasma lipid levels of **A)** triglycerides and **B)** cholesterol. CTRL n=13; T2D n=8; *p<0,05.

Because of the relevance of hyperlipidemias in type 2 diabetes, specifically in associated cardiovascular complications, we tested whether plasma levels of triglycerides and total cholesterol were increased after 4 weeks of diabetes. These

results reveal a significant increase in plasma triglycerides and cholesterol in type 2 diabetic animals (figure 42 A, B). This gives our type 2 diabetic model more clinical interest because reproduces a main metabolic feature of type 2 diabetes associated with higher risk of cardiovascular complications [204].

1.4. TYPE 2 DIABETES DOES NOT CAUSE OBESITY IN RATS BUT INCREASES FAT ACCUMULATION

Although obesity and overweight are often associated with insulin resistance and type 2 diabetes, not all diabetic patients have obesity or overweight. However, they often have excess of metabolic active fat, especially accumulation of visceral adipose tissue [205]. In rodents, visceral fat is composed of several adipose depots, including mesenteric, epididymal white adipose tissue (EWAT), and perirenal depots [206]. Epididymal fat pads are typically the largest and most readily accessible fat pads and, for these reasons, they are the most frequently used in the literature.
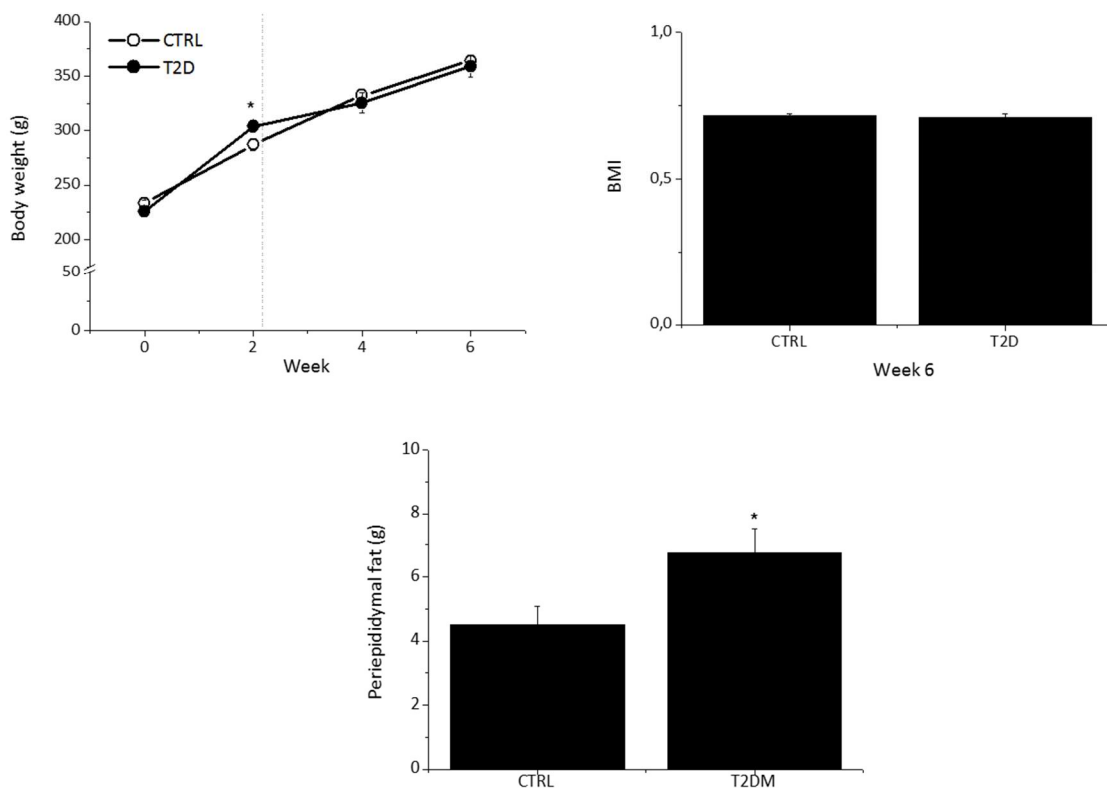
Figure 43. Changes in fat accumulation, but not in body weight, in the type 2 diabetic model. **A)** Body weight. **B)** Body mass index (BMI) at the end of the experimental period (week 6). CTRL n=20; T2D n=22 **C)** Periepididymal fat. CTRL n=12; T2D n=16; *p<0,05.

We make weekly weight measurements during the experimental period. We observed that two weeks on high-fat diet significantly increased the body weight of diabetic animals, but the STZ injection truncated the tendency and, the body weight of control and type 2 diabetic rats did not show significant differences at the end of the experimental period (figure 43 A). The effect of STZ injection in body weight has been previously reported in other models for Type 2 diabetes induction. It may be caused by a decreased glucose metabolism and increased fat metabolism [207].

Furthermore, body mass index, used to correlate weight and height, is similar in control and diabetic animals at the end of the experimental period (figure 45 B). However, although type 2 diabetes induction does not cause overweight or obesity, the periepididymal fat is significantly increased in diabetic animals (figure 43 C). Thus, type 2 diabetic rats reproduce the excess of regional adipose tissue accumulation without increased body weight, frequently observed in type 2 diabetic patients, that may play a central role in the development of T2D [208].

1.5. TYPE 2 DIABETES INDUCTION CAUSES POLYDIPSIA AND POLYPHAGIA

Higher needs of food (polyphagia) and water (polydipsia) intake are common symptoms of T2DM. Polydipsia is caused by increased blood glucose levels, whereas polyphagia by insulin resistance [209]. We weekly monitored the food and water intake and observed that type 2 diabetic rats consumed more water and food than age-matched controls (figure 44 A, B). Therefore, the combination of high fat diet and STZ injection reproduces the polydipsia and polyphagia reported in diabetic patients.
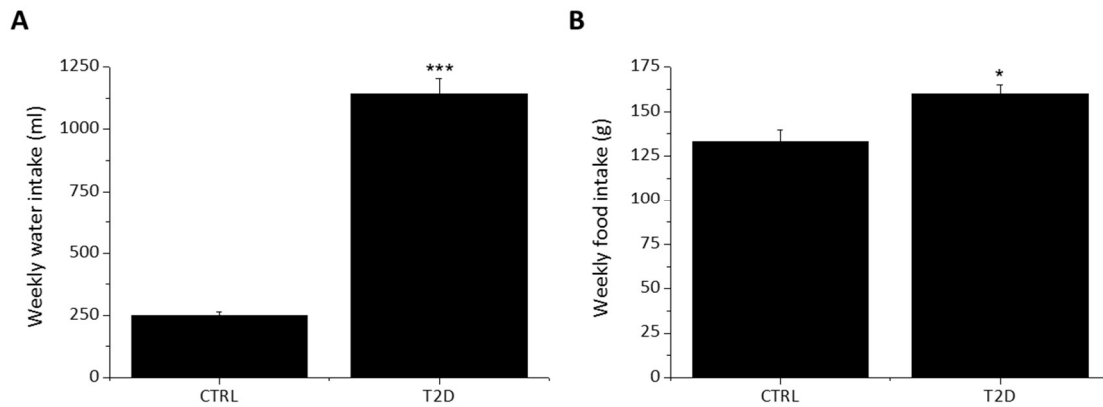
Figure 44. Diabetic rats have both polydipsia and polyphagia. **A)** Weekly water intake. **B)** Weekly Food intake. CTRL n=15; T2D n=22; *p<0,05; ***p<0,005.

1.6. ADDITIONAL CONTROL GROUPS STRENGTHEN THE BIOCHEMICAL VALIDATION OF THE ANIMAL MODEL

As previously explained, we created two more control groups for the type 2 diabetic rat model to test the effects *per se* of HFD and STZ injection and their roles in the development of the disease. Data from these groups indicate that fasting plasma glucose levels in Chow+STZ and HFD groups, although significantly higher than in control, were lower than in the diabetic group and remained close to or below physiological limits (table 4). Hence, STZ alone and HFD feeding alone are not sufficient to induce the hyperglycemia observed in the diabetic group. Although 35 mg/kg STZ injection initially caused pancreatic β-cell damage and hyperglycemia, damage was not enough to maintain consistent hyperglycemia for 4 weeks. This fact has been previously described [210] and indicates that STZ induced mild impairment instead of complete dysfunction in the pancreas. Thus, it is the combination of STZ injection and HFD feeding that causes consistent hyperglycemia for 4 weeks.

Four weeks after diabetes induction, plasma insulin levels were not significantly different between the four experimental groups. Nevertheless, the HFD group showed insulin resistance in the IPIGTT (table 4). This demonstrates that HFD, and not STZ injection, induces insulin resistance after 6 weeks. Feeding with a high-fat diet caused a significantly higher accumulation of epididymal fat, both in the HFD an in the T2D group, that is related to the development of insulin resistance [208]. It also caused an increase

in body weight (table 4). Conversely, as reported in the literature [207], Chow+STZ animals had a significant decrease in both epididymal fat accumulation and body weight (table 4). Regarding the lipid profile, high-fat diet feeding induced hypercholesterolemia and slightly (not significantly) elevated circulating triglycerides. This dyslipidemia is caused by the fatty acids of the diet [211].

This group of results are consistent with publications using similar type 2 diabetes models [210, 212]. It is the combination of both STZ injection and HFD feeding that accurately reproduces a type 2 diabetes rat model.

	CONTROL	CHOW+STZ	HFD	DIABETIC
Body weight (g)	364.1±4.2	331.7±12.3*	374±4.7*	346.8±10
Glucose (mg/dL)	101.1±2.5	127.8±7.2**#	122±5.6**#	175.05±12***
Cholesterol (mg/dL)	67.1±9.4	100±34	198.6±16.8**	183±20.6**
Triglycerides (mg/dL)	146.1±32	205.1±60.3	169.2±57	207.7±15.5*
IPIGTT (AUC)	394±16	413±92	519±107*	723±56**
Insulin (ng/mL)	2.4±0.3	1.9±0.01*	2.2±0.1	2.2±0.2
Epididymal Fat (g)	4.1±0.4	3.3±0.4* ##	7.2±0.5**	6.2±0.5**

Table 4. Animal characteristics for control, chow+streptozotocin, high-fat diet (HFD), and DIABETIC (HFD+STZ) groups, measured at week 6. Data are mean ± SEM, n=8-17 per group; *p< 0.05, **p<0.01 compared to control; #p<0.05, ##p<0.01 compared to diabetic group.

2. CARDIAC ELECTRICAL REMODELING OF DIABETIC RATS

2.1. TYPE 2 DIABETICS RATS DO NOT DEVELOP APPARENT CARDIAC HYPERTROPHY

Diabetes associates with changes in the structure and function of the myocardium that is not directly attributable to other confounding factors such as coronary artery disease or hypertension. These changes result in cardiac hypertrophy that has been associated with ventricular arrhythmias. The Framingham Heart Study identified cardiac hypertrophy as a blood pressure-independent risk for sudden cardiac death [213]. Thus,

cardiac hypertrophy may be a cause of arrhythmia and sudden death in type 2 diabetes rats.
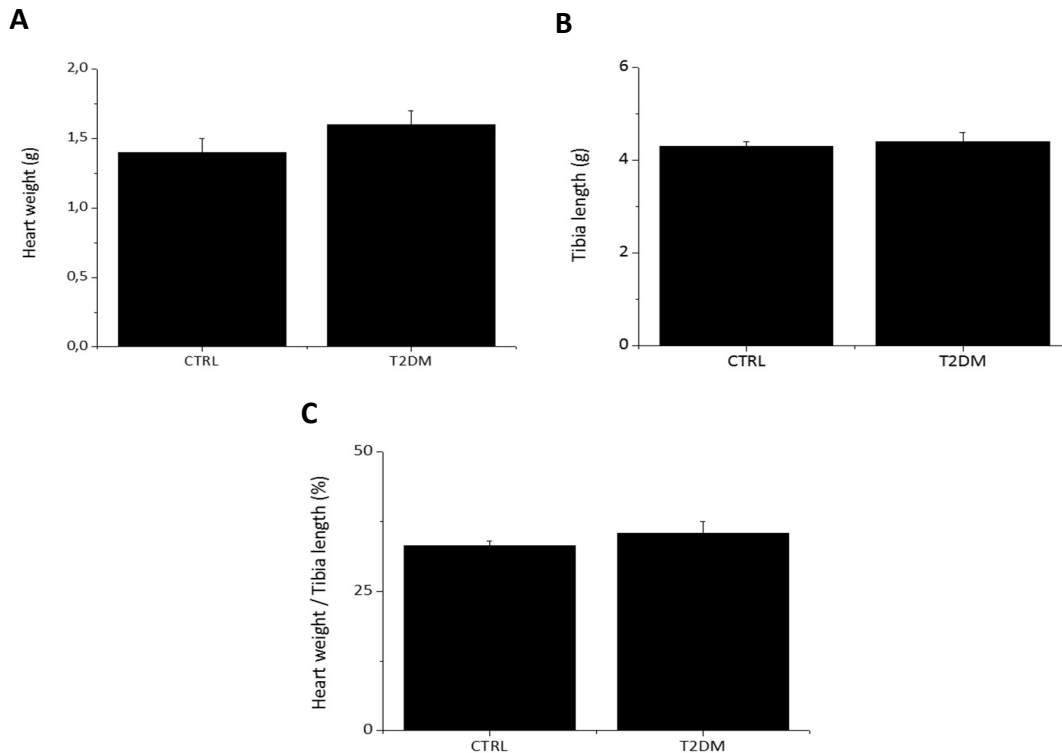
Figure 45. Type 2 diabetes rat model does not show apparent cardiac hypertrophy. A) Heart weight. **B)** Tibia Length. **C)** Hypertrophy index consisting in a ratio between heart weight and tibia length. CTRL n=10; T2D n=10.

Different ways can be used to assess the degree of cardiac hypertrophy. Some authors use the absolute increase in heart weight as an index, whereas others use the heart weight-body weight ratio. However, there are limitations that restrict their usefulness. The heart weight measurements overlook the contribution of the animal size. The heart weight-body weight ratio implicitly assumes either that body weight remains constant or that heart weight changes in parallel with body weight under normal conditions. Since this may yield misleading results, body weight is not a good parameter to assess cardiac hypertrophy relative to body. In mature rats, the tibia length changes minimally, and the tibia growth curve is not affected by lesions that might appear during the lifetime of the rat or changes in body weight. Therefore, we considered that the heart weight/tibia length is the most accurate index to determine cardiac hypertrophy [214]. We compared the heart weights and the heart weight/tibia

length ratio. Type 2 diabetes animals do not seem to have cardiac hypertrophy because there is no significant variation in heart weight or the hypertrophy index with the control group (Fig 45 A, C). Although additional experiments could be performed to further confirm absence of cardiac hypertrophy, our data indicate that in our diabetic animals cardiac dysfunctions are not caused by cardiac hypertrophy.

2.2. TYPE 2 DIABETIC ANIMALS SHOW ALTERATIONS IN THE ELECTROCARDIOGRAM

The epidemiological studies in general population samples have shown that patients with type 2 diabetes are at higher risk of sudden cardiac death. However, the causes underlying the increased vulnerability of the cardiac electrical substrate in diabetic patients are unclear. One of the described predictors of severe ventricular arrhythmia and subsequent sudden death are the ECG repolarization abnormalities such as a prolonged QT interval [215]. Prolonged QT interval duration has been consistently reported in diabetic patients [103, 135]. Therefore, we aimed to develop a type 2 diabetic animal model with electrocardiographic, besides metabolic, disturbances. To analyze the cardiac electrical characteristics of our diabetic model, we recorded the II-lead of the ECG to conscious animals weekly (figure 46 A). In diabetic animals, waves and intervals of the ECG related to atrial function and ventricular depolarization were normal (figure 46 B, C, D). Diabetes did not modify either atrial or ventricular depolarization, measured as P wave and QRS complex duration respectively (figure 46 C, D). The PR interval duration, an indicator of cardiac impulse conduction at the atrioventricular node, was also similar in control and diabetic animals (figure 46 B, table 5). Diabetes is an independent risk factor for atrial fibrillation, although the mechanisms underlying the increased susceptibility to AF in DM are not completely understood [216]. Unlike Zucker rats, a genetic model of type 2 diabetes who have higher susceptibility to AF [94], our metabolic-induced model does not affect atrial function.

However, the electrocardiograms of diabetic animals and age-matched controls showed clear differences. At the end of the experimental period diabetic animals, as well as the animals in the Chow+STZ group, had a lower heart rate than control animals.

RR interval duration in diabetic and Chow+ STZ rats was significantly longer than in control animals (figure 47 A, table 5). This effect in heart rate has been also described in type 2 diabetic patients and is due to the T2D-associated cardiac autonomic neuropathy [217]. In our animals, as Chow+STZ rats also show variability in the heart rate, the effect may also be produced by the effect of STZ injection. Nevertheless, only animals in the diabetic group (high-fat diet plus STZ) had repolarization abnormalities.
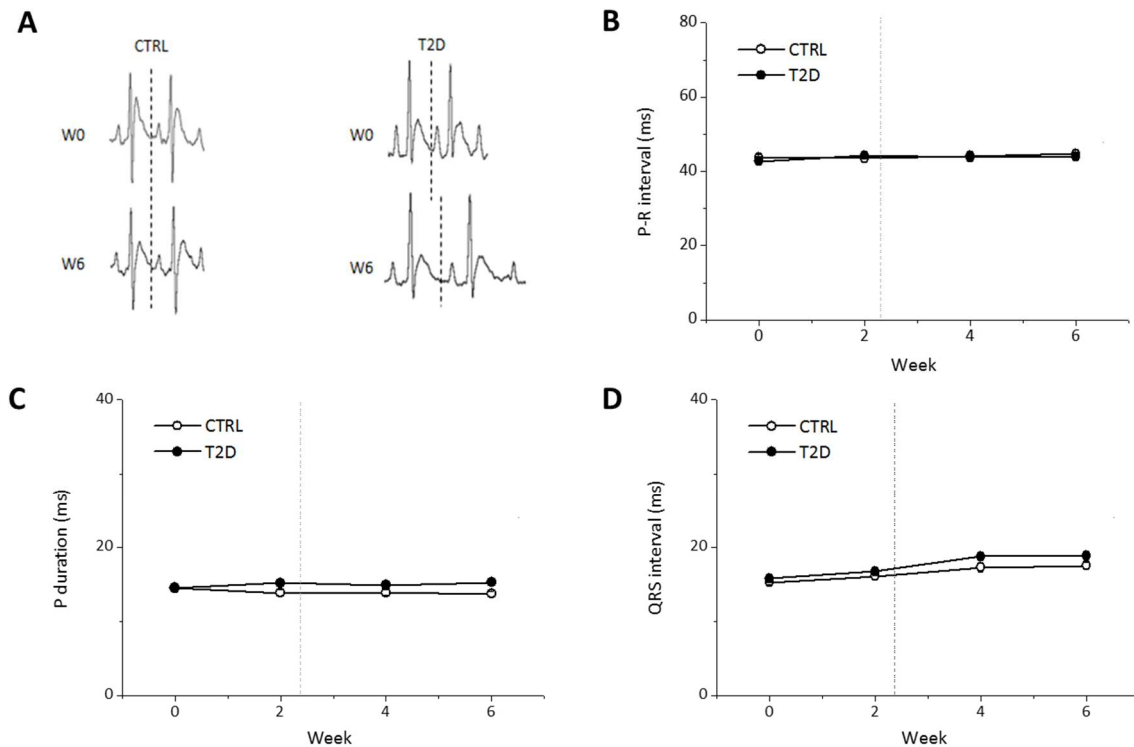
Figure 46. Cardiac electrical remodeling of the diabetic heart reduces heart rate but does not affect the atria and the ventricular depolarization. **A)** Electrocardiographic recordings in a control and a diabetic animal before and after the 6 weeks experimental period. The dotted line shows the end of the T wave. **B)** PR interval; **C)** P wave duration; and **D)** QRS complex of the ECG throughout the experimental period. CTRL n=19; T2D n=30; **p < 0.01. The dotted line in B-D shows the moment of STZ or vehicle injection.

From the first week after STZ injection diabetic rats showed the expected prolongation of the repolarization time, seen as the prolonged QT and QTc intervals, and the prolonged Tpeak-Tend, an electrocardiographic marker of the transmural dispersion of repolarization (figure 47 A-D). As diabetic patients show repolarization abnormalities associated with increased risk of ventricular arrhythmias and mortality, prolonged QTc and Tpeak-Tend are used in clinical settings to predict the risk of sudden cardiac death [87, 217, 218].
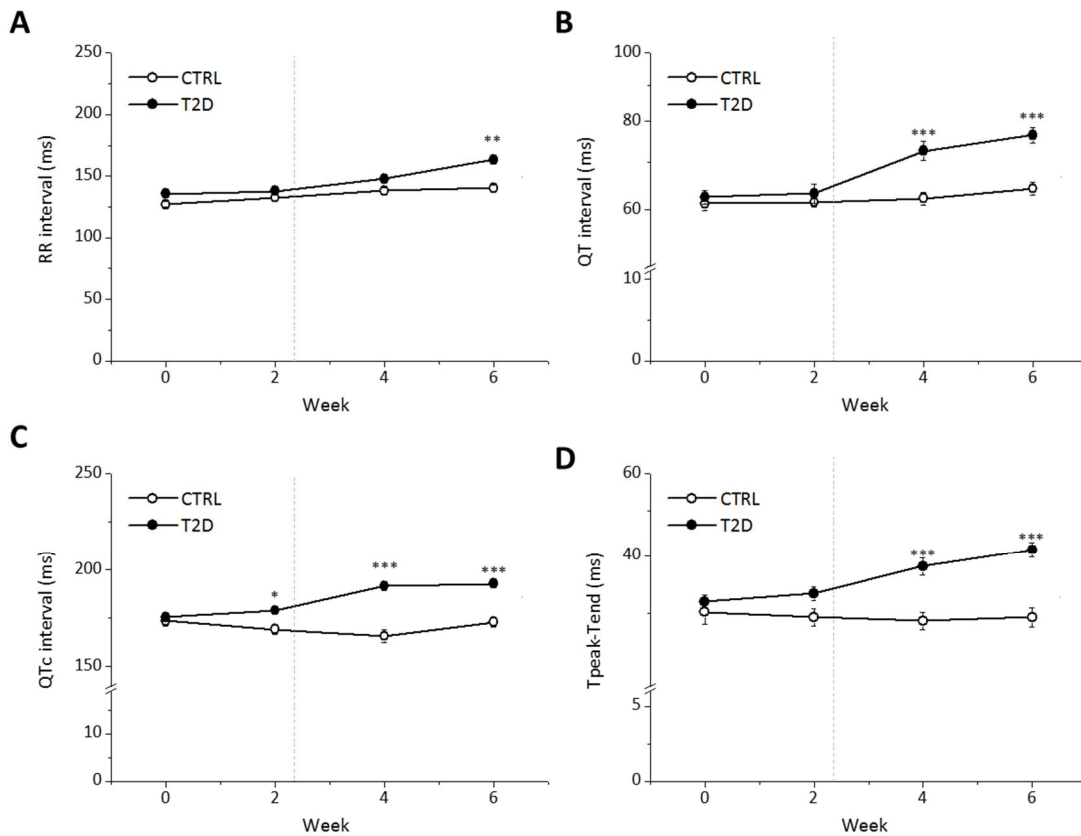
Figure 47. Cardiac electrical remodeling of diabetic heart induces abnormalities in ventricular repolarization. **A)** Heart rate represented by the RR interval of the ECG **B-D)** Main repolarization parameters of the ECG: QT, QTc, and Tpeak-Tend. CTRL n=19; T2D n=30; *p < 0.05, **p < 0.01; **p < 0.005. The dotted line in B-G shows the moment of STZ or vehicle injection.

2.3. ADDITIONAL CONTROL GROUPS ALSO VALIDATE THE ECG RESULTS OF THE DIABETIC ANIMAL MODEL

As was made for the metabolic disturbances, we also analyzed the ECG recordings of the additional control groups for the diabetic model, in order to identify whether the ECG were due to either STZ injection or HFD alone.

Only one abnormality was found in these control groups. Like diabetic rats, animals in the Chow+STZ group showed a prolongation in the R-R duration (figure 47, table 5). Thus, the longer R-R interval of the diabetic group may be a result of the STZ injection.

	CONTROL	Chow+STZ	HFD	DIABETIC
RR (ms)	141.2 ± 2.5	159.6 ± 7.24**	136.2 ± 1.17	157.6 ± 3.9**
PR (ms)	44.48 ± 1.01	44.41 ± 1.36	45.34 ± 1.16	44.07 ± 0.92
P (ms)	13.65 ± 0.35	14.68 ± 0.82	15 ± 0.58	14.94 ± 0.42
QRS (ms)	17.16 ± 0.3	17.04 ± 0.71	16.32 ± 0.82	18.79 ± 0.93
QT (ms)	64.2±1.3	66±2.2	67.5±1.5	76.5±1.5**
QTc (ms)	122.8 ±1	125.5 ± 1.56	116.6 ± 1.2	141.4 ±1.3**
T_{peak}-T_{end} (ms)	29.4±1.4	33.9±1.1	35±1.5	42.4±1.3**

Table 5. ECG analysis of the control groups for the diabetic model. Data are mean ± SEM, n=6-30 per group; **$p<0.01$ compared to control.

2.4. TYPE 2 DIABETIC HEART IS MORE PRONE TO LIFE-THREATENING ARRHYTHMIA

The ECGs of Type 2 diabetes rats showed alterations in the cardiac repolarization, which is related with a higher risk of ventricular arrhythmia. Prolongations of QT and Tpeak-Tend interval durations are arrhythmia surrogates, so we next tested the arrhythmia susceptibility of control and diabetic animals under a caffeine/dobutamine cardiac challenge (figure 48 A). Arrhythmia-induction protocol was performed as previously described [198]. It consisted in an intravenous injection of dobutamine, a beta2-sympathomimetic agonist, followed by an intraperitoneal injection of caffeine. Both substances have effects that increase the heart contractility and rate as well as the left ventricular output. Ventricular arrhythmia were classified according to Lambeth convention [219], and only life-threatening arrhythmia were quantified. Torsade de Pointes, the most severe type of ventricular tachycardia, was considered apart.
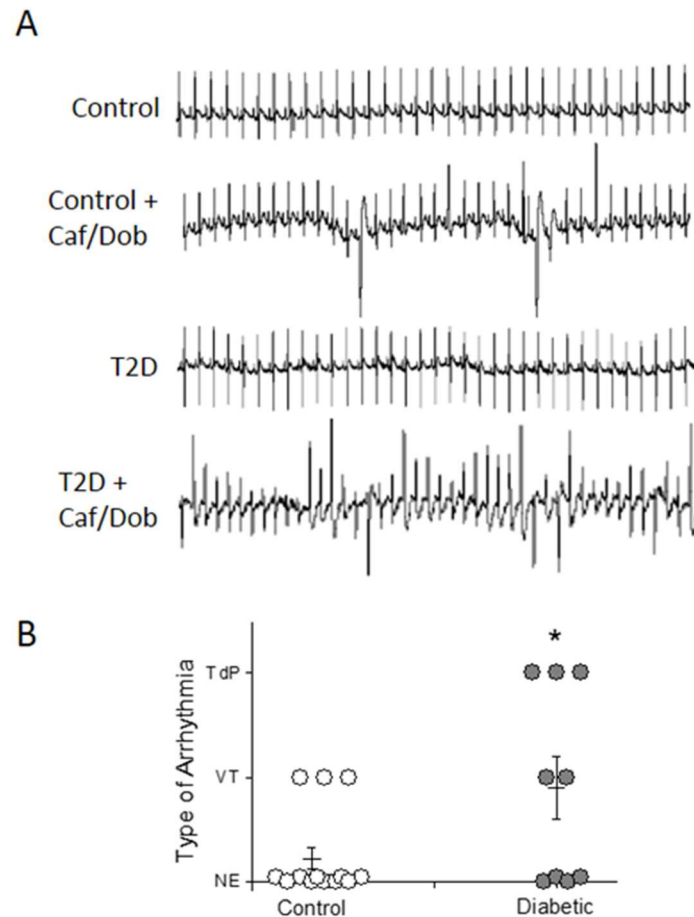
Figure 48. Increased arrhythmia susceptibility in diabetic heart. A) Examples of non-arrhythmic and arrhythmic electrocardiographic recordings in control and diabetic animals before and after caffeine/dobutamine challenge (Caf/Dob). **B)** Incidence and severity of ventricular tachycardias and TdP in control and diabetic animals. Each arrhythmia was scored as No Events (NE) = 0; Ventricular Tachycardia (VT) = 1; and TdP = 2. CTRL n=14; T2D n=10; *p < 0.05.

In this sense, when subjected to proarrhythmic conditions with the caffeine/dobutamine challenge, diabetic animals developed more arrhythmic episodes and more severe than control animals (figure 48 B). Cardiac challenge results show that ventricular tachyarrhythmias were more frequent in type 2 diabetes than in control animals (55% vs 23%). It is also important to note that cardiac challenge induced the potentially lethal arrhythmia torsade de pointes in one out of three type 2 diabetic animals. By contrast, none of the control animals developed torsade de pointes under the same challenge (figure 48 B). Thus, as previous described [100, 103, 105], the prolongation of QT and Tpeak-Tend of the type 2 diabetes rats translates into a higher susceptibility to life-threatening ventricular arrhythmia and therefore, higher risk of

sudden death. Type 2 diabetes patients have more prevalence of ventricular arrhythmia [220] and animals of the type 2 diabetes model reproduce this fact.

2.5. TYPE 2 DIABETES MODEL AFFECTS THE REPOLARIZATION CAPABILITY OF THE HEART

Prolongation of cardiac repolarization is related with alterations in the electrical activity of the cardiomyocytes. At the cellular level, diabetes can induce lengthening in the cardiac repolarization time by affecting the expression and activity of several cardiac ionic channels and their corresponding ionic currents. In several animal models of diabetes (mainly type 1 diabetes), reduction of the transient outward K^+ current (Ito) has been proposed as a main cause of prolonged repolarization [58, 60]. The Ito is responsible for the early repolarization phase of the ventricular action potential and influences the amplitude and duration of the currents involved in the plateau phase, thereby modulating the length of the action potential. Prominent Ito currents have been recorded in ventricular myocytes isolated from the hearts of many mammalian species, including rats and humans. Specially in rodents, Ito is the prominent repolarization current in ventricular myocytes [67].

Due to the critical role of the Ito in ventricular repolarization we recorded and quantified Ito current density in left ventricular myocytes isolated from control and diabetic animals (figure 49 A). Our results in the type 2 diabetic model are in agreement with the previous published results that determined that prolonged repolarization is caused by a reduction of the Ito in type 1 diabetes. We found that Ito density in type 2 diabetic animals is smaller than in control animals. In diabetic cardiomyocytes Ito was significantly smaller that in control cells at positive voltages (figure 49 B). At +50 mV, Ito density was approximately 50% smaller in diabetic than in control cells (Figure 49 C).

The strong reduction on Ito density caused by diabetes reduced the repolarization capacity of the ventricular cells. This can explain the prolonged repolarization time of the whole heart observed in the electrocardiogram. Therefore, these data confirmed that our metabolic-induced diabetic model reduces Ito amplitude, which may lead to the prolonged QTc observed in the ECG.
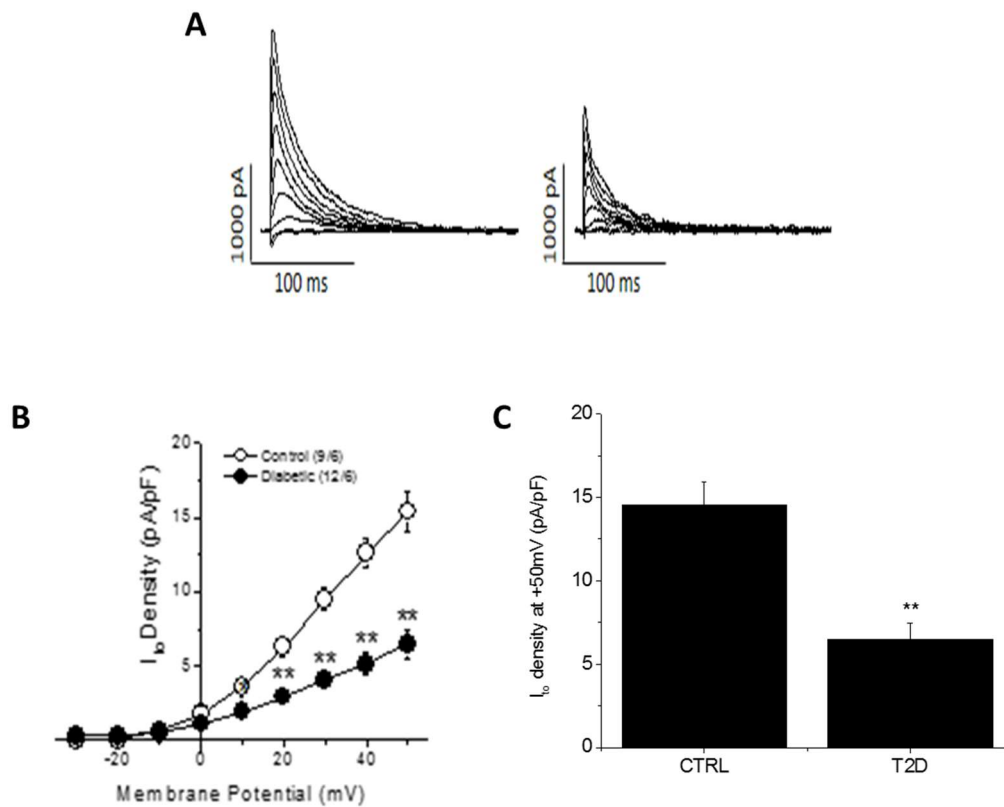
Figure 49. Type 2 diabetes animals show a reduction in the Ito current density. **A)** Current traces of a current-voltage protocol of the transient outward current (Ito) elicited in ventricular control and diabetic cells of similar size. **B)** Ito density/voltage relationships. **C)** Ito density at +50 mV in control and diabetic cells. CTRL= 9/6, T2D= 12/6 (number of cells/number of animals). **p < 0.01.

2.6. TYPE 2 DIABETES REDUCES THE EXPRESSION OF THE Ito CHANNEL

Changes in ionic currents are often caused by a decrease in the channel protein expression. In type 1 diabetes, Ito current reduction is accompanied by the decrease of the channel protein expression [221]. In rats, the Ito channels are formed by two α-subunits of the Kv4 family: Kv4.2 and Kv4.3, which is the most expressed subunit of Ito channels in rat adult cardiac cardiomyocytes. We analyzed by western blotting the semi-quantitative expression of the Kv4.3 channel subunit in diabetic and control rat cardiac cardiomyocytes (figure 50 A).

The western blot analysis shows a significant reduction in the expression of the Kv4.3 protein in diabetic cells compared to control. Relative densitometry of the Kv4.3 subunit

is lower in type 2 diabetes samples, which indicates a reduction in the expression of Kv4.3 (Figure 50 B). Thus, the observed reduction of Ito in diabetic cardiomyocytes is completely or partially caused by the reduction of Kv4.3 expression.

A

CTRL T2D

Kv 4.3 (75 kDa)

Tubulin (50 kDa)

B
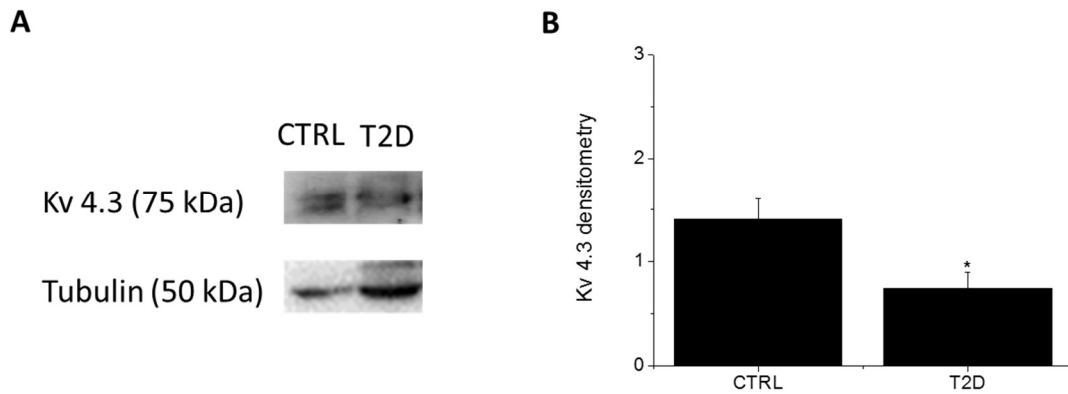
Figure 50. Type 2 diabetes cardiomyocytes reduce Kv4.3 expression in rat adult ventricular cardiomyocytes. **A)** Representative western blot images of Kv4.3 and the used charge control (tubulin). **B)** Relative densitometry of Kv4.3 expression to tubulin expression. CTRL= 3/3, T2D= 3/3 (amount of cells/number of animals). *p < 0.05.

2.7. INCREASING IN SPONTANEOUS CALCIUM SPARKS IS AN ARRHYTHMOGENIC MECHANISM PRESENT IN THE TYPE 2 DIABETES RAT MODEL

Calcium plays a central role in the contraction of the heart. It is the bi-directional link between electrical excitation of the heart and contraction. A misbalance in the calcium cytoplasmic levels such as elevated intracellular calcium concentrations can lead to a cardiac arrhythmia by triggering the initiation event of excitation-contraction coupling. Calcium misbalance is often caused by a calcium release from the sacroplasmatic reticulum (SR) that elevates intracellular calcium concentration. These calcium release events are called calcium sparks and are detected as a microscopic release of calcium [222]. Studies in type 1 diabetic rats identified alterations of Ca^{2+} signaling via changes in critical processes that regulate intracellular free Ca^{2+} concentration [223]. Other studies [113, 123] also reveal that ventricular myocytes isolated from STZ-induced diabetic rat hearts exhibit an increased frequency of spontaneous Ca^{2+} sparks leading to an increased basal $[Ca^{2+}]i$ due to calcium leaking from SR that is associated with

hyperphosphorylation of RyR. Thus, Calcium sparks are a described intracellular mechanism that causes ventricular arrhythmia in type 2 diabetes [224]. Then, understanding the dynamics of Ca^{2+} sparks is essential for understanding the function of the heart. Investigation of Ca^{2+} sparks in diseases like type 2 diabetes has also begun to provide novel insights into underlying physiopathology such as cardiac arrhythmias and heart failure.
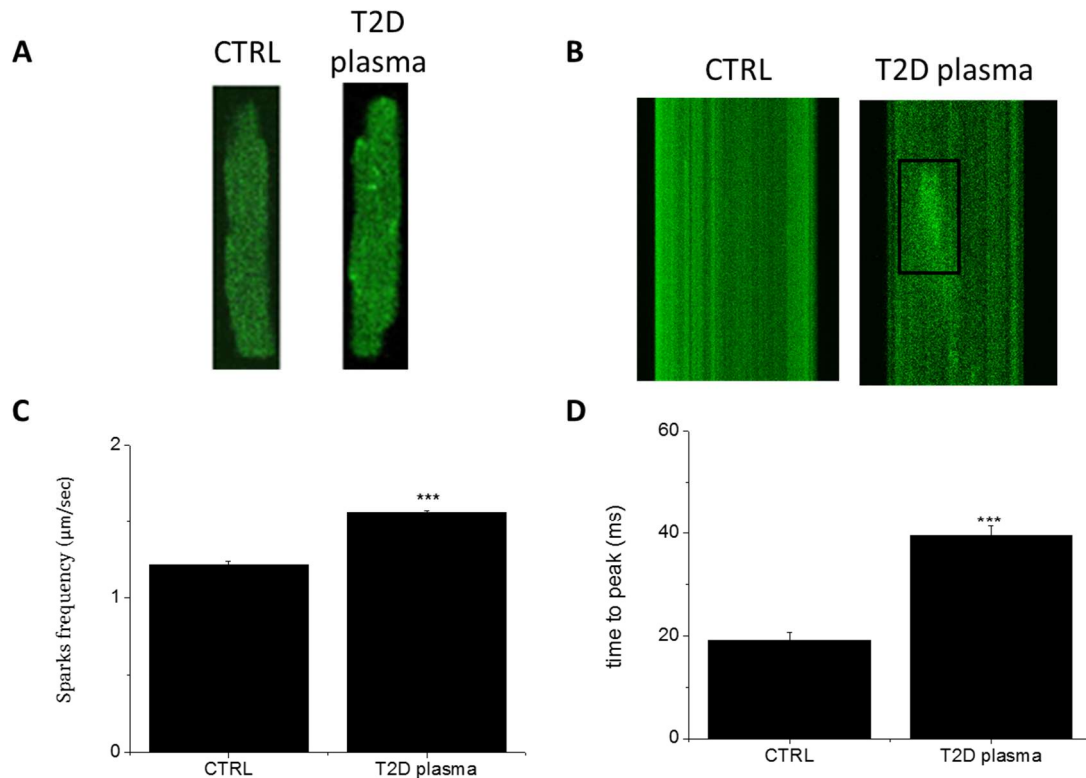
Figure 51. Type 2 diabetes serum induces higher spontaneous calcium sparks in control cardiomyocytes. **A)** Original confocal images recorded in Fluo-3-loaded isolated left ventricular cardiomyocytes after 24 incubation with DMEM supplemented with control serum and DMEM supplemented with T2D serum. **B)** Representative individual line-scan images (x vs t) of the cardiomyocytes from the control and type 2 diabetes serum that display a calcium spark marked with a square. **C)** Comparison of Ca^{2+} sparks frequency. More sparks per cell were observed in cardiomyocytes incubated with Type 2 diabetes serum **D)** Time to peak. Measurements of the time of the peak amplitude. CTRL= 30/10; T2D plasma= 15/5. In parenthesis (number of cells/number of animals); ***p<0.005 with respect to control.

Hence, we hypothesized that the spontaneous calcium sparks are another intracellular mechanism that leads to the previously described higher risk of life-threatening ventricular arrhythmia in the type 2 diabetes rats. To confirm the hypothesis, ventricular myocytes isolated from control rats were incubated 24 hours in only DMEM, in DMEM supplemented with plasma obtained from healthy animals, and

in DMEM supplemented with plasma extracted from type 2 diabetic animals. Following the incubations, calcium sparks from cardiomyocytes were recorded by loading with Fluo-3. As expected, incubation with plasma extracted from control animals had no relevant effect on the calcium sparks of control myocytes, and therefore we decided to pooled control results (table 7). However, diabetic-serum incubated cardiomyocytes showed a significant increase in the number of events and in the Time to peak parameter (figure 51, table 6). These results indicate that in the cardiomyocytes incubated with diabetic serum sparks were more frequent and faster. Higher frequency leads to a higher risk of ventricular arrhythmia. Therefore, calcium sparks are another intracellular mechanism that leads to type 2 diabetic rats of our metabolic-induced model to generate arrhythmia.

	AMPLITU F/F$_0$	FWHM (µm)	FDHM (ms)	SPARKS/100 µm/sec	TIME TO PEAK (ms)
CTRL	0,4± 0,0	4,14± 0,1*	55,41± 3,3***	1,22± 0,0	27,81± 2,2
T2D plasma	0,4± 0,0	3,9± 0,1	48,1± 1,7	1,6± 0,0***	39,5± 0 ,8***

Table 6. **Spontaneous calcium sparks parameters and characteristics determined with the aid of computer programming analysis.** Sparks frequency determined as spark per 100 µm and per second (SPARKS/100µm/sec). Peak amplitude determined as F/F at the peak of Ca^{2+} spark (AMPLITUD F/F0). Spatial width determines as sparks width at half-maximal amplitude (FWHM). Duration determined as full duration at half-maximal amplitude (FDHM. The rising phase (time to peak), CTRL= 30/10; T2D plasma= 15/5. In parenthesis (number of cells/number of animals); ***$p<0.005$ with respect to control

	AMPLITD F/F$_0$	FWHM (µm)	FDHM (ms)	SPARKS/100µ m/sec	TIME TO PEAK (ms)
Ø	0,6± 0,0	4,1± 0,1	66,7± 4,9	1,04± 0,0	29,4± 2,9
CTRL plasma	0,6± 0,0	4,2± 0,1	44,1± 1,7***	1,08± 0,0	26,2± 1,6
Pooled Control	0,6± 0,0	4,1± 0,1	55,4± 3,3	1,22± 0,0	27,8± 2,2

Table 7. Summary of quantitative data for Ca^{2+} spark parameters and characteristics in control groups. CTRL Ø= 10/4; CTRL plasma= 20/6. In parenthesis (number of cells/number of animals); ***$p<0.005$ with respect to control.

3. DIABETIC RATS SHOW A LOW-GRADE INFLAMMATION STATUS

Cytokines are a diverse group of cells signaling proteins expressed and mainly secreted by immune cells such as macrophages, lymphocytes, and adipocytes. These proteins interact with specific receptors on target cells to mediate important physiological responses such as immunity and inflammation. Dysregulation of expression that causes a low-grade inflammation is associated with pathological conditions ranging from cancer and diabetes to infection and autoimmune disease. The accumulation of abdominal fat is recognized as the origin of a generalized low grade inflammatory status of the whole body [42]. Type 2 diabetes as well as obesity and overweight that are related with a higher accumulation of fat associate with systemic chronic low-grade inflammation. Among other features, Low-grade inflammation is characterized by higher levels of circulating proinflammatory cytokines such as IL-6, TNFα, IFN-γ, TGF-β, MCP-1 or IL-1β [225]. These can interfere with normal insulin function and thereby, induce insulin resistance as well as β-cell dysfunction. Thus, determining the circulating levels of pro-inflammatory cytokines could help us to understand the underlying physiopathology of type 2 diabetes.

We analyzed whether our diabetic animals displayed the low-grade inflammatory status observed in type 2 diabetes patients. Using a multiplex commercial kit, we measured plasmatic levels of the proinflammatory cytokines associated with diabetes (figure 52 A-G). The experiments showed that at the end of the experimental period, diabetic animals had an altered inflammatory profile compared to control animals (figure 52 B-G). This included higher levels of IL-2, IL-5, IL-6, IL-12p70, GM-CSF, IFN-γ, as well as TNFα and IL-1β, two cytokines known to be upregulated in type 2 diabetic patients [226].

Therefore, like in diabetic patients, our type 2 diabetic model has an inflammatory component that can affect different organs including the heart, and is responsible for insulin resistance.

H

I
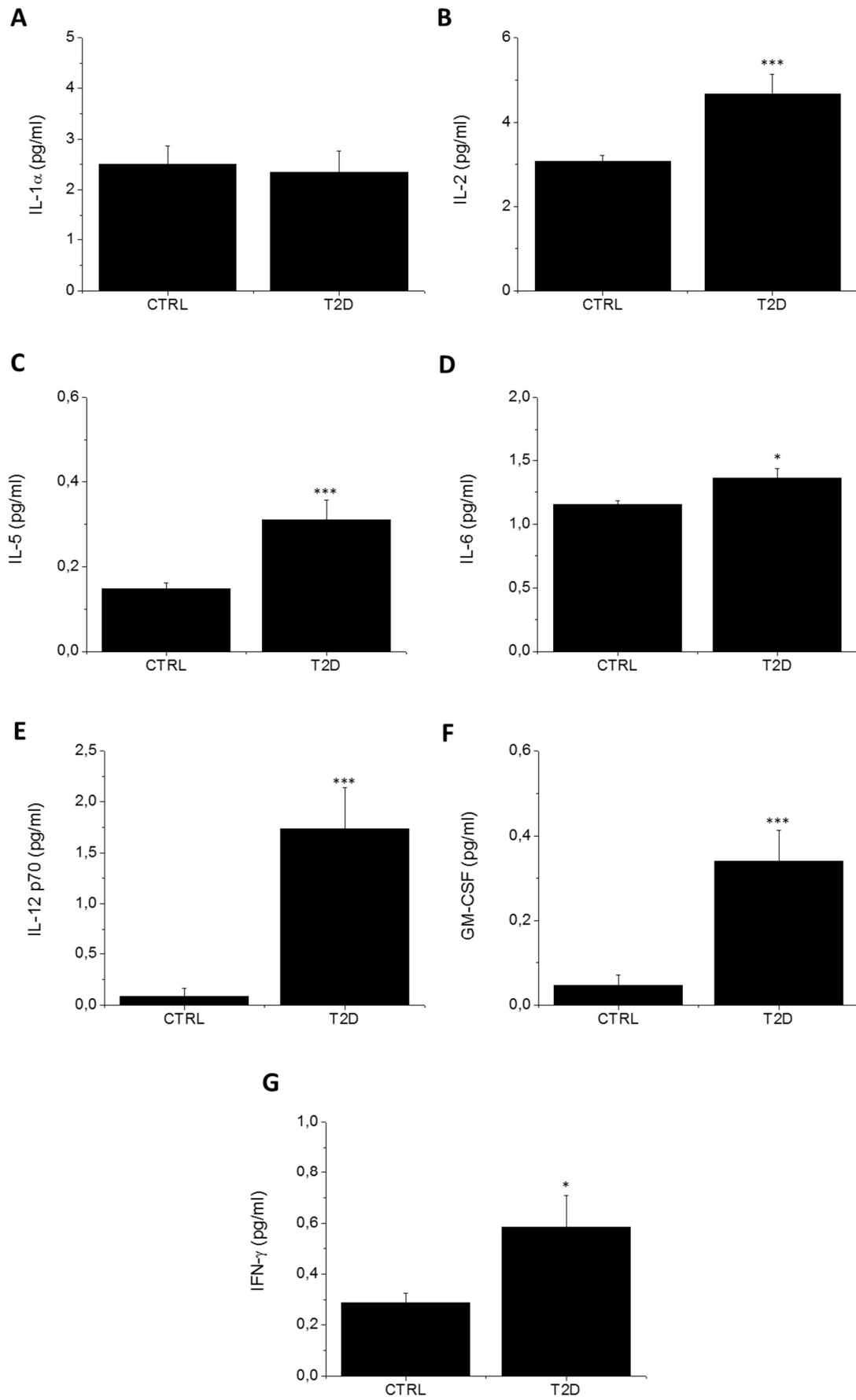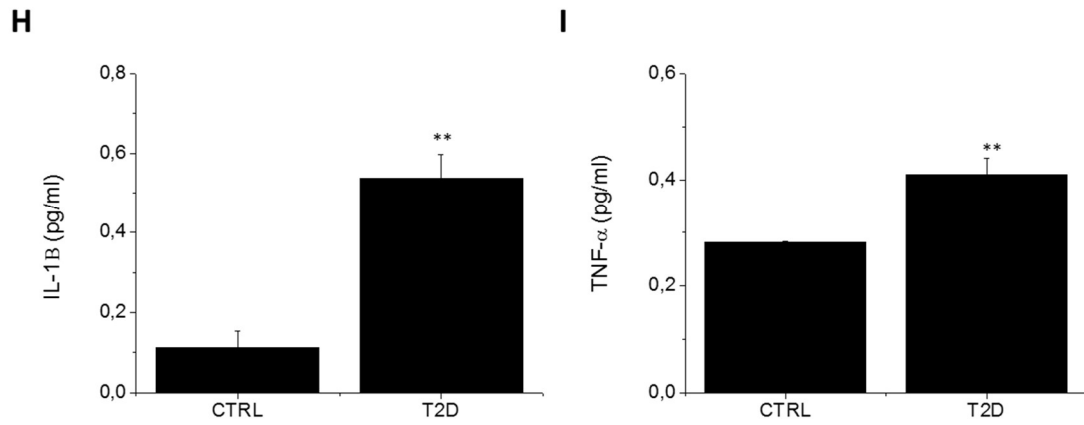
Figure 52. Type 2 diabetes model has a low-grade proinflammatory status. **A-I)** Plasmatic levels of proinflammatory cytokines. CTRL= 16; T2D= 12. *p < 0.05; **p<0.01; ***p<0.005

PART 2. ROLE OF DIABETES-ASSOCIATED CIRCULATING PROINFLAMMATORY FACTORS IN PATHOPHYSIOLOGY AND CARDIAC ELECTRICAL REMODELING OF TYPE 2 DIABETIC RATS

1. TYPE 2 DIABETES INFLAMMATORY STATUS CAUSES ACTION POTENTIAL PROLONGATION

In type 1 diabetic animals, Ito inhibition has been attributed to proinflammatory cytokines of the diabetic inflammatory status. Thus, TNFα and IL-1β reduce the functional expression of the cardiac repolarizing current Ito [130] *in vivo* and *in vitro*. Moreover, it has been recently demonstrated the role of both TNFα and IL-1β in the initiation and maintenance of cardiac arrhythmias in humans [227]. However, although the key role of low-grade inflammatory status in the pathophysiology of diabetes is broadly accepted, little is known about its role in cardiac electrophysiology.

Our previous results suggest that in this type 2 diabetic model, elevation of plasmatic TNFα and IL-1β levels could cause Ito reduction. This could lead to prolonged repolarization and higher susceptibility to arrhythmia under cardiac challenge. To test this hypothesis, we analyzed the repolarization in the context of the cardiac action potential (AP). We exposed cardiomyocytes isolated from control rats to plasma extracted from diabetic animals, and recorded AP to confirm whether diabetes-associated circulating factors like TNFα and IL-1β could induce cardiac electrical remodeling. In these experiments, ventricular myocytes isolated from healthy rats were incubated 24 hours in DMEM supplemented with: i) plasma obtained from healthy animals; ii) DMEM supplemented with plasma extracted from type 2 diabetic animals; or iii) DMEM supplemented with plasma extracted from type 2 diabetic animals with the addition of TNFα (50 μM) and IL-1β (50 μg/ml) receptor blockers (figure 53 A and table 8).

	RMP (mV)	APA (mV)	APD_{90} (ms)	APD_{50} (ms)	APD_{30} (ms)
Control	-64,0±6,7	72,4±7,8	24,7±4,5	9,0±2,1	6,3±1,2
T2D Plasma	-63±8,2	74,7±8	57,4±14,5*	20,7±5,6*	13±3,9*
T2D Plasma Block	-64,4±2	68,4±4,4	33,3±3,2	8,3±1,9[#]	5,2±1,5[#]

Table 8. Effects of diabetic circulating factors in the ventricular action potential characteristics. Effects of Control Plasma, T2D Plasma and T2D Plasma with blockers of TNFα and IL-1β receptors on ventricular action potential. Resting membrane potential (RMP), action potential amplitude (APA), and action potential duration (APD) at 30, 50 and 90% of repolarization. CTRL= 17/10; T2D plasma= 8/4; T2D plasma block= 13/4. In parenthesis (number of cells/number of animals); *$p<0.05$ with respect to control; # $p<0.05$ with respect to T2D plasma.

As expected, incubation with plasma extracted from control animals had no effect on the action potential of control myocytes (figure 53 A-D). Incubation with plasma obtained from diabetic animals did not affect resting membrane potential and AP amplitude, but significantly prolonged AP duration (figure 53 A-D). Therefore, Incubation of control myocytes with plasma obtained from diabetic animals resulted in a diabetic-like electrical phenotype, and confirmed that high plasmatic levels of TNFα and IL-1β cause a cellular electrical remodeling that impairs the ability of cardiac myocytes to repolarize. Prolonged APD was prevented by preincubating the diabetic plasma with TNFα and IL-1β receptor blockers. Thus, diabetes associated circulating proinflammatory factors induce electrical remodeling in cardiac cells. As a result, there is an impairment in major pro-arrhythmic parameters, increasing the risk to generate arrhythmia.
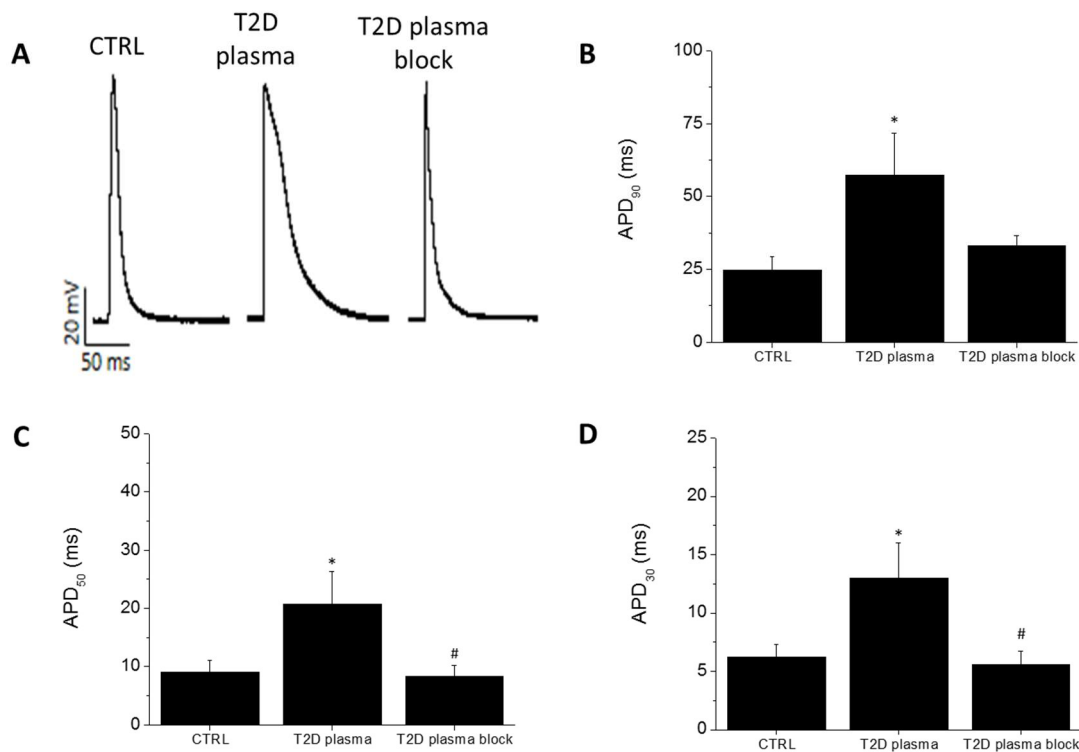
Figure 53. Role of circulating mediators on cardiac electrical remodeling. **A)** Typical action potentials recorded in myocytes isolated from the right ventricle of healthy animals incubated 24 hours in DMEM supplemented with plasma from healthy animals (Ctrl); in DMEM supplemented with plasma from diabetic animals (T2D plasma); or DMEM supplemented with plasma extracted from type 2 diabetic animals with TNFα and IL1β receptor blockers (T2D plasma block). **B)** 90% of repolarization (APD90) in all the experimental conditions. **C)** 50% of repolarization (APD50) in all the experimental conditions. **D)** 90% of repolarization (APD90) in all the experimental conditions. Data are mean ± SEM; CTRL= 17/10; T2D plasma = 8/4; T2in parenthesis (number of cells/number of animals); *p<0.05 with respect to control; # p<0.05 with respect to T2D plasma.

2. INMUNOMODULATION BY PHARMACOLOGICAL INHIBITION OF Kv1.3 CHANNEL, A POTENTIAL TREATMENT FOR TYPE 2 DIABETES

In previous experiments, we determined that the metabolic-induced model of type 2 diabetes rat reproduces the pathophysiology of the disease including insulin resistance, hyperglycemia, and the higher risk of life-threatening ventricular arrhythmia observed in type 2 diabetes patients [228] (figure 39-43, 48). In this model of type 2 diabetic rat, we have described the cardiac electrical remodeling of the rat diabetic heart, including the prolonged QT of the ECG (figure 47) caused by the reduction of the Ito potassium

current (figure 49) that leads to prolongation of the repolarization phase of action potential in type 2 diabetic cardiomyocytes (figure 52). We have also shown the molecular and intracellular mechanism that induce this electrical remodeling of the heart; the reduction in Kv4.3 expression that reduce Ito currents (figure 50); and the higher frequency of calcium sparks that triggers arrhythmia (figure 51). Moreover, is known that low-grade inflammatory status including higher circulating cytokines like TNFα and IL-1β play a critical role in the development of insulin resistance and subsequent hyperglycemia in type 2 diabetes patients [229, 230]. In this sense, overexpression of these cytokines also cause electrical remodeling and arrhythmia in the diabetic heart [130]. Our metabolic-induced model of type 2 diabetes shows a low-grade inflammatory status that translates into elevated circulating proinflammatory cytokines (figure 51). We have also found that plasma isolated from diabetic animals, with high levels of TNFα and IL-1β, induced APD prolongation in control myocytes (figure 52). Moreover, prolongation of APD in type 2 diabetic cardiomyocytes was prevented by the inhibition of these cytokines (figure 53).

According to these results, it is obvious the role of the immune system and proinflammatory cytokines in both the metabolic alterations and the cardiac electrical remodeling of type 2 diabetes. Therefore, we thought that the modulation of the inflammatory status by a therapeutic target could improve both insulin resistance and cardiac electrical remodeling of type 2 diabetes. In this sense, potassium Kv1.3 channel has a prominent role in the modulation of the inflammatory status and therefore is an interesting target.

The inhibition of Kv1.3 channel is a very promising strategy for the treatment of type 2 diabetes. Kv1.3 channel expression and activation modulate proliferation and differentiation of some relevant cells in inflammation like macrophages, T-lymphocytes, and adipocytes. Effects on these cells also modulate the production of inflammatory cytokines that are related to underlying mechanisms of T2D such as insulin resistance and arrhythmia. It is known that pharmacological and genetic inhibition of Kv1.3 channel improves insulin resistance [183]. Thus, we blocked the Kv1.3 channel in our type 2 diabetic animals to determine whether immunomodulation improved the pathophysiology of the disease.

PAP-1 (5-(4-Phenoxybutoxy) psoralen) is derived from 5-methoxy psoralen, a natural compound. It is a potent, most selective, and orally active Kv1.3 blocker (EC50=2 nM). Moreover, PAP-1 does not exhibit cytotoxic or phototoxic effects [231]. Thus, in the following set of experiments we treated our diabetic animals with PAP-1 for 4 weeks. We also compared PAP-1 treatment with metformin treatment since metformin is the first-choice drug for T2D [232]. In both treatments, when needed, doses were adjusted to achieve intensive glucose control. According to the clinical use, metformin doses ranged from 50 mg/kg to 200 mg/kg. According to its pharmacokinetics [193], PAP-1 doses ranged from 5 mg/kg to 10 mg/kg.

2.1. INHIBITION OF Kv1.3 WITH PAP-1 IMPROVES THE INFLAMMATORY STATUS OF TYPE 2 DIABETIC RATS

Low-grade inflammation is a clinical characteristic of type 2 diabetic patients. This inflammatory status consists of an increased circulating level of proinflammatory cytokines such as TNFα and IL-1β. Cytokine levels are not as high as in severe infections but are elevated with respect to healthy people. Low-grade inflammation plays a critical role in insulin resistance because circulating cytokines like TNFα and IL-1β desensitize the insulin receptor [42, 50, 230, 233]. In addition, elevated circulating levels of TNFα induce cardiac electrical remodeling and risk of arrhythmia and sudden death [91, 234]. Thus, low-grade inflammation is key in the progression of type 2 diabetes and its associated complications. As presented before (figure 51 to 53), animals with metabolic-induced model of type 2 diabetes displayed alterations in the proinflammatory profile that are important for the development of the diabetic cardiac electrical remodeling. On the other hand, Kv1.3 potassium channel has role in the inflammatory system. Pharmacological or genetic inhibition of Kv1.3 reduces the proliferation and differentiation of macrophages, T-lymphocytes and adypocytes, which implies the reduction of cytokine secretion by these cells [176, 184, 235]. According to this, we hypothesized that treatment with PAP-1, which pharmacologically inhibits the Kv1.3 potassium channel, would improve the proinflammatory profile of type 2 diabetes.
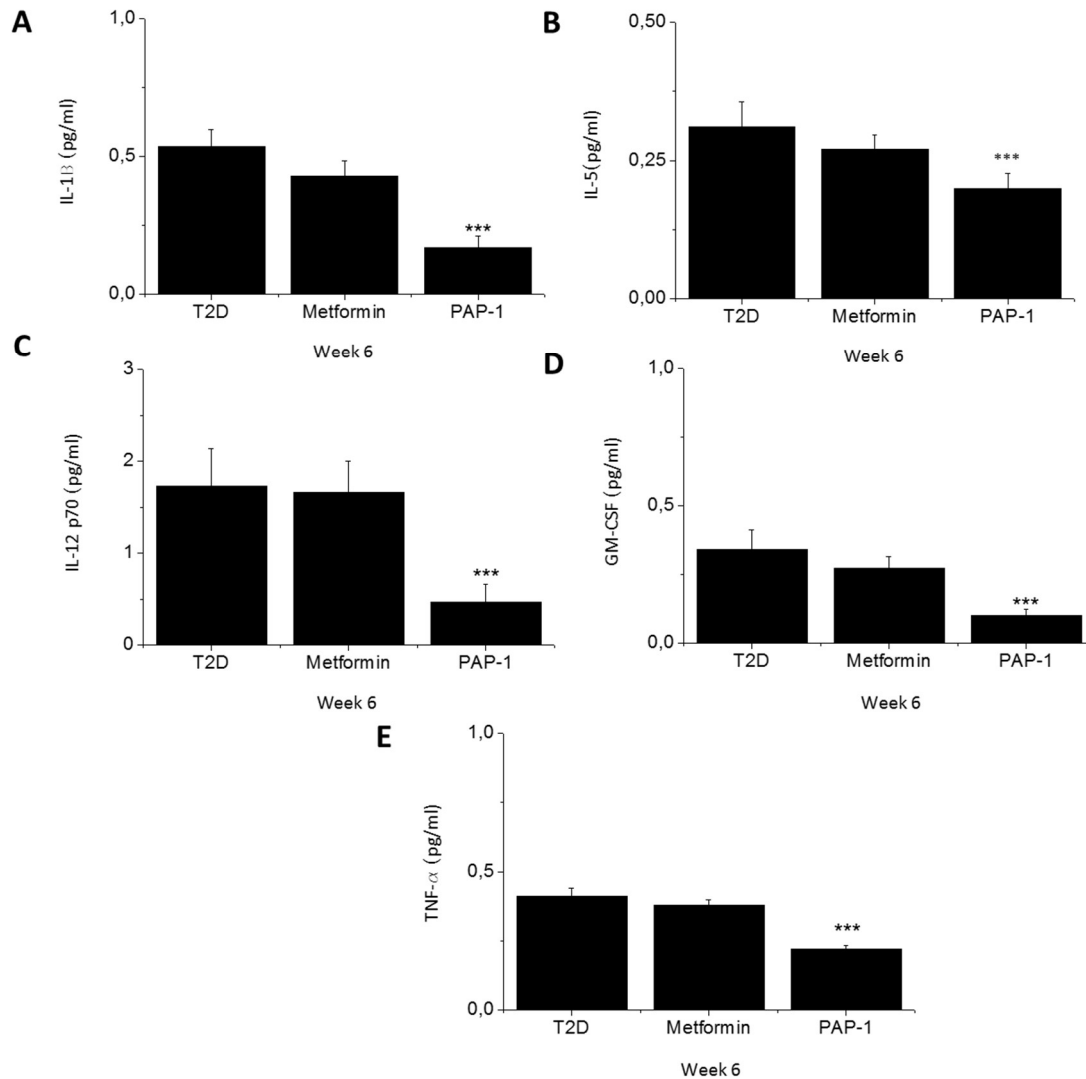
Figure 54. Kv1.3 pharmacological inhibition, and not metformin, reduces the levels of some proinflammatory cytokines in type 2 diabetic animals. **A-E)** Plasmatic levels of proinflammatory cytokines elevated in diabetic animals are significantly reduced by treatment with PAP-1. T2D= 12; Metformin= 11; PAP-1= 5. ***$p<0.005$ to T2D

We analyzed the levels of some proinflammatory cytokines in animals treated with metformin or PAP-1 for four weeks (figure 54 A-E, figure 54 A). This analysis reveals that, at the end of the experimental period, many circulating cytokines that were elevated in type 2 diabetes are reduced by PAP-1 treatment, and not by metformin (figure 54 A). Among them, we were particularly interested in TNFα and IL-1β because we had previously determined their role in type 2 diabetic cardiac remodeling. Both TNFα and IL-1β are reduced by the inhibition of Kv1.3 and not by the metformin therapy (figure 54 A- E) at week 6. However, PAP-1 treatment failed to restore the levels of some cytokines. Neither metformin nor PAP-1 reduce the levels of IL-2, IL-6, and IFN-y after 4 weeks of

diabetes (figure 55 with A-C). Therefore, blockade of Kv1.3 potassium channel with PAP-1 immunomodulates the inflammatory profile of type 2 diabetic animals by reducing the levels of IL-1β, IL-5, IL-12, GM-CSF and TNFα. A reduction in TNFα has been reported after Kv1.3-inhibition with the ShK-186 peptide in obese mice [183].
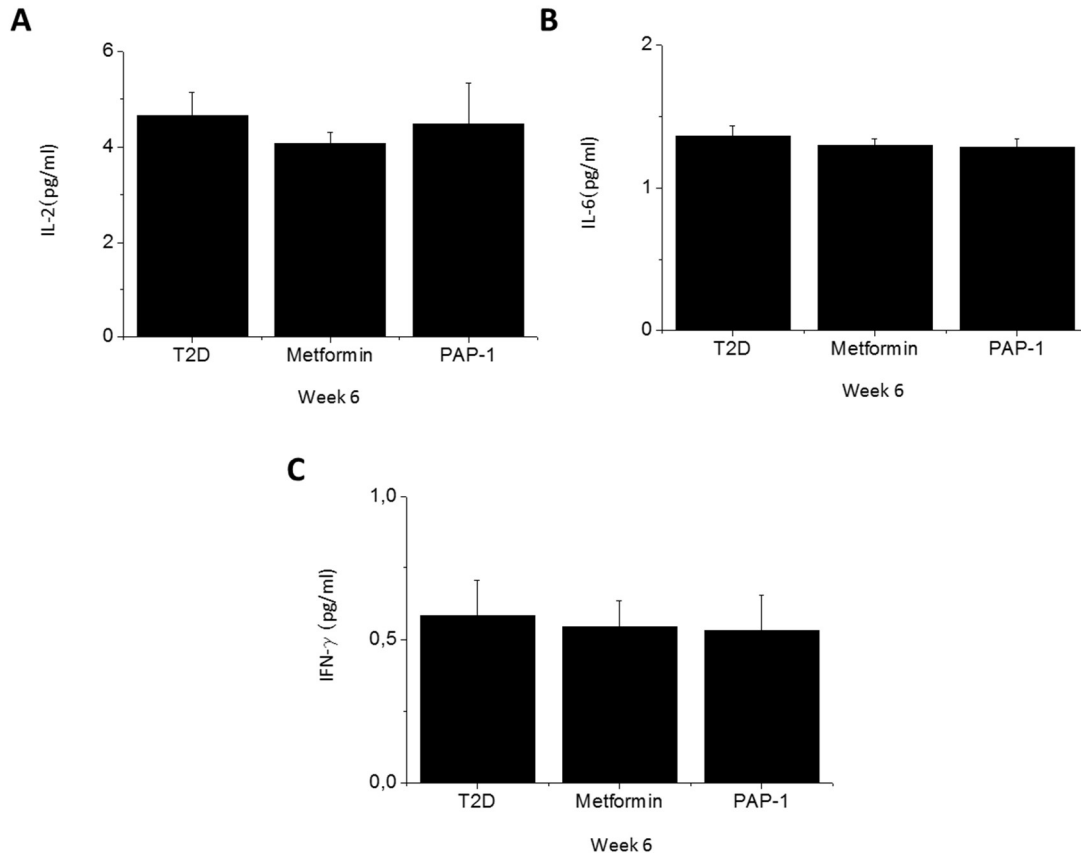
Figure 55. Proinflammatory cytokines elevated in diabetes that were not restored by PAP-1 or metformin treatments. **A-C)** Plasmatic levels of proinflammatory cytokines that were higher in type 2 diabetes animals than in controls and are not reduced after the treatments. T2D= 12; Metformin= 11; PAP-1= 5. ***$p<0.005$ to T2D

2.2. ANTIDIABETIC EFFECTS OF THE INMUNOMODULATION INDUCED BY Kv1.3 INHIBITION

Since chronic hyperglycemia is the defining characteristic of the type 2 diabetes, treatment has focused on an anti-hyperglycemic effect that does not cause hypoglycemia, underestimating underlying mechanisms and the pathophysiology of the disease. Although its mechanism of action is not completely understood, metformin fulfills these premises [137].

A potential new anti-diabetic drug is expected to have anti-hyperglycemic effects comparable to those of metformin, as well as avoid hypoglycemic episodes. Inhibition of Kv1.3 reduces blood glucose levels by improving insulin resistance and the translocation of GLUT4 [182, 185].
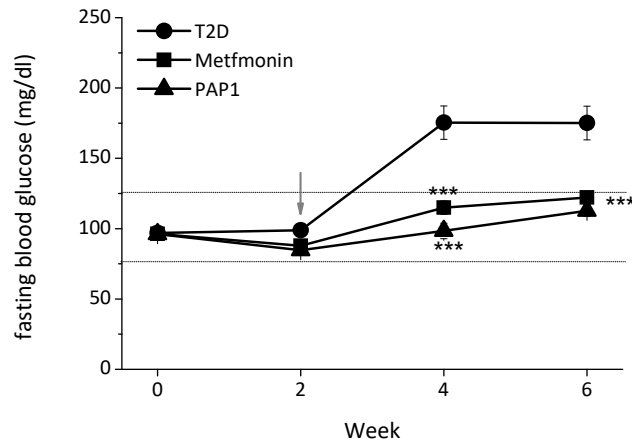
Figure 56. PAP-1 treatment reduces to normalize the fasting blood glucose levels. Weekly fasting plasma glucose throughout the experimental period. The dotted lines indicate the healthy interval levels for plasma glucose. The arrow indicates the injection of STZ or vehicle. T2D n=18; Metformin= 19; PAP-1= 7 ***p<0,005 to T2D group

In our experiments, treatment with PAP-1 for 4 weeks prevented the diabetes-induced hyperglycemia. Moreover, blood glucose levels did not rise above the physiological range throughout the experimental period. Thus, inhibition of Kv1.3 was as effective as metformin in improving hyperglycemia. Both PAP-1 and metformin normalized fasting blood glucose after STZ injection until the end of the experimental period (figure 56).

A. PAP-1 TREATMENT IMPROVES INSULIN SENSITIVITY IN TYPE 2 DIABETIC RATS

Nowadays, insulin resistance is considered the main pathophysiology feature underlying T2D, since persistent insulin resistance causes hyperglycemia [21]. However, pharmacologic therapy does not usually focus on the improvement of insulin resistance [139]. Previous publication determined the role of inflammation in the insulin resistance of the obesity and type 2 diabetes [42]. Moreover, Upadhyay et al [183] reported that

the pharmacological inhibition of the Kv1.3 improved insulin sensitivity in an obesity mouse model. Thus, the glucose control observed in type 2 diabetic rats with PAP-1 treatment might be due to an improvement of insulin sensitivity. However, the effect of PAP-1 on insulin resistance in T2D animals has not been described. Hence, to test whether pharmacological blockade of Kv1.3 reduces insulin resistance, we performed IPIGTT and measured plasmatic insulin levels after 4 weeks of diabetes.
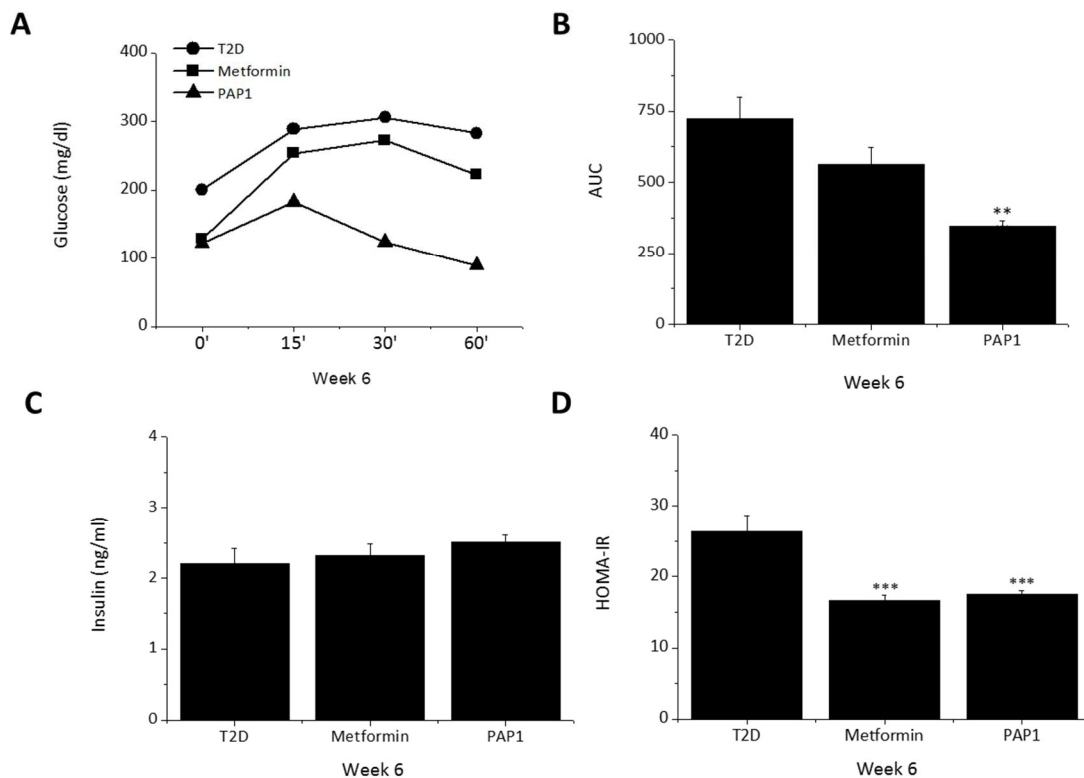
Figure 57. PAP-1 treatment reduced insulin resistance by improving insulin sensitivity. **A)** IPIGTT performed at the end of the experimental period (week 6). **B)** The corresponding Area Under the Curve (AUC) of IPIGTT graph. T2D n=18; Metfromin= 14; PAP-1= 7 **C)** Plasma Insulin levels after 4 weeks of diabetes. T2D n=11; Metfromin= 14; PAP-1= 7. **D)** Homa-IR index after 4 weeks of diabetes. T2D n=11; Metfromin= 14; PAP-1= 7. **p<0,01; ***p<0,005 to T2D group

After analyzing insulin resistance as the area under the curve of the IPIGTT, we found that PAP-1 treatment, but not metformin, significantly reduced insulin resistance in diabetic animals (figure 57A, B). Plasmatic insulin levels were similar in PAP-treated, metformin-treated and in untreated diabetic animals (figure 57 C). Therefore, the improvement in insulin resistance after pharmacological inhibition of Kv1.3 is caused by an improvement of insulin sensitivity, as was described in obesity mice [183]. Moreover, metformin and PAP-1 therapy also reduced the HOMA-IR (figure 57 D).

B. THE BLOCKADE OF Kv1.3 IMPROVES THE DYSLIPIDEMIA OF TYPE 2 DIABETES

Dyslipidemia is a frequent complication of type 2 diabetes and often associates with a higher risk of cardiovascular complications in diabetic patients [38]. We have previous described hypercholesterolemia and hypertriglyceridemia in the type 2 diabetic rats model. A treatment that also corrects dyslipidemia in type 2 diabetes would improve underlying pathologies of the disease. Hence, we tested whether PAP-1 treatment improved total cholesterol and triglycerides levels. Interestingly, only the Kv1.3 blockade with PAP-1 significantly reduces levels of both cholesterol and triglycerides (figure 58 A, B). Metformin treatment did not normalize the hyperlipidemia in diabetic rats (figure 58 A, B). Impaired plasma lipid profile in diabetic animals is corrected by PAP-1 treatment, but not by metformin, through a reduction of the circulating cholesterol and triglycerides. A reduction in plasmatic cholesterol has been also described in obese mice [183].
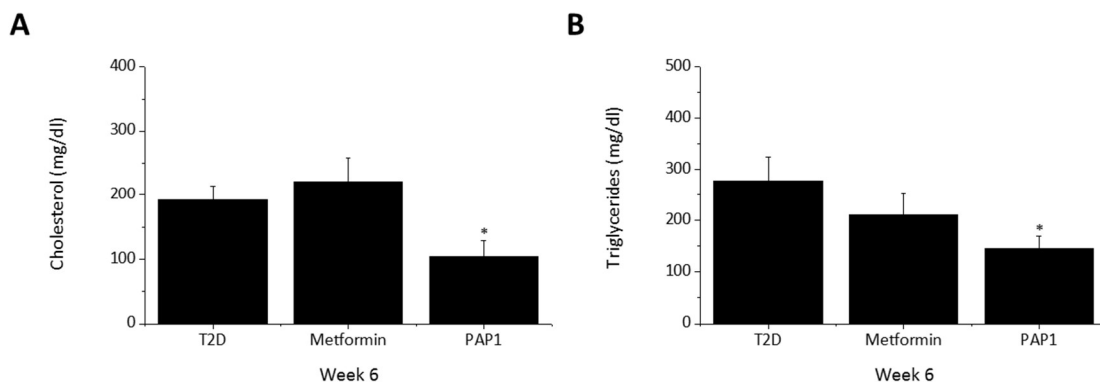
Figure 58. Kv1.3 blockade with PAP-1, but not metformin, corrects the dyslipidemia of the type 2 diabetes animal mode. A) Triglycerides and **B)** cholesterol.T2D n=8; metformin=10; PAP-1=7 *p<0,05 to T2D group

C. PAP-1 TREATMENT REDUCES BODY WEIGHT AND ADIPOSITY IN TYPE 2 DIABETIC RATS

Obesity is a risk factor for a number of pathologies including type 2 diabetes. In this sense, a reduction in the body weight of type 2 diabetic patients decreases the risk of type 2 diabetes and its associated cardiovascular complications [8].

Kv 1.3 blockade reduced weight gain in mice on obesity-inducing diet [183]. Although the type 2 diabetic animals do not have obesity, we tested if pharmacological inhibition of kv1.3 with PAP-1 affected body weight. Daily injection of PAP-1 reduced the body weight as well as the body mass index in T2D animals (figure 59 A, B). This reduction was not observed in diabetic animals treated with metformin (figure 59 A, B). Thus, PAP-1 treatment, but not metformin, prevents the body weight gain in type 2 diabetes. This is in agreement with the literature [183].
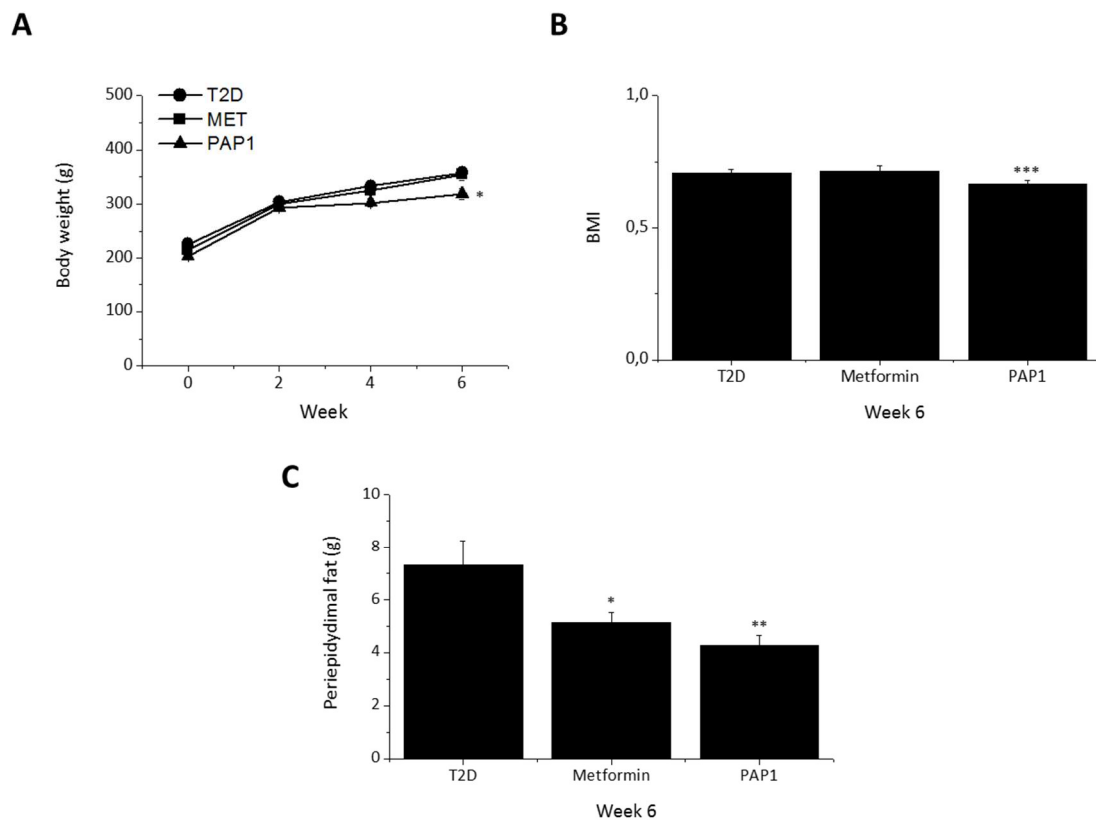
Figure 59. PAP-1 treatment reduces body weight and fat accumulation in type 2 diabetic animals. **A)** Body weight. **B)** Body mass index (BMI). **C)** Periepididymal fat accumulation. T2D n=16; Metformin= 12; PAP1= 5. *p<0,05; **p<0,01; ***p<0,005

On the other hand, increased adiposity is another frequent feature of the type 2 diabetes patients. Aside from being a cause of obesity, increased adiposity participates in metabolic alterations of type 2 diabetes like insulin resistance in non-obese patients. Adipocytes of the abdominal fat have a role in the generation of the low-grade inflammation status [47, 229, 236]. Therefore, adiposity acts as a link between metabolic alterations like insulin resistance and proinflammatory status, and a treatment that also reduces adipose accumulation would improve the pathophysiology of type 2 diabetes.

We analyzed whether blockade of Kv1.3 with PAP-1 reduces the periepidydimal fat, an adiposity marker, in diabetic rats. Data shows that both treatments significantly reduce adiposity compared to untreated diabetic rats, but in PAP-1 treatment, the reduction is more drastic (figure 59 C). The effect of Kv1.3 inhibition in the reduction of adiposity has been also determined in mice on obesity diet [183].

In our metabolic-induced model of type 2 diabetes, inhibition of Kv1.3 by PAP-1 normalized blood levels of cholesterol and glucose, insulin sensitivity and reduced weight gain and adiposity. The effects of PAP-1 therapy and metformin therapy are remarkably different. This strongly suggests that the antidiabetic activities of PAP-1 are predominantly due to pharmacological actions on Kv 1.3, probably in peripheral tissues because PAP-1 hardly crosses the blood–brain barrier [193]. In this sense, at least three mechanisms contribute to the antidiabetic effects of Kv 1.3 inhibition: brown adipose tissue (BAT) activation leading to increased energy expenditure, heightens activity of metabolic pathways involved in energy and lipid metabolism in the liver, and reduction of inflammation of abdominal white adipose tissue (WAT) [183].

D. PHARMACOLOGICAL INHIBITON OF Kv 1.3 ALSO REDUCES POLYDIPSIA AND POLYPHAGIA

The reduction of diabetes-associated polydipsia and polyphagia would indicate an improvement of the underlying physiopathology of the disease, and might facilitate the quality of life of the patients. We analyzed the effect of the pharmacological inhibition of Kv1.3 on polydipsia and polyphagia at the end of the experimental period (week 6).

Only PAP-1 treatment decreased both weekly water and food intake (figure 60 A, B). Metformin therapy also significantly reduced water intake compared to untreated animals, but PAP-1 was significantly more effective (figure 60 A). Our results show that inhibition of Kv1.3 prevents the development of polydipsia and polyphagia in type 2 diabetic animals. Since polydipsia and polyphagia associate with hyperglycemia and insulin resistance [201], these data are consistent with the normalization of hyperglycemia and insulin resistance observed in PAP-1 treated rats.
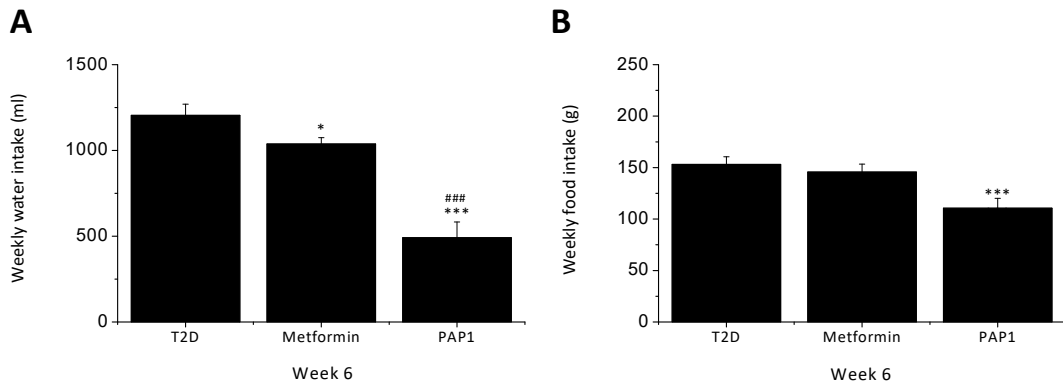
Figure 60. Only PAP-1 treatment prevents polydipsia and polyphagia in type 2 diabetic animals. **A)** Weekly water intake at the end of the experimental period. PAP-1 and metformin treatments reduce polydipsia compared to untreated type 2 diabetes. **B)** Weekly Food intake at the end of the experimental period. Blockade of Kv 1.3 with PAP-1 decreases the polyphagia compared to type 2 diabetes. T2D n=22; Metformin= 14; PAP-1= 8. *p<0,05; ***p<0,005 to T2D. ###<p0,005 to Metformin

2.3. EFFECTS OF THE INMUNOMODULATION INDUCED BY Kv1.3 INHIBITION IN CARDIAC ELECTRICAL REMODELING OF TYPE 2 DIABETIC RATIS

A. PAP-1 TREATMENT IMPROVES REPOLARIZATION ALTERATIONS OF TYPE 2 DIABETIC RATS

A Cardiac electrical remodeling has been described in type 2 diabetes patients [103]. It mainly affects the repolarization leading to prolongation of the action potential and the QT interval of the ECG [94, 103]. These electrophysiological changes of the heart increase the risk of ventricular arrhythmia and sudden death [99], and are often unknown and understudied in type 2 diabetes patients. Metabolic-induced model of type 2 diabetic rat reproduced the cardiac electrical remodeling of the diabetic heart (figure 46-51) as well as inflammatory status underlying type 2 diabetes (figure 52). In addition, we defined the role of this proinflammatory status in the development of the cardiac electrical remodeling of type 2 diabetes as well as in the involved mechanism (figures 52, 53).

Thus, the inhibition of a potential therapeutic target like Kv1.3 channel that is known to modulate the immune system could control blood glucose levels and improve insulin sensitivity in diabetic patients while preventing the development of cardiac electrical alterations that might end up in arrhythmia and sudden death.
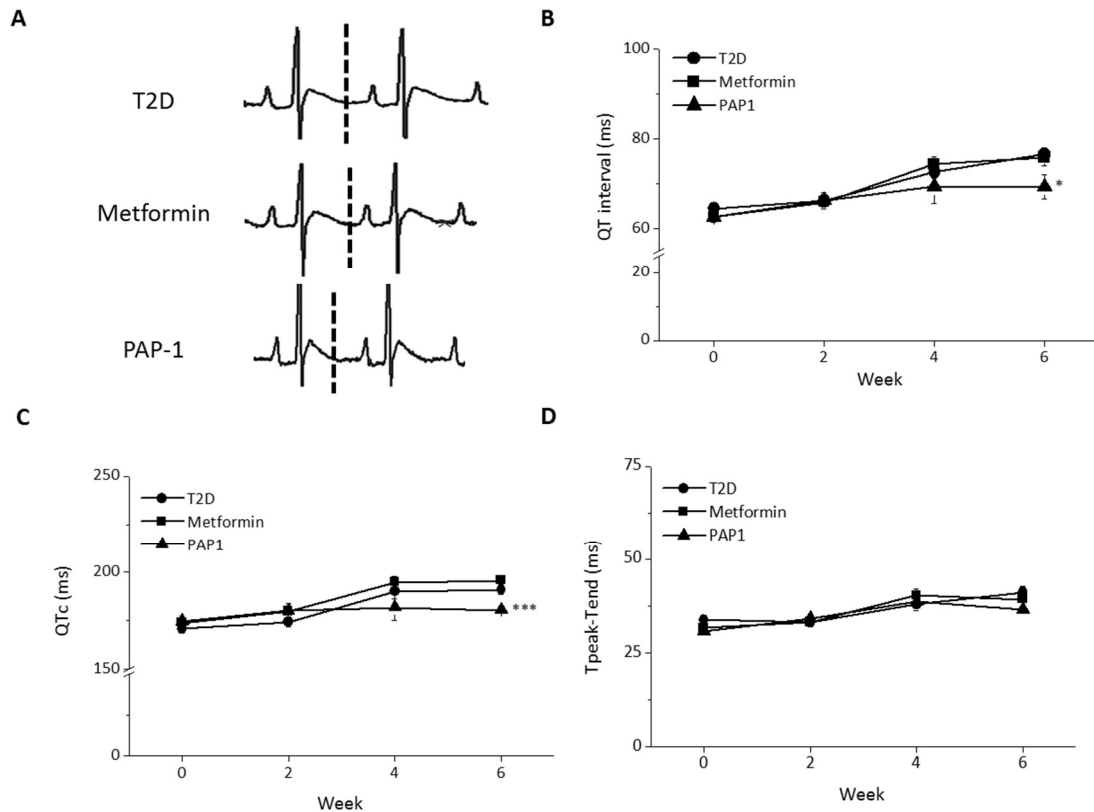
Figure 61. Inhibition of Kv1.3 channel with PAP-1 prevents diabetes-induced repolarization defects. **A)** Electrocardiographic recordings in diabetic animals treated with metformin, PAP-1 or vehicle during 4 weeks. The dotted line shows the end of the T wave. **B)** Cardiac repolarization expressed as QT interval and **C)** heart rate-corrected QT interval. **D)** The transmural dispersion of repolarization expressed as Tpeak-Tend. T2D n=30; Metformin= 14; PAP-1= 5. *p < 0.05; **p < 0.005 to T2D.

To confirm this, we compared the ECG of type 2 diabetic animals to those treated with metformin or PAP-1. We analyzed different parameters after 4 weeks of diabetes (table 9), and as expected, the results only showed differences in the ECG elements related to the ventricular repolarization (figure 61 A-C). Therefore, QT interval and QT interval related to heart rate (QTc) durations are significantly reduced in animals treated with PAP-1, but not in metformin animals (figure 61 B and C). Due to the influence of the heart rate in the QT interval, the effect is better observed in the QTc. Prolonged QT and QTc intervals are also described in type 2 diabetic patients [103], and are used in the clinical settings to predict the risk of ventricular arrhythmia and sudden cardiac

death [218, 237]. Thus, a reduction in the duration of the repolarization decreases the risk of ventricular arrhythmia and sudden death in type 2 diabetic patients. Another ECG marker that predicts the risk of ventricular arrhythmia and sudden death is the reduction in the transmural dispersion of repolarization, expressed as Tpeak-Tend. Neither metformin nor PAP-1 affected this parameter (figure 61 D). On the other hand, both metformin and PAP-1 treatment reduce the R-R interval duration (table 9), which inversely correlates with the heart rate. Bradycardia, a decreasing in the heart rate is often observed in diabetes due to the cardiac autonomic neuropathy [98]. Our results show that both PAP-1 and metformin treatments normalize the heart rate. In conclusion, only inhibition of Kv1.3 with PAP-1 prevents altered cardiac repolarization in type 2 diabetic animals, expressed as prolongation of QT and QTc intervals in the ECG.

	RR Interval	PR Interval	P duration	QRS interval	QT interval	QTc interval	Tpeak - Tend
T2D	163,5± 5,8	43,5± 1,0	15,1± 0,4	17,9± 0,6	76,5± 1,4	192,0± 2,1	41,2± 1,5
Metformin	145,1± 7,0***	41,4± 0,8	14,5± 0,5	17,6± 0,4	72,8± 1,8	195,7± 2,1	38,3± 1,9
PAP-1	139± 1,2***	44,4± 0,9	14,7± 0,3	17,8±0,7	70,2± 2,7*	182,4± 0,6***	38,5± 2,1

Table 9. ECG analysis from diabetic rats treated 4 weeks with metformin, PAP-1 or vehicle. Data are mean ± SEM, n=5-30 per group; **p<0.01 compared to T2D

B.   INHIBITION OF Kv1.3 BY PAP-1 REDUCES SUSCEPTIBILITY OF ARRHYTHMIA IN TYPE 2 DIABETIC RATS

Diabetic patients have higher prevalence of cardiac arrhythmia and sudden death [135, 220]. Metabolic-induced model of type 2 diabetic rats reproduce the cardiac electrical remodeling and the higher risk of arrhythmia (figure 46-51). In addition, we observed that the pharmacological blockade of Kv1.3 with PAP-1 corrected the ECG alterations (figure 61). As it directly relates with the risk of ventricular arrhythmia, this

correction may translate into a reduced risk of life-threatening arrhythmia and sudden death. To confirm this hypothesis, we subjected the diabetic animals treated with metformin or PAP-1 to the protocol of cardiac challenge that triggers arrhythmia. Our results showed that pharmacological inhibition of Kv1.3 channel reduces the risk of life-threatening arrhythmia. Only the 40% of PAP-1 treated animals develop ventricular arrhythmia after the caffeine/dobutamine challenge. This is significantly lower value than the 55% obtained for the diabetic animals. On the other hand, metformin treatment increased the susceptibility to arrhythmia, since 66% of the animals developed ventricular tachycardia or TdP (figure 62). Thus, only the antagonist targeting of Kv1.3 improves cardiac repolarization and protects against the risk of ventricular arrhythmia and sudden death in type 2 diabetic animals.
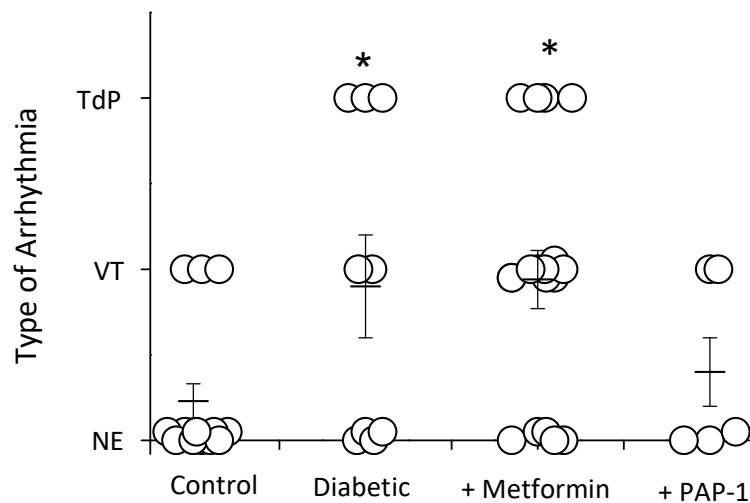
Figure 62. Inhibition of Kv1.3 by PAP-1 reduces arrhythmia susceptibility in type 2 diabetic rats. CTRL= 11; T2D n= 9; Metformin= 16; PAP-1= 5. *p < 0.05; to T2D

DISCUSSION SUMMARY

DISCUSSION SUMMARY

In this work, we characterized a type 2 diabetic rat model that reproduced the physiopathology of the disease and displayed cardiac electrical remodeling. Diabetic animals had prolonged QTc, reduced Ito and high susceptibility to develop arrhythmia under cardiac challenge. We also found that diabetes accompanied with an inflammatory status, caused by the increased plasmatic levels of proinflammatory cytokines like TNFα and IL-1β observed in type 2 diabetic rats. These circulating proinflammatory factors were demonstrated to be related with different features of the type 2 diabetes pathophysiology. Immunomodulation by PAP-1, an inhibitor of the potassium channel Kv1.3, reduced the levels of several circulating proinflammatory cytokines including TNFα and IL-1β. PAP-1 therapy showed antidiabetic effects. It also reduced the prolongation of QTc interval and the susceptibility to arrhythmia in type 2 diabetic rats. In this sense, it was also determined that TNFα and IL-1β impaired ventricular repolarization, which increases the susceptibility to arrhythmia in type 2 diabetes.

Different combinations of high-caloric diets (fructose rich, fat rich) and low STZ doses have been used to induce type 2 diabetes in mammals [63, 65]. In this work, we used a diet with 45% Kcal from lipids to cause progressive insulin resistance. After two weeks, we injected a low dose of STZ intraperitoneal to facilitate some beta cell destruction. 48 hours after STZ administration diabetes was confirmed by elevated fasting blood glucose and animals continued consuming high fat diet. We measured metabolic and electrocardiographic parameters and found that the expected diabetes-associated changes were well stablished four weeks after STZ injection. Thus, in this work we characterized an animal model with the main metabolic and electrocardiographic characteristics of type 2 diabetic patients in a reasonable period of 6 weeks.

Diabetic animals replicated the classical high fasting plasma glucose and insulin resistance characteristics of type 2 diabetic patients. Since fasting plasma insulin was similar in diabetics than in control animals, the high blood glucose was due to insulin resistance and the inability of the pancreas to compensate by increasing insulin

production. In addition, as described for type 2 diabetic patients [238], our type 2 diabetic animals had more abdominal fat than control animals, hypercholesterolemia and hypertriglyceridemia. Our experimental data are in are in line with the clinical findings in humans with type 2 diabetes [201].

Correspondingly, the ECGs of diabetic patients show slower heart rate and prolonged duration of the QT interval, the latter indicating repolarization abnormalities associated with increased risk of ventricular arrhythmias and mortality [87, 228]. In fact, diabetic animals, as well as the animals in the Chow+STZ group, had lower heart rate than control animals, measured as longer RR interval. Although a decreasing in the heart rate have been described in type 2 diabetes patients due to a cardiac autonomous neuropathy [217], the reduction in the heart rate can be also caused by the STZ injection. However, only animals in the diabetic group (high-fat diet plus STZ injection) had repolarization abnormalities. Diabetic rats showed the expected prolongation of the repolarization time [135], determined by the prolonged QT and QTc intervals and also by the prolonged Tpeak-Tend, an electrocardiographic marker of the transmural dispersion of repolarization. Prolonged QTc and Tpeak-Tend are used in the clinical settings to predict risk of ventricular arrhythmia and sudden cardiac death [218, 237, 239]. In this sense, when subjected to proarrhythmic conditions with the caffeine/dobutamine challenge [198], diabetic animals developed more arrhythmic episodes and more severe than control animals. It is important to note that cardiac challenge induced the potentially lethal arrhythmia torsade de pointes in one out of three type 2 diabetic animals. By contrast, none of the control animals developed torsade de pointes under the same challenge.

At the cellular level, diabetes lengthens the cardiac repolarization time by affecting the expression and activity of several cardiac ionic channels and their corresponding ionic currents. In models of type 1 diabetes, prolonged repolarization is caused by a reduction of Ito, the transient outward K^+ current [58, 60, 61, 106]. Our results in the type 2 diabetic model are in agreement with that. We found that Ito density and channel expression is smaller in type 2 diabetic animals than in control animals. The strong reduction on Ito density caused by diabetes reduced the repolarization capacity of the

ventricular cells. This can explain the prolonged repolarization time of the whole heart observed in the electrocardiogram.

The accumulation of abdominal fat is recognized as the origin of a generalized low-grade inflammatory status of the whole body in type 2 diabetes, with increased circulating cytokines such as IL-6, TNFα, IFN-γ, TGF-β, or IL-1β [208, 240]. In this sense, low-grade inflammatory status plays a critical role in pathophysiology and development of type 2 diabetes mellitus [42]. In addition, TNFα and IL-1β are two cytokines known to be upregulated in type 2 diabetic patients [226], which can reduce the functional expression of the cardiac repolarizing current Ito [130, 234]. It has been recently demonstrated the role of both TNFα and IL-1β in the initiation and maintenance of cardiac arrhythmias in humans [227, 241]. Here, we found that plasma levels of proinflammatory cytokines including TNFα and IL-1β were significantly higher in our type 2 diabetic animals than in their age-matched controls. Therefore, as in diabetic patients, our type 2 diabetic model had an inflammatory component that can affect different organs including the heart. Then, we hypothesized that in type 2 diabetes high plasmatic levels of TNFα and IL-1β were the cause of a cellular electrical remodeling that impairs the ability of cardiac myocytes to repolarize. Incubation of control cardiomyocytes with plasma obtained from diabetic animals resulted in a diabetic-like cardiac electrical phenotype. Prolonged APD was prevented by preincubating the diabetic plasma with TNFα and IL-1β receptor blockers. Thus, diabetes-associated circulating proinflammatory factors induce electrical remodeling in cardiac cells. As a result, there is an impairment in major pro-arrhythmic parameters, increasing the risk to generate arrhythmia. On the other hand, a dysfunction in the intracellular calcium homeostasis has been determined as a mechanism of arrhythmia triggering in diabetic animals. Frequently, the SR of diabetic cardiomyocytes spontaneously releases calcium to the cytosol generating calcium sparks, which lead to an unexpected cardiac contraction and generate arrhythmia [222-224]. Our results revealed a higher frequency of calcium sparks in control myocytes incubated 24h with serum obtained from type 2 diabetic rats. Control cardiomyocytes incubated with control serum showed significantly fewer calcium sparks than cells incubated with diabetic serum. Thus, factors present in

diabetic plasma increase the frequency of calcium sparks, another arrhythmia triggering mechanism in type 2 diabetic animals.

According to these previous results, we tested whether an immunomodulation that reduce the circulating proinflammatory cytokines would have antidiabetic effects and improve the cardiac electrical remodeling of type of 2 diabetes. We used PAP-1, a selective Kv1.3 blocker, as immunomodulator. Kv1.3 is a potassium channel expressed in a number of tissues like neurons or immune cells, but not in cardiomyocytes. The inhibition of the Kv1.3 channel have antidiabetic effects mediated by its role in the immune system [178, 181]. Kv1.3 blockade reduces the proliferation and migration of T-lymphocytes and macrophages as well as reduces the cytokine secretion by these cells [165, 174, 185]. As expected, treatment of type 2 diabetic rats with PAP-1 reduced the levels of circulating proinflammatory cytokines including TNFα and IL-1β. Pharmacological inhibition of Kv1.3 with PAP-1 showed antidiabetic effects. It induced the glucose control by reducing the insulin resistance in type 2 diabetic rats and caused a reduction in the fat accumulation and dyslipidemia.

Furthermore, Kv1.3 blockade with PAP-1 prevented from the cardiac electrical remodeling observed in type 2 diabetic rats. 4 weeks after diabetes was diagnosed, PAP-1 treated animals did not display a prolonged QT interval of the electrocardiogram. Prevention of cardiac electrical remodeling translated in that PAP-1 treated animals had less susceptibility to arrhythmia than diabetic animals. The mechanism of these effects are not completely understood and further investigation will be need. However, since Kv1.3 it is no expressed in cardiomyocytes, we could affirm that the immunomodulation induced by Kv1.3 pharmacological inhibition improves diabetic pathophysiology, including the cardiac electrical remodeling, by reducing the circulating levels of TNFα and IL-1β. As Kv1.3 blockade was more effective than metformin and gave more protection against arrhythmia in the cardiac challenge, our results place Kv1.3 inhibition as an interesting potential therapeutic target for the treatment of type 2 diabetes and its associated complications like cardiac electrical remodeling.

CONCLUSIONS

CONCLUSIONS

1.   Metabolic-induced model of type 2 diabetic rats reproduces the pathophysiology of type 2 diabetes. Diabetic animals show hyperglycemia, insulin resistance, adiposity and dyslipidemia.

2.   Electrocardiograms of type 2 diabetic rats display a cardiac electrical remodeling that affects cardiac repolarization. ECGs show prolonged QT, QTc and Tpeak-Tend intervals, which are markers of cardiac repolarization.

3.   Type 2 diabetic animals are at higher risk of developing ventricular arrhythmia, which is related with the cardiac electrical remodeling. Diabetic animals have higher susceptibility to lethal ventricular arrhythmia than age-matched control rats.

4.   Type 2 diabetic cardiomyocytes have reduced Ito density due to a reduction in the expression of Kv4.3, the main Ito channel-forming protein. This reduced expression causes prolonged cardiac repolarization.

5.   Metabolic-induced model of type 2 diabetic rats show an altered inflammatory status with higher levels of circulating cytokines including TNFα and IL-1β.

6.   Type 2 diabetic cardiomyocytes show a prolonged AP that is reverted by the preincubation of diabetic plasma with TNFα and IL-1β blockers.

7.   Plasmatic factors of type 2 diabetes also induce a higher frequency of calcium sparks, that is another arrhythmia triggering mechanism.

8.   Inmunomodulation by Kv1.3 inhibition has antidiabetic effects. It normalizes glucose levels by reducing insulin resistance and reduces the fat accumulation and dyslipidemia of type 2 diabetic rats.

9.   Pharmacological inhibition of Kv1.3 by PAP-1 have immunomodulatory effect on type 2 diabetic rats. It reduce the levels of circulating proinflammatory cytokines including TNFα and IL-1β.

10. Pharmacological blockade of Kv1.3 prevents the electric cardiac remodeling. PAP-1 therapy prevents the prolongation of the repolarization in ECG. Diabetic animals treated with PAP-1 do not show prolonged QT interval.

11. Kv1.3 inhibition reduces the susceptibility to arrhythmia of type 2 diabetic rats.

BIBLIOGRAPHY

BIBLIOGRAPHY

1. NCD Risk Factor Collaboration NCD-. NCD risk factor collaboration (NCD-RisC). worldwide trends in diabetes since 1980: A pooled analysis of 751 population-based studies with 4.4 million participants (vol 387, pg 1513, 2016). *Lancet*. 2017;389(10068):E2. doi: 10.1016/S0140-6736(16)32060-8.

2. Schellenberg ES, Dryden DM, Vandermeer B, Ha C, Korownyk C. Lifestyle interventions for patients with and at risk for type 2 diabetes A systematic review and meta-analysis. *Ann Intern Med*. 2013;159(8):543-+. doi: 10.7326/0003-4819-159-8-201310150-00007.

3. Fuchsberger C, Flannick J, Teslovich TM, et al. The genetic architecture of type 2 diabetes. *Nature*. 2016;536(7614):41-+. doi: 10.1038/nature18642.

4. Ross R. Does exercise without weight loss improve insulin sensitivity? *Diabetes Care*. 2003;26(3):944-945. doi: 10.2337/diacare.26.3.944.

5. Venkatasamy VV, Pericherla S, Manthuruthil S, Mishra S, Hanno R. Effect of physical activity on insulin resistance, inflammation and oxidative stress in diabetes mellitus. *Journal of Clinical and Diagnostic Research*. 2013;Vol-7: 1764-1766(8):1-3.

6. Papakonstantinou E, Panagiotakos DB, Pitsavos C, et al. Food group consumption and glycemic control in people with and without type 2 diabetes: The ATTICA study. *Diabetes Care*. 2005;28(10):2539-2540. doi: 10.2337/diacare.28.10.2539.

7. Cusi K. *The epidemic of type 2 diabetes mellitus: Its links to obesity, insulin resistance, and lipotoxicity.* ; 2009:54. 10.1007/978-1-59745-260-1_1.

8. Bellou V, Belbasis L, Tzoulaki I, Evangelou E. Risk factors for type 2 diabetes mellitus: An exposure-wide umbrella review of meta-analyses. *Plos One*. 2018;13(3):e0194127. doi: 10.1371/journal.pone.0194127.

9. Willi C, Bodenmann P, Ghali WA, Faris PD, Cornuz J. Active smoking and the risk of type 2 diabetes - A systematic review and meta-analysis. *Jama-Journal of the American Medical Association*. 2007;298(22):2654-2664. doi: 10.1001/jama.298.22.2654.

10. Polonsky KS, Sturis J, Bell GI. Non-insulin-dependent diabetes mellitus - A genetically programmed failure of the beta cell to compensate for insulin resistance. *N Engl J Med*. 1996;334(12):777-783. doi: 10.1056/NEJM199603213341207.

11. Stumvoll M, Goldstein BJ, van Haeften TW. Type 2 diabetes: Principles of pathogenesis and therapy. *Lancet*. 2005;365(9467):1333-1346. doi: 10.1016/S0140-6736(05)61032-X.

12. Czech MP. Insulin action and resistance in obesity and type 2 diabetes. *Nat Med*. 2017;23(7):804-814. doi: 10.1038/nm.4350.

13. Jiang ZY, Zhou QL, Coleman KA, Chouinard M, Boese Q, Czech MP. Insulin signaling through akt/protein kinase B analyzed by small interfering RNA-mediated gene silencing. *Proc Natl Acad Sci U S A*. 2003;100(13):7569-7574. doi: 10.1073/pnas.1332633100.

14. Titchenell PM, Quinn WJ, Lu M, et al. Direct hepatocyte insulin signaling is required for lipogenesis but is dispensable for the suppression of glucose production. *Cell Metabolism*. 2016;23(6):1154-1166. doi: 10.1016/j.cmet.2016.04.022.

15. Rosen ED, Spiegelman BM. Adipocytes as regulators of energy balance and glucose homeostasis. *Nature*. 2006;444(7121):847-853. doi: 10.1038/nature05483.

16. Zick Y. Uncoupling insulin signalling by serine/threonine phosphorylation: A molecular basis for insulin resistance. *Biochem Soc Trans*. 2004;32:812-816. doi: 10.1042/BST0320812.

17. Montagnani M, Ravichandran LV, Chen H, Esposito DL, Quon MJ. Insulin receptor substrate-1, and phosphoinositide-dependent kinase-1 are required for insulin-stimulated production of nitric oxide in endothelial. *Molecular Endocrinology*. 2002;16(8):1931-1942. doi: 10.1210/me.2002-0074.

18. Petersen KF, Shulman GI. Pathogenesis of skeletal muscle insulin resistance in type 2 diabetes mellitus. *Am J Cardiol*. 2002;90(5A):11G-18G.

19. Wu H, Ballantyne CM. Skeletal muscle inflammation and insulin resistance in obesity. *J Clin Invest*. 2017;127(1):43-54. doi: 10.1172/JCI88880.

20. Rosen ED, Spiegelman BM. Adipocytes as regulators of energy balance and glucose homeostasis. *Nature*. 2006;444(7121):847-853. doi: 10.1038/nature05483.

21. Galicia-Garcia U, Benito-Vicente A, Jebari S, et al. Pathophysiology of type 2 diabetes mellitus. *International Journal of Molecular Sciences*. 2020;21(17):6275. doi: 10.3390/ijms21176275.

22. ZHOU YP, GRILL V. Long-term exposure to fatty-acids and ketones inhibits B-cell functions in human pancreatic-islets of langerhans. *Journal of Clinical Endocrinology & Metabolism*. 1995;80(5):1584-1590. doi: 10.1210/jc.80.5.1584.

23. Hotamisligil GS, Peraldi P, Budavari A, Ellis R, White MF, Spiegelman BM. IRS-1-mediated inhibition of insulin receptor tyrosine kinase activity in TNF-alpha- and obesity-induced insulin resistance. *Science*. 1996;271(5249):665-668. doi: 10.1126/science.271.5249.665.

24. KERN PA, SAGHIZADEH M, ONG JM, BOSCH RJ, DEEM R, SIMSOLO RB. The expression of tumor-necrosis-factor in human adipose-tissue - regulation by obesity, weight-loss, and relationship to lipoprotein-lipase. *J Clin Invest*. 1995;95(5):2111-2119. doi: 10.1172/JCI117899.

25. HOTAMISLIGIL GS, ARNER P, CARO JF, ATKINSON RL, SPIEGELMAN BM. Increased adipose-tissue expression of tumor-necrosis-factor-alpha in human obesity and insulin-resistance. *J Clin Invest*. 1995;95(5):2409-2415. doi: 10.1172/JCI117936.

26. Czech MP. Mechanisms of insulin resistance related to white, beige, and brown adipocytes. *Molecular Metabolism*. 2020;34:27-42. doi: 10.1016/j.molmet.2019.12.014.

27. Edgerton DS, Lautz M, Scott M, et al. Insulin's direct effects on the liver dominate the control of hepatic glucose production. *J Clin Invest*. 2006;116(2):521-527. doi: 10.1172/JCI27073.

28. Meshkani R, Adeli K. Hepatic insulin resistance, metabolic syndrome and cardiovascular disease. *Clin Biochem*. 2009;42(13-14):1331-1346. doi: 10.1016/j.clinbiochem.2009.05.018.

29. Steneberg R, Rubins N, Bartoov-Shifman R, Walker MD, Edlund H. The FFA receptor GPR40 links hyperinsulinemia, hepatic steatosis, and impaired glucose homeostasis in mouse. *Cell Metabolism*. 2005;1(4):245-258. doi: 10.1016/j.cmet.2005.03.007.

30. Christensen AA, Gannon M. The beta cell in type 2 diabetes. *Current Diabetes Reports*. 2019;19(9):81. doi: 10.1007/s11892-019-1196-4.

31. Halban PA, Polonsky KS, Bowden DW, et al. Beta-cell failure in type 2 diabetes: Postulated mechanisms and prospects for prevention and treatment. *Diabetes Care*. 2014;37(6):1751-1758. doi: 10.2337/dc14-0396.

32. Oanh Hoang Do, Thorn P. Insulin secretion from beta cells within intact islets: Location matters. *Clinical and Experimental Pharmacology and Physiology*. 2015;42(4):406-414. doi: 10.1111/1440-1681.12368.

33. Butler AE, Janson J, Bonner-Weir S, Ritzel R, Rizza RA, Butler PC. Beta-cell deficit and increased beta-cell apoptosis in humans with type 2 diabetes. *Diabetes*. 2003;52(1):102-110. doi: 10.2337/diabetes.52.1.102.

34. MARTIN BC, WARRAM JH, KROLEWSKI AS, BERGMAN RN, SOELDNER JS, KAHN CR. Role of glucose and insulin resistance in development of type-2 diabetes-mellitus - results of a 25-year follow-up-study. *Lancet*. 1992;340(8825):925-929. doi: 10.1016/0140-6736(92)92814-V.

35. Liu YQ, Jetton TL, Leahy JL. Beta-cell adaptation to insulin resistance - increased pyruvate carboxylase and malate-pyruvate shuttle activity in islets of nondiabetic zucker fatty rats. *J Biol Chem*. 2002;277(42):39163-39168. doi: 10.1074/jbc.M207157200.

36. Poitout V, Robertson RP. Glucolipotoxicity: Fuel excess and beta-cell dysfunction. *Endocr Rev*. 2008;29(3):351-366. doi: 10.1210/er.2007-0023.

37. Verges B. Pathophysiology of diabetic dyslipidaemia: Where are we? *Diabetologia*. 2015;58(5):886-899. doi: 10.1007/s00125-015-3525-8.

38. Taskinen MR. Diabetic dyslipidaemia: From basic research to clinical practice. *Diabetologia*. 2003;46(6):733-749. doi: 10.1007/s00125-003-1111-y.

39. Adiels M, Boren J, Caslake MJ, et al. Overproduction of VLDL1 driven by hyperglycemia is a dominant feature of diabetic dyslipidemia. *Arteriosclerosis Thrombosis and Vascular Biology*. 2005;25(8):1697-1703. doi: 10.1161/01.ATV.0000172689.53992.25.

40. Gordts, Philip L. S. M., Nock R, Son N, et al. ApoC-III inhibits clearance of triglyceride-rich lipoproteins through LDL family receptors. *J Clin Invest*. 2016;126(8):2855-2866. doi: 10.1172/JCI86610.

41. Laatsch A, Merkel M, Talmud PJ, Grewal T, Beisiegel U, Heeren J. Insulin stimulates hepatic low density lipoprotein receptor-related protein 1 (LRP1) to increase postprandial lipoprotein clearance. *Atherosclerosis*. 2009;204(1):105-111. doi: 10.1016/j.atherosclerosis.2008.07.046.

42. Dandona P, Aljada A, Bandyopadhyay A. Inflammation: The link between insulin resistance, obesity and diabetes. *Trends Immunol*. 2004;25(1):4-7. doi: 10.1016/j.it.2003.10.013.

43. Tajiri Y, Mimura K, Umeda F. High-sensitivity C-reactive protein in japanese patients with type 2 diabetes. *Obes Res*. 2005;13(10):1810-1816. doi: 10.1038/oby.2005.220.

44. Wang P, Mariman E, Renes J, Keijer J. The secretory function of adipocytes in the physiology of white adipose tissue. *J Cell Physiol*. 2008;216(1):3-13. doi: 10.1002/jcp.21386.

45. Halberg N, Wernstedt-Asterholm I, Scherer PE. The adipocyte as an endocrine cell. *Endocrinol Metab Clin North Am*. 2008;37(3):753-+. doi: 10.1016/j.ecl.2008.07.002.

46. Shi H, Kokoeva MV, Inouye K, Tzameli I, Yin H, Flier JS. TLR4 links innate immunity and fatty acid-induced insulin resistance. *J Clin Invest*. 2006;116(11):3015-3025. doi: 10.1172/JCI28898.

47. Antuna-Puente B, Feve B, Fellahi S, Bastard J-. Adipokines: The missing link between insulin resistance and obesity. *Diabetes Metab*. 2008;34(1):2-11. doi: 10.1016/j.diabet.2007.09.004.

48. Weisberg SP, McCann D, Desai M, Rosenbaum M, Leibel RL, Ferrante AW. Obesity is associated with macrophage accumulation in adipose tissue. *J Clin Invest*. 2003;112(12):1796-1808. doi: 10.1172/JCI200319246.

49. Bastard JP, Maachi M, Lagathu C, et al. Recent advances in the relationship between obesity, inflammation, and insulin resistance. *Eur Cytokine Netw*. 2006;17(1):4-12.

50. Feve B, Bastard J. The role of interleukins in insulin resistance and type 2 diabetes mellitus. *Nature Reviews Endocrinology*. 2009;5(6):305-311. doi: 10.1038/nrendo.2009.62.

51. Hirosumi J, Tuncman G, Chang LF, et al. A central role for JNK in obesity and insulin resistance. *Nature*. 2002;420(6913):333-336. doi: 10.1038/nature01137.

52. Gao ZG, Hwang D, Bataille F, et al. Serine phosphorylation of insulin receptor substrate 1 by inhibitor kappa B kinase complex. *J Biol Chem*. 2002;277(50):48115-48121. doi: 10.1074/jbc.M209459200.

53. Maedler K, Sergeev P, Ris F, et al. Glucose-induced beta cell production of IL-1 beta contributes to glucotoxicity in human pancreatic islets (vol 110, pg 851, 2002). *J Clin Invest*. 2017;127(4):1589. doi: 10.1172/JCI92172.

54. Boeni-Schnetzler M, Boller S, Debray S, et al. Free fatty acids induce a proinflammatory response in islets via the abundantly expressed interleukin-1 receptor I. *Endocrinology*. 2009;150(12):5218-5229. doi: 10.1210/en.2009-0543.

55. King A, Bowe J. Animal models for diabetes: Understanding the pathogenesis and finding new treatments. *Biochem Pharmacol*. 2016;99:1-10. doi: 10.1016/j.bcp.2015.08.108.

56. King AJF. The use of animal models in diabetes research. *Br J Pharmacol*. 2012;166(3):877-894. doi: 10.1111/j.1476-5381.2012.01911.x.

57. Masiello P. Animal models of type 2 diabetes with reduced pancreatic beta-cell mass. *Int J Biochem Cell Biol*. 2006;38(5-6):873-893. doi: 10.1016/j.biocel.2005.09.007.

58. MAGYAR J, RUSZNAK Z, SZENTESI P, SZUCS G, KOVACS L. Action-potentials and potassium currents in rat ventricular muscle during experimental diabetes. *J Mol Cell Cardiol*. 1992;24(8):841-853. doi: 10.1016/0022-2828(92)91098-P.

59. SHIMONI Y, FIREK L, SEVERSON D, GILES W. Short-term diabetes alters K+ currents in rat ventricular myocytes. *Circ Res*. 1994;74(4):620-628. doi: 10.1161/01.RES.74.4.620.

60. Casis O, Gallego M, Iriarte M, Sanchez-Chapula JA. Effects of diabetic cardiomyopathy on regional electrophysiologic characteristics of rat ventricle. *Diabetologia*. 2000;43(1):101-109. doi: 10.1007/s001250050013.

61. Lengyel C, Virag L, Biro T, et al. Diabetes mellitus attenuates the repolarization reserve in mammalian heart. *Cardiovasc Res*. 2007;73(3):512-520. doi: 10.1016/j.cardiores.2006.11.010.

62. Lengyel C, Virag L, Kovacs PP, et al. Role of slow delayed rectifier K+-current in QT prolongation in the alloxan-induced diabetic rabbit heart. *Acta Physiol*. 2008;192(3):359-368. doi: 10.1111/j.1748-1716.2007.01753.x.

63. Ionut V, Liu H, Mooradian V, et al. Novel canine models of obese prediabetes and mild type 2 diabetes. *Am J Physiol -Endocrinol Metab*. 2010;298(1):E38-E48. doi: 10.1152/ajpendo.00466.2009.

64. Podell BK, Ackart DF, Richardson MA, DiLisio JE, Pulford B, Basaraba RJ. A model of type 2 diabetes in the guinea pig using sequential diet-induced glucose intolerance and streptozotocin treatment. *Dis Model Mech*. 2017;10(2):151-162. doi: 10.1242/dmm.025593.

65. Ti Y, Xie G, Wang Z, et al. TRB3 gene silencing alleviates diabetic cardiomyopathy in a type 2 diabetic rat model. *Diabetes*. 2011;60(11):2963-2974. doi: 10.2337/db11-0549.

66. Grant AO. Cardiac ion channels. *Circulation-Arrhythmia and Electrophysiology*. 2009;2(2):185-194. doi: 10.1161/CIRCEP.108.789081.

67. Nerbonne JM, Kass RS. Molecular physiology of cardiac repolarization. *Physiol Rev*. 2005;85(4):1205-1253.

68. Barry DM, Nerbonne JM. Myocardial potassium channels: Electrophysiological and molecular diversity. *Annu Rev Physiol*. 1996;58:363-394. doi: 10.1146/annurev.physiol.58.1.363.

69. Zimmet PZ, Magliano DJ, Herman WH, Shaw JE. Diabetes: A 21st century challenge. *Lancet Diabetes & Endocrinology*. 2014;2(1):56-64. doi: 10.1016/S2213-8587(13)70112-8.

70. Litwak L, Goh S, Hussein Z, Malek R, Prusty V, Khamseh ME. Prevalence of diabetes complications in people with type 2 diabetes mellitus and its association with baseline characteristics in the multinational A(1)chieve study. *Diabetology & Metabolic Syndrome*. 2013;5:57. doi: 10.1186/1758-5996-5-57.

71. KANNEL WB, HJORTLAND M, CASTELLI WP. Role of diabetes in congestive heart-failure - framingham study. *Am J Cardiol*. 1974;34(1):29-34. doi: 10.1016/0002-9149(74)90089-7.

72. Patel A, MacMahon S, Chalmers J, et al. Intensive blood glucose control and vascular outcomes in patients with type 2 diabetes. *N Engl J Med*. 2008;358(24):2560-2572. doi: 10.1056/NEJMoa0802987.

73. Moritz T, Duckworth W, Abraira C. Glucose control and vascular complications in veterans with type 2 diabetes (vol 360, pg 129, 2009). *N Engl J Med*. 2009;361(10):1024-1025. doi: 10.1056/NEJMc096250.

74. RUBLER S, YUCEOGLU YZ, KUMRAL T, GRISHMAN A, BRANWOOD AW, DLUGASH J. New type of cardiomyopathy associated with diabetic glomerulosclerosis. *Am J Cardiol*. 1972;30(6):595-&. doi: 10.1016/0002-9149(72)90595-4.

75. Jia G, Hill MA, Sowers JR. Diabetic cardiomyopathy: An update of mechanisms contributing to this clinical entity. *Circ Res*. 2018;122(4):624-638. doi: 10.1161/CIRCRESAHA.117.311586.

76. Lee M, Gardin JM, Lynch JC, et al. Diabetes mellitus and echocardiographic left ventricular function in free-living elderly men and women: The cardiovascular health study. *Am Heart J*. 1997;133(1):36-43. doi: 10.1016/S0002-8703(97)70245-X.

77. Devereux RB, Roman MJ, Paranicas M, et al. Impact of diabetes on cardiac structure and function - the strong heart study. *Circulation*. 2000;101(19):2271-2276. doi: 10.1161/01.CIR.101.19.2271.

78. Bugger H, Abel ED. Molecular mechanisms of diabetic cardiomyopathy. *Diabetologia*. 2014;57(4):660-671. doi: 10.1007/s00125-014-3171-6.

79. Casis O, Echevarria E. Diabetic cardiomyopathy: Electromechanical cellular alterations. *Curr Vasc Pharmacol*. 2004;2(3):237-248. doi: 10.2174/1570161043385655 [doi].

80. Onay-Besikci A. *Substrate metabolism in the diabetic heart.* Vol 9. NEW YORK; 233 SPRING STREET, NEW YORK, NY 10013, UNITED STATES: SPRINGER; 2014:76. 10.1007/978-1-4614-9317-4_4.

81. Palomer X, Pizarro-Delgado J, Vazquez-Carrera M. Emerging actors in diabetic cardiomyopathy: Heartbreaker biomarkers or therapeutic targets? *Trends Pharmacol Sci*. 2018;39(5):452-467. doi: 10.1016/j.tips.2018.02.010.

82. Hotamisligil GS, Erbay E. Nutrient sensing and inflammation in metabolic diseases. *Nature Reviews Immunology*. 2008;8(12):923-934. doi: 10.1038/nri2449.

83. Jia G, DeMarco VG, Sowers JR. Insulin resistance and hyperinsulinaemia in diabetic cardiomyopathy. *Nature Reviews Endocrinology*. 2016;12(3):144-153. doi: 10.1038/nrendo.2015.216.

84. Schilling JD, Machkovech HM, Kim AHJ, Schwendener R, Schaffer JE. Macrophages modulate cardiac function in lipotoxic cardiomyopathy (vol 303, pg H1366, 2012). *American Journal of Physiology-Heart and Circulatory Physiology*. 2013;304(4):H632. doi: 10.1152/ajpheart.zh4-0687-corr.2013.

85. Gallego M, Casis O. *Cellular mechanism underlying the misfunction of cardiac ionic channels in diabetes.* Vol 9. NEW YORK; 233 SPRING STREET, NEW YORK, NY 10013, UNITED STATES: SPRINGER; 2014:199. 10.1007/978-1-4614-9317-4_11.

86. Hegyi B, Bers DM, Bossuyt J. CaMKII signaling in heart diseases: Emerging role in diabetic cardiomyopathy. *J Mol Cell Cardiol*. 2019;127:246-259. doi: 10.1016/j.yjmcc.2019.01.001.

87. Tse G, Lai ETH, Tse V, Yeo JM. Molecular and electrophysiological mechanisms underlying cardiac arrhythmogenesis in diabetes mellitus. *J Diabetes Res*. 2016:2848759. doi: 10.1155/2016/2848759.

88. Chen C, Wang W, Zhou W, et al. Nocturnal ventricular arrhythmias are associated with the severity of cardiovascular autonomic neuropathy in type 2 diabetes. *J Diabetes*. 2019;11(10):794-801. doi: 10.1111/1753-0407.12908.

89. Spallone V, Ziegler D, Freeman R, et al. Cardiovascular autonomic neuropathy in diabetes: Clinical impact, assessment, diagnosis, and management. *Diabetes-Metab Res Rev*. 2011;27(7):639-653. doi: 10.1002/dmrr.1239.

90. Jermendy G. Clinical consequences of cardiovascular autonomic neuropathy in diabetic patients. *Acta Diabetol*. 2003;40:S370-S374. doi: 10.1007/s00592-003-0122-y.

91. Karam BS, Chavez-Moreno A, Koh W, Akar JG, Akar FG. Oxidative stress and inflammation as central mediators of atrial fibrillation in obesity and diabetes. *Cardiovasc Diabetol*. 2017;16:120. doi: 10.1186/s12933-017-0604-9.

92. Huxley RR, Alonso A, Lopez FL, et al. Type 2 diabetes, glucose homeostasis and incident atrial fibrillation: The atherosclerosis risk in communities study. *Heart*. 2012;98(2):133-138. doi: 10.1136/heartjnl-2011-300503.

93. Goudis CA, Korantzopoulos P, Ntalas IV, Kallergis EM, Liu T, Ketikoglou DG. Diabetes mellitus and atrial fibrillation: Pathophysiological mechanisms and potential upstream therapies. *Int J Cardiol*. 2015;184:617-622. doi: 10.1016/j.ijcard.2015.03.052.

94. Fu L, Rao F, Lian F, et al. Mechanism of electrical remodeling of atrial myocytes and its influence on susceptibility to atrial fibrillation in diabetic rats. *Life Sci*. 2019;239:116903. doi: 10.1016/j.lfs.2019.116903.

95. Singleton MJ, German C, Hari KJ, et al. QRS duration is associated with all-cause mortality in type 2 diabetes: The diabetes heart study. *J Electrocardiol*. 2020;58:150-154. doi: 10.1016/j.jelectrocard.2019.11.053.

96. BELLAVERE F, FERRI M, GUARINI L, et al. Prolonged qt period in diabetic autonomic neuropathy - a possible role in sudden cardiac death. *Br Heart J*. 1988;59(3):379-383.

97. CHAMBERS JB, SAMPSON MJ, SPRIGINGS DC, JACKSON G. Qt prolongation on the electrocardiogram in diabetic autonomic neuropathy. *Diabetic Med*. 1990;7(2):105-110. doi: 10.1111/j.1464-5491.1990.tb01342.x.

98. EWING DJ, BOLAND O, NEILSON J, CHO CG, CLARKE BF. Autonomic neuropathy, qt interval lengthening, and unexpected deaths in male diabetic-patients. *Diabetologia*. 1991;34(3):182-185. doi: 10.1007/BF00418273.

99. Naas A, Davidson NC, Thompson C, et al. QT and QTc dispersion are accurate predictors of cardiac death in newly diagnosed non-insulin dependent diabetes: Cohort study. *Br Med J*. 1998;316(7133):745-746. doi: 10.1136/bmj.316.7133.745.

100. Cox AJ, Azeem A, Yeboah J, et al. Heart rate- corrected QT interval is an independent predictor of AllCause and cardiovascular mortality in individuals WithType 2 diabetes: The diabetes heart study. *Diabetes Care*. 2014;37(5):1454-1461. doi: 10.2337/dc13-1257.

101. Kumar R, Fisher M, Whitaker R, MacFarlane PW. Effect of controlling hyperglycemia with diet on QT abnormalities in newly diagnosed patients with type 2 diabetes. *Diabetes Care*. 2004;27(11):2767-2768. doi: 10.2337/diacare.27.11.2767-a.

102. Li C, Lv L, Li H, Yu D. Cardiac fibrosis and dysfunction in experimental diabetic cardiomyopathy are ameliorated by alpha-lipoic acid. *Cardiovasc Diabetol*. 2012;11:73. doi: 10.1186/1475-2840-11-73.

103. Ninkovic VM, Ninkovic SM, Miloradovic V, et al. Prevalence and risk factors for prolonged QT interval and QT dispersion in patients with type 2 diabetes. *Acta Diabetol*. 2016;53(5):737-744. doi: 10.1007/s00592-016-0864-y.

104. Ferrannini E, DeFronzo RA. Impact of glucose-lowering drugs on cardiovascular disease in type 2 diabetes. *Eur Heart J*. 2015;36(34):2288-U19. doi: 10.1093/eurheartj/ehv239.

105. Cardoso C, Salles G, Bloch K, Deccache W, Siqueira AG. Clinical determinants of increased QT dispersion in patients with diabetes mellitus. *Int J Cardiol*. 2001;79(2-3):253-262. doi: 10.1016/S0167-5273(01)00443-0.

106. Torres-Jacome J, Gallego M, Rodriguez-Robledo JM, Sanchez-Chapula JA, Casis O. Improvement of the metabolic status recovers cardiac potassium channel synthesis in experimental diabetes. *Acta Physiol*. 2013;207(3):447-459. doi: 10.1111/apha.12043.

107. TSUCHIDA K, WATAJIMA H, OTOMO S. Calcium current in rat diabetic ventricular myocytes. *Am J Physiol -Heart Circul Physiol*. 1994;267(6):H2280-H2289.

108. JOURDON P, FEUVRAY D. Calcium and potassium currents in ventricular myocytes isolated from diabetic rats. *J Physiol -London*. 1993;470:411-429. doi: 10.1113/jphysiol.1993.sp019866.

109. Lu Z, Jiang Y, Xu X, Ballou LM, Cohen IS, Lin RZ. Decreased L-type Ca2+ current in cardiac myocytes of type 1 diabetic akita mice due to reduced phosphatidylinositol 3-kinase signaling. *Diabetes*. 2007;56(11):2780-2789. doi: 10.2337/db06-1629.

110. Pereira L, Matthes J, Schuster I, et al. Mechanisms of [Ca2+](i) transient decrease in cardiomyopathy of db/db type 2 diabetic mice. *Diabetes*. 2006;55(3):608-615. doi: 10.2337/diabetes.55.03.06.db05-1284.

111. REGAN TJ, ETTINGER PO, KHAN MI, et al. Altered myocardial-function and metabolism in chronic diabetes-mellitus without ischemia in dogs. *Circ Res*. 1974;35(2):222-237. doi: 10.1161/01.RES.35.2.222.

112. FEUVRAY D, IDELLWENGER JA, NEELY JR. Effects of ischemia on rat myocardial-function and metabolism in diabetes. *Circ Res*. 1979;44(3):322-329. doi: 10.1161/01.RES.44.3.322.

113. FEIN FS, KORNSTEIN LB, STROBECK JE, CAPASSO JM, SONNENBLICK EH. Altered myocardial mechanics in diabetic rats. *Circ Res*. 1980;47(6):922-933. doi: 10.1161/01.RES.47.6.922.

114. Teshima Y, Takahashi N, Saikawa T, et al. Diminished expression of sarcoplasmic reticulum Ca2+-ATPase and ryanodine sensitive Ca2+ channel mRNA in streptozotocin-induced diabetic rat heart. *J Mol Cell Cardiol*. 2000;32(4):655-664. doi: 10.1006/jmcc.2000.1107.

115. Netticadan T, Temsah RM, Kent A, Elimban V, Dhalla NS. Depressed levels of Ca2+-cycling proteins may underlie sarcoplasmic reticulum dysfunction in the diabetic heart. *Diabetes*. 2001;50(9):2133-2138. doi: 10.2337/diabetes.50.9.2133.

116. ALLO SN, LINCOLN TM, WILSON GL, GREEN FJ, WATANABE AM, SCHAFFER SW. Non-insulin-dependent diabetes-induced defects in cardiac cellular calcium regulation. *Am J Physiol*. 1991;260(6):C1165-C1171.

117. Singh RM, Waqar T, Howarth FC, Adeghate E, Bidasee K, Singh J. Hyperglycemia-induced cardiac contractile dysfunction in the diabetic heart. *Heart Fail Rev*. 2018;23(1):37-54. doi: 10.1007/s10741-017-9663-y.

118. Razeghi P, Young ME, Cockrill TC, Frazier OH, Taegtmeyer H. Downregulation of myocardial myocyte enhancer factor 2C and myocyte enhancer factor 2C-regulated gene expression in diabetic patients with nonischemic heart failure. *Circulation*. 2002;106(4):407-411. doi: 10.1161/01.CIR.0000026392.80723.DC.

119. Zhong Y, Ahmed S, Grupp IL, Matlib MA. Altered SR protein expression associated with contractile dysfunction in diabetic rat hearts. *Am J Physiol -Heart Circul Physiol*. 2001;281(3):H1137-H1147.

120. FEIN FS, ZOLA BE, MALHOTRA A, et al. Hypertensive-diabetic cardiomyopathy in rats. *Am J Physiol*. 1990;258(3):H793-H805.

121. HORACKOVA M, MURPHY MG. Effects of chronic diabetes-mellitus on the electrical and contractile activities, C-45(2+) transport, fatty-acid profiles and ultrastructure of isolated rat ventricular myocytes. *Pflugers Arch*. 1988;411(5):564-572. doi: 10.1007/BF00582379.

122. PENPARGKUL S, FEIN F, SONNENBLICK EH, SCHEUER J. Depressed cardiac sarcoplasmic reticular function from diabetic rats. *J Mol Cell Cardiol*. 1981;13(3):303-309. doi: 10.1016/0022-2828(81)90318-7.

123. Golfman LS, Takeda N, Dhalla NS. Cardiac membrane ca(2+)-transport in alloxan-induced diabetes in rats. *Diabetes Res Clin Pract*. 1996;31 Suppl:73. doi: 0168-8227(96)01233-8 [pii].

124. Chiamvimonvat N, Ye Chen-Izu, Clancy CE, et al. Potassium currents in the heart: Functional roles in repolarization, arrhythmia and therapeutics. *J Physiol -London*. 2017;595(7):2229-2252. doi: 10.1113/JP272883.

125. Xu Z, Patel KP, Rozanski GJ. Metabolic basis of decreased transient outward K+ current in ventricular myocytes from diabetic rats. *Am J Physiol -Heart Circul Physiol*. 1996;271(5):H2190-H2196.

126. Qin DY, Huang BY, Deng LL, et al. Downregulation of K+ channel genes expression in type I diabetic cardiomyopathy. *Biochem Biophys Res Commun*. 2001;283(3):549-553. doi: 10.1006/bbrc.2001.4825.

127. Gallego M, Fernandez D, Ahyayauch H, Casis E, Casis O. Reduced calmodulin expression accelerates transient outward potassium current inactivation in diabetic rat heart. *Cell Physiol Biochem*. 2008;22(5-6):625-634. doi: 10.1159/000185546.

128. Zhang Y, Xiao J, Lin H, et al. Ionic mechanisms underlying abnormal QT prolongation and the associated arrhythmias in diabetic rabbits: A role of rapid delayed rectifier K+ current. *Cell Physiol Biochem*. 2007;19(5-6):225-238. doi: 10.1159/000100642.

129. Zhang Y, Xiao J, Wang H, et al. Restoring depressed HERG K+ channel function as a mechanism for insulin treatment of abnormal QT prolongation and associated arrhythmias in diabetic rabbits. *Am J Physiol -Heart Circul Physiol*. 2006;291(3):H1446-H1455. doi: 10.1152/ajpheart.01356.2005.

130. Monnerat G, Alarcon ML, Vasconcellos LR, et al. Macrophage-dependent IL-1 beta production induces cardiac arrhythmias in diabetic mice. *Nat Commun*. 2016;7:13344. doi: 10.1038/ncomms13344.

131. Tsuchida K, Watajima H. Potassium currents in ventricular myocytes from genetically diabetic rats. *Am J Physiol -Endocrinol Metab*. 1997;273(4):E695-E700.

132. Shimoni Y, Chuang M, Abel ED, Severson DL. Gender-dependent attenuation of cardiac potassium currents in type 2 diabetic db/db mice. *J Physiol -London*. 2004;555(2):345-354. doi: 10.1113/jphysiol.2003.055590.

133. Sato T, Kobayashi T, Kuno A, et al. Type 2 diabetes induces subendocardium-predominant reduction in transient outward K+ current with downregulation of Kv4.2 and KChIP2. *Am J Physiol -Heart Circul Physiol*. 2014;306(7):H1054-H1065. doi: 10.1152/ajpheart.00414.2013.

134. Ashrafi R, Modi P, Oo AY, et al. Arrhythmogenic gene remodelling in elderly patients with type 2 diabetes with aortic stenosis and normal left ventricular ejection fraction. *Exp Physiol*. 2017;102(11):1424-1434. doi: 10.1113/EP086412.

135. Hancox JC. A basis for human QT interval prolongation and arrhythmia risk in type 2 diabetes? *Exp Physiol*. 2017;102(11):1395-1396. doi: 10.1113/EP086618.

136. Knowler WC, Barrett-Connor E, Fowler SE, et al. Reduction in the incidence of type 2 diabetes with lifestyle intervention or metformin. *N Engl J Med*. 2002;346(6):393-403. doi: 10.1056/nejmoa012512.

137. Viberti G, Kahn SE, Greene DA, et al. A diabetes outcome progression trial (ADOPT). *Diabetes Care*. 2002;25(10):1737-1743. doi: 10.2337/diacare.25.10.1737.

138. Boussageon R, Supper I, Bejan-Angoulvant T, et al. Reappraisal of metformin efficacy in the treatment of type 2 diabetes: A meta-analysis of randomised controlled trials. *PLos Med*. 2012;9(4):e1001204. doi: 10.1371/journal.pmed.1001204.

139. Boussageon R, Gueyffier F, Cornu C. Metformin as firstline treatment for type 2 diabetes: Are we sure? *BMJ-British Medical Journal*. 2016;352:h6748. doi: 10.1136/bmj.h6748.

140. Hemmingsen B, Schroll JB, Wetterslev J, et al. Sulfonylurea versus metformin monotherapy in patients with type 2 diabetes: A cochrane systematic review and meta-analysis of randomized clinical trials and trial sequential analysis. *CMAJ Open*. 2014;2(3):162. doi: 10.9778/cmajo.20130073 [doi].

141. Jin X, Jiang Y, Xue G, et al. Increase of late sodium current contributes to enhanced susceptibility to atrial fibrillation in diabetic mice. *Eur J Pharmacol*. 2019;857:UNSP 172444. doi: 10.1016/j.ejphar.2019.172444.

142. Turner RC, Cull CA, Frighi V, Holman RR, UK Prospective Diabet Study Grp. Glycemic control with diet, sulfonylurea, metformin, or insulin in patients with type 2 diabetes mellitus - progressive requirement for multiple therapies (UKPDS 49). *JAMA-J Am Med Assoc*. 1999;281(21):2005-2012. doi: 10.1001/jama.281.21.2005.

143. Fox CS, Coady S, Sorlie PD, et al. Trends in cardiovascular complications of diabetes. *JAMA-J Am Med Assoc*. 2004;292(20):2495-2499. doi: 10.1001/jama.292.20.2495.

144. Preis SR, Pencina MJ, Hwang S, et al. Trends in cardiovascular disease risk factors in individuals with and without diabetes mellitus in the framingham heart study. *Circulation*. 2009;120(3):212-U52. doi: 10.1161/CIRCULATIONAHA.108.846519.

145. Turner RC, Holman RR, Stratton IM, et al. Effect of intensive blood-glucose control with metformin on complications in overweight patients with type 2 diabetes (UKPDS 34). *Lancet*. 1998;352(9131):854-865. doi: 10.1016/s0140-6736(98)07037-8.

146. Dormandy JA, Charbonnel B, Eckland D, et al. Secondary prevention of macrovascular events in patients with type 2 diabetes in the PROactive study (PROspective pioglitAzone clinical trial in macroVascular events): A randomised controlled trial. *Lancet*. 2005;366(9493):1279-1289. doi: 10.1016/S0140-6736(05)67528-9.

147. Singh S, Loke YK, Furberg CD. Long-term risk of cardiovascular events with rosiglitazone - A meta-analysis. *JAMA-J Am Med Assoc*. 2007;298(10):1189-1195. doi: 10.1001/jama.298.10.1189.

148. Lincoff AM, Wolski K, Nicholls SJ, Nissen SE. Pioglitazone and risk of cardiovascular events in patients with type 2 diabetes mellitus - A meta-analysis of randomized trials. *JAMA-J Am Med Assoc*. 2007;298(10):1180-1188. doi: 10.1001/jama.298.10.1180.

149. Scirica BM, Bhatt DL, Braunwald E, et al. Saxagliptin and cardiovascular outcomes in patients with type 2 diabetes mellitus. *N Engl J Med*. 2013;369(14):1317-1326. doi: 10.1056/NEJMoa1307684.

150. Zannad F, Cannon CP, Cushman WC, et al. Heart failure and mortality outcomes in patients with type 2 diabetes taking alogliptin versus placebo in EXAMINE: A multicentre, randomised, double-blind trial. *Lancet*. 2015;385(9982):2067-2076. doi: 10.1016/S0140-6736(14)62225-X.

151. Green JB, Bethel MA, Armstrong PW. Effect of sitagliptin on cardiovascular outcomes in type 2 diabetes (vol 373, pg 232, 2015). *N Engl J Med*. 2015;373(6):586.

152. Marso SP, Bain SC, Consoli A, et al. Semaglutide and cardiovascular outcomes in patients with type 2 diabetes. *N Engl J Med*. 2016;375(19):1834-1844. doi: 10.1056/NEJMoa1607141.

153. Marso SP, Nauck MA, Fries TM, et al. Myocardial infarction subtypes in patients with type 2 diabetes mellitus and the effect of liraglutide therapy (from the LEADER trial). *Am J Cardiol*. 2018;121(12):1467-1470. doi: 10.1016/j.amjcard.2018.02.030.

154. Zinman B, Wanner C, Lachin JM, et al. Empagliflozin, cardiovascular outcomes, and mortality in type 2 diabetes. *N Engl J Med*. 2015;373(22):2117-2128. doi: 10.1056/NEJMoa1504720.

155. Baartscheer A, Schumacher CA, Wust RCI, et al. Empagliflozin decreases myocardial cytoplasmic na+ through inhibition of the cardiac na+/H+ exchanger in rats and rabbits. *Diabetologia*. 2017;60(3):568-573. doi: 10.1007/s00125-016-4134-x.

156. Durak A, Olgar Y, Degirmenci S, Akkus E, Tuncay E, Turan B. A SGLT2 inhibitor dapagliflozin suppresses prolonged ventricular-repolarization through augmentation of mitochondrial function in insulin-resistant metabolic syndrome rats. *Cardiovasc Diabetol*. 2018;17:144. doi: 10.1186/s12933-018-0790-0.

157. Xu J, Rajaratnam R. Cardiovascular safety of non-insulin pharmacotherapy for type 2 diabetes. *Cardiovasc Diabetol*. 2017;16:18. doi: 10.1186/s12933-017-0499-5.

158. Darpo B, Garnett C, Benson CT, et al. Cardiac safety research consortium: Can the thorough QT/QTc study be replaced by early QT assessment in routine clinical pharmacology studies? scientific update and a research proposal for a path forward. *Am Heart J*. 2014;168(3):262-272. doi: 10.1016/j.ahj.2014.06.003.

159. Sager PT, Nebout T, Darpo B. ICH E14: A new regulatory guidance on the clinical evaluation of QT/QTc internal prolongation and proarrhythmic potential for non-antiarrhythmic drugs. *Drug Inf J*. 2005;39(4):387-394. doi: 10.1177/009286150503900407.

160. Heller S, Darpoe B, Mitchell MI, et al. Considerations for assessing the potential effects of antidiabetes drugs on cardiac ventricular repolarization: A report from the cardiac safety research consortium. *Am Heart J*. 2015;170(1):23-35. doi: 10.1016/j.ahj.2015.03.007.

161. Jiang YX, Lee A, Chen JY, et al. X-ray structure of a voltage-dependent K+ channel. *Nature*. 2003;423(6935):33-41. doi: 10.1038/nature01580.

162. Zhu J, Yan J, Thornhill WB. The Kv1.3 potassium channel is localized to the cis-golgi and Kv1.6 is localized to the endoplasmic reticulum in rat astrocytes. *Febs Journal*. 2014;281(15):3433-3445. doi: 10.1111/febs.12871.

163. Vicente R, Villalonga N, Calvo M, et al. Kv1.5 association modifies Kv1.3 traffic and membrane localization. *J Biol Chem*. 2008;283(13):8756-8764. doi: 10.1074/jbc.M708223200.

164. Szabo I, Bock J, Jekle A, et al. A novel potassium channel in lymphocyte mitochondria. *J Biol Chem*. 2005;280(13):12790-12798. doi: 10.1074/jbc.M413548200.

165. PAHAPILL PA, SCHLICHTER LC. Modulation of potassium channels in intact human lymphocytes-T. *Journal of Physiology-London*. 1992;445:407-430. doi: 10.1113/jphysiol.1992.sp018931.

166. McCormack T, McCormack K, Nadal MS, Vieira E, Ozaita A, Rudy B. The effects of shaker beta-subunits on the human lymphocyte K+ channel Kv1.3. *J Biol Chem*. 1999;274(29):20123-20126. doi: 10.1074/jbc.274.29.20123.

167. GRISSMER S, NGUYEN AN, AIYAR J, et al. Pharmacological characterization of 5 cloned voltage-gated K+ channels, types Kv1.1, Kv1.2, Kv1.3, Kv1.5, and Kv3.1, stably expressed in mammalian-cell lines. *Mol Pharmacol*. 1994;45(6):1227-1234.

168. DOUGLASS J, OSBORNE PB, CAI YC, WILKINSON M, CHRISTIE MJ, ADELMAN JP. Characterization and functional expression of a rat genomic dna clone encoding a lymphocyte potassium channel. *Journal of Immunology*. 1990;144(12):4841-4850.

169. Jang SH, Byun JK, Jeon W, et al. Nuclear localization and functional characteristics of voltage-gated potassium channel Kv1.3. *J Biol Chem*. 2015;290(20):12547-12557. doi: 10.1074/jbc.M114.561324.

170. Xu JC, Koni PA, Wang PL, et al. The voltage-gated potassium channel Kv1.3 regulates energy homeostasis and body weight. *Hum Mol Genet*. 2003;12(5):551-559. doi: 10.1093/hmg/ddg049.

171. Panyi G, Vamosi G, Bacso Z, et al. Kv1.3 potassium channels are localized in the immunological synapse formed between cytotoxic and target cells. *Proc Natl Acad Sci U S A*. 2004;101(5):1285-1290. doi: 10.1073/pnas.0307421100.

172. Hu L, Pennington M, Jiang Q, Whartenby KA, Calabresi PA. Characterization of the functional properties of the voltage-gated potassium channel Kv1.3 in human CD4(+) T lymphocytes. *Journal of Immunology*. 2007;179(7):4563-4570. doi: 10.4049/jimmunol.179.7.4563.

173. Vallejo-Gracia A, Bielanska J, Hernandez-Losa J, et al. Emerging role for the voltage-dependent K+ channel Kv1.5 in B-lymphocyte physiology: Expression associated with human lymphoma malignancy. *J Leukoc Biol*. 2013;94(4):779-789. doi: 10.1189/jlb.0213094.

174. Villalonga N, Escalada A, Vicente R, et al. Kv1.3/Kv1.5 heteromeric channels compromise pharmacological responses in macrophages. *Biochem Biophys Res Commun*. 2007;352(4):913-918. doi: 10.1016/j.bbrc.2006.11.120.

175. Cahalan MD, Chandy KG. The functional network of ion channels in T lymphocytes. *Immunol Rev*. 2009;231:59-87. doi: 10.1111/j.1600-065X.2009.00816.x.

176. Perez-Verdaguer M, Capera J, Ortego-Dominguez M, et al. Caveolar targeting links Kv1.3 with the insulin-dependent adipocyte physiology. *Cellular and Molecular Life Sciences*. 2018;75(21):4059-4075. doi: 10.1007/s00018-018-2851-7.

177. Doczi MA, Morielli AD, Damon DH. Kv1.3 channels in postganglionic sympathetic neurons: Expression, function, and modulation. *American Journal of Physiology-Regulatory Integrative and Comparative Physiology*. 2008;295(3):R733-R740. doi: 10.1152/ajpregu.00077.2008.

178. Tucker K, Overton JM, Fadool DA. Diet-induced obesity resistance of Kv1.3-/- mice is olfactory bulb dependent. *J Neuroendocrinol*. 2012;24(8):1087-1095. doi: 10.1111/j.1365-2826.2012.02314.x.

179. Fadool DA, Levitan IB. Modulation of olfactory bulb neuron potassium current by tyrosine phosphorylation. *Journal of Neuroscience*. 1998;18(16):6126-6137.

180. Bielanska J, Hernandez-Losa J, Moline T, et al. Differential expression of Kv1.3 and Kv1.5 voltage-dependent K+ channels in human skeletal muscle sarcomas. *Cancer Invest*. 2012;30(3):203-208. doi: 10.3109/07357907.2012.654872.

181. Xu JC, Koni PA, Wang PL, et al. The voltage-gated potassium channel Kv1.3 regulates energy homeostasis and body weight. *Hum Mol Genet*. 2003;12(5):551-559. doi: 10.1093/hmg/ddg049.

182. Li YY, Wang PL, Xu JC, Desir GV. Voltage-gated potassium channel Kv1.3 regulates GLUT4 trafficking to the plasma membrane via a Ca2+-dependent mechanism. *American Journal of Physiology-Cell Physiology*. 2006;290(2):C345-C351. doi: 10.1152/ajpcell.00091.2005.

183. Upadhyay SK, Eckel-Mahan KL, Mirbolooki MR, et al. Selective Kv1.3 channel blocker as therapeutic for obesity and insulin resistance. *Proc Natl Acad Sci U S A*. 2013;110(24):E2239-E2248. doi: 10.1073/pnas.1221206110.

184. Beeton C, Wulff H, Standifer NE, et al. Kv1.3 channels are a therapeutic target for T cell-mediated autoimmune diseases. *Proc Natl Acad Sci U S A*. 2006;103(46):17414-17419. doi: 10.1073/pnas.0605136103.

185. Perez-Verdaguer M, Capera J, Serrano-Novillo C, Estadella I, Sastre D, Felipe A. The voltage-gated potassium channel Kv1.3 is a promising multitherapeutic target against human pathologies. *Expert Opinion on Therapeutic Targets*. 2016;20(5):577-591. doi: 10.1517/14728222.2016.1112792.

186. Koni PA, Khanna R, Chang MC, et al. Compensatory anion currents in Kv1.3 channel-deficient thymocytes. *J Biol Chem*. 2003;278(41):39443-39451. doi: 10.1074/jbc.M304879200.

187. You M, Song MS, Lee SK, Ryu PD, Lee SY, Kim D. Voltage-gated K+ channels in adipogenic differentiation of bone marrow-derived human mesenchymal stem cells. *Acta Pharmacol Sin*. 2013;34(1):129-136. doi: 10.1038/aps.2012.142.

188. Tucker K, Overton JM, Fadool DA. Kv1.3 gene-targeted deletion alters longevity and reduces adiposity by increasing locomotion and metabolism in melanocortin-4 receptor-null mice. *Int J Obes*. 2008;32(8):1222-1232. doi: 10.1038/ijo.2008.77.

189. Yang Y, Wang Y, Yang X, et al. Specific Kv1.3 blockade modulates key cholesterol-metabolism-associated molecules in human macrophages exposed to ox-LDL. *J Lipid Res*. 2013;54(1):34-43. doi: 10.1194/jlr.M023846.

190. Schmitz A, Sankaranarayanan A, Azam P, et al. Design of PAP-1, a selective small molecule Kv1.3 blocker, for the suppression of effector memory T cells in autoimmune diseases. *Mol Pharmacol*. 2005;68(5):1254-1270. doi: 10.1124/mol.105.015669.

191. Srinivasan S, Bernal-Mizrachi E, Ohsugi M, Permutt MA. Glucose promotes pancreatic islet beta-cell survival through a PI 3-kinase/akt-signaling pathway. *American Journal of Physiology-Endocrinology and Metabolism*. 2002;283(4):E784-E793. doi: 10.1152/ajpendo.00177.2002.

192. Schmitz A, Sankaranarayanan A, Azam P, et al. Design of PAP-1, a selective small molecule Kv1.3 blocker, for the suppression of effector memory T cells in autoimmune diseases. *Mol Pharmacol*. 2005;68(5):1254-1270. doi: 10.1124/mol.105.015669.

193. Azam P, Sankaranarayanan A, Homerick D, Griffey S, Wulff H. Targeting effector memory T cells with the small molecule Kv1.3 blocker PAP-1 suppresses allergic contact dermatitis. *J Invest Dermatol*. 2007;127(6):1419-1429. doi: 10.1038/sj.jid.5700717.

194. Zhang FL, Ye CZ, Li G, et al. The rat model of type 2 diabetic mellitus and its glycometabolism characters. *Experimental Animals*. 2003;52(5):401-407. doi: 10.1538/expanim.52.401.

195. Fernandez-Ruocco J, Gallego M, Rodriguez-de-Yurre A, et al. High thyrotropin is critical for cardiac electrical remodeling and arrhythmia vulnerability in hypothyroidism. *Thyroid*. 2019;29(7):934-945. doi: 10.1089/thy.2018.0709.

196. Elsokkari I, Reyneke E, William M. Left atrial septal pouch causing an ischaemic stroke in association with aortic coarctation. *European Journal of Echocardiography*. 2011;12(12):916. doi: 10.1093/ejechocard/jer224.

197. Lumkwana D, Botha A, Samodien E, Hanser S, Lopes J. Laminin, laminin-entactin and extracellular matrix are equally appropriate adhesive substrates for isolated adult rat cardiomyocyte culture and experimentation. *Cell Adhesion & Migration*. 2018;12(5):503-511. doi: 10.1080/19336918.2017.1387693.

198. Erickson JR, Pereira L, Wang L, et al. Diabetic hyperglycaemia activates CaMKII and arrhythmias by O-linked glycosylation. *Nature*. 2013;502(7471):372-+. doi: 10.1038/nature12537.

199. NEHER E, SAKMANN B. Single-channel currents recorded from membrane of denervated frog muscle-fibers. *Nature*. 1976;260(5554):799-802. doi: 10.1038/260799a0.

200. Durak A, Olgar Y, Degirmenci S, Akkus E, Tuncay E, Turan B. A SGLT2 inhibitor dapagliflozin suppresses prolonged ventricular-repolarization through augmentation of mitochondrial function in insulin-resistant metabolic syndrome rats. *Cardiovascular Diabetology*. 2018;17:144. doi: 10.1186/s12933-018-0790-0.

201. Chatterjee S, Khunti K, Davies MJ. Type 2 diabetes. *Lancet*. 2017;389(10085):2239-2251. doi: 10.1016/S0140-6736(17)30058-2.

202. Kuzuya T, Nakagawa S, Satoh J, et al. Report of the committee on the classification and diagnostic criteria of diabetes mellitus. *Diabetes Res Clin Pract*. 2002;55(1):65-85. doi: 10.1016/S0168-8227(01)00365-5.

203. Haffner SM, Amer Diabet Assoc. Management of dyslipidemia in adults with diabetes. *Diabetes Care*. 2000;23:S57-S60.

204. Mooradian AD. Dyslipidemia in type 2 diabetes mellitus. *Nature Clinical Practice Endocrinology & Metabolism*. 2009;5(3):150-159. doi: 10.1038/ncpendmet1066.

205. Vaag A, Lund SS. Non-obese patients with type 2 diabetes and prediabetic subjects: Distinct phenotypes requiring special diabetes treatment and (or) prevention? *Applied Physiology Nutrition and Metabolism*. 2007;32(5):912-920. doi: 10.1139/H07-100.

206. Chusyd DE, Wang D, Huffman DM, Nagy TR. Relationships between rodent white adipose fat pads and human white adipose fat depots. *Frontiers in Nutrition*. 2016;3:10. doi: 10.3389/fnut.2016.00010.

207. Rossmeisl M, Rim JS, Koza RA, Kozak LP. Variation in type 2 diabetes-related traits in mouse strains susceptible to diet-induced obesity. *Diabetes*. 2003;52(8):1958-1966. doi: 10.2337/diabetes.52.8.1958.

208. Guilherme A, Virbasius JV, Puri V, Czech MP. Adipocyte dysfunctions linking obesity to insulin resistance and type 2 diabetes. *Nature Reviews Molecular Cell Biology*. 2008;9(5):367-377. doi: 10.1038/nrm2391.

209. Bibak B, Khalili M, Rajaei Z, Soukhtanloo M, Hadjzadeh M, Hayatdavoudi P. Effects of melatonin on biochemical factors and food and water consumption in diabetic rats. *Advanced biomedical research*. 2014;3:173. doi: 10.4103/2277-9175.139191.

210. Srinivasan K, Viswanad B, Asrat L, Kaul CL, Ramarao P. Combination of high-fat diet-fed and low-dose streptozotocin-treated rat: A model for type 2 diabetes and pharmacological screening. *Pharmacological Research*. 2005;52(4):313-320. doi: 10.1016/j.phrs.2005.05.004.

211. Jia Y, Liu J, Guo Y, Xu R, Sun J, Li J. Dyslipidemia in rat fed with high-fat diet is not associated with PCSK9-LDL-receptor pathway but ageing. *Journal of Geriatric Cardiology*. 2013;10(4):361-368. doi: 10.3969/j.issn.1671-5411.2013.04.007.

212. Guo X, Wang Y, Wang K, Ji B, Zhou F. Stability of a type 2 diabetes rat model induced by high-fat diet feeding with low-dose streptozotocin injection. *Journal of Zhejiang University-Science B*. 2018;19(7):559-569. doi: 10.1631/jzus.B1700254.

213. Boudina S, Abel ED. Diabetic cardiomyopathy, causes and effects. *Reviews in Endocrine & Metabolic Disorders*. 2010;11(1):31-39. doi: 10.1007/s11154-010-9131-7.

214. YIN F, SPURGEON HA, RAKUSAN K, WEISFELDT ML, LAKATTA EG. Use of tibial length to quantify cardiac-hypertrophy - application in the aging rat. *Am J Physiol*. 1982;243(6):H941-H947.

215. Cox AJ, Azeem A, Yeboah J, et al. Heart rate- corrected QT interval is an independent predictor of AllCause and cardiovascular mortality in individuals WithType 2 diabetes: The diabetes heart study. *Diabetes Care*. 2014;37(5):1454-1461. doi: 10.2337/dc13-1257.

216. Bohne LJ, Johnson D, Rose RA, Wilton SB, Gillis AM. The association between diabetes mellitus and atrial fibrillation: Clinical and mechanistic insights. *Frontiers in Physiology*. 2019;10:135. doi: 10.3389/fphys.2019.00135.

217. Benichou T, Pereira B, Mermillod M, et al. Heart rate variability in type 2 diabetes mellitus: A systematic review and meta-analysis. *Plos One*. 2018;13(4):e0195166. doi: 10.1371/journal.pone.0195166.

218. Tse G, Yan BP. Traditional and novel electrocardiographic conduction and repolarization markers of sudden cardiac death. *Europace*. 2017;19(5):712-721. doi: 10.1093/europace/euw280.

219. Curtis MJ, Hancox JC, Farkas A, et al. The lambeth conventions (II): Guidelines for the study of animal and human ventricular and supraventricular arrhythmias. *Pharmacol Ther*. 2013;139(2):213-248. doi: 10.1016/j.pharmthera.2013.04.008.

220. Movahed M, Hashemzadeh M, Jamal M. Increased prevalence of ventricular fibrillation in patients with type 2 diabetes mellitus. *Heart Vessels*. 2007;22(4):251-253. doi: 10.1007/s00380-006-0962-9.

221. Gallego M, Alday A, Urrutia J, Casis O. Transient outward potassium channel regulation in healthy and diabetic hearts. *Can J Physiol Pharmacol*. 2009;87(2):77-83. doi: 10.1139/Y08-106.

222. Hoang-Trong TM, Ullah A, Jafri MS. Calcium sparks in the heart: Dynamics and regulation. *Research and Reports in Biology*. 2015;6:203-214. doi: 10.2147/RRB.S61495.

223. Yaras N, Ugur M, Ozdemir S, et al. Effects of diabetes on ryanodine receptor ca release channel (RyR2) and Ca2+ homeostasis in rat heart. *Diabetes*. 2005;54(11):3082-3088. doi: 10.2337/diabetes.54.11.3082.

224. Pereira L, Matthes J, Schuster I, et al. Mechanisms of [Ca2+](i) transient decrease in cardiomyopathy of db/db type 2 diabetic mice. *Diabetes*. 2006;55(3):608-615. doi: 10.2337/diabetes.55.03.06.db05-1284.

225. Zatterale F, Longo M, Naderi J, et al. Chronic adipose tissue inflammation linking obesity to insulin resistance and type 2 diabetes. *Frontiers in Physiology*. 2020;10:1607. doi: 10.3389/fphys.2019.01607.

226. Dasu MR, Devaraj S, Park S, Jialal I. Increased toll-like receptor (TLR) activation and TLR ligands in recently diagnosed type 2 diabetic subjects. *Diabetes Care*. 2010;33(4):861-868. doi: 10.2337/dc09-1799.

227. Bello F, Marchi A, Prisco D, Olivotto I, Emmi G. Antiarrhythmic efficacy of anakinra in a young patient with autoimmune lymphocytic myocarditis. *Rheumatology*. 2020;59(11):E88-E90. doi: 10.1093/rheumatology/keaa207.

228. Pfister R, Cairns R, Erdmann E, Schneider CA, PROactive Invest. Prognostic impact of electrocardiographic signs in patients with type 2 diabetes and cardiovascular disease: Results from the PROactive study. *Diabetic Med*. 2011;28(10):1206-1212. doi: 10.1111/j.1464-5491.2011.03281.x.

229. HOTAMISLIGIL GS, ARNER P, CARO JF, ATKINSON RL, SPIEGELMAN BM. Increased adipose-tissue expression of tumor-necrosis-factor-alpha in human obesity and insulin-resistance. *J Clin Invest*. 1995;95(5):2409-2415. doi: 10.1172/JCI117936.

230. Shoelson SE, Lee J, Goldfine AB. Inflammation and insulin resistance. *J Clin Invest*. 2006;116(7):1793-1801. doi: 10.1172/JCI29069.

231. Schmitz A, Sankaranarayanan A, Azam P, et al. Design of PAP-1, a selective small molecule Kv1.3 blocker, for the suppression of effector memory T cells in autoimmune diseases. *Mol Pharmacol*. 2005;68(5):1254-1270. doi: 10.1124/mol.105.015669.

232. Aguayo Rojas LB, Gomes MB. Metformin: An old but still the best treatment for type 2 diabetes. *Diabetol Metab Syndr*. 2013;5:6.

233. Hotamisligil GS. Inflammation and metabolic disorders. *Nature*. 2006;444(7121):860-867. doi: 10.1038/nature05485.

234. Fernandez-Velasco M, Ruiz-Hurtado G, Hurtado O, Moro MA, Delgado C. TNF-alpha downregulates transient outward potassium current in rat ventricular myocytes through iNOS overexpression and oxidant species generation. *American Journal of Physiology-Heart and Circulatory Physiology*. 2007;293(1):H238-H245. doi: 10.1152/ajpheart.01122.2006.

235. Vicente R, Escalada A, Villalonga N, et al. Association of Kv1.5 and Kv1.3 contributes to the major voltage-dependent K+ channel in macrophages. *J Biol Chem*. 2006;281(49):37675-37685. doi: 10.1074/jbc.M605617200.

236. Scherer PE. Adipose tissue - from lipid storage compartment to endocrine organ. *Diabetes*. 2006;55(6):1537-1545. doi: 10.2337/db06-0263.

237. Yan GX, Antzelevitch C. Cellular basis for the normal T wave and the electrocardiographic manifestations of the long-QT syndrome. *Circulation*. 1998;98(18):1928-1936. doi: 10.1161/01.CIR.98.18.1928.

238. Jialal I, Singh G. Management of diabetic dyslipidemia: An update. *World Journal of Diabetes*. 2019;10(5):280-290. doi: 10.4239/wjd.v10.i5.280.

239. Blom LJ, Groeneveld SA, Wulterkens BM, et al. Novel use of repolarization parameters in electrocardiographic imaging to uncover arrhythmogenic substrate. *J Electrocardiol*. 2020;59:116-121. doi: 10.1016/j.jelectrocard.2020.02.003.

240. Zatterale F, Longo M, Naderi J, et al. Chronic adipose tissue inflammation linking obesity to insulin resistance and type 2 diabetes. *Frontiers in Physiology*. 2020;10:1607. doi: 10.3389/fphys.2019.01607.

241. Maida CD, Vasto S, Di Raimondo D, et al. Inflammatory activation and endothelial dysfunction markers in patients with permanent atrial fibrillation: A cross-sectional study. *Aging-Us*. 2020;12(9):8423-8433. doi: 10.18632/aging.103149.